The University of Nottingham

UNITED KINGDOM · CHINA · MALAYSIA

CARBON FROM CARBON DIOXIDE VIA MOLTEN CARBONATE ELECTROLYSIS: FUNDAMENTAL INVESTIGATIONS

By

RICHARD CHARLES LAWRENCE

MEng (Hons) AMIChemE

Thesis submitted to the University of Nottingham

for the degree of Doctor of Philosophy

Department of Chemical and Environmental Engineering

The University of Nottingham

December 2013

ABSTRACT

Conversion of carbon dioxide into useful products has become highly desirable in recent years in order to both mitigate carbon dioxide emissions to the atmosphere and develop non-fossil energy sources. A variety of methods exist for the electro-reduction of carbon dioxide in solution to useful products, such as carbon monoxide and hydrocarbons. However, none of these processes are able to directly convert carbon dioxide to carbon.

In this thesis, the conversion of carbon dioxide into solid carbon via molten carbonate electrolysis has been investigated. Both the past literature and the present work have shown that carbon nanopowder can be produced via this process, so it is highly likely that the electro-deposited carbon obtained is a valuable product. Although this process has been known since the 1960s, there are still many areas where our knowledge of the process is lacking. Hence, this thesis is focussed primarily on the reactions occurring in the molten carbonate electrolyte, the properties of the electro-deposited carbon and the re-oxidation of the electro-deposited carbon.

Using cyclic voltammetry carried out at platinum working electrodes, it was found that carbon was electro-deposited at the cathodic limit in the Li_2CO_3-Na_2CO_3 and Li_2CO_3-K_2CO_3 electrolytes at temperatures of ca. 600 °C and ca. 700 °C, probably by the following reaction:

$$CO_3^{2-} + 4e^- \rightarrow C + 3O^{2-} \qquad \text{(i)}$$

One novel finding of this research is that carbon electro-deposition competed with other cathodic reactions at the cathodic limit, which included alkali metal formation, carbon monoxide formation and alkali metal carbide formation. However, the carbon electro-deposition reaction dominated over the other cathodic reactions once the metal working electrode surface had become covered with a layer of electro-deposited carbon. This was probably because a lower overpotential is required to deposit carbon onto carbon, as opposed to carbon onto metal. Moreover, the other cathodic reactions may have been catalysed by the bare metal working electrode surface before it became covered with carbon.

Electrochemical re-oxidation of electro-deposited carbon was found to occur via a process consisting of at least two stages, which was deduced using cyclic voltammetry in conjunction with the re-oxidation of electro-deposited carbon via galvanostatic chronopotentiometry. These stages may have corresponded to the oxidation of portions of the carbon with different morphologies.

Carbon was electro-deposited onto mild steel working electrodes via chronoamperometry in the Li_2CO_3-Na_2CO_3, Li_2CO_3-K_2CO_3 and Li_2CO_3-Na_2CO_3-K_2CO_3 electrolytes. The highest apparent electro-deposition rate obtained was 0.183 g/cm^2.h at an applied potential of -2.98 V vs. Ag/AgCl, using the Li_2CO_3-K_2CO_3 electrolyte at 708 °C. The average current efficiencies obtained for carbon electro-deposition were: 74.4 % for Li_2CO_3-Na_2CO_3, 79.0 % for Li_2CO_3-K_2CO_3 and 51.2 % for Li_2CO_3-Na_2CO_3-K_2CO_3. Scanning electron microscopy (SEM), X-ray diffraction (XRD) and energy dispersive X-ray (EDX) spectroscopy revealed that the washed carbon deposits mostly consisted of fine quasi-spherical carbon particles, some as small as 60 nm in diameter. All of the electro-deposited carbon appeared to be amorphous.

ACKNOWLEDGEMENTS

Firstly, I would like to thank my supervisors Prof. George Zheng Chen and Prof. Trevor Drage for their supervision, guidance and encouragement throughout this project. I am indebted to Dr. Nancy Siambun, Happiness Ijije, Dr. Han Wang and Dr. Di Hu for their invaluable assistance and advice in molten salt experimental matters. Rustam Akhmetov rendered considerable help in translating the Delimarskii et al. (1975) patent from Russian into English. Other friends and colleagues to whom I am grateful include: Archi Sarroza, Mark Jennings, Kar-sheng Lee, Guan Li, Junghoon Chae, Gwangjun Kim, Dr. Matthew Li, Ebenezer Igunnu, Anthony Stevenson, Dr. Linpo Yu, Dr. Yun Gao, Chidi Ogbuka, Abolore Abdulahi, Ezekiel Agunlejika, Dr. Hui Deng, and Tom Bennett.

I would like to thank the Engineering and Physical Sciences Research Council for financial support. Furthermore, I am grateful to the staff in the Department of Chemical and Environmental Engineering, including but not limited to: Dr. Douglas Brown, Donna Astill, Marion Bryce, Vikki Archibald, Dave Mee, David Clift, Phil Bennett, Mick Fletcher, Jim Oswin, Terry Cullinan, Reg Briggs, Mel Hemsley, and Fred Anderton. Thanks are also due to Phil Davies and Mike Marsden from TA Instruments for assistance in operating the Chen research group's SDT Q600 combined TGA-DSC machine. I would like to thank Dr. Vernon Collis, Dr. David Whitley, Dr. Paul Langston and Prof. Barry Azzopardi for giving me the opportunity to help teach undergraduates whilst I was carrying out this PhD.

Finally, I wish to thank my parents, my sister, and my fiancée Ming-ying Chen for their support and encouragement during this PhD project.

TABLE OF CONTENTS

LIST OF FIGURES

LIST OF TABLES

CHAPTER 1

INTRODUCTION

Conversion of carbon dioxide into useful products has become highly desirable in recent years in order to both mitigate carbon dioxide emissions to the atmosphere and develop non-fossil energy sources (Whipple and Kenis, 2010). This thesis focuses on one method of electro-reducing carbon dioxide to carbon using a molten carbonate electrolyte. Before discussing how this process works, the electro-reduction of carbon dioxide in solution will be considered first.

1.1 Electrochemical Reduction of Carbon Dioxide in Solution

1.1.1Features and general overview

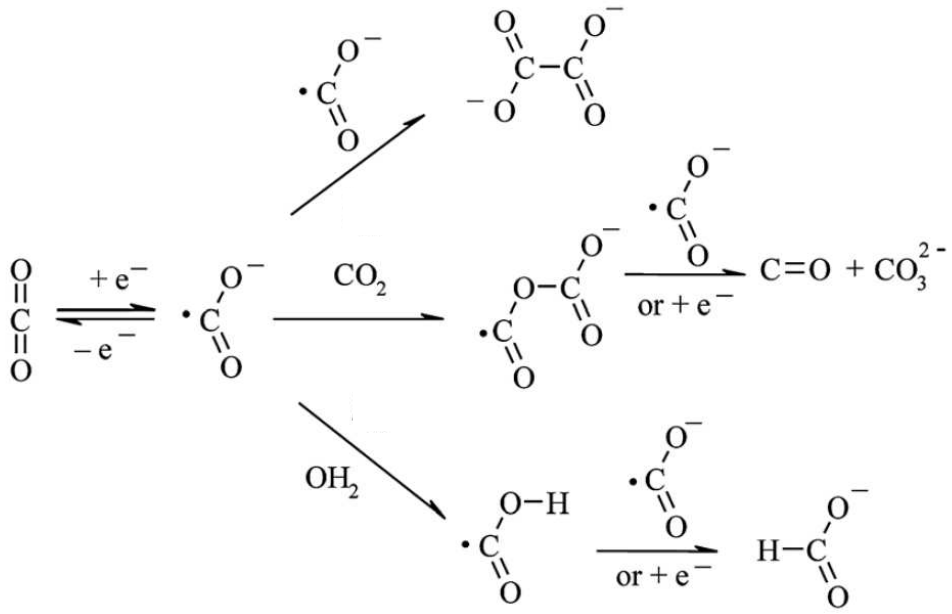

Figure 1.1: Three reaction pathways for the electro-reduction of carbon dioxide at an inert electrode (From Costentin et al., 2013).

There are a great many published works that have demonstrated the electro-reduction of carbon dioxide in solution, under a variety of different conditions. This short overview focuses mainly on aqueous solutions, although the electro-reduction of carbon dioxide has been carried out in

ionic liquids (Barrosse-Antle and Compton, 2009; Snuffin et al., 2011), and organic solvents such as methanol (Kaneco et al., 1999; Kaneco et al., 2007).

Naturally, the electro-reduction conditions affect the type and quantity of product that can be obtained. Firstly, the choice of electrode material is one that has a profound impact on carbon dioxide electro-reduction (Mikkelsen et al., 2009). When carbon or unreactive metal is used as an electrode, the electro-reduction of carbon dioxide gives rise to a carbon dioxide radical anion, which may either undergo disproportionation to carbonate and carbon monoxide, or it may undergo dimerisation to form oxalate (Creutz and Fujita, 2001). Alternatively, the radical anion may react with water in the electrolyte to form formate (Costentin et al., 2013). These three reaction pathways are illustrated in Figure 1.1.

On the other hand, when an 'active metal' is used as an electrode material, it is possible to convert carbon dioxide to hydrogenated products at much lower applied voltages due to the fact that the heterogeneous catalysis is very efficient. The dual role of delivering electrons and stabilising reduced fragments is provided by the metal in such situations (Creutz and Fujita, 2001).

Examples of metals that are not 'active' include iron, aluminium, platinum, nickel, titanium and gadolinium, which can reduce carbon dioxide to form carbon monoxide, but not at very high current efficiencies because hydrogen is the principal product of electrolyses in aqueous solution at these electrodes (Hori and Murata, 1990; Taguchi and Aramata, 1994).

One important point that should be mentioned here is that if the electro-reduction of carbon dioxide is carried out in a water-based or methanol electrolyte, then hydrogen formation will compete with carbon dioxide reduction (Mikkelsen et al., 2009). For instance, when Azuma et al. (1990) carried out electro-reduction using a carbon electrode, the current efficiency of hydrogen evolution was 92.5 %, making the electro-reduction process very inefficient. However, if hydrogen and carbon monoxide could be produced in a ratio of 2:1, syngas would be produced, which could be converted to methanol (Olah and Prakash, 2010).

Electrode materials such as thallium, mercury, lead, cadmium, indium and tin are able to electro-reduce carbon dioxide at high current efficiencies, but are not good catalysts due to the fact that the primary product is formic acid, in which the carbon-oxygen bond remains unbroken (Jitaru et al., 1997). In methanol, lead and mercury have been shown to lead to oxalate production (Eggins et al., 1997). Silver, zinc and gold can also produce carbon monoxide at relatively high current efficiencies; Azuma et al. (1990) recorded current efficiencies of 40.7 %, 9.8 % and 16.9 % for these three metals respectively.

Copper is also capable of electro-reducing carbon dioxide to carbon monoxide at relatively high current efficiencies; however, it can also convert carbon monoxide into more reduced species, including methane, ethane, alcohols and aldehydes (Gattrell et al., 2006). Hori et al. (1986) were able to electro-reduce carbon dioxide to methane at current efficiencies up to 65 % in bicarbonate solutions – although the overpotential necessary for this was rather large (1.5 V). The principal reactions occurring during the electro-reduction of carbon dioxide at a copper electrode are as follows (Gattrell et al., 2006):

$$2H^+ + 2e^- \rightarrow H_2 \quad (1.1)$$

$$2CO_2 + 12H^+ + 12e^- \rightarrow C_2H_4 + 4H_2O \quad (1.2)$$

$$CO_2 + 8H^+ + 8e^- \rightarrow CH_4 + 2H_2O \quad (1.3)$$

$$CO_2 + 2H^+ + 2e^- \rightarrow CO + H_2O \quad (1.4)$$

$$CO_2 + H^+ + 2e^- \rightarrow HCOO^- \quad (1.5)$$

Thus, it is evident that quite a range of different products can be produced during electro-reduction at a copper electrode.

Besides the electrode material, the product composition obtained from the electro-reduction of carbon dioxide can be affected by the electrolyte medium. For example, the pH of the electrolyte can influence the current efficiencies obtained. Whipple et al. (2010) used a 5 mol/dm^3 KCl electrolyte and investigated electro-reduction at pH values of 4, 7 and 10. They

found that lowering the pH improved the reaction kinetics and current efficiencies for the formation of formic acid.

Hara et al. (1995) investigated the effect of pressure on the electro-reduction of carbon dioxide at 1 atm and 30 atm pressure, in a 0.1 mol/dm^3 $KHCO_3$ solution at various working electrode materials. They found that using Group 8-10 metals, such as rhodium, palladium, platinum, nickel, cobalt and iron, led to the production of formic acid and/or carbon monoxide at 30 atm pressure, whilst at 1 atm pressure the principal product was hydrogen from the electrolysis of water.

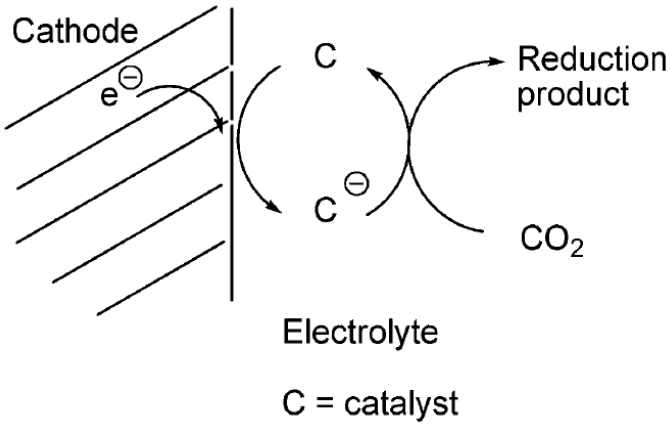

Figure 1.2: Schematic illustration of the catalysed electro-reduction of carbon dioxide (from Mikkelsen et al., 2009).

Rather than focusing on changing the operating conditions of electrolysis, a substantial amount of research effort has recently been expended on finding suitable catalysts for the electro-reduction of carbon dioxide. Large overpotentials are required to directly reduce carbon dioxide on most electrode surfaces, which leads to lower conversion efficiencies as a result. Therefore, electrocatalysts can be utilised to decrease the overpotential, improve reaction kinetics and enhance selectivity (Mikkelsen et al., 2009). Figure 1.2 shows a schematic illustration of the catalysed electro-reduction of carbon dioxide.

Three types of homogeneous catalyst that have been studied in the literature are: metal complexes with macrocyclic ligands (Bhugun et al., 1996), metal complexes with bipyridine

ligands (Hawecker et al., 1984) and transition metal phosphine complexes (Raebiger et al., 2006). An example of the first type are Ni(II) cyclam complexes, which can catalyse the reduction of carbon dioxide to carbon monoxide and are able to attain current efficiencies of up to 96 % at -0.86 V vs. SCE (the standard calomel electrode) in aqueous solution (Beley et al., 1986). An example of the second type are Re(bpy) $(CO)_3Cl$ complexes, which can also selectively catalyse the electro-reduction of carbon dioxide to carbon monoxide, yielding current efficiencies up to 98 %. However, this particular catalyst suffers from two limitations. Firstly, increasing the amount of water in the electrolyte causes the selectivity for carbon monoxide to decrease. Secondly, the electro-reduction has a low turnover frequency of 21.4 h^{-1} (Hawecker et al., 1984). Considering the third type of catalyst, a representative example are $[Pd(triphosphine)(CH_3CN)]^{2+}$ complexes, which can lead to the formation of carbon monoxide at current efficiencies over 90 %. Two limitations of this catalyst are its decomposition to Pd(I) dimers and hydrides, which eventually terminates its catalytic activity, and low turnover numbers between 10 and 100 (Raebiger et al., 2006).

1.1.2 Limitations

In order for the electrochemical reduction of carbon dioxide to be feasible, it must satisfy two principal criteria (Whipple and Kenis, 2010): high energy efficiency and high reaction rates[1]. Regarding the electro-reduction of carbon dioxide in solution, Whipple and Kenis (2010) considered that "current research efforts in the electrochemical conversion of CO_2 have achieved moderate efficiencies and reasonably high current densities, although not at the same time." For instance, many researchers obtained current efficiencies that were typically greater than 90 % for formic acid and carbon monoxide production, but at the expense of high overpotentials, hence limiting the energy efficiency attained (Whipple and Kenis, 2010).

From the brief overview given in Section 1.1.1, a number of other limitations are apparent in the electro-reduction of carbon dioxide in solution. Firstly, the process can produce quite a wide range of products, but cannot produce pure carbon. For example, Azuma et al. (1990)

[1] A higher current density is indicative of a higher rate of reaction.

reported quite a wide range of different reduction products: CH_4, C_2H_4, C_2H_6, C_3H_6, C_3H_8, CO, HCOOH and H_2. Evidently, separating products that exist in the same phase would increase the overall cost of using the process to generate valuable products. However, if hydrogen and carbon monoxide were the only products of the process then they could be used as syngas if produced in the correct 2:1 ratio (Olah and Prakash, 2010). Furthermore, the reaction rates that can be obtained from the process are limited by the relatively low temperatures used, which are imposed by the boiling points of the electrolytes. If high-temperature electrolytes like molten salts were used, it may be possible to significantly increase the rate of electro-reduction of carbon dioxide (Kaplan et al. 2010).

1.2 Production of Solid Carbon from Carbon Dioxide via Molten Carbonate Electrolysis

One alternative way of converting carbon dioxide to a useful product is to convert it to solid carbon via molten alkali metal carbonate electrolysis. In this process, the multiple product and separation issues mentioned in Section 1.1.2 do not arise because the main product is solid carbon.

The process for electro-depositing carbon from carbonate ions was first proposed in the 1960s (Delimarskii et al., 1964), but comparatively few workers in the literature have considered using carbon dioxide as the carbon source. Figure 1.3 gives a simplified illustration of the process and the laboratory-scale molten salt reactor that was utilised in this PhD.

During electrolysis, carbonate ions are electro-reduced to solid carbon and oxide ions at the cathode (Le Van et al., 2009):

$$CO_3^{2-} + 4e^- \rightarrow C + 3O^{2-} \qquad (1.6)$$

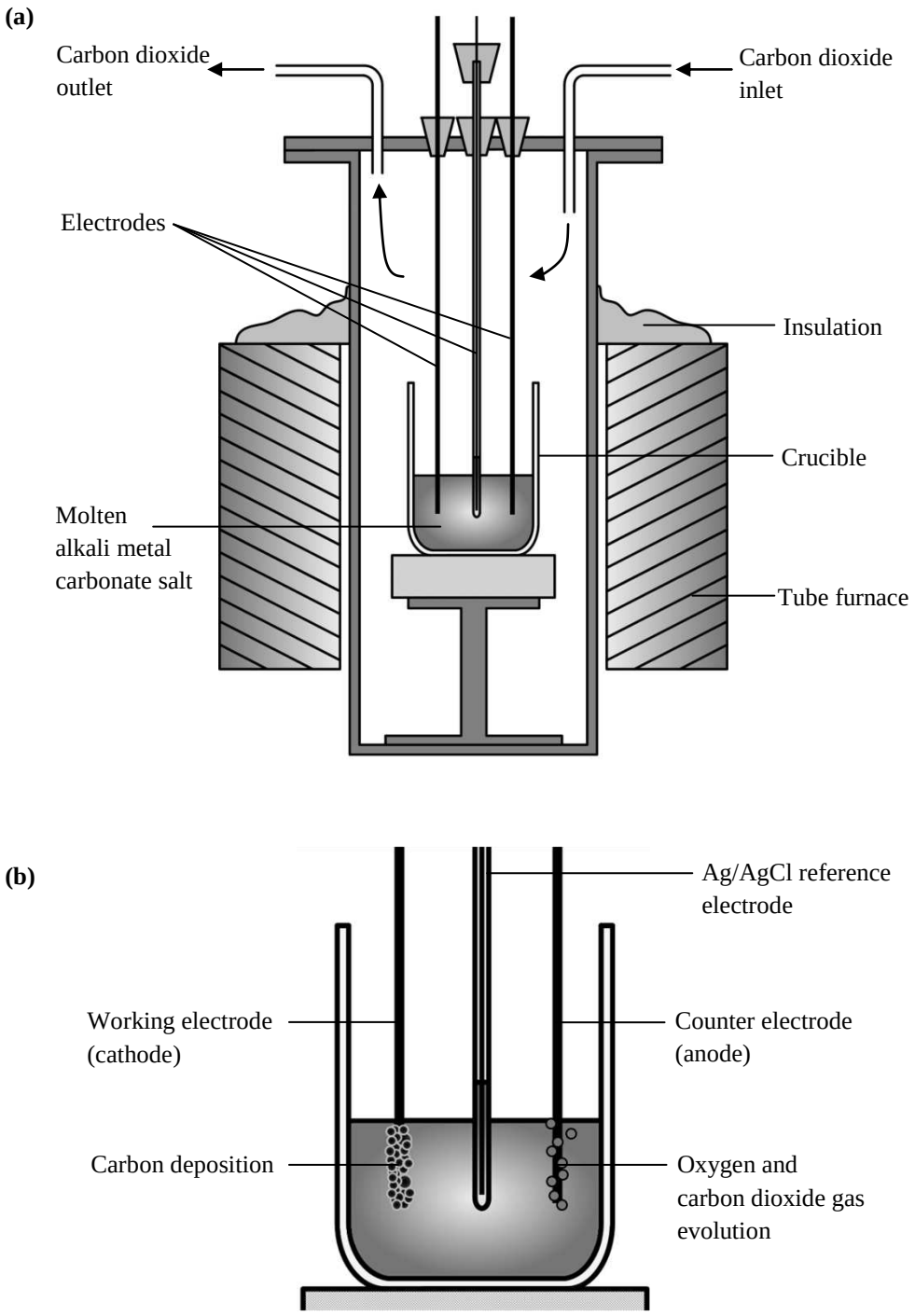

Figure 1.3: The laboratory-scale conversion of carbon dioxide to solid carbon via molten carbonate electrolysis. (a) Simplified view of the molten salt reactor, showing its key features. (b) Close-up view of the crucible containing the molten carbonate electrolyte, showing the electrode processes that take place during electrolysis.

The oxide ions produced can react with carbon dioxide from the reactor atmosphere to regenerate the carbonate ions (Kawamura and Ito, 2000):

$$CO_2 + O^{2-} \rightleftharpoons CO_3^{2-} \quad (1.7)$$

At the anode, two reactions can occur: the oxidation of oxide ions and/or the oxidation of carbonate ions (Lorenz and Janz, 1970):

$$O^{2-} \rightarrow \tfrac{1}{2}O_2 + 2e^- \quad (1.8)$$

$$CO_3^{2-} \rightarrow CO_2 + \tfrac{1}{2}O_2 + 2e^- \quad (1.9)$$

The evidence for Reactions 1.6 to 1.9, and the details of the process conditions used, are considered in Chapter 2 of this thesis. The overall reactions for carbonate ion electro-reduction can be written as follows for anodic Reactions 1.8 and 1.9 respectively, taking the lithium ion to be the cation:

$$Li_2CO_3 \rightarrow Li_2O + O_2 + C \quad (1.10)$$

$$3Li_2CO_3 \rightarrow 3Li_2O + 2CO_2 + O_2 + C \quad (1.11)$$

Note that even though two moles of carbon dioxide are produced in Reaction 1.11, three moles of lithium oxide are also produced. As a result, two moles of lithium oxide can react with the carbon dioxide from the anodic off-gases, whilst the third mole of lithium oxide can react with carbon dioxide from the reactor atmosphere. Therefore, when Reactions 1.10 and 1.11 take place under a carbon dioxide atmosphere, the net reaction is the conversion of carbon dioxide to solid carbon, since carbon dioxide is used to regenerate any carbonate ions that are consumed:

$$CO_2 \rightarrow C + O_2 \quad (1.12)$$

Many workers in the literature have also found that the electro-deposited carbon produced from molten carbonates possesses many unique properties, which could make it a valuable and viable commercial product. In particular, the electro-deposited carbon can possess high specific surface areas. Le Van et al. (2009) achieved specific surface areas as high as 1315 m^2/g for carbon that was electro-deposited from a Li_2CO_3-Na_2CO_3-K_2CO_3 molten salt at 450 °C. Such high surface areas mean that the carbon is likely to perform favourably in electrochemical devices such as capacitors (Ito, 2011), and this has indeed been found. For example, when some electro-deposited carbon was tested in electrochemical capacitors, capacitances similar to activated carbon were attained without subjecting the electro-deposited carbon to activation treatments (Ijije, 2012). The electro-deposited carbon has also been tested as an anode material in lithium-ion batteries, where it has shown reversible capacities approximately three times higher than natural graphite (Groult et al., 2006).

Besides these promising electrochemical uses, the molten salt process also has good prospects in a number of other areas. For instance, the process can be used to carburise metals (Siambun et al., 2011a) in a way that is inherently much safer than the conventional carburisation process, which uses toxic molten cyanide baths (Davis, 2002). Furthermore, the process can also be used to coat metals with carbon (Kawamura and Ito, 2000). The conventional method for producing such carbon coatings is via chemical vapour deposition, which requires temperatures of around 1500 °C (Chen et al., 2010). The present molten salt process only requires temperatures between 400 and 850 °C.

Energy storage is another potential use of the molten salt process. Since electrical energy is used to produce carbon from carbon dioxide, the electro-deposited carbon acts as a store of that energy. This energy could be released by burning or by using the carbon as a fuel in a direct carbon fuel cell. Two recently proposed variants of the molten salt process involve using solar energy to provide the electricity and part of the heating requirements of the process (Chen et al., 2009; Licht et al., 2010).

1.3 Topics Needing Further Study

Chapter 2 reviews what is known in the literature concerning carbon electro-deposition in molten carbonates. Although the production of carbon from molten carbonates has been studied by a number of workers, there are still many areas where our knowledge of the process is lacking. Firstly, the fundamental reactions occurring in the system have not been subjected to a thoroughly rigorous investigation. Some workers have conducted limited studies of specific electrolytes using cyclic voltammetry, but no thorough study of several electrolyte compositions under similar conditions has been carried out.

Secondly, there is a paucity of results in the literature regarding the production rates and current efficiencies of carbon deposition. This issue must be addressed if commercialisation of the process is ever to be achieved. In addition, such results are essential for determining the energy efficiency of the process. Le Van et al. (2009) carried out a comprehensive study on the effects of several process conditions on the properties of electro-deposited carbon, for a ternary Li_2CO_3-Na_2CO_3-K_2CO_3 molten salt, but no worker has directly compared the carbon deposits produced from different carbonate electrolyte compositions.

Thirdly, Ingram et al. (1966) are the only workers to have ever studied the electrochemical re-oxidation of electro-deposited carbon in molten carbonates, but their study only considered a relatively narrow set of conditions. Further investigations are required in order to determine if electro-deposition/re-oxidation of carbon is a viable method of energy storage. These investigations would also shed more light on the nature of carbon oxidation reactions in the molten salt process.

This research aims to help address the issues raised above through the findings of the following investigations:

- A comprehensive study of the cyclic voltammetry of various alkali metal carbonate electrolytes, considering the effects of temperature, electrolyte composition and electrode material.

- Studies of carbon electro-deposition at different temperatures from several alkali metal carbonate electrolytes, collecting data to determine production rates and current efficiencies.
- A study of the properties of the electro-deposited carbon.
- Analyses of the re-oxidation of the electro-deposited carbon, focussing on the effects of temperature, electrolyte composition, and re-oxidation current.

Thus, the principal aim of this research is to improve our fundamental understanding of carbon electro-deposition and its re-oxidation in molten carbonates.

1.4 Scope of this Thesis

Chapter 1 introduces the research topic. This chapter gives the background to the research, as well as a brief summary of the key features of the production of carbon from carbon dioxide via molten carbonate electrolysis. The aims of the research and the scope of this thesis are also defined.

The literature on the subject of carbon electro-deposition, from carbon dioxide and/or carbonate ions in molten salts, is reviewed in Chapter 2.

In Chapter 3, the methodologies used to conduct the research and experiments considered in this thesis are described. Some justification for experimental design is also given.

A detailed study of carbon electro-deposition and re-oxidation reactions is presented in Chapter 4. This chapter focuses on the cyclic voltammetry of the Li_2CO_3-Na_2CO_3 electrolyte at a platinum working electrode. The results are interpreted and compared with the literature, and their implications for carbon deposition are discussed.

In Chapter 5, the effect of cations present in molten carbonate electrolytes on the electro-deposition and re-oxidation of carbon is considered. The cyclic voltammetry of the Li_2CO_3-

K_2CO_3 electrolyte is presented and compared with the voltammetry of the Li_2CO_3-Na_2CO_3 electrolyte, which was presented in Chapter 4.

Chapter 6 complements Chapters 4 and 5 in that it contains the results of a comparative study of the cyclic voltammetry of four alkali metal carbonate electrolytes at stainless steel working electrodes. The four electrolytes considered are: Li_2CO_3-Na_2CO_3, Li_2CO_3-K_2CO_3, Na_2CO_3 and K_2CO_3. As with Chapters 4 and 5, the findings are interpreted and compared with the literature.

The electro-deposition of carbon via potentiostatic electrolysis is considered in Chapter 7. The rates and current efficiencies of carbon deposition are given in this chapter, along with several analyses of the properties of the electro-deposited carbon.

Chapter 8 considers the electrochemical re-oxidation of electro-deposited carbon in molten carbonates. The effects of changing process variables such as the temperature, electrolyte composition, deposition potential and discharge current are discussed.

A summary of the work presented in this thesis is provided in Chapter 9, focussing on the main conclusions. Suggestions for future work are also given.

CHAPTER 2

LITERATURE REVIEW

In this chapter, a critical review of the literature pertaining to carbon electro-deposition in molten salts is given, with particular emphasis on carbon electro-deposition via the electrolysis of carbonate ions. The direct electrochemical reduction of carbon dioxide to carbon will be discussed first in Section 2.1, before discussing the mechanisms for the indirect conversion of carbon dioxide to carbon via molten carbonate electrolysis in Section 2.2. The reactions that have been reported to occur in molten carbonate electrolytes, along with the effects of process conditions, are also considered. Finally, the properties of electro-deposited carbon are described, followed by a brief discussion of the potential uses of such carbon.

2.1 Mechanisms for the Direct Reduction of Carbon Dioxide to Carbon

In direct electrochemical reduction, carbon dioxide simply dissolves in the molten salt electrolyte and is reduced at the cathode to elemental carbon (Delimarskii et al. 1975). Delimarskii et al. (1968) considered that direct electrochemical reduction to carbon occurred according to a single-step reaction:

$$CO_2 + 4e^- \rightarrow C + 2O^{2-} \qquad (2.1)$$

However, Novoselova et al. (2003; 2007; 2008a; 2008b) postulated that direct electrochemical reduction to produce carbon proceeded via a three-stage electrochemical-chemical-electrochemical (ECE) mechanism, which involved a hypothetical CO_2^{2-} ion whose existence has been suggested by Borucka (1977). The mechanism is as follows (Novoselova et al., 2003):

Quasi-reversible reduction of carbon dioxide to the hypothetical CO_2^{2-} ion:

$$CO_2 + 2e^- \rightleftharpoons CO_2^{2-} \qquad (2.2)$$

Chemical formation of carbon monoxide:

$$CO_2^{2-} \rightarrow CO + O^{2-} \qquad (2.3)$$

Irreversible electro-reduction of carbon monoxide to carbon:

$$CO + 2e^- \rightarrow C + O^{2-} \quad (2.4)$$

The oxide ions produced in Reaction 2.4 were then said to react with carbon dioxide to produce carbonate, such that the overall cathodic reaction may be written as follows:

$$3CO_2 + 4e^- \rightarrow C + 2CO_3^{2-} \quad (2.5)$$

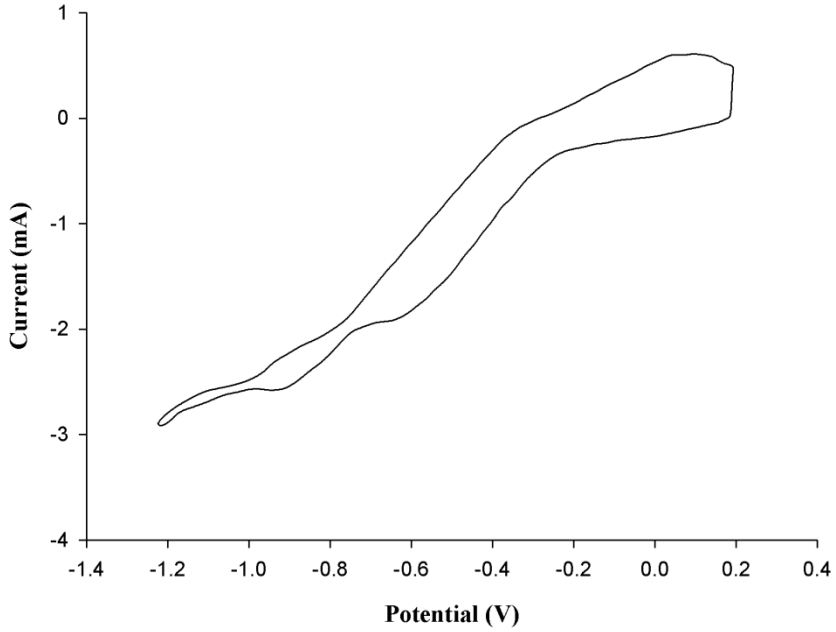

Figure 2.1: Cyclic voltammogram obtained at a gold working electrode using a NaCl-KCl melt (molar ratio of 1:1) at a temperature of 750 °C under a carbon dioxide pressure of 1.0 MPa. Counter electrode: glassy carbon or platinum crucible; reference electrode: platinum quasi-reference electrode; scan rate: 0.1 V/s. Figure re-plotted from Novoselova et al. (2008b).

Novoselova et al. (2003; 2007; 2008a; 2008b) considered that this mechanism was correct due to the occurrence of two cathodic waves in cyclic voltammograms conducted at gold and platinum working electrodes, in a NaCl-KCl molten salt at a temperature of 750 °C under a carbon dioxide pressure of 1.0 MPa. Figure 2.1 shows a cyclic voltammogram obtained at a gold working electrode. Furthermore, this mechanism was supported by the fact that Novoselova et al. (2003) could not obtain carbonaceous deposits at potentials that were less

negative than the second cathodic peak potential, which is the peak at a potential of around -0.9 V vs. Pt in Figure 2.1.

However, one issue that was not raised by Novoselova et al. (2003; 2007; 2008a; 2008b) is that chloride molten salts may contain non-negligible amounts of oxide ions due to their inherently hygroscopic nature. These oxide ions could help to absorb carbon dioxide by forming carbonate ions, which could in turn be electro-reduced to carbon via the mechanisms given in Section 2.2. As consequence, the mechanism for the electrochemical conversion of carbon dioxide to carbon in molten chlorides is likely to be more complicated than that proposed by Novoselova et al. (2003; 2007; 2008a; 2008b). Another issue with the work of Novoselova et al. (2003; 2007; 2008a; 2008b) is that they used a pseudo-reference electrode, which makes it difficult to identify the electrochemical reactions occurring in the system.

The fact that Novoselova et al. (2003; 2007; 2008a; 2008b) were able to obtain carbon deposits from a pure chloride molten salt shows that the direct reduction of dissolved carbon dioxide can occur in molten chloride salts. Apart from early papers such as that of Delimarskii et al. (1968) and the works of Novoselova et al. (2003; 2007; 2008a; 2008b), most authors in the literature did not report that carbon deposition occurred via the direct electro-reduction of carbon dioxide.

2.2 Mechanisms for the Conversion of Carbon Dioxide to Carbon via Carbonate Electrolysis

Electrolysis cells that can be used to reduce alkali or alkali earth metal carbonates to carbon can be used to indirectly reduce carbon dioxide (Ingram et al., 1966). This is possible due to the following equilibrium, using the example of Li_2CO_3:

$$Li_2CO_3 \rightleftharpoons Li_2O + CO_2 \qquad (2.6)$$

All of the suggested mechanisms for the electro-reduction of carbonate ions lead to the production of oxide ions as well as carbon (Deanhardt et al., 1986; Ito et al., 1992; Le Van et al, 2009). Thus, as carbonates are electro-reduced to carbon and their respective oxides, carbon dioxide can then react with the oxides as per the reverse reaction of Reaction 2.6, producing more carbonates that can be electro-reduced (Kawamura and Ito, 2000).

Three principal mechanisms for the reduction of carbonate ions to carbon have been suggested. Note that many studies of the electrochemical reduction of carbonate ions did not consider or use carbon dioxide as an indirect carbon source, although these studies are still very relevant, as carbonate ion reduction to carbon can occur regardless of whether an atmosphere containing carbon dioxide is used or not (Ingram et al., 1966).

Firstly, it has been suggested that carbonate ions can be electro-reduced to carbon in a single-step reaction (Ingram et al., 1966):

$$CO_3^{2-} + 4e^- \rightarrow C + 3O^{2-} \quad (2.7)$$

The carbonate ions could alternatively be electro-reduced in a two-step reaction (Ito et al., 1992); note again the presence of the hypothetical CO_2^{2-} ion suggested by Borucka (1977):

$$CO_3^{2-} + 2e^- \rightarrow CO_2^{2-} + O^{2-} \quad (2.8)$$

$$CO_2^{2-} + 2e^- \rightarrow C + 2O^{2-} \quad (2.9)$$

The third possible mechanism involves the reduction of metal ions to metal, followed by the reaction of the reduced metal with metal carbonate (Deanhardt et al., 1986):

$$M^+ + e^- \rightarrow M \quad (2.10)$$

$$4M + M_2CO_3 \rightarrow C + 3M_2O \quad (2.11)$$

Most evidence presented in the literature appears to support the first carbonate ion reduction mechanism, given by Reaction 2.7.

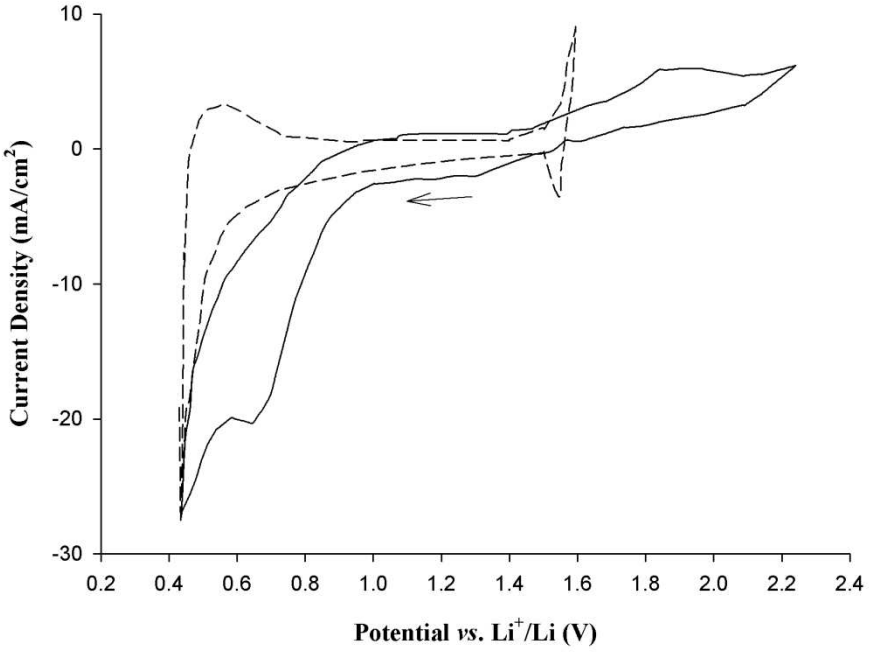

Figure 2.2: Cyclic voltammograms obtained from a molten binary eutectic mixture of LiCl-KCl (dashed line) and a molten mixture of LiCl-KCl containing 1.0 mol % of K_2CO_3 (solid line). Temperature: 450 °C; scan rate: 0.05 V/s; working electrode: aluminium; counter electrode: glassy carbon; reference electrode: Ag/AgCl calibrated with reference to a lithium-coated nickel dynamic reference electrode; atmosphere: Ar. Figure re-plotted from Kawamura and Ito (2000).

Kawamura and Ito (2000) studied the electro-deposition of carbon onto an aluminium working electrode in a LiCl-KCl-K_2CO_3 melt (molar ratio of 57.9:41.1:1.0), at a temperature of 450 °C under an argon atmosphere. Figure 2.2 shows the cyclic voltammograms that they obtained from a molten eutectic mixture of LiCl-KCl (molar ratio of 58.5:41.5) and the LiCl-KCl-K_2CO_3 melt. An obvious difference between the two cyclic voltammograms is that there is a very clear cathodic reduction peak at around 0.7 V vs. Li^+/Li for the melt containing K_2CO_3, which was attributed to the reduction of carbonate ions to carbon via Reaction 2.7. This was confirmed when carbon deposits were obtained at potentials in the range of 0.60 V to 1.00 V,

but not at potentials more positive than 1.10 V. Note that the cathodic limit in this case was ascribed to the formation of a Li-Al alloy (Kawamura and Ito, 2000).

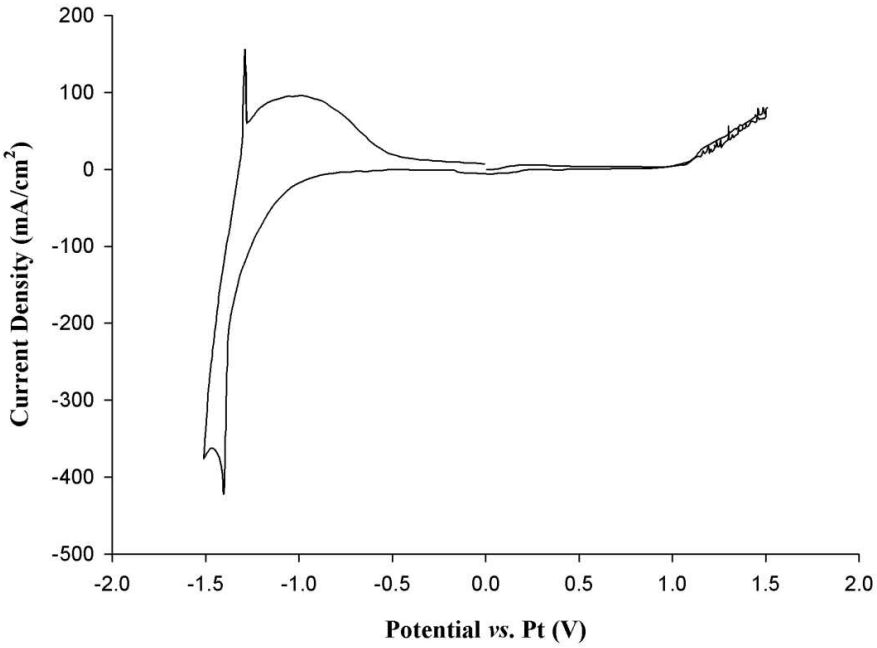

Figure 2.3: Cyclic voltammogram obtained from a LiF-NaF eutectic mixture containing 2% by mass of Na_2CO_3. Working electrode: gold; counter electrode: vitreous carbon; reference electrode: platinum quasi-reference electrode; scan rate: 100 mV/s; temperature: 800 °C; atmosphere: Ar. Figure re-plotted from Massot et al. (2002).

Massot et al. (2002) obtained a similar result to Kawamura and Ito (2000). A LiF-NaF-Na_2CO_3 molten salt (molar ratio of 59.6:39.8:0.6) was studied at temperatures of 700-800 °C under an argon atmosphere, using gold and copper working electrodes. Figure 2.3 shows a cyclic voltammogram obtained using a gold working electrode. The cathodic peak at approximately −1.38 V vs. Pt was shown to be due to the reduction of carbonate ions, as the current density of this peak increased in direct proportion with the concentration of carbonate ions.

The fact that both Massot et al. (2002) and Kawamura and Ito (2000) obtained single peaks for the reduction of carbonate ions seems to imply that the reduction mechanism involved only one electrochemical step. However, one major limitation of the studies of Massot et al. (2002) and

Kawamura and Ito (2000) is that they used pseudo-reference electrodes, which can make identification of the electrode reactions problematic.

Note that even though oxide ions are produced at the cathode according to Reaction 2.7, oxygen evolution has not been reported there. For example, Kaplan et al. (2010) studied electrolysis in a Li_2CO_3-Na_2CO_3-K_2CO_3 eutectic mixture at temperatures between 500 and 800 °C, using a nickel cathode and a graphite anode. No cathodic gas evolution was reported at current densities between 0 and 2 A/cm^2. Thus any oxide ions produced must either react with carbon dioxide to form carbonate ions again (Kawamura and Ito, 2000) or the oxide ions are discharged at the anode as oxygen gas (Delimarskii et al., 1965). Note that if a graphite or transition metal anode is used, carbon dioxide (Barnett et al., 2009) or metal oxides may be formed from the oxide ions.

In summary, carbon deposits were claimed to have been produced via direct or indirect reduction of carbon dioxide. However, it is possible that carbon dioxide reduction could occur both directly and indirectly at the same time, provided that the process conditions used allow reduction via both routes at significant rates. Before considering the process conditions necessary for carbon deposition in greater detail, an overview of the principal anodic reactions will be given in the next section to complete the description of the main electrochemical reactions.

2.3 Principal Anodic Reactions

Irrespective of whether carbon was deposited directly from the reduction of carbon dioxide or indirectly via the reduction of carbonates, most authors considered that a significant anodic reaction occurring during carbon deposition was the oxidation of the carbonate ion, in accordance with the following reaction (Bartlett and Johnson, 1967; Novoselova et al., 2007; Le Van et al., 2009):

$$CO_3^{2-} \rightarrow CO_2 + \tfrac{1}{2}O_2 + 2e^- \qquad (2.12)$$

Reaction 2.12 is plausible, as the evolution of the oxidation products oxygen and carbon dioxide was observed at the anode by Delimarskii et al. (1965) during carbon deposition in an equimolar mixture of Li_2CO_3 and K_2CO_3 at temperatures between 580 °C and 600 °C. Chen et al. (2010) also observed vigorous bubbling at the anode during carbon deposition in a LiF-NaF-Na_2CO_3 molten salt (molar ratio: 59.3:39.5:1.26) at 700 °C, implying that some gas-releasing anodic reaction was occurring.

However, the work carried out by Lorenz and Janz (1970) has shown that Reaction 2.12 is not the only principal anodic reaction that can occur. Electrolysis was carried out in a molten eutectic mixture of Li_2CO_3-Na_2CO_3-K_2CO_3 (molar ratio of 43.5:31.5:25.0) at a temperature of 500 °C under an argon atmosphere (a carbon dioxide atmosphere was used when electrolysis was not taking place). Oxide ions produced during the carbon deposition reaction could be oxidised at the anode according to the following reaction (Lorenz and Janz, 1970):

$$O^{2-} \rightarrow \tfrac{1}{2}O_2 + 2e^- \qquad (2.13)$$

Results from gas chromatography showed that the ratio of carbon dioxide to oxygen in the anodic off-gases increased with increasing anode potential and current density (Lorenz and Janz, 1970), as shown in Figures 2.4(a) and 2.4(b). This implies that Reaction 2.12 became more dominant at higher potentials and current densities.

Similar observations to Lorenz and Janz (1970) were made by Delimarksii et al. (1969), also using a platinum working electrode, but for a Li_2CO_3-K_2CO_3 melt at temperatures between 500-580 °C. Delimarskii et al. (1969) observed greater current efficiencies for anodic oxygen evolution at current densities lower than 30 mA/cm^2.

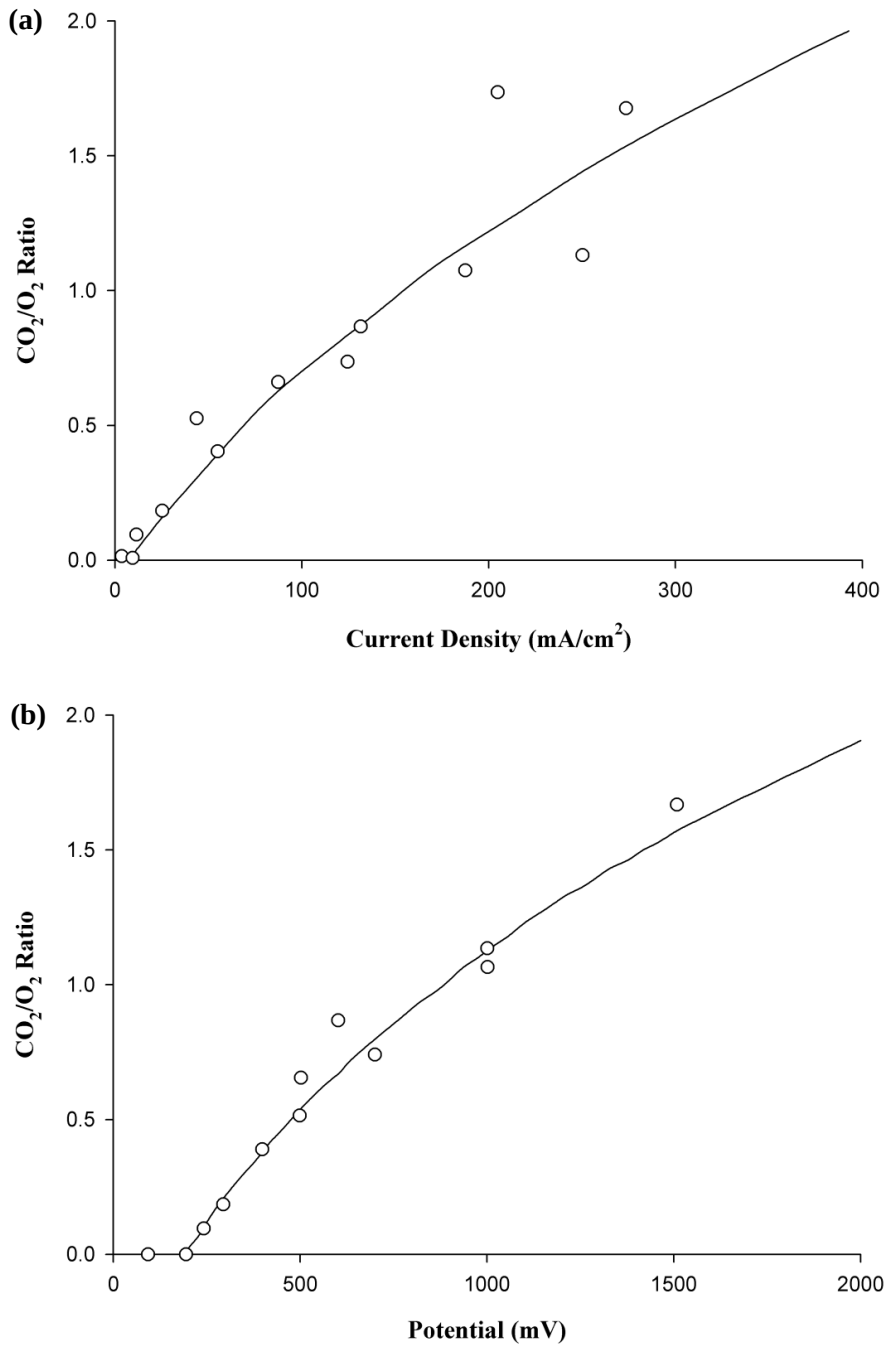

Figure 2.4: CO_2/O_2 ratio in the anodic off-gases versus (a) current density and (b) anodic potential used in electrolysis. Molten salt: Li_2CO_3-Na_2CO_3-K_2CO_3 (molar ratio of 43.5:31.5:25.0); temperature: 500 °C; atmosphere during electrolysis: argon; working electrode: platinum; counter-electrode: 20 % palladium-80 % gold alloy crucible. Potentials are given versus a Pyrex membrane platinum reference electrode described in detail by Lorenz and Janz (1970). Re-plotted from Lorenz and Janz (1970).

Other anodic and cathodic reactions can also occur in the molten salt system; some of these will be discussed in Section 2.5. In the next section, the effect of process conditions on carbon deposition will be considered.

2.4 Process Conditions

In the above sections, the effect of the process conditions on the anodic and cathodic reactions was not considered in order to clearly explain the principal reactions. However, the reactions that occur in a molten salt electrolysis cell are significantly influenced by the process conditions, such as the salt composition, pressure, atmosphere, temperature and electrode materials. Indeed carbon cannot be deposited under certain process conditions. In this section an overview of the effects of such process conditions is given.

Table 2.1 shows the conditions under which authors in the literature produced carbon, via either the direct reduction of carbon dioxide or the reduction of carbonates. From this table it is clear that, at atmospheric pressures of carbon dioxide, carbon was only deposited when carbonate ions were present, as well as either lithium ions or barium ions. Alternatively, carbon deposits could be obtained under high carbon dioxide pressures of at least 1.5 atm (gauge pressure). It would appear that lithium ions do not have to be present for the direct reduction of carbon dioxide.

Table 2.1: Experimental conditions from the literature under which carbon deposits were produced during electrolysis in molten salts. Note that certain rows have some blank entries due to information being unavailable (only the abstracts of some papers could be obtained).

Composition of Molten Salt (Molar Ratio in Brackets)	**Temperatures (°C)**	**Atmosphere**	**Absolute Pressures (atm)**	**Working Electrode/Cathode Materials**	**References**
Li_2CO_3	750	Ar or CO_2	1	Au, Au-20%Pd alloy, Pt, Ag, stainless steel	Ingram et al. (1966)
Li_2CO_3	780, 840	Ar	1	Graphite	Dimitrov (2009)
Li_2CO_3	750-900	CO_2	1	Pt, Ni, inconel (Ni alloy), monel (Ni alloy), Ti, C	Licht et al. (2010)
Li_2CO_3-Na_2CO_3 (53.3:46.7)	550	N_2	1	Pt	Bartlett and Johnson (1967)
Li_2CO_3-K_2CO_3 (1:1)	580-600			Pt, Au	Delimarskii et al. (1964 and 1965)
Li_2CO_3-K_2CO_3 (62:38)	600	CO_2	2.5-3.5		Delimarskii et al. (1970a)
Li_2CO_3-K_2CO_3 (62:38)	450				Delimarskii et al. (1970b)
Li_2CO_3-K_2CO_3	500	CO_2	4		Delimarskii et al. (1975)
Li_2O-Li_2CO_3 (7.1:92.9)	750				Smirnov et al. (1965)
Li_2CO_3-Na_2CO_3-K_2CO_3 (43.5:31.5:25.0)	600	CO_2	1	Au, Pt, Ag, Ni, Au-20%Pd alloy	Janz and Conte (1964a)
Li_2CO_3-Na_2CO_3-K_2CO_3 (43.5:31.5:25.0)	600, 750	Ar or CO_2	1	Au	Ingram et al. (1966)
Li_2CO_3-Na_2CO_3-K_2CO_3 (43.5:31.5:25.0)	500	Ar	1	Au	Lorenz and Janz (1970)

Composition of Molten Salt (Molar Ratio in Brackets)	Temperatures (°C)	Atmosphere	Absolute Pressures (atm)	Working Electrode/Cathode Materials	References
Li_2CO_3-Na_2CO_3-K_2CO_3 (43.5:31.5:25.0)	450	CO_2	1	Al, Pt, Cu, Ni, glassy carbon	Lantelme et al. (1999)
Li_2CO_3-Na_2CO_3-K_2CO_3 (43.5:31.5:25.0)	450	CO_2	1	Ni, glassy carbon	Kaplan et al. (2002)
Li_2CO_3-Na_2CO_3-K_2CO_3 (43.5:31.5:25.0)	450-700	CO_2	1	Ni, vitreous carbon	Le Van et al. (2009)
Li_2CO_3-Na_2CO_3-K_2CO_3 (43.5:31.5:25.0)	500-800	CO_2	1	Ni	Kaplan et al. (2010)
NaCl-KCl	680	CO_2	2.5		Delimarskii et al. (1968)
NaCl-KCl (1:1)	700-800	CO_2	10.9-16.0		Kushkhov et al. (1987)
NaCl-KCl (1:1)	700-850	CO_2	17.8	Pt	Novoselova et al. (2003)
NaCl-KCl (1:1)	500-800	CO_2	15.8	Pt, Au	Novoselova et al. (2007)
NaCl-KCl (1:1)	750	CO_2	11	Pt, Au	Novoselova et al. (2008a)
NaCl-KCl-CsCl (30:24.5:45.5)	500-800	CO_2	15.8	Pt, Au	Novoselova et al. (2007)
NaCl-KCl-CsCl (30:24.5:45.5)	550	CO_2	15.8	Pt, Au	Novoselova et al. (2008a)
NaCl-KCl-CsCl (30:24.5:45.5)	550	CO_2	15.8	Glassy carbon, Pt	Novoselova et al. (2008b)
Li_2CO_3-LiCl	700	Ar	1	Mo	Dimitrov (2009)

Composition of Molten Salt (Molar Ratio in Brackets)	Temperatures (°C)	Atmosphere	Absolute Pressures (atm)	Working Electrode/Cathode Materials	References
Li_2CO_3-NaCl-KCl	680	No CO_2			Delimarskii et al. (1968)
Li_2CO_3-NaCl-KCl	700			Pt	Delimarskii et al. (1971)
K_2CO_3-LiCl-KCl (1.0:57.9:41.1)	450	Ar	1	Al	Kawamura and Ito (2000)
K_2CO_3-LiCl-KCl (1.0:57.9:41.1)	500	Ar	1	TiO	Song et al. (2012)
Na_2CO_3-K_2CO_3-KCl-$BaCO_3$	680				Delimarskii et al. (1968)
Na_2CO_3-K_2CO_3-KCl-Li_2CO_3	680				Delimarskii et al. (1968)
Na_2CO_3-K_2CO_3-KCl-Li_2CO_3	700				Delimarskii et al. (1970b)
LiF-NaF-Na_2CO_3 (59.6:39.8:0.6)	700-800	Ar, 80% Ar-20% CO_2	1	Au, Cu	Massot et al. (2002)
LiF-NaF-Na_2CO_3 (59.7:39.8:0.4)	670-750	Ar	1	Au	Massot et al. (2003)
LiF-NaF-Na_2CO_3 (59.3:39.5:1.26)	700	Ar	1	W, Pt	Chen et al. (2010)
LiF-KF-K_2CO_3	600	CO_2	9		Delimarskii et al. (1975)
LiF-NaF-KF-K_2CO_3 (45.1:11.2:40.8:2.9)	500, 750	He	1	Pt, Ni	Deanhardt et al. (1986)

The findings of Ingram et al. (1966) and Delimarskii et al. (1968) both corroborate well with these two observations. Ingram et al. (1966) deposited carbon from both Li_2CO_3 and Li_2CO_3-Na_2CO_3-K_2CO_3 melts at 750 °C using gold working electrodes under a carbon dioxide atmosphere, but no carbon could be obtained from a binary mixture of Na_2CO_3-K_2CO_3 (molar ratio of 58:42) under the same conditions. Similarly, Delimarskii et al. (1968) obtained carbon deposits from a NaCl-KCl-Li_2CO_3 mixture but could not obtain carbon deposits from a NaCl-KCl-K_2CO_3 mixture. However, if an equimolar mixture of NaCl-KCl was held under a carbon dioxide pressure of 1.5 atm at a temperature of 680 °C for 2 to 3 hours prior to electrolysis, carbon deposits were obtained. From these findings it may be inferred that the direct reduction of carbon dioxide to carbon only takes place at significant rates under relatively high carbon dioxide pressures of at least 1.5 atm, presumably because a sufficient quantity of carbon dioxide must be physically dissolved in the molten salt.

However, at a carbon dioxide pressure of 1.5 atm, carbon dioxide is unlikely to be dissolved in the molten chloride salt in substantial quantities. When Delimarskii et al. (1968) obtained carbon deposits from a NaCl-KCl molten salt held under carbon dioxide at 1.5 atm, it is plausible that carbon dioxide reacted with oxide ions present in the melt to form carbonate ions, which could in turn be electro-reduced to solid carbon. Oxide ions may have been present in the chloride electrolyte due to its hygroscopic nature, as was remarked in Section 2.1.

The activity of oxide ions in the molten salt is likely to have a significant effect on the electro-reduction of carbonate ions to carbon. If the activity of oxide ions is lower, the reduction of carbonate ions to carbon via Reaction 2.7 becomes easier in terms of both thermodynamics and kinetics. In addition, at higher pressures of carbon dioxide, it is likely that the equilibrium activity of oxide ions would be reduced, due to the reduced tendency for carbonate ions to thermally decompose. One other effect of a higher carbon dioxide pressure might be to discourage carbonate oxidation to carbon dioxide and oxygen at the anode via Reaction 2.12. This would encourage the direct discharge of oxide ions at the anode, forming oxygen and as a result reducing the activity of oxide ions in the electrolyte. Thus, it is likely that carbonate ion reduction to carbon becomes easier under higher carbon dioxide pressures, which also allows

the carbon deposition reaction to compete better with the cathodic reduction of alkali metal cations to alkali metal. This may be why Delimarskii et al. (1968) were able to obtain carbon deposits from NaCl-KCl held under a carbon dioxide pressure of 1.5 atm. Carbonate ions may have been formed and the high carbon dioxide pressure could have made their electro-reduction to carbon more favourable, allowing carbon deposition to compete better with alkali metal formation.

As was mentioned above, the reduction of carbonates to carbon seems to only take place when lithium or barium ions are present. Thermodynamic calculations can provide evidence that Li_2CO_3 reduction to carbon is more thermodynamically favourable than Na_2CO_3 or K_2CO_3 reduction to carbon, under certain conditions, but this does not explain why carbon has not been obtained from carbonate electrolytes lacking lithium ions. Two other possible cathodic reactions that can take place are the reduction of carbonate ions to carbon monoxide (Lorenz and Janz, 1970) and the reduction of alkali metal ions to alkali metal (Le Van et al., 2009). Thus, three principal cathodic reactions can occur, where M represents an alkali metal element (Le Van et al., 2009; Lorenz and Janz, 1970):

i) Metal ion reduction: $M^+ + e^- \rightarrow M$ (2.14)

ii) Carbonate ion reduction to carbon: $CO_3^{2-} + 4e^- \rightarrow C + 3O^{2-}$ (2.15)

iii) Carbonate ion reduction to CO: $CO_3^{2-} + 2e^- \rightarrow CO + 2O^{2-}$ (2.16)

For convenience, use the oxidation of the carbonate ion as the anodic reference reaction (Le Van et al., 2009):

$$2CO_3^{2-} \rightarrow 2CO_2 + O_2 + 4e^- \quad (2.17)$$

Therefore, when metal ion reduction occurs at the cathode, the overall reaction is (Le Van et al., 2009):

$$M_2CO_3 \rightarrow CO_2 + \tfrac{1}{2}O_2 + 2M \quad (2.18)$$

The standard Gibbs free energy of this reaction is given by (Le Van et al., 2009):

$$\Delta G^{o}_{M_2CO_3/M} = \Delta G^{o}_{CO_2} - \Delta G^{o}_{M_2CO_3} \quad (2.19)$$

Where: $\Delta G°_X$ = Standard Gibbs free energy change of formation of substance X.

As a result the standard potential of the cathode for metal reduction vs. CO_3^{2-}/CO_2-O_2 is (Le Van et al., 2009):

$$E^{o}_{M} = -\frac{\Delta G^{o}_{M_2CO_3/M}}{2F} \quad (2.20)$$

Where: $E°_M$ = standard potential for metal reduction and F = Faraday's constant (96.48 kC/mol).

Considering the reduction of carbonate ions to carbon, the overall reaction, its corresponding standard Gibbs free energy and the standard potential of the cathode are given by (Le Van et al., 2009):

$$3M_2CO_3 \rightarrow 3M_2O + 2CO_2 + O_2 + C \quad (2.21)$$

$$\Delta G^{o}_{M_2CO_3/C} = 3\Delta G^{o}_{M_2O} + 2\Delta G^{o}_{CO_2} - 3\Delta G^{o}_{M_2CO_3} \quad (2.22)$$

$$E^{o}_{C} = -\frac{\Delta G^{o}_{M_2CO_3/C}}{4F} \quad (2.23)$$

Where: $E°_C$ = standard potential for carbonate ion reduction to carbon.

However, if carbonate ions are reduced to carbon monoxide instead of carbon, the overall reaction, its corresponding standard Gibbs free energy and the standard potential of the cathode are given by:

$$2M_2CO_3 \rightarrow 2M_2O + CO_2 + \tfrac{1}{2}O_2 + CO \quad (2.24)$$

$$\Delta G^{o}_{M_2CO_3/CO} = 2\Delta G^{o}_{M_2O} + \Delta G^{o}_{CO_2} + \Delta G^{o}_{CO} - 2\Delta G^{o}_{M_2CO_3} \quad (2.25)$$

$$E^{o}_{CO} = -\frac{\Delta G^{o}_{M_2CO_3/CO}}{2F} \quad (2.26)$$

Where: $E°_{CO}$ = standard potential for carbonate ion reduction to carbon monoxide.

Table 2.2: Standard Gibbs free energy changes for the conversion of metal carbonate to pure metal, carbon or carbon monoxide, and their corresponding standard potentials vs. CO_3^{2-}/CO_2-O_2, for Li, Na and K carbonates at several different temperatures. Values of $\Delta G°_{M2CO3/M}$, $E°_M$, $\Delta G°_{M2CO3/C}$ and $E°_C$ were taken from Le Van et al. (2009), whilst the values of $\Delta G°_{M2CO3/CO}$ and $E°_{CO}$ were calculated by the present author using data from Chase (1998).

T (°C)	Metal, M	$\Delta G°_{M2CO3/M}$ (kJ/mol)	$E°_M$ (V)	$\Delta G°_{M2CO3/C}$ (kJ/mol)	$E°_C$ (V)	$\Delta G°_{M2CO3/CO}$ (kJ/mol)	$E°_{CO}$ (V)
450	Li	602.5	-3.12	687.4	-1.78	414.8	-2.15
	Na	522.6	-2.71	1007.2	-2.61	502.0	-2.60
	K	534.9	-2.77	1217.4	-3.15	768.0	-3.98
540	Li	581.3	-3.01	661.4	-1.71	388.4	-2.01
	Na	500.3	-2.59	978.1	-2.53	599.3	-3.11
	K	511.0	-2.65	1181.8	-3.06	735.1	-3.81
620	Li	562.5	-2.91	638.4	-1.65	365.9	-1.89
	Na	480.5	-2.49	952.1	-2.47	575.0	-2.98
	K	489.7	-2.54	1150.1	-2.98	706.7	-3.66
700	Li	543.6	-2.82	615.3	-1.59	344.6	-1.79
	Na	460.7	-2.39	926.2	-2.40	551.6	-2.86
	K	468.5	-2.43	1118.4	-2.90	679.9	-3.52

Table 2.2 gives some results for these thermodynamic calculations for Li_2CO_3, Na_2CO_3 and K_2CO_3 at four different temperatures. For Li_2CO_3, $E°_C$ is less negative than $E°_M$ at all of the temperatures given, whereas for Na_2CO_3 and K_2CO_3, $E°_M$ is the least negative potential. Thus these results support the observation made that carbon deposits can be obtained from molten salts containing lithium ions and carbonate ions. On the other hand, carbon deposits have not been obtained when lithium ions are not present, at least at carbon dioxide atmospheres below 1.5 atm, as metal ion reduction occurs instead. These calculations are therefore in agreement with the experimental observations made by Ingram et al. (1966) and Delimarskii et al. (1968).

As can be seen from Table 2.2, for Li_2CO_3, the $E°_{CO}$ values are less negative than the $E°_M$ values but are more negative than the $E°_C$ values; this implies that carbon production is more favourable than carbon monoxide formation at these temperatures. However, the results of

Lorenz and Janz (1970) have indicated that as the temperature increases the formation of carbon monoxide becomes increasingly favourable. This is shown in Figure 2.5, where the theoretical potential for the formation of carbon monoxide becomes less negative than that for carbon formation at temperatures exceeding approximately 870 °C. The experimental results of Lorenz and Janz (1970) agree well with their theoretical predictions.

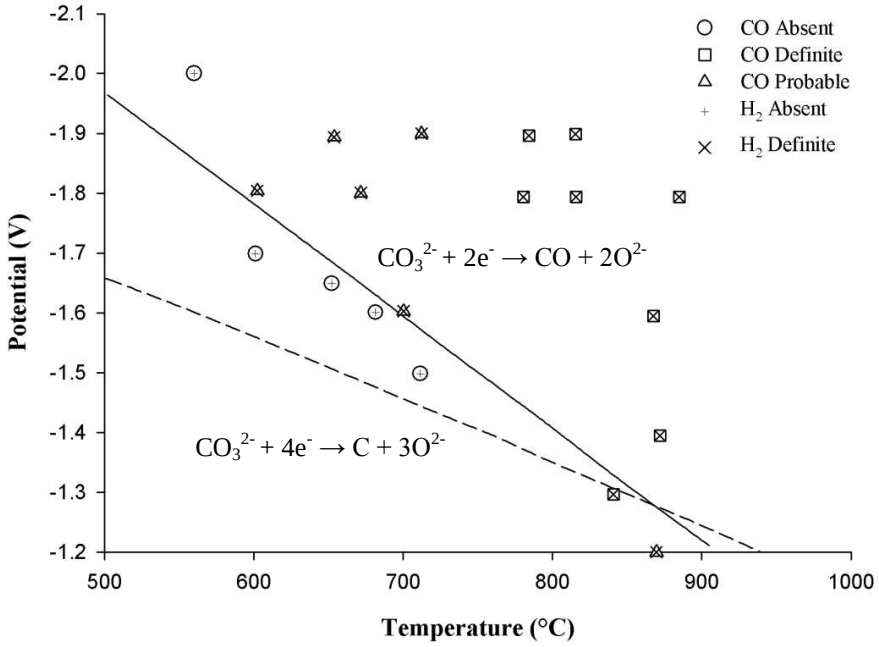

Figure 2.5: Potential versus temperature for a molten ternary eutectic mixture of Li_2CO_3-Na_2CO_3-K_2CO_3. The solid and dashed lines represent the theoretically calculated potentials for carbon monoxide and carbon production respectively. The points correspond to the gases observed to be produced from electrolysis at the cathode. Potentials are given versus a Pyrex membrane platinum reference electrode described in detail by Lorenz and Janz (1970). Figure re-plotted from Lorenz and Janz (1970).

Carbon monoxide formation has been observed to occur at the same time as carbon formation (Kaplan et al., 2010) and as a consequence would lead to a drop in the current efficiency of carbon formation. Since carbon monoxide formation is favourable at higher temperatures, it would appear that the best way to avoid it is to use lower temperatures (Delimarskii et al., 1975).

Several other factors aside from the electrochemical production of carbon monoxide would appear to affect the current efficiency of carbonate ion reduction to carbon. Ingram et al. (1966) conducted a study into the effect of temperature, atmosphere and voltage on the current efficiency of carbon deposition, the results of which are shown in Table 2.3.

Table 2.3: The effects of temperature, atmosphere and voltage on the current efficiency of carbon deposition. These results were obtained from electrolysis using a molten Li_2CO_3-Na_2CO_3-K_2CO_3 eutectic mixture; a gold cathode was used. Adapted from Ingram et al. (1966).

Temperature (°C)	**Atmosphere**	**Voltage (V)**	**Current (A)**	**Current Efficiency (%)**
600	Ar	-2.0	-0.005	0
600	Ar	-2.5	-0.0965	64
600	Ar	-2.6	-0.193	97
600	CO_2	-2.6	-0.193	67
750	Ar	-2.5	-0.193	55

The results presented in Table 2.3 clearly show that the current efficiency reduced when the temperature was raised from 600 °C to 750°C, under an argon atmosphere at constant current density (cf. rows 3 and 5). Ingram et al. (1966) attributed this to the following reaction:

$$C + CO_2 \rightleftharpoons 2CO \qquad (2.27)$$

However, this drop in current efficiency could also have been due to the production of carbon monoxide via Reaction 2.24. When the atmosphere was changed from argon to carbon dioxide, at the same temperature and constant current density (cf. rows 3 and 4), the current efficiency also reduced, which was attributed to the reaction of carbon according to Reaction 2.27. Note that even though a carbon dioxide atmosphere appears to lead to a reduction in the current efficiency, it must still be used if indirect reduction of carbon dioxide is to occur continuously.

Table 2.3 also shows that the current efficiency increased at increasingly negative voltages and greater current densities, obviously with a concurrent increase in the input energy. Lantelme et al. (1999) made a similar observation from a Li_2CO_3-Na_2CO_3-K_2CO_3 melt under a carbon

dioxide atmosphere at 450 °C using a nickel working electrode. The current efficiency increased as the applied potential was made more negative, albeit Lantelme et al. (1999) also obtained current efficiencies in excess of 100% at potentials more negative than -1.9 V vs. CO_3^{2-}/CO_2-O_2. For example, at -2.30 V vs. CO_3^{2-}/CO_2-O_2 a current efficiency of 175% was obtained. There are two possible reasons for such high current efficiencies. Current efficiencies over 100% typically imply that electrochemical-chemical mechanisms (either EC or CE) are occurring (Le et al., 2011). Alternatively, Lantelme et al. (1999) may not have accurately determined the mass of carbon in their sample, as metal, oxide and carbonate impurities may have been present that were unaccounted for. Since no other current efficiency data exists in the literature for this system it is not possible to comment further on the reliability of these results here. However, it would appear that it is possible to obtain higher current efficiencies under a carbon dioxide atmosphere than the 67 % reported by Ingram et al. (1966).

The effects of salt composition, pressure, temperature, atmosphere and potential on carbon deposition in molten salts have now been described. The electrode materials used can also influence the reactions that take place – some aspects of this are considered in the next section on the voltammetry of molten carbonate electrolytes.

2.5 Voltammetry of Carbonate Molten Salts

Many of the reactions that can occur in the aforementioned molten salt electrolytes have been deduced using cyclic voltammetry, or the older technique linear sweep voltammetry. In this section the voltammetry of carbonate electrolytes is discussed for various working electrode materials. This section focuses on carbonate-only molten salts due to the fact that they were used as the electrolytes in the experimental studies of the present work.

2.5.1 Vitreous carbon and gold working electrodes – inert electrode materials

In the work of Ingram et al. (1966), gold was found to be an inert working electrode material in the carbonate salts studied: that is, only reactions associated with the carbonate electrolyte

components took place. Similarly, Le Van et al. (2009) found that vitreous carbon was an inert working electrode material. The justification for these observations will be given in more detail in the discussion that follows. The apparent fact that gold and vitreous carbon are inert materials makes them useful for studying the reactions taking place without complications arising from reactions involving the electrode materials themselves.

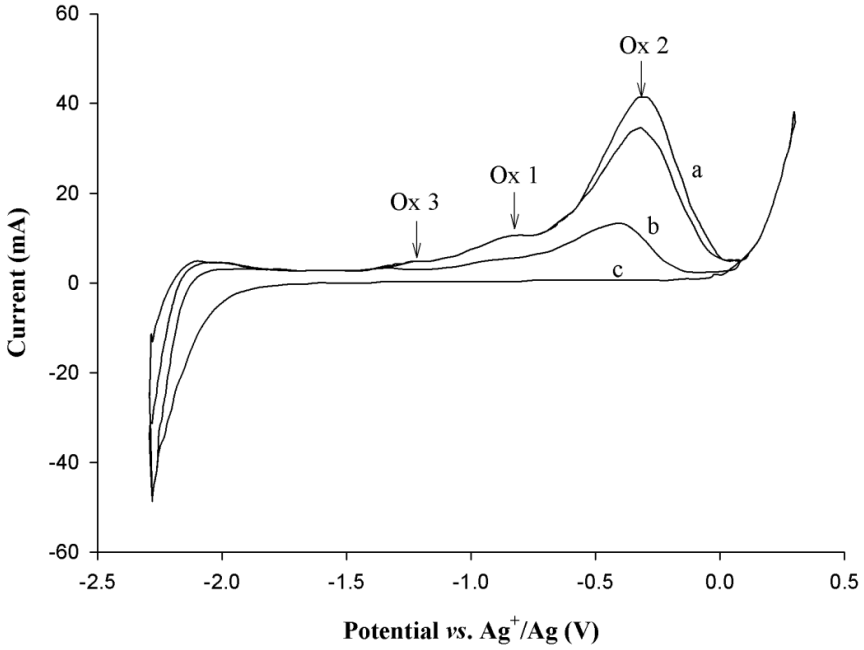

Figure 2.6: Cyclic voltammograms obtained using a vitreous carbon working electrode at 450 °C in a molten ternary eutectic mixture of Li_2CO_3-Na_2CO_3-K_2CO_3 (molar ratio of 43.5:31.5:25.0). Scan rate: 0.1 V/s; counter electrode: graphite; reference electrode: alumina tube containing Ag/Ag_2SO_4; atmosphere: 1 atm CO_2. The voltammograms labelled from (a) to (c) were obtained when the potential was held at -2.3 V vs. Ag^+/Ag for (a) 10 s, (b) 5 s and (c) 1 s. Re-plotted from Le Van et al. (2009).

Figure 2.6 shows the cyclic voltammograms obtained by Le Van et al. (2009) for a vitreous carbon working electrode in a ternary eutectic Li_2CO_3-Na_2CO_3-K_2CO_3 electrolyte (molar ratio of 43.5:31.5:25.0). Unlike Figures 2.2 and 2.3, which were obtained from chloride and halide-based melts respectively, Figure 2.6 was obtained from a carbonate-based melt, i.e. only carbonate ions were present in the added salts. Thus the carbonate ion reduction reaction to carbon (given by Reaction 2.7) was assigned to the cathodic limit in Figure 2.6 (Le Van et al.,

2009). This is reasonable since it should not be possible to deplete the diffusion layer around the electrode of carbonate ions in a pure carbonate molten salt. Furthermore, as shown by the data in Table 2.2, carbon formation via the reduction of Li_2CO_3 is the most thermodynamically favourable reaction that can occur in the ternary carbonate salt. The anodic limit on the other hand was attributed to the oxidation of carbonate ions via Reaction 2.12 (Le Van et al., 2009).

Lantelme et al. (1999) showed the vitreous carbon electrode to be inert, based on the absence of any reduction peaks between the anodic and cathodic limits. These observations were also made in the works of Kaplan et al. (2002) and Le Van et al. (2009). Furthermore, the absence of any cathodic peaks makes it less likely that the direct reduction of carbon dioxide was occurring under these conditions. If the direct reduction of carbon dioxide had occurred, at least one reduction peak might be expected in Figure 2.6.

Figure 2.6 shows two principal anodic peaks labelled Ox 1 and Ox 2, which were said to be due to oxidation of the electro-deposited carbon according to the following two reactions respectively (Le Van et al., 2009):

$$C + 2O^{2-} \rightarrow CO_2 + 4e^- \quad (2.28)$$

$$C + 2CO_3^{2-} \rightarrow 3CO_2 + 4e^- \quad (2.29)$$

The fact that these two anodic peaks increased in height when the potential was held at -2.3 V vs. Ag^+/Ag for several seconds implied that these peaks were indeed responsible for the oxidation of the carbon deposited at the cathodic limit (Le Van et al., 2009). However, no difference in the height of Ox 1 was observed when the potential was held at -2.3 V vs. Ag^+/Ag for 5 s and 10 s. This was attributed to oxide ions leaving the bulk of the deposit by diffusing into the electrolyte (Le Van et al., 2009). Such an inference may be reasonable, as the activity of oxide ions at or near the electrode remains approximately constant under potential control according to the Nernst equation.

The anodic peak labelled Ox 3 was assigned to the oxidation of lithium carbide, Li_2C_2. Li_2C_2 was considered to be formed according to the following cathodic reaction (Le Van et al., 2009):

$$2Li^+ + 2CO_3^{2-} + 10e^- \rightarrow 6O^{2-} + Li_2C_2 \qquad (2.30)$$

According to the thermodynamic calculations carried out by Le Van et al. (2009), the calculated standard potentials vs. CO_3^{2-}/CO_2-O_2 for the formation of Li_2C_2 and carbon from Li_2CO_3 at 450 °C are -2.00 V and -1.78 V respectively. Since the standard potential for Li_2C_2 formation is relatively close to that for carbon formation, it was considered to be likely that Li_2C_2 formation occurred. Li_2C_2 would probably react with water to form other products during the washing process used by Le Van et al. (2009), hence explaining why no Li_2C_2 was detected in the X-ray diffraction (XRD) studies that they carried out.

As the cathodic limit was made more negative, the height of the anodic peak Ox 3 increased (Le Van et al., 2009), which was presumed to be as a consequence of increased Li_2C_2 production. Le Van et al. (2009) therefore took this observation to be evidence for the Ox 3 peak being due to Li_2C_2 oxidation.

There is also a fourth anodic peak in Figure 2.6 at ca. -2.2 V vs. Ag^+/Ag that Le Van et al. (2009) entirely neglected to discuss. This peak is significant, as it is at least as high as the peak labelled Ox 3. However, this peak was not observed in other cyclic voltammograms presented by Le Van et al. (2009), which may be why no explanation was attempted. Based on the position of the peak, it could be due to the re-oxidation of alkali metal back to alkali metal ions.

Based on the holding and negative potential limit studies carried out by Le Van et al. (2009), it seems likely that Ox 1 and Ox 2 were associated with the re-oxidation of electro-deposited carbon (Le Van et al., 2009). The supposition that Li_2C_2 was formed is also quite reasonable: both Lantelme et al. (1999) and Song et al. (2012) detected it in their unwashed electro-deposited carbon. However, no other evidence was presented for the attribution of the anodic peaks to specific reactions.

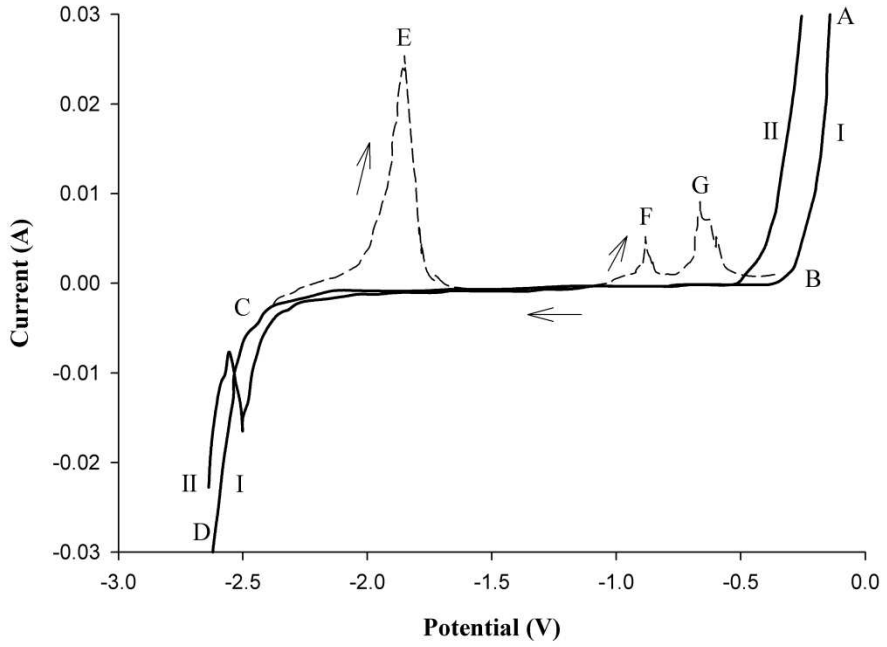

Figure 2.7: Linear sweep voltammograms obtained from a molten ternary eutectic mixture of Li_2CO_3-Na_2CO_3-K_2CO_3 (molar ratio of 43.5:31.5:25.0) at a temperature of 600 °C. The lines denoted by the Roman numerals I and II correspond to the results obtained under (I) a CO_2 atmosphere and (II) an Ar atmosphere respectively. The solid line represents the cathodic sweep whilst the dashed line corresponds to the anodic sweep (carried out after the cathodic sweep). WE: gold; CE: gold-palladium crucible; RE: Danner-Rey RE; scan rate: 5 mV/s. Re-plotted from Ingram et al. (1966).

On the other hand, Ingram et al. (1966) conducted anodic stripping coulometry of electro-deposited carbon, in addition to linear sweep voltammetry. This gave them supporting evidence for the identification of anodic peaks in their linear sweep voltammograms. Figure 2.7 shows the linear sweep voltammograms obtained by Ingram et al. (1966) for a gold working electrode in a ternary eutectic Li_2CO_3-Na_2CO_3-K_2CO_3 electrolyte (molar ratio of 43.5:31.5:25.0), under carbon dioxide and argon atmospheres. Note that no fundamental difference in behaviour between the two atmospheres was observed. In addition, no cathodic peaks were observed between the anodic and cathodic limits, thus indicating that gold was inert in the molten salt. The cathodic limit was ascribed to the reduction of carbonate ions to carbon, as per Reaction 2.7, whilst the anodic limit was attributed to carbonate ion oxidation via

Reaction 2.12. With regards to the identification of the anodic and cathodic limits, both Ingram et al. (1966) and Le Van et al. (2009) draw the same conclusions. Ingram et al. (1966) confirmed that carbon deposition occurred at the cathodic limit by observing substantial carbon deposits at potentials beyond -2.5 V vs. the Danner-Rey reference electrode.

Ingram et al. (1966) did not attribute the peaks in the anodic sweep to specific reactions; they merely stated that the current wave C-E (in Figure 2.7) was due to the oxidation of the carbon deposit. The anodic peaks F and G were said to correspond to the removal of the final traces of carbon on the electrode. These peak attributions seem to corroborate well with their anodic stripping coulometry results, which shall now be considered, before continuing the present discussion on cyclic/linear sweep voltammetry.

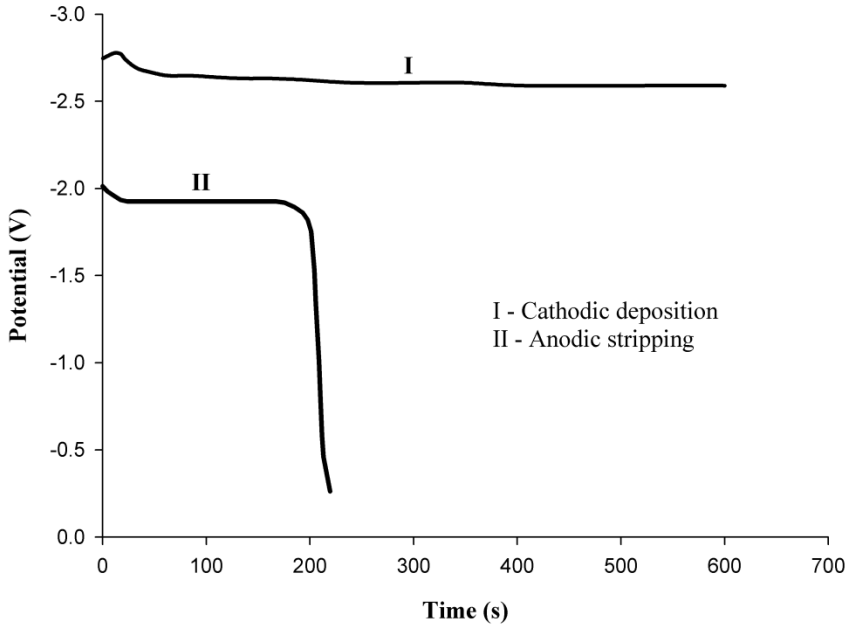

Figure 2.8: Chronopotentiograms for the electro-deposition and anodic stripping of carbon in a ternary eutectic mixture of Li_2CO_3-Na_2CO_3-K_2CO_3 (molar ratio of 43.5:31.5:25.0) at a temperature of 600 °C. The line labelled I corresponds to the cathodic deposition of carbon at a constant cathodic current of 0.193 A. The line labelled II refers to the anodic stripping of the electro-deposited carbon at a constant anodic current of 0.193 A. WE: gold; CE: gold-palladium crucible; RE: Danner-Rey RE. Re-plotted from Ingram et al. (1966).

Figure 2.8 shows typical chronopotentiograms obtained by Ingram et al. (1966) during constant-current electro-deposition and anodic stripping coulometry (lines I and II respectively). During stripping, when they passed an anodic current of 0.193 A, the potential remained constant at -1.95 V for about one-third of the deposition period. The potential then increased significantly to -0.2 V, where the oxidation of the molten salt electrolyte took place. However, despite the fact that the potential had risen to the melt oxidation potential, they still observed a layer of carbon on the working electrode surface. At very low currents they observed that further carbon removal could take place at a potential of -1.0 V, although even then the last portion of the carbon fell away from the electrode and could not be re-oxidised. From these results, Ingram et al. (1966) deduced that there were two stages to carbon oxidation: the first stage took place at -1.95 V, whilst the second took place at -1.0 V. These potentials coincide with the anodic peaks in observed in Figure 2.7, which thus provides supporting evidence for the supposition that these peaks were caused by carbon oxidation.

Ingram et al. (1966) also studied three different carbonate electrolytes at a temperature of 750 °C: pure Li_2CO_3, Na_2CO_3-K_2CO_3 (molar ratio of 58:42) and Li_2CO_3-Na_2CO_3-K_2CO_3 (molar ratio of 43.5:31.5:25.0). Figure 2.9 shows the linear sweep voltammograms they obtained at a gold working electrode. The behaviour of the ternary eutectic denoted by line II is very similar to that shown in Figure 2.7, which was at a lower temperature of 600 °C. Comparing lines I and II in Figure 2.9, Ingram et al. (1966) stated that the range of electroactivity of pure Li_2CO_3 (line I) was 1.7 V, which is 0.3 V smaller than that of the ternary eutectic at the same temperature. The cathodic limit for Li_2CO_3 was more positive than for the ternary eutectic, and the anodic peak at which carbon was oxidised was also more positive.

Na_2CO_3-K_2CO_3, which is indicated by line III in Figure 2.9, showed markedly different behaviour to the electrolytes containing Li_2CO_3. As has already been mentioned above, Ingram et al. (1966) observed that no carbon could be deposited from Na_2CO_3-K_2CO_3, and thus the cathodic limit of this electrolyte was attributed to alkali metal ion reduction. Two stages in this reduction were considered to occur. Firstly, at -2.25 V alkali metal was liberated to such an extent as to amalgamate with the gold surface. Secondly, at -2.7 V alkali metal appeared on the

metal surface, which was chemically confirmed by Ingram et al. (1966). Note the close correspondence of the anodic and cathodic current trends for this electrolyte, which they took to be evidence of the reversibility of the alkali metal deposition process.

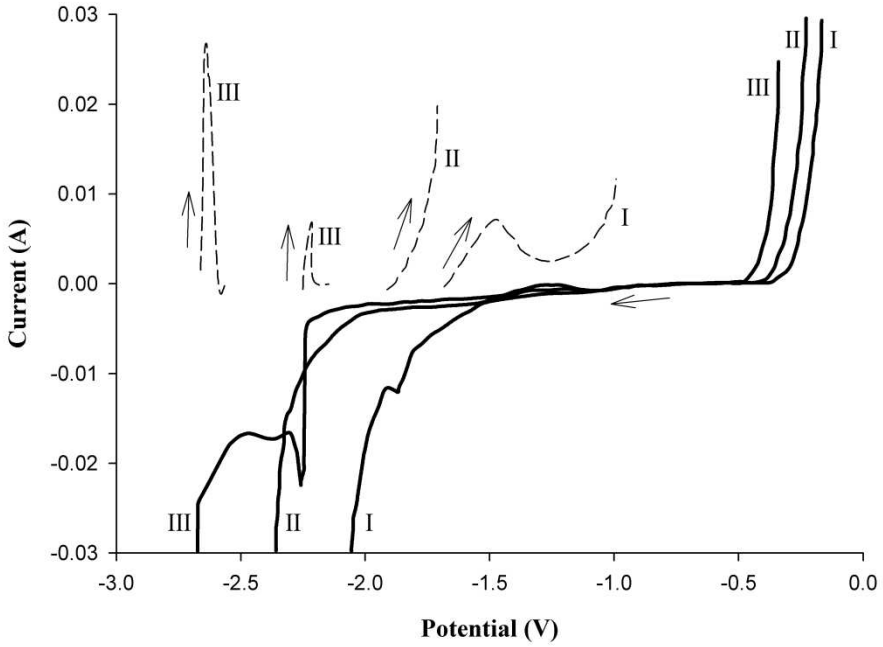

Figure 2.9: Linear sweep voltammograms obtained from three different molten salt compositions at a temperature of 750 °C. The lines denoted by the Roman numerals I, II and III correspond to the results obtained using molten salts of the following compositions: (I) pure Li_2CO_3; (II) ternary eutectic mixture of Li_2CO_3, Na_2CO_3 and K_2CO_3; (III) binary mixture of Na_2CO_3 and K_2CO_3. The solid lines represent the cathodic sweeps whilst the dashed lines correspond to the anodic sweeps. Atmosphere: CO_2. WE: gold; CE: gold-palladium crucible; RE: Danner-Rey RE; scan rate: 5 mV/s. Re-plotted from Ingram et al. (1966).

A number of other working electrode materials besides vitreous carbon and gold have been studied in the literature; several relevant ones shall now be discussed in the following sub-sections.

2.5.2 Studies of Lantelme et al. (1999)

Lantelme et al. (1999) studied the cyclic voltammetry of several different working electrodes in a ternary Li_2CO_3-Na_2CO_3-K_2CO_3 (molar ratio of 43.5:31.5:25.0) molten salt electrolyte at 450 °C. The materials studied included aluminium, gold, copper, nickel, platinum and vitreous carbon. In general, for all of these materials except gold, carbon deposition was considered to occur at the cathodic limit. However, the observation that no carbon could be obtained at a gold electrode contradicts the results of Delimarskii et al. (1964), Ingram et al. (1966) and Massot et al. (2002), who did obtain carbon using gold electrodes. Another general observation that can be drawn from the work of Lantelme et al. (1999) is that additional anodic and cathodic peaks usually arose from reactions involving the electrode metal.

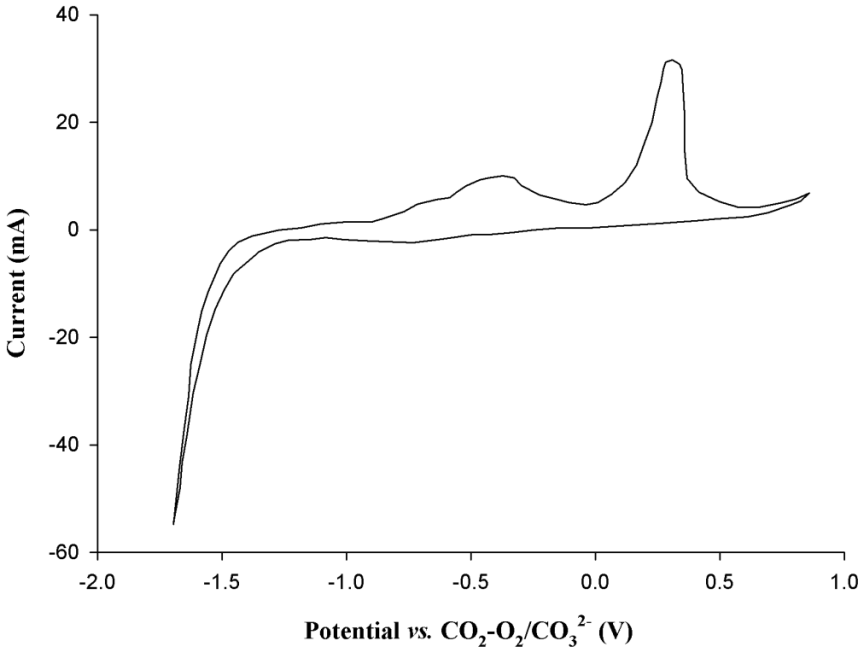

Figure 2.10: Cyclic voltammogram obtained using a platinum working electrode at 450 °C in a molten ternary eutectic mixture of Li_2CO_3-Na_2CO_3-K_2CO_3 (molar ratio of 43.5:31.5:25.0). Scan rate: 1 V/s; counter electrode: gold sheet; reference electrode: CO_2-O_2/CO_3^{2-}; atmosphere: CO_2. Re-plotted from Lantelme et al. (1999).

In the present thesis, some important studies of cyclic voltammetry were carried out using platinum working electrodes. Therefore, in this sub-section the platinum cyclic voltammogram obtained by Lantelme et al. (1999) is discussed.

Figure 2.10 shows the cyclic voltammogram obtained by Lantelme et al. (1999) at a platinum working electrode. Carbon deposits were obtained on a freshly polished platinum electrode at a potential of -1.65 V vs. CO_3^{2-}/CO_2-O_2, which corresponds to the cathodic limit. The anodic limit was attributed to the oxidation of carbonate ions. Janz et al. (1963) observed the formation of Li_2PtO_3 when platinum was immersed in carbonate-based molten salts, so the cathodic peak was said to be due to the following reaction (Lantelme et al., 1999):

$$PtO_3^{2-} + 4e^- \rightarrow Pt + 3O^{2-} \qquad (2.31)$$

The generation of PtO_3^{2-} ions was considered to be responsible for one of the three anodic peaks observed in Figure 2.10, in accordance with the following reaction (Lantelme et al., 1999):

$$3CO_3^{2-} + Pt \rightarrow 3CO_2 + PtO_3^{2-} + 4e^- \qquad (2.32)$$

As for the other two anodic peaks, Lantelme et al. (1999) attributed these to the oxidation of carbon according to a two-step mechanism. However, Lantelme et al. (1999) did not specifically refer to any particular anodic peaks in their explanation of the voltammogram, which makes their attributions somewhat less reliable.

2.5.3 Studies of Keijzer et al. (1999) – 304 stainless steel electrodes

Keijzer et al. (1999) studied the cyclic voltammetry of 304 stainless steel in Li_2CO_3-Na_2CO_3 (molar ratio of 60:40) and Li_2CO_3-K_2CO_3 (molar ratio of 62:38) molten salts at a temperature of 650 °C. The atmospheres used were humidified molten carbonate fuel cell (MCFC) anode and cathode gases. The humidified anode gas consisted of 60.9 % H_2, 8.4 % CO_2, 21.6 % H_2O

and 9.1 % CO, whilst the humidified cathode gas consisted of 14.3 % O_2, 29.2 % CO_2, 2.8 % H_2O and 53.7 % N_2. Keijzer et al. (1999) did not intentionally produce any carbon deposits during their study, although they recognised that carbon could be formed at the cathodic limit in the two binary carbonates studied. The study is relevant because it describes the metal-related reactions that occur at 304 stainless steel working electrodes.

Figure 2.11 shows the cyclic voltammograms obtained after the stainless steel was subjected to 30 minutes of exposure to the Li_2CO_3-Na_2CO_3 and Li_2CO_3-K_2CO_3 electrolytes. Keijzer et al. (1999) recognised that carbon could be formed at more negative potentials, as observed by Vossen et al. (1995). Hence, the anodic peak A at -1.5 V was attributed to carbon oxidation:

$$C + 2CO_3^{2-} \rightarrow 3CO_2 + 4e^- \qquad (2.33)$$

At a similar potential, chromium was also said to be oxidised to $LiCrO_2$, albeit this reaction does not produce a peak in the cyclic voltammogram, as was shown by Vossen et al. (1996). The formation of $LiCrO_2$ is given by the following (Keijzer et al., 1999):

$$\frac{2}{3}Cr + \frac{2}{3}Li^+ + \frac{4}{3}CO_3^{2-} \rightarrow \frac{2}{3}LiCrO_2 + \frac{4}{3}CO_2 + 2e^- \qquad (2.34)$$

The peak B was ascribed to the oxidation of iron metal by carbonate ions (Keijzer et al., 1999):

$$Fe + CO_3^{2-} \rightarrow FeO + CO_2 + 2e^- \qquad (2.35)$$

The combination of the anodic peaks B and C was attributed to the formation of a solid solution of FeO and $LiFeO_2$ (Keijzer et al., 1999):

$$\frac{2}{3}Fe + \frac{2}{3}Li^+ + \frac{4}{3}CO_3^{2-} \rightarrow \frac{2}{3}LiFeO_2 + \frac{4}{3}CO_2 + 2e^- \qquad (2.36)$$

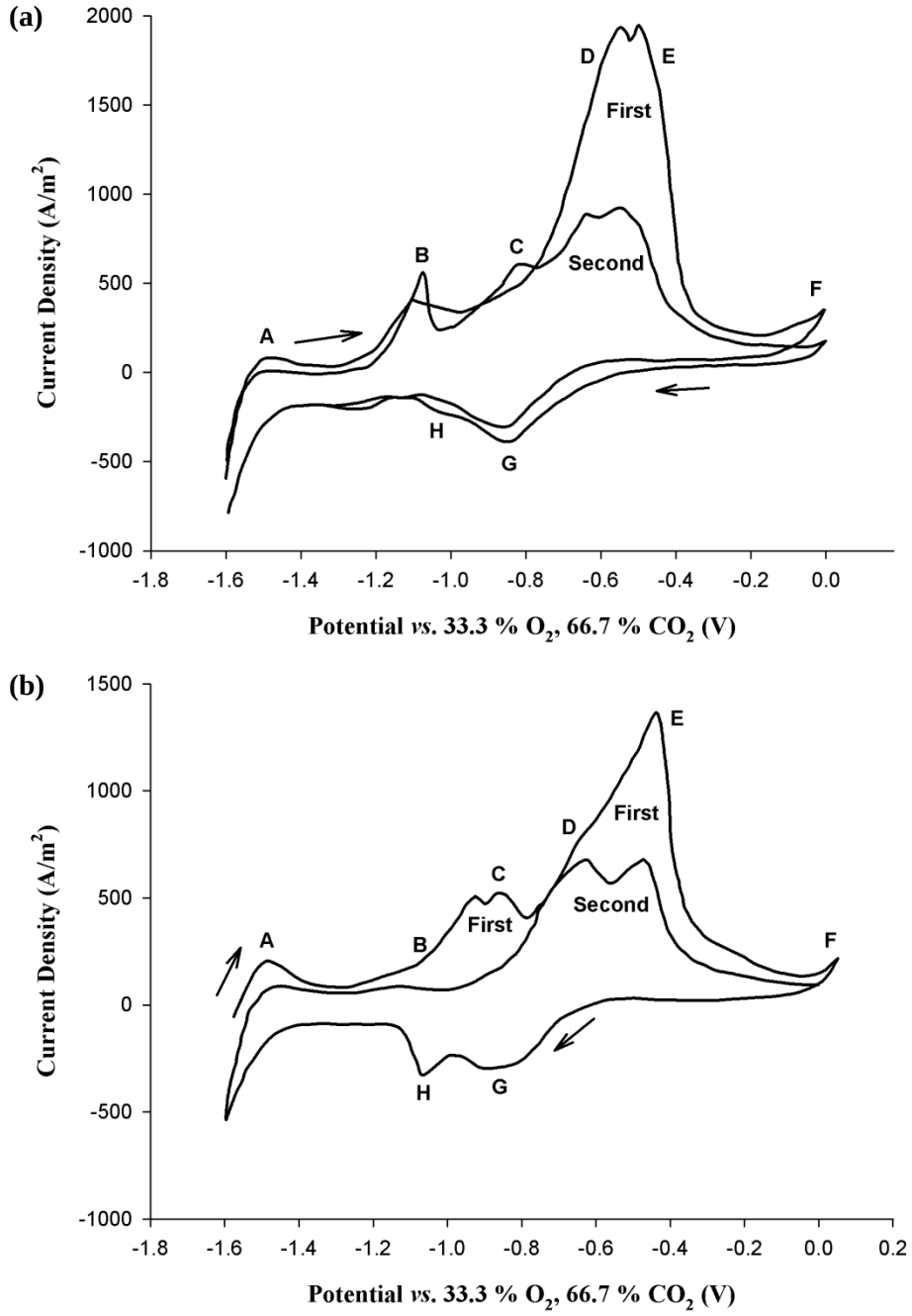

Figure 2.11: Cyclic voltammograms of 304 stainless steel obtained after 30 minutes of exposure to the electrolyte. Voltammogram (a) was obtained using a Li_2CO_3-K_2CO_3 molten salt (molar ratio of 62:38) under MCFC anode gas. Voltammogram (b) was obtained using a Li_2CO_3-Na_2CO_3 molten salt (molar ratio of 60:40) under MCFC cathode gas. Temperature: 650 °C; scan rate: 50 mV/s; reference electrode: gold under reference gas (33.3 % O_2, 66. 7 % CO_2, 1 atm). Re-plotted from Keijzer et al. (1999).

Collectively, the anodic peaks D and E were considered to be caused by oxidation reactions involving the principal components of the stainless steel: iron, nickel and chromium. One point worth noting here is that peaks D and E appear to be formed from several peaks that were too close together to be adequately resolved. Iron oxide formed in Reaction 2.35 was said to be successively oxidised according to the following two reactions (Keijzer et al., 1999):

$$2FeO + 2Li^{+} + 2CO_3^{2-} \rightarrow 2LiFeO_2 + 2CO_2 + 2e^{-} \quad (2.37)$$

$$4Fe + LiFeO_2 + 6CO_3^{2-} \rightarrow LiFe_5O_8 + 6CO_2 + 12e^{-} \quad (2.38)$$

Nickel oxidation probably occurred according to the following reaction (Keijzer et al., 1999):

$$Ni + CO_3^{2-} \rightarrow NiO + CO_2 + 2e^{-} \quad (2.39)$$

As for chromium, the peak at -0.9 V was said to be caused by the oxidation of bivalent chromium ions that were present in the oxide scale (Keijzer et al., 1999). Keijzer et al. (1999) considered that the anodic peak at -0.7 V may have been due to the oxidation of metallic chromium to Li_2CrO_4, which dissolves in the molten salt as chromate ions:

$$\frac{1}{3}Cr + \frac{4}{3}\,CO_3^{2-} \rightarrow \frac{1}{3}CrO_4^{2-} + \frac{4}{3}CO_2 + 2e^{-} \quad (2.40)$$

The anodic limit (peak F) was attributed to carbonate ion oxidation according to Reaction 2.12 (Keijzer et al., 1999).

Keijzer et al. (1999) ascribed the two cathodic peaks G and H to the reductions of $LiFe_5O_8$, $LiFeO_2$, and NiO according to the following reactions:

$$LiFe_5O_8 + 4e^{-} \rightarrow LiFeO_2 + 4FeO + 2O^{2-} \quad (2.41)$$

$$LiFeO_2 + 4e^{-} \rightarrow FeO + Li^{+} + O^{2-} \quad (2.42)$$

$$NiO + 2e^{-} \rightarrow Ni + O^{2-} \quad (2.43)$$

The cyclic voltammograms produced by Keijzer et al. (1999), and shown in Figure 2.11, were produced in an unconventional way compared to the other cyclic voltammograms presented in this review. The cyclic voltammograms in Figure 2.11 were started at the most cathodic potential, and the anodic sweep was carried out prior to the cathodic sweep. Since cyclic voltammetry was started at the most cathodic potential, it is likely that some carbon may have been formed. Keijzer et al. (1999) did account for the presence of carbon in their analysis. Although based on the observations of Ingram et al. (1966) and Le Van et al. (2009), carbon oxidation is likely to have produced other peaks as well. However, if the amount of carbon produced was small, the carbon oxidation peaks may be very small in other places compared to the other anodic peaks observed.

2.5.4 Other electrode materials

Carbon deposition at several other electrode materials has also been reported in the literature. However, Janz and Conte (1964b) were unable to obtain carbon deposits on a stainless steel electrode, in a ternary eutectic mixture of Li_2CO_3-Na_2CO_3-K_2CO_3 at 600-700 °C, albeit this was probably due to the fact that low current densities were employed.

Carbon has also been obtained under various conditions on tungsten (Chen et al., 2010), silver (Janz and Conte, 1964a) and molybdenum (Dimitrov, 2009) electrodes, as shown in Table 2.1 in Section 2.4.

In addition, Dimitrov (2009) reported that carbon could be deposited on a graphite working electrode in a pure Li_2CO_3 melt at 740 °C and 840 °C under an argon atmosphere. However, this seems to contradict the result of Kaplan et al. (2010), who were unable to obtain carbon deposits on a graphite cathode in a ternary eutectic mixture of Li_2CO_3-Na_2CO_3-K_2CO_3 at temperatures between 500-800 °C under a carbon dioxide atmosphere. Instead Kaplan et al. (2010) observed that the graphite cathode swelled and thus inferred that metal intercalation had taken place. The difference in atmospheres between the two experiments is unlikely to have been the cause for the contradictory observations, since Ingram et al. (1966) observed carbon

deposition under both carbon dioxide and argon atmospheres. Possibly the manner in which cathodic polarisation was applied to the cathode was responsible for the difference between the observations for graphite.

2.5.5 Summary

From the findings already described, it is apparent that carbon deposits can be obtained on a variety of different electrode materials in molten salts where carbonate ions are the only added anions; the carbon formation reaction occurs at the cathodic limit. The anodic peaks observed by Le Van et al. (2009) and Ingram et al. (1966) for the oxidation of carbon and possibly carbide compounds (see Figures 2.6, 2.7 and 2.9) could potentially occur when any electrode material is used, provided that carbon can be deposited on the electrode in the first place. This is because the mechanism for carbon deposition does not seem to be affected by the electrode material, on the basis of the majority of evidence available, and thus electro-deposited carbon is likely to be oxidised in a fairly similar way regardless of the electrode material.

However, other reactions involving the electrode material itself and its oxides (if any) have been shown to vary considerably (Lantelme et al., 1999; Keijzer et al., 1999). The exact nature of these reactions has not yet been reliably ascertained, since cyclic voltammograms are open to various interpretations and also few studies into these subsidiary electrode reactions have been reported. Regardless, these subsidiary electrode reactions involving the electrode materials may not have a drastic effect on the deposition of carbon, as the submerged cathode surface becomes rapidly coated with carbon, which then functions as the cathode surface due to the fact that the carbon deposit is an electrical conductor (Ingram et al., 1966).

However, the interactions between the molten salt electrolyte and the anode material are more significant, since the bare anode surface is exposed to the electrolyte for the entire duration of electrolysis, unlike the working electrode, which becomes coated with a layer of carbon after a relatively short time. The importance of anode selection is illustrated in the next section on anode performance.

2.6 Anode Performance Studies

As was remarked above, the interactions between the anode material and the electrolyte are more commonly observed in practice than the interactions between the cathode material and the electrolyte. This is because the anode does not become coated with a protective layer of carbon. At present, only Siambun (2011b) has carried out a comparison of different anode materials for carbon electro-deposition from carbonates. Three different anode materials were tested in an equimolar Li_2CO_3-K_2CO_3 molten salt at temperatures between 544-547 °C, under a carbon dioxide atmosphere. Carbon electro-deposition was carried out in each experiment at an applied potential difference of 4 V for 60 minutes. The cathode was a mild steel rod, whilst the three types of anode used were a tin oxide rod, a nickel rod and a stainless steel rod. Figure 2.12 shows the current-time curves obtained using each of the anode materials.

Siambun (2011b) observed that the tin oxide anode became soft and disintegrated after 60 minutes of electrolysis. Furthermore, as Figure 2.12 shows, the charge passed when the tin oxide anode was used was considerably smaller than in the other two experiments: only 2952 C. This was probably due to the tin oxide possessing an inherently higher resistivity than the other two materials. Based on these two disadvantages, Siambun (2011b) deemed tin oxide to be an unsuitable anode material.

When the nickel anode was used, the charge passed was substantially higher than the other two materials: 11040 C. However, Siambun (2011b) observed that after 60 minutes of electrolysis, where the nickel rod had been immersed in the electrolyte, its surface had become green and pitted. The rod was subsequently subjected to a further 14 hours of electrolysis, after which significant anodic dissolution was observed. These phenomena were attributed to the formation of nickel oxide, which could dissolve in the electrolyte. Since nickel could not withstand prolonged electrolysis, Siambun (2011b) also considered it to be an inappropriate anode material.

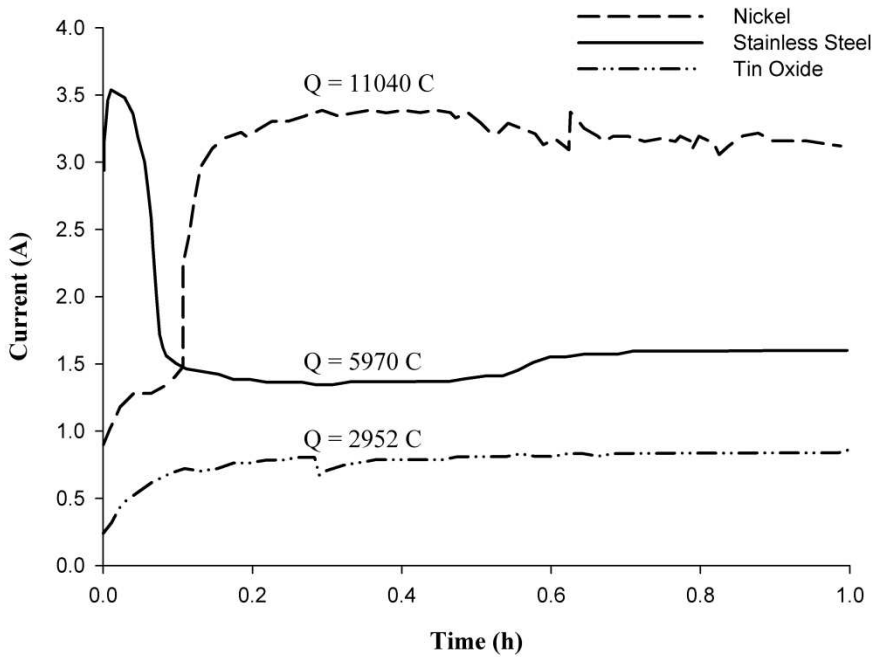

Figure 2.12: Current versus time trends during carbon electro-deposition for three different anode materials: stainless steel, nickel and tin oxide. Electrolysis was carried out using an applied potential difference of 4 V in a Li_2CO_3-K_2CO_3 molten salt (molar ratio of 1:1) at temperatures between 544-547 °C, under a carbon dioxide atmosphere. The working electrode material was mild steel. Re-plotted from Siambun (2011b).

Siambun (2011b) found that stainless steel was the most favourable anode material. The charge passed in 60 minutes was intermediate compared to the other two materials (5970 C), indicating a reasonable electrical conductivity. Furthermore, Siambun (2011b) observed that the stainless steel did not undergo pitting or thinning during electrolysis. This lack of significant corrosion was probably due to the formation of two layers at the surface of the stainless steel (Keijzer et al., 1999). The innermost chromium oxide layer, which also contained nickel, prevented the outward diffusion of metal ions and the inward diffusion of oxide ions. As a result, the growth of the outermost iron oxide layer was retarded (Tzvetkov and Kolchakov, 2004). Due to its reasonable current-time behaviour and lack of substantial corrosion, stainless steel was considered to be the best anode material out of the three studied (Siambun, 2011b).

So far in this review, the following subjects have been considered: the direct and indirect methods of carbon deposition, the effect of process conditions, the voltammetry of carbonate electrolytes and anode performance. In the next section, the properties of the electro-deposited carbon shall be discussed.

2.7 Properties of Electro-deposited Carbon

2.7.1 General properties

Before discussing the effect of process conditions on the properties of electro-deposited carbon, it is necessary to give an overview of the general characteristics of such carbon. Most of the systematic studies of the properties of electro-deposited carbon have been carried out using carbon deposited from Li_2CO_3-Na_2CO_3-K_2CO_3 molten salt mixtures (molar ratio of 43.5:31.5:25.0) at temperatures between 450 and 700 °C.

Regardless of the precise conditions used to obtain electro-deposited carbon, it was generally found that at least some of the carbon possessed an amorphous structure (Bartlett and Johnson, 1967; Ito et al., 1992; Novoselova et al., 2008a). Kawamura and Ito (2000) found that their electro-deposited carbon possessed largely sp^2 hybridisation, using X-ray Photoelectron Spectroscopy (XPS) and X-ray Excited Auger Electron Spectroscopy (XAES). However, some of the carbon at the surface of the deposit was found to possess sp^3 hybridisation and this was attributed to the partial oxidation of the surface (Kawamura and Ito, 2000). Presumably these observations would apply to any other carbon deposited using molten salt electrolytes.

Le Van et al. (2009) obtained carbon deposits on a nickel working electrode in a Li_2CO_3-Na_2CO_3-K_2CO_3 molten salt mixture (molar ratio of 43.5:31.5:25.0), at temperatures between 450-700 °C and at applied potential differences between -3 and -6 V. To prepare the carbon for analysis, the working electrode was first immersed in distilled water to cause the deposit to disintegrate. The powders were then washed with HCl solution and then dried under vacuum for 15 hours; the drying temperature was varied between 250 °C and 2000 °C.

Le Van et al. (2009) observed particle sizes of between 30-50 nm in their transmission electron microscopy (TEM) results, as Figures 2.13(a) and (b) show. Thus the electro-deposited carbon was described by Le Van et al. (2009) as carbon nanopowder. Such carbon powder can possess a relatively high specific surface area, depending on the process conditions used; the highest specific surface area obtained by Le Van et al. (2009) was 1315 m^2/g, at a salt temperature of 450 °C, an applied potential difference of -6 V and a drying temperature of 600 °C.

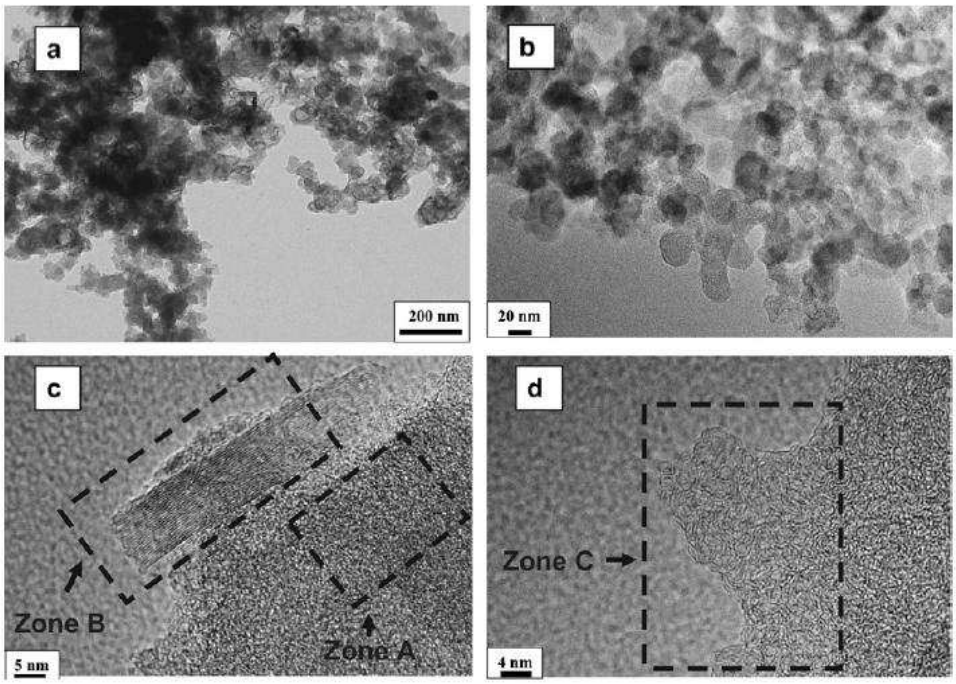

Figure 2.13: TEM images of carbon nano-powders deposited at an applied potential difference of -4 V in a molten Li_2CO_3-Na_2CO_3-K_2CO_3 eutectic mixture at 450 °C and subjected to different heat-treatment temperatures after washing: (a) 400 °C; (b) 2000 °C; (c and d) 600 °C. Taken from Le Van et al. (2009).

Irrespective of the process and post-treatment conditions, Le Van et al. (2009) observed three characteristic types of domain in their electro-deposited carbon, which are illustrated in Figure 2.13. The three kinds of domain were: amorphous domains (zone A in Figure 2.13(c)), graphitised domains with a random orientation (zone C in Figure 2.13(d)) and graphitised domains with a consistent orientation (zone B in Figure 2.13(c)). The graphitised domains with a consistent orientation possessed a fringe spacing of 0.34 nm, which is very similar to the

distance between adjacent graphene sheets in graphite (Le Van et al., 2009). Kaplan et al. (2002) observed a similar fringe spacing value from TEM images. Furthermore, the X-ray diffraction (XRD) results obtained by Le Van et al. (2009) indicated an average interlayer distance of 0.335 nm.

Nano-structured carbon phases have also been reported in the literature. Kaplan et al. (2001) deposited carbon on a nickel working electrode in a Li_2CO_3-Na_2CO_3-K_2CO_3 molten salt mixture (molar ratio of 43.5:31.5:25.0), at a temperature of 450 °C and at an applied potential of -1.6 V vs. CO_3^{2-}/CO_2-O_2. The electro-deposited carbon obtained was said to contain graphite, amorphous carbon and carbon nano-fibres. These carbon nano-fibres possessed an average diameter of approximately 10 nm. The nano-structures obtained were of nearly uniform size and were self-arranged into long 'ropes', with 10-50 nano-fibres per rope. The average diameter of a 'rope' was 100-500 nm and the maximum rope length obtained was 1 μm.

Novoselova et al. (2008a, 2008b) reported that they obtained carbon nanotubes (CNTs) in their electro-deposited carbon. The outer diameter of these CNTs varied from 5 nm to 250 nm, whilst the internal diameter varied from 2 nm to 140 nm. These CNTs were filled with solidified salt (Novoselova et al., 2008a).

Ijije (2012) deposited carbon from a eutectic Li_2CO_3-Na_2CO_3-K_2CO_3 molten salt mixture at a temperature of 598 °C and an applied potential difference of 4 V. Figure 2.14 shows a TEM image of the electro-deposited carbon obtained. Ijije (2012) observed irregularly arranged, sheet-like structures in the deposit, which could possibly be graphene sheets.

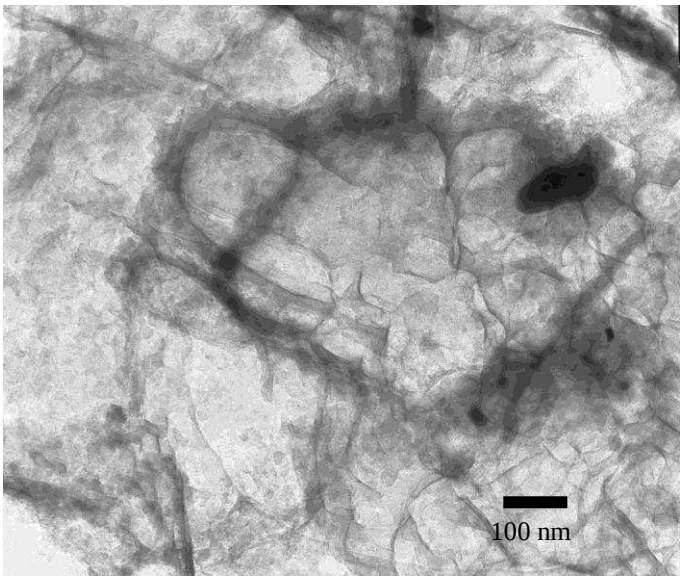

Figure 2.14: TEM image of carbon powder deposited at an applied potential difference of 4 V in a molten Li_2CO_3-Na_2CO_3-K_2CO_3 eutectic mixture at a temperature 598 °C. Prior to analysis, the sample was washed with distilled water and 2.3 M HCl solution. Taken from Ijije (2012).

XRD analysis has yielded evidence of substances other than carbon in the deposits. Lantelme et al. (1999) deposited carbon on a nickel working electrode in a Li_2CO_3-Na_2CO_3-K_2CO_3 molten salt mixture (molar ratio of 43.5:31.5:25.0), at a temperature of 450 °C and at applied potentials between -1.70 and -2.30 V vs. CO_3^{2-}/CO_2-O_2. Some of the carbon samples were washed using hot water, treated with dilute HCl solution and dried under vacuum at 150 °C. When XRD analysis was carried out on these deposits, peaks associated with lithium peroxide, Li_2O_2, and lithium carbide, Li_2C_2, were detected. Some other carbon samples were heated to 650 °C (presumably under vacuum although this was not explicitly stated), crushed and washed with boiling hydrochloric acid. No peaks for Li_2O_2 or Li_2C_2 were observed after such treatment (Lantelme et al., 1999). The formation of Li_2C_2 has already been mentioned in the section on subsidiary reactions. Le Van et al. (2009) considered that peroxide ions could be formed in the following reaction:

$$2CO_3^{2-} + 2e^- \rightarrow 2C + 3O_2^{2-} \qquad (2.44)$$

However, Le Van et al. (2009) considered that this reaction was only likely to occur at very negative potentials, at a standard potential of -5.98 V vs. CO_3^{2-}/CO_2-O_2.

Furthermore, metals from the electrode and electrolysis cell materials have also been detected in electro-deposited carbon. When Novoselova et al. (2008a) analysed their electro-deposited carbon using XRD, they detected the presence of platinum metal from the working electrode, as well as iron, nickel and chromium from the electrolysis cell materials. Lantelme et al. (1999) also detected the presence of lithium-nickel-oxide Li_2NiO in their carbon deposits and this nickel probably originated from their working electrode.

A number of other properties depend strongly on the process variables and the post-treatment of the deposits, such as the specific surface area and the average particle size of the carbon deposits. In the following sub-sections the effect of these factors on the properties of the carbon deposits are considered.

2.7.2 Effect of molten salt temperature

Le Van et al. (2009) found that the molten salt temperature primarily affected the specific surface area, the crystallinity and the average particle size. Figure 2.15 shows scanning electron microscope (SEM) images of carbon deposits obtained at an applied potential difference of -4 V at several different molten salt temperatures. At 450 °C a typical particle was less than 100 nm in size. As the molten salt temperature was increased, however, the particles became larger and more elongated; the apparent porosity also appeared to decrease (Le Van et al., 2009).

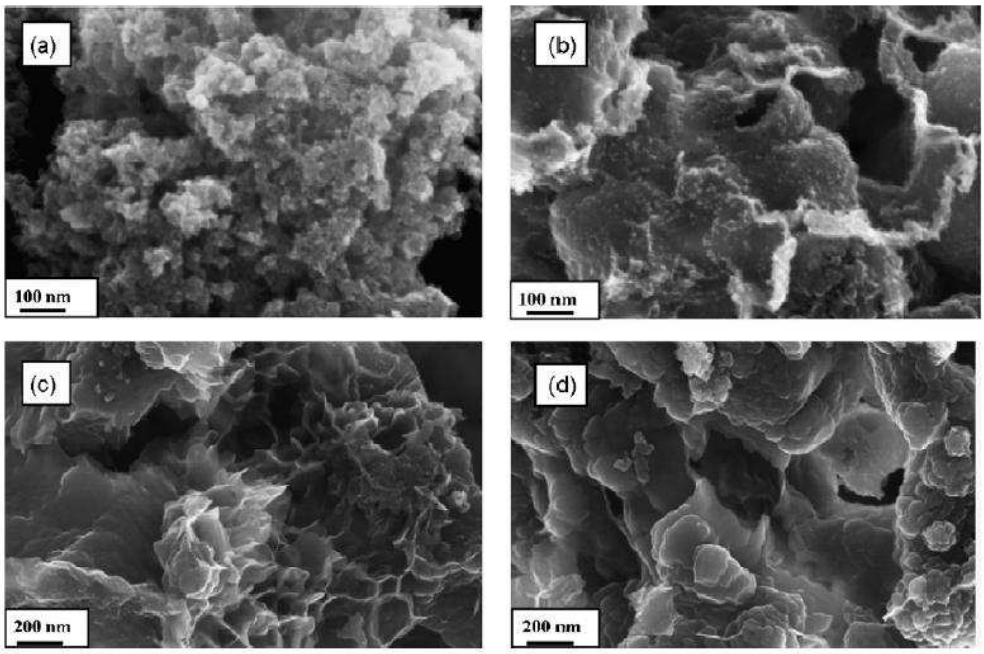

Figure 2.15: SEM images of carbon nano-powders deposited at an applied potential difference of -4 V in a molten Li_2CO_3-Na_2CO_3-K_2CO_3 eutectic mixture at various electrolyte temperatures: (a) 450 °C; (b) 540 °C; (c) 620 °C; (d) 700 °C. Taken from Le Van et al. (2009).

Le Van et al. (2009) used the Brunauer-Emmett-Teller (BET) method to ascertain the specific surface areas of their carbon nano-powders. Figure 2.16 shows their results for carbon powders produced at four different electrolyte temperatures and six different post-production annealing (or drying) temperatures. Evidently the specific surface area dropped rapidly with increasing electrolyte temperature (Le Van et al., 2009), which corroborates well with their SEM observations.

In addition, Le Van et al. (2009) considered that the carbon deposited at a temperature of 450 °C had a higher crystallinity than the carbon deposited at the higher temperatures of 540 °C, 620 °C and 700 °C. During XRD analysis, the carbon deposited at 450 °C had the highest peak intensity for the diffraction peak due to the Miller index plane (002), which corresponds to diffraction due to adjacent graphene sheets, as in graphite. Thus it was inferred that the carbon deposited at 450 °C had the highest crystallinity. However, the coherent length of graphite crystallites appeared to be largely independent of the electrolyte temperature (Le Van et al., 2009).

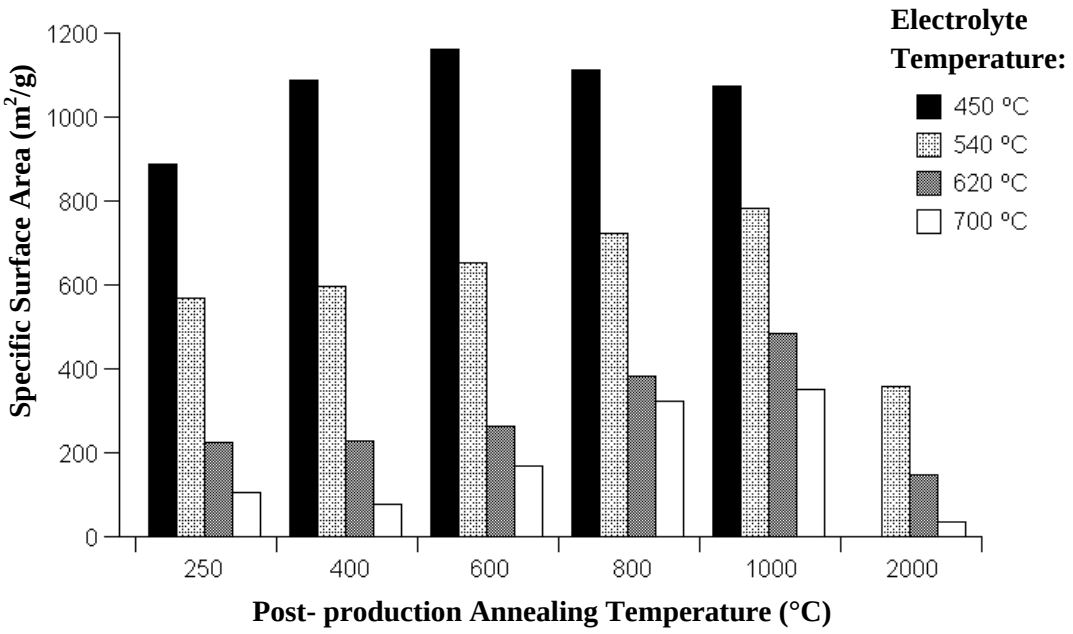

Figure 2.16: Specific surface areas from BET analysis of carbon nano-powders obtained from Li_2CO_3-Na_2CO_3-K_2CO_3 at an applied potential difference of -4 V, at several different electrolyte temperatures and post-production annealing temperatures after washing. Re-plotted from Le Van et al. (2009).

2.7.3 Effect of potential/voltage

Lantelme et al. (1999) found that as the deposition potential became more negative, the amounts of lithium-based compounds in the carbon deposits were found to increase, probably due to the formation of compounds such as Li_2C_2.

Le Van et al. (2009) found that the deposition potential difference had an effect on the macro- and microporosities of the carbon deposits obtained. At more negative applied potential differences, the degree of microporosity was found to be higher, whereas the degree of macroporosity was found to be lower, in comparison with the porosities obtained at less negative applied potential differences. In addition, Le Van et al. (2009) found that the more negative the deposition potential difference, the greater the specific surface area obtained; this is shown in Figure 2.17. However, Kaplan et al. (2002) reported the reverse trend: the specific surface areas of samples deposited at potentials of -2.4 V vs. CO_3^{2-}/CO_2-O_2 and -6.0 V vs.

CO_3^{2-}/CO_2-O_2 were 850 m^2/g and 500 m^2/g respectively. Kaplan et al. (2002) only reported two results, however, so it is quite possible that their results may have been anomalous. Comparing Figures 2.16 and 2.17, it is apparent that the changing the electrolyte temperature has a more significant effect on the specific surface area obtained, as opposed to changing the deposition potential.

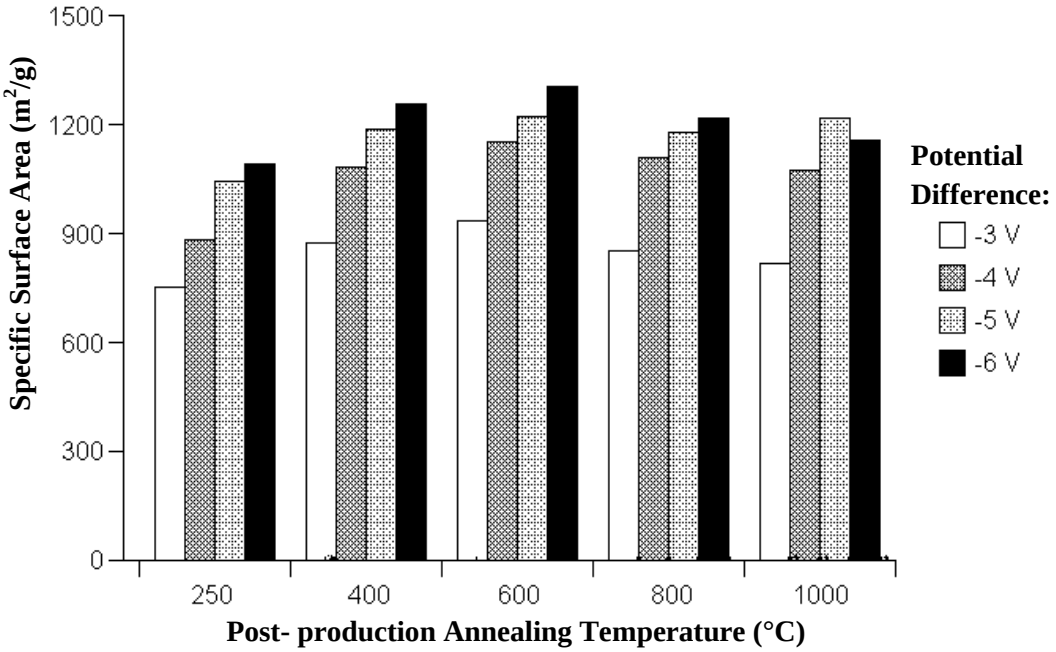

Figure 2.17: Specific surface areas of carbon nano-powders obtained from a molten eutectic mixture of Li_2CO_3-Na_2CO_3-K_2CO_3 at a temperature of 450 °C, at several different potential differences and annealing temperatures after washing. Re-plotted from Le Van et al. (2009).

2.7.4 Effect of post-production treatment

For carbon deposition in electrolytes consisting solely of carbonate salts, post-production treatment would appear to be essential prior to analysis or use. Table 2.4 gives the solubilities of various chloride, fluoride and carbonate compounds in water at a temperature of 25 °C. As Table 2.4 shows, lithium carbonate is not highly soluble in water (Linke, 1958) and thus many authors in the literature have used acid treatment to remove it. Similarly, the data in Table 2.4 implies that carbon deposits obtained from fluoride salts would also require acid treatment, due to the low solubilities of LiF and NaF in water (Linke, 1958). Prior to washing, Lantelme et al. (1999) found that their deposits contained only 10% carbon, whereas after washing with dilute

hydrochloric acid, Bartlett and Johnson (1967) reported that their deposit contained 90% carbon.

Table 2.4: Solubilities of various chloride, fluoride and carbonate compounds in water at a temperature of 25 °C; values were taken from Linke (1958).

Substance	**Mass Dissolved per dm^3 of Water at 25 °C (g)**
Li_2CO_3	12.63
LiCl	574.0
LiF	1.510
Na_2CO_3	293.1
NaCl	358.1
NaF	41.45
K_2CO_3	1118
KCl	357.6
KF	1017
$CaCO_3$	0.056
$CaCl_2$	808.1

Despite such significant differences in composition most authors in the literature have paid little attention to post-production acid treatment. In many investigations, such as that of Ingram et al. (1966), even the concentration and volume of the hydrochloric acid used was not quantitatively specified, so it is not possible to deduce the effect of the acid strength on the properties of the carbon deposit obtained.

On the other hand, deposits produced from chloride-based melts do not seem to require such aggressive post-production treatment and are generally reported to have been washed in water only. This is presumably due to the comparatively higher solubility of chlorides in water, generally speaking (Linke, 1958). Kawamura and Ito (2000) produced carbon deposits in chloride-based molten salts; they apparently produced satisfactory carbon by merely washing the electro-deposited films with distilled water.

Groult et al. (2003; 2006) and Le Van et al. (2009) subjected their electro-deposited carbon to heat treatment under vacuum at several different temperatures. Groult et al. (2006) found that, as the heat treatment temperature increased from 80 °C, through 400 °C to 1000 °C, the degree of surface disordering of the carbon increased. As Figures 2.16 and 2.17 show, the heat

treatment temperature only had a relatively weak influence on the specific surface area (Le Van et al., 2009).

2.7.5 Summary

Regardless of the exact process conditions used to produce electro-deposited carbon in molten salts, most authors have reported that such carbon contains regions of amorphous carbon, as well as some graphitised portions. Nano-structured carbon has also been observed, including nano-fibres (Kaplan et al., 2001; 2002) and graphene sheets (Ijije, 2012).

The findings of Le Van et al. (2009) showed that as the molten salt temperature was increased, the average particle size, degree of crystallinity and specific surface area all decreased. As the deposition potential was increased, the specific surface area increased (Le Van et al., 2009); also more lithium-based compounds such as Li_2C_2 were found to be present at more negative deposition potentials (Lantelme et al., 1999).

Acid treatment of carbon deposits seems to be essential when carbon is produced from carbonate-based and fluoride-based electrolytes, as opposed to chloride ones. This is due to the low solubility of Li_2CO_3, LiF and NaF in water (Linke, 1958). However, no authors have presented quantitative studies of the effect of such acid treatment on the composition of the deposits produced.

Furthermore, Groult et al. (2003; 2006) and Le Van et al. (2009) reported the use of heat-treatment of carbon under vacuum after washing. Such treatment had only a relatively weak influence on the specific surface area (Le Van et al., 2009), albeit the level of surface disordering of the carbon increased with increasing heat-treatment temperature.

Having now discussed the properties of electro-deposited carbon, the uses to which such carbon and the carbon deposition process can be put shall now be discussed.

2.8 Practical Applications

Two areas of practical application of the carbon deposition process can be considered: the applications to which the carbon itself can be put and the other potential uses of the molten salt process. These shall now be discussed in turn.

2.8.1 Uses of electro-deposited carbon

Carbon is a popular choice of electrode material in a variety of electrochemical processes, mainly due to its high heat resistance, corrosion resistance and low cost (Massot et al., 2002). Carbon is used as an anode material in fluorine production (Groult and Devilliers, 1998), supercapacitors (Kaplan et al., 2002) and rechargeable lithium-ion batteries (Tokumitsu et al., 1996), just to mention a few.

The structural characteristics of a given carbon material are an important factor in the choice of electrode materials (Kaplan et al., 2002). As shown by Le Van et al. (2009), the carbon that can be electro-deposited from carbonate molten salts can possess very high specific surface areas, which is useful for electrochemical devices such as lithium-ion batteries and supercapacitors.

An important function of the carbon anode in lithium-ion batteries is that it allows lithium to intercalate between the graphite layers, preventing the formation of metallic lithium at the anode surface. Avoiding metallic lithium deposition at the anode surface is important due to the fact that it is liable to catch fire (Flavell-While, 2011). Groult et al. (2003; 2006) have already investigated the use of their electro-deposited carbon as an anode material in lithium-ion batteries. The most favourable reversible capacity obtained by Groult et al. (2006) was 1100 mAh/g, approximately three times higher than that obtained for pure graphite (372 mAh/g).

Furthermore, Ito (2011) considered that the micro-porous structure of electro-deposited carbon films would be advantageous for use in electrochemical capacitors. Recently at the University of Nottingham, Ijije (2012) and Lee (2012) have demonstrated that the carbon electro-deposited from certain molten carbonates does indeed exhibit promising behaviour in electrochemical capacitors. Carbon produced from Li_2CO_3-K_2CO_3 appears to possess the highest capacitance compared to carbon produced from Li_2CO_3-Na_2CO_3, Li_2CO_3-Na_2CO_3-K_2CO_3 and Li_2CO_3 (Lee, 2012). For example, Ijije (2012) electro-deposited carbon from a Li_2CO_3-K_2CO_3 electrolyte (molar ratio: 62:38) at a temperature of 593 °C, at an applied potential difference of 4 V under a carbon dioxide atmosphere. After washing with dilute HCl solution, this carbon was tested using a symmetrical capacitor using 3M KCl solution as the electrolyte; galvanostatic charge-discharge was carried out using a voltage of 1 V, and yielded a capacitance value of 101 F/g (Ijije 2012). Two commercial-grade activated carbons studied by Guo et al. (2003) possessed capacitances of 78 F/g and 100 F/g, in a symmetrical capacitor using the same electrolyte as Ijije (2012). Since the electro-deposited carbon produced by Ijije (2012) can already attain capacitance values similar to those of activated carbon, but without further treatment, it would definitely seem that the electro-deposited carbon is well suited to use in electrochemical capacitors.

Kaplan et al., (2002) considered that another possible use of the electro-deposited carbon could be to use it as an anode in fluorine production: pure graphite cannot be used as an anode due to the fact that exfoliation occurs. However, if graphite can undergo exfoliation, it is likely that the electro-deposited carbon would be even worse due to the fact that the majority of the carbon consists of agglomerated carbon nano-particles.

Aside from the use of the electro-deposited carbon in electrochemical technologies, the carbon produced could also be used as a fuel. In this way, the electrical energy used to electro-deposit the carbon would be stored until the carbon is burned. The electro-deposited carbon might also be useful as a fuel in direct carbon fuel cells (DCFCs).

2.8.2 Uses of the molten salt carbon-producing process

Besides creating carbon that could be burned as fuel or used in electrochemical technologies, the molten salt carbon-producing process considered in this thesis could be put to several other uses. Such purposes include the production of carbon films on metal substrates, the production of carbide compounds and the carburisation of metals. In addition, the molten salt carbon-producing process could be harnessed for carbon capture or energy storage purposes.

Firstly, Kawamura and Ito (2000) suggested that the process could be used to coat metals with a layer of carbon in order to improve the thermal and corrosion resistance of the substrate metal, since carbon may possess better thermal and corrosion resistances than the substrate. Such carbon-coated metal could also be used in a similar way to carbon electrodes as described in the previous sub-section.

Carbon coatings are currently prepared using chemical-vapour deposition, which is highly costly due to the use of very high temperatures of around 1500 °C (Chen et al., 2010). Carbon can also be produced via the pyrolysis of organic compounds at temperatures of up to 1000 °C, followed by calcination at 1600 °C to remove gases incorporated into the crystal structures (Kaplan et al., 2002). Evidently the molten salt carbon-producing process has an inherent advantage over these two techniques due its lower operating temperatures (typically lower than 850 °C).

Song et al. (2012) were able to obtain carbon films with enhanced adhesion onto a titanium substrate; this involved producing a graded Ti-O-C interlayer between the bulk titanium and carbon phases. The resulting carbon film had a significantly higher adhesion strength value of 9.1 N according to scratch test, as opposed to 4.9 N for a carbon film on bare titanium.

Stern and Rolison (1989) and Stern (1992) used a variant of the molten salt carbon-producing process to produce transition metal carbides, such as tantalum carbide, vanadium carbide and titanium carbide. In their process, transition metals and carbon were simultaneously electro-

deposited onto the working electrode surface. The deposited transition metals then reacted with electro-deposited carbon to form transition metal carbides. This process used a LiF-NaF-KF molten salt electrolyte (molar ratio of 46.5:11.5:42.0), to which K_2CO_3 and a metal fluoride such as K_2TaF_7 were added; a temperature of 750 °C and a helium atmosphere were used. Transition metal carbides are typically used in industry as protective coatings, as they possess a high hardness and wear resistance (Martínez et al., 2002).

Siambun et al. (2011a) developed a method for carburising mild steel using the carbon-producing molten salt process. Two electrolytes were studied at an operating temperature of 800 °C under carbon dioxide: Na_2CO_3-NaCl (molar ratio of 4:1) and Li_2CO_3-K_2CO_3 (molar ratio of 1:1). The mild steel to be carburised was used as the cathode, whilst a tin oxide rod was used as the anode. Significant surface hardening occurred at applied potential differences between 2.0 and 2.5 V: Vickers micro-hardness values at the metal surface were observed to increase from around 300 HV (for the as-received mild steel) to values in excess of 1000 HV. The conventional carburisation process uses toxic molten cyanide baths (Davis, 2002); therefore the process developed by Siambun et al. (2011a) is considerably safer.

Licht et al. (2010) proposed a process whereby solar energy was used to help power a carbon dioxide-capturing molten salt electrolysis cell. This works on the principle that carbonate ion reduction yields carbon and/or carbon monoxide, as well as oxide ions. The oxide ions react with carbon dioxide from the cell atmosphere, therefore simultaneously regenerating the carbonate that is consumed and capturing the carbon dioxide. The cell contained pure Li_2CO_3 electrolyte at temperatures of 750-950 °C, and the electrodes used were a platinum cathode and a nickel anode. They suggested that solar energy could be harnessed to help meet the energy requirements of the process in two ways. Firstly, solar energy could be used to power the electrolysis via electricity generated by a photovoltaic panel. Secondly, the carbon dioxide could be pre-heated using thermal energy from the incident solar radiation. Licht et al. (2010) envisaged that it would also be possible to use solar radiation to heat the molten carbonate electrolyte as well. The work of Licht et al. (2010) is the only work in the literature at present

that considers the energy consumption of the molten salt process, although Ingram et al. (1966) and Lantelme et al. (1999) did determine current efficiencies for carbon electro-deposition.

One further use of the molten salt process could be to utilise it as an energy storage method; this strategy has not been considered in the literature. The process could also be used to store energy by electro-depositing carbon, which could then be re-oxidised to release the energy. Apart from the limited work of Ingram et al. (1966), no authors in the literature have studied the electrochemical re-oxidation of the electro-deposited carbon produced in the molten salt process.

2.9 Summary

In this literature review, the molten salt processes for the electrochemical conversion of carbon dioxide to carbon have been described. The review has encompassed a diverse range of topics related to this, including: chemical and electro-chemical reactions, the effect of process conditions, voltammetry in carbonate electrolytes, the properties of electro-deposited carbon and the uses of the process and electro-deposited carbon. The principal findings of this review are summarised in the following paragraphs.

Novoselova et al. (2003; 2007; 2008a; 2008b) proposed a three-step mechanism for the direct reduction of carbon dioxide:

$$CO_2 + 2e^- \rightleftharpoons CO_2^{2-} \quad (2.45)$$

$$CO_2^{2-} \rightarrow CO + O^{2-} \quad (2.46)$$

$$CO + 2e^- \rightarrow C + O^{2-} \quad (2.47)$$

Indirect reduction of carbon dioxide can occur in molten salt electrolytes containing carbonate ions. Most evidence presented in the literature suggests that carbonate ion electro-reduction to carbon proceeds according to the following reaction (Le Van et al., 2009):

$$CO_3^{2-} + 4e^- \rightarrow C + 3O^{2-} \quad (2.48)$$

Process conditions have a significant impact on the direct and indirect reduction of carbon dioxide to carbon. Typically, the direct reduction of carbon dioxide only occurs under elevated carbon dioxide pressures. However it is possible that the carbon dioxide simply reacts with dissolved oxide ions in the salt to form carbonate ions, which are then electro-reduced to carbon. The prerequisite for the indirect conversion of carbon dioxide to carbon via the electrolysis of carbonate ions has been shown to be the presence of lithium ions in the molten salt electrolyte, at least at carbon dioxide pressures less than 1.5 atm. Carbon can be deposited from Li_2CO_3 at a less negative potential than the reduction of the lithium cation to lithium metal, whereas for Na_2CO_3 and K_2CO_3, metal cation reduction takes place at a less negative potential than carbon deposition (Le Van et al., 2009).

For processes using carbonate ion reduction, temperature is a significant parameter, as carbon monoxide formation from carbonates becomes increasingly favourable at higher temperatures (Lorenz and Janz, 1970).

Carbon can be deposited on a significant range of electrode materials, including: vitreous carbon, gold, platinum, stainless steel, titanium, silver, nickel and aluminium. When the voltammetry of 'inert' materials such as vitreous carbon or gold was carried out in pure carbonates containing Li_2CO_3, carbon deposition was found to occur at the cathodic limit (Le Van et al., 2009). The anodic peaks were considered to correspond to carbon oxidation (Ingram et al., 1966) and possibly Li_2C_2 oxidation (Le Van et al., 2009). When 'non-inert' materials such as stainless steel were studied using voltammetry, anodic and cathodic peaks arose due to the reactions between the electrolyte and the electrode material (Keijzer et al., 1999).

According to Le Van et al. (2009), electro-deposited carbon produced from molten Li_2CO_3-Na_2CO_3-K_2CO_3 consists of three types of carbon: amorphous carbon, graphitised carbon with a random orientation and graphitised carbon with a clear orientation. Nano-structured carbon has also been observed, such as nano-fibres (Kaplan et al., 2001; 2002) and graphene sheets (Ijije,

2012). The particle sizes in electro-deposited carbon have been reported to be of the order of 30-50 nm (Le Van et al., 2009). Carbon with very high specific surface areas can be obtained, depending on the process conditions used. The highest obtained by Le Van et al., (2009) was 1315 m^2/g. The lower the electrolyte temperature or the more negative the cathode potential, the greater the specific surface area attained.

The molten salt carbon-producing process (reduction of carbonates to carbon) has been suggested for a variety of applications, for instance: the production of carbon for lithium-ion battery anodes (Groult et al., 2006), the capture of carbon dioxide using solar energy (Licht et al., 2010) and the production of carbide coatings for metals (Stern, 1992). The process can also be used to carburise metals (Siambun et al., 2011a). Furthermore, the carbon produced by the process has shown particular promise as an electrode material for electrochemical capacitors, where capacitance values have been attained that are similar to activated carbon materials, but without further treatment being necessary (Ijije, 2012).

CHAPTER 3

METHODOLOGY

In this chapter the general research methodology, experimental procedures and apparatus used in this PhD project are outlined.

3.1 General Research Methodology

The work carried out in this PhD project can be split into two categories: theoretical studies and empirical studies. Various theoretical studies were carried out. Phase diagrams were studied in order to determine the eutectic compositions and temperatures of the molten carbonate mixtures used as electrolytes. The theoretical standard potentials of possible electrochemical reactions were calculated, where HSC Chemistry software (Version 6.12; Outokumpu Research) was used to determine the standard Gibbs free energies of reaction. Reference works were also consulted on the use of analytical techniques such as scanning electron microscopy (SEM) and X-ray diffraction (XRD).

The remainder of this chapter describes the empirical methodologies employed. Firstly, the electrochemical molten salt reactor used for three-electrode and two-electrode experimentation is described, along with the materials, electrodes and electrolytes used in the reactor. This is followed by an outline of the various types of electrochemical experiment performed using the reactor. Finally, the carbon sample analysis methods used are considered.

3.2 Electrochemical Molten Salt Reactor

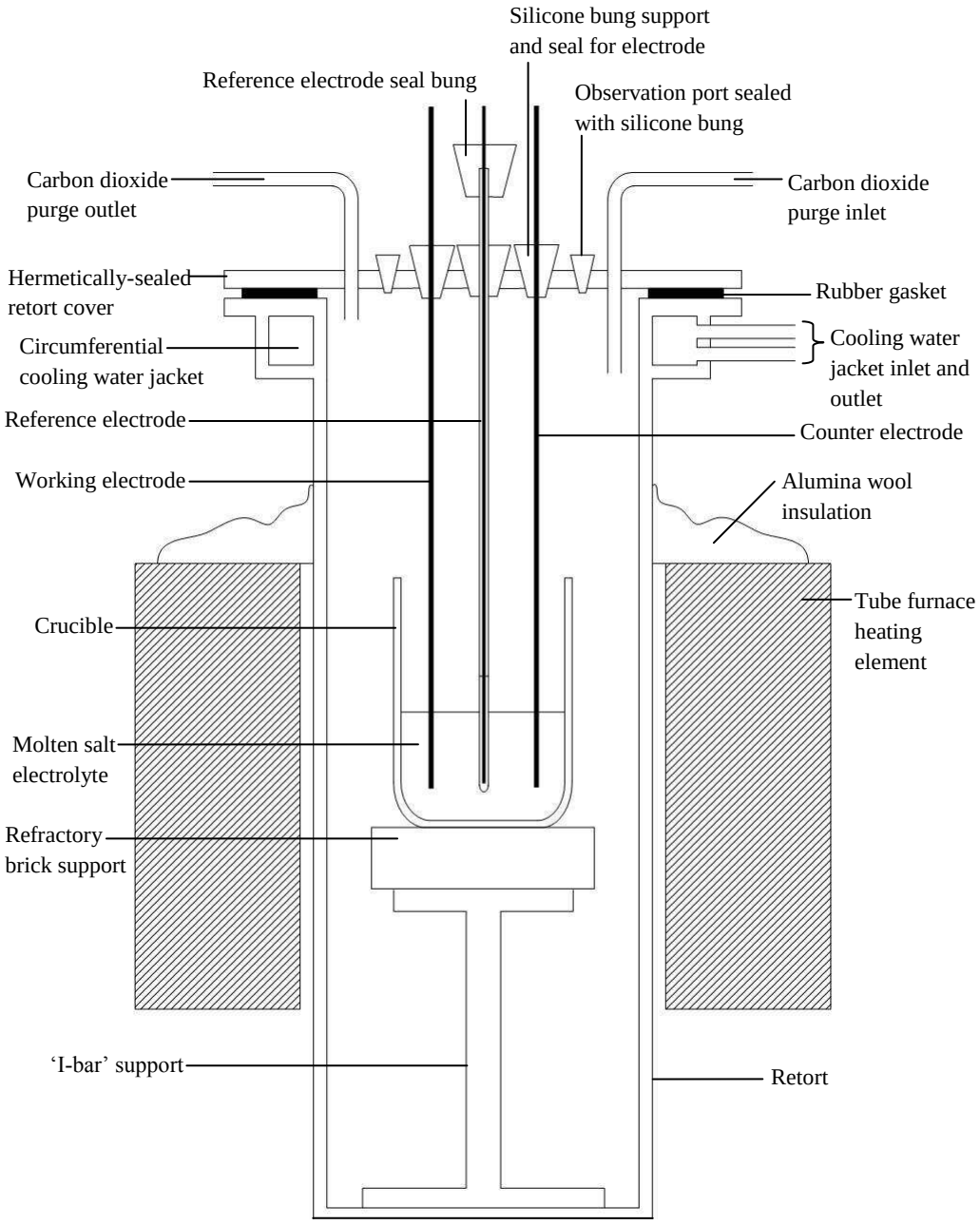

Figure 3.1: Schematic representation of the electrochemical molten salt reactor used in this study, set up in a three-electrode arrangement. For a two-electrode arrangement, the reference electrode was not used and the two electrodes used were called the anode and cathode. NB. This diagram is not to scale.

Figure 3.1 shows the general experimental set-up used for electrochemical experiments. In basic terms, the set-up consisted of a custom-built stainless steel retort placed through the bore of a vertical tube furnace. The molten salt electrolyte was held in a crucible placed in the hottest zone of the retort. The furnace was custom-made by Vecstar Furnaces Ltd. and consisted of two shells, allowing it to be opened. The bore of the furnace had an internal diameter of 160 mm and a tube length of 500 mm. A 2416CG Eurotherm PID 8 segment programmable controller was used to the control the furnace, which had a maximum achievable temperature of 1100 °C. The controller had an accuracy of ±1 °C and also had a power consumption meter for monitoring the energy consumption of the furnace.

The cylindrical retort used in this study was produced in-house from 316-grade stainless steel; Figure 3.2(a) shows a schematic diagram of the retort. Alumina wool was used to cover the gap between the retort and the furnace in order to reduce heat losses. The retort was hermetically sealed using a rubber gasket and a flange-type stainless steel cover (also made from 316-grade stainless steel), which had holes for the insertion of electrodes as well as for observation purposes. Figure 3.2(b) shows a schematic diagram of the retort lid. Silicone rubber bungs (Fisher Scientific Ltd.) were used to hold the electrodes in place and to seal the observation holes. A cooling water jacket was employed to prevent the bungs from overheating/melting and to allow safe handling.

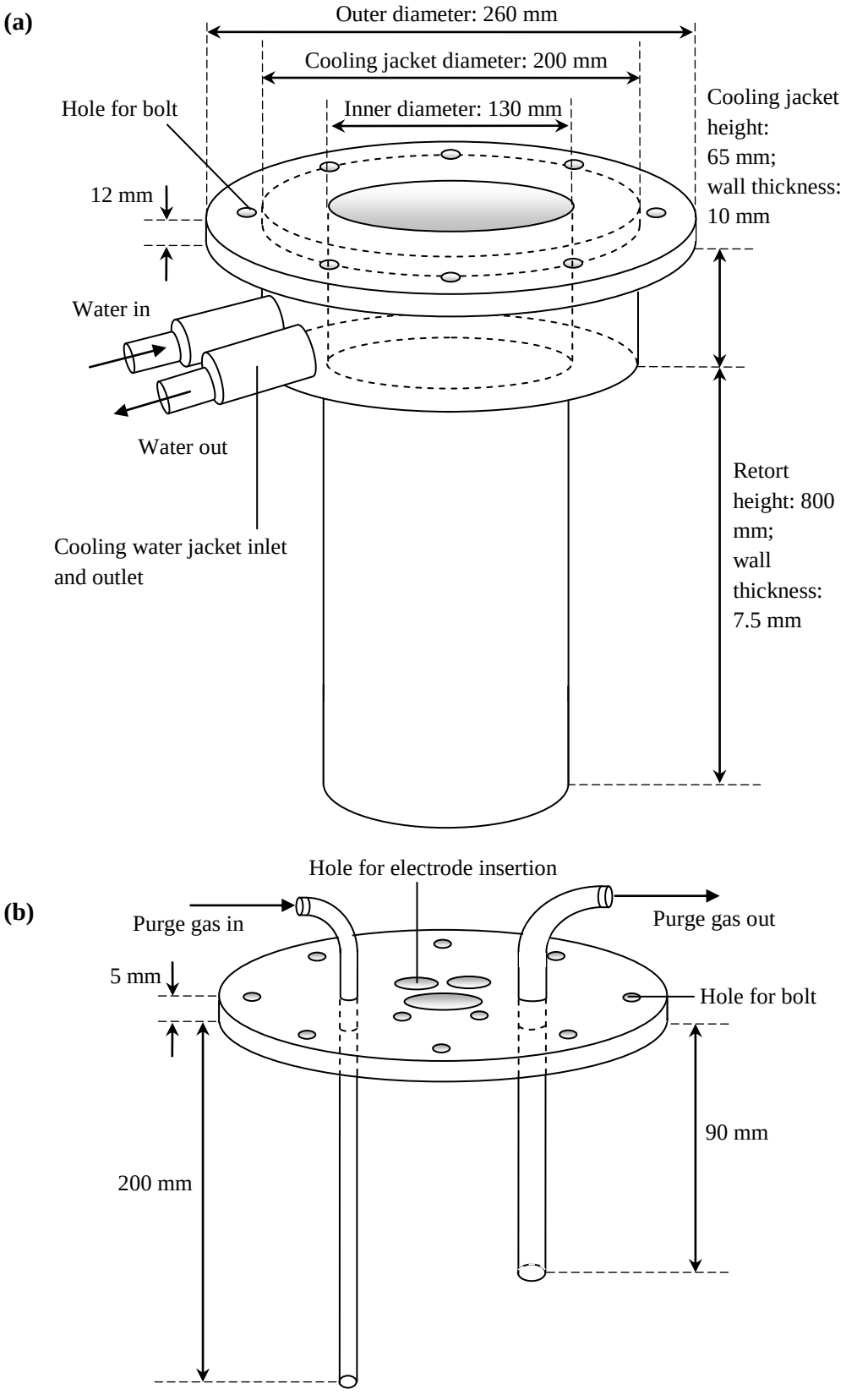

Figure 3.2: Schematic representation of (a) the retort and (b) the retort lid, showing dimensions and important features. NB. These diagrams are not to scale.

Metal pipes were welded to the retort lid to allow carbon dioxide purge gas (99.99 % pure; Air Products Ltd.) to be supplied to the retort from a gas cylinder. The carbon dioxide cylinder was fitted with a two-stage brass carbon dioxide regulator (GIS Leengate), whose outlet pressure was set at 0.2 bar g for at least twelve hours prior to and during experimentation. To ensure that the purge gas reached the surface of the molten salt with a high velocity, the inlet pipe was longer and narrower than the outlet, thus encouraging better mixing with any gases produced during electrolysis. The gas outlet pipe was shorter and wider than the inlet and therefore encouraged flow from the bottom of the retort to the top. The wide diameter of the outlet also prevented it from becoming blocked with condensed salt (Jewell, 2009). A calibrated rotameter (Roxspur Measurement and Control) was used to control the purge gas flowrate, which was typically 200 mL/min at atmospheric temperature and pressure (ATP). The operating range of the rotameter was 20-200 mL/min at ATP. A Dreschel bottle containing 'Labovac 10' mineral oil (Jencons) was used at the gas outlet to prevent the entry of air into the system.

The molten salt electrolyte was contained in an alumina crucible, which was placed in the hottest area of the furnace. The crucible was supported on a refractory brick, which was in turn supported on a stainless steel stand (manufactured in-house). Cup-shaped alumina crucibles (Pi-kem Ltd.) were used, with dimensions of 80 mm outer diameter at the top, 40 mm outer diameter at the bottom and a height of 100 mm. The crucible had a wall thickness of 2 mm. The purity of the alumina was 99.0 % and the total volume of the crucible was around 275 cm^3.

Prior to experimentation, after the purge gas flow was initiated, the furnace temperature was raised above the electrolyte melting temperature and maintained at that temperature for the duration of the experiment. Temperatures inside the crucible were taken using a YCT-727D thermometer (TC Ltd.) with an attached 3 mm diameter 1 m long mineral insulated thermocouple (310-grade stainless steel K or Pyrosil insulated type N). The thermocouple was placed within the molten salt for up to a minute in order to obtain an accurate temperature reading but minimise electrolyte contamination.

3.3 Electrolytes

Table 3.1: Electrolyte components used in this study, with the supplier and purity of each chemical. All of the salts were purchased in anhydrous form.

Substance	Supplier	Specification
Li_2CO_3	Sigma Aldrich	Purum grade, ≥99.0% pure
Na_2CO_3	Sigma-Aldrich	ACS reagent grade, ≥99.5% pure
K_2CO_3	Sigma-Aldrich	ACS reagent grade, 99.0% pure

Table 3.2: Electrolytes used in this study; the composition and melting/eutectic temperature of each electrolyte is given. References: * from Ingram et al. (1966); † from Stern and Weise (1969); ‡ from Facility for the Analysis of Chemical Thermodynamics (2012).

Electrolyte	Composition (mol. %)			Melting/Eutectic Temperature (°C)
	Li_2CO_3	Na_2CO_3	K_2CO_3	
Li_2CO_3	100	0.00	0.00	726 *
Na_2CO_3	0.00	100	0.00	856 †
K_2CO_3	0.00	0.00	100	898 †
Li_2CO_3-Na_2CO_3	52.0	48.0	0.00	501 ‡
Li_2CO_3-K_2CO_3	62.0	0.00	38.0	489 ‡
Na_2CO_3-K_2CO_3	0.00	58.0	42.0	709 ‡
Li_2CO_3-Na_2CO_3-K_2CO_3	43.5	31.5	25.0	397 *

Carbonate electrolytes were used throughout this study, thus preventing the carbon deposition rate from becoming limited by the carbonate ion concentration in the electrolyte (Le Van et al., 2009). Table 3.1 lists the electrolyte components used, along with their purities and manufacturers. Note that all of the salts were purchased in anhydrous form. Table 3.2 gives the seven electrolyte compositions used in this study, as well as their melting/eutectic temperatures at these compositions. Eutectic compositions of binary and ternary salts were chosen due to the fact that they have the lowest temperatures on the liquidus line of their respective phase diagrams.

3.4 Electrodes

3.4.1 Working and counter electrodes

Table 3.3 gives the materials used as working or counter electrodes in this study. The mild steel and stainless steel rods were simply held in place using silicone bungs as illustrated in Figure 3.1.

Table 3.3: Electrode materials used, with the supplier and type of each material.

Material	Manufacturer	Type/Grade
Stainless Steel Rod (6 mm diameter)	Unicorn Metals	304
Mild Steel Rod (5 mm diameter)	Unicorn Metals	CR4
Stainless Steel Wire (0.25 mm diameter) Fe/Cr18/Ni10	Advent Research Materials	B/1
Platinum Wire (0.25 mm diameter)	Advent Research Materials	99.99+% pure Temper hard
Graphite Rod (10 mm diameter, 300 mm long)	Multi-lab	DC-10

The stainless steel wire and graphite rods needed to be attached to metal rods in order to use them as electrodes. When stainless steel wire or platinum wire was used, it was tied to a clean stainless steel rod using another piece of stainless steel wire. The stainless steel rod with attached wire could then be held in place using a silicone bung as shown in Figure 3.1. When graphite was used, the graphite rods were drilled and given screw threads such that they would fit a threaded 6 mm diameter stainless steel rod, which could in turn be held in place using a silicone bung.

A variety of combinations of these electrodes were used in electrochemical experiments, these are discussed in Sections 3.5 and 3.6. Stainless steel was usually chosen as the anode or counter electrode material due to its apparent stability during electrolysis and its reasonable electrical conductivity, as discussed in Section 2.6 on anode performance.

3.4.2 Reference electrodes

All three-electrode electrochemical experiments required the use of a reference electrode. The reference electrode used in this study was a high temperature alumina membrane Ag/AgCl reference electrode based on that developed by Wang et al. (2012). This reference electrode exhibits good stability, reproducibility and reusability, as shown by Wang et al. (2012). When electrolysis was carried out in Li_2CO_3-K_2CO_3 (molar ratio of 1:1) for 80 hours at a temperature of 540 °C, the cathodic limit potential variation from cyclic voltammetry was less than ±5 mV over that period (Wang et al., 2012). Since ±5 mV is the typical error in cyclic voltammetry, this observation indicated that the reference electrode possessed good stability in the carbonate electrolyte. Furthermore, Wang et al. (2012) found that prolonged electrolysis in Li_2CO_3-K_2CO_3 for up to one week did not lead to any visible damage to the alumina sheath.

Figure 3.3 shows a schematic diagram of the reference electrode used. The reference electrode consisted of a 50 cm long alumina tube (99.7 % pure; Multilab Ltd.), sealed at one end, with inner and outer diameters of 3 mm and 5 mm respectively. Near the closed end the alumina tube walls were ground down to a thickness of less than 0.3 mm in order to provide an ion conducting membrane. 0.3 g of salt of the same composition as the main electrolyte was put into the tube, which also contained 10 mol. % of AgCl (greater than 99% pure; Acros Organics). Prior to three-electrode experimentation, the end of this tube containing the salt was submerged in the molten electrolyte. Once the salt inside the tube had melted, silver wire (99.99% pure; Advent Research Materials Ltd.) was submerged in the salt inside the tube. Stainless steel wire was used to connect the silver wire to the potentiostat-connecting wire. The reference electrode was then hermetically sealed with a silicone bung through which the stainless steel wire passed as shown in Figure 3.3.

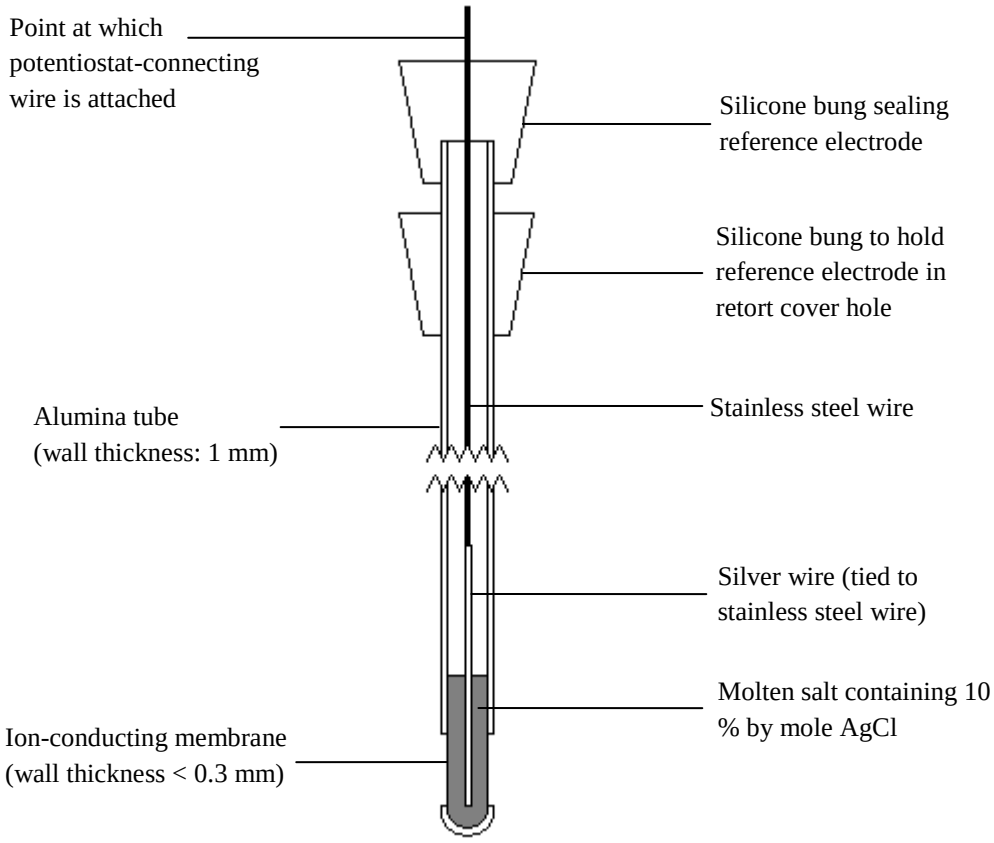

Figure 3.3: Schematic diagram of the high temperature Ag/AgCl reference electrode used in this study. NB. This diagram is not to scale.

Use of a reference electrode in a three-electrode system allows issues associated with iR drop to be addressed in a controlled manner. Considering a two-electrode system, if a significant electrical resistance is present or a large current is flowing, the attained voltage can be markedly different from the applied voltage due to ohmic losses (Heinze et al., 1984):

$$E_{actual} = E_{applied} - iR \qquad (3.1)$$

Where: E_{actual} = practically realised cell voltage, $E_{applied}$ = set cell voltage, i = current and R = resistance.

Therefore, if the electrical resistance across the cell is 0.5 Ω, a current flow of 1 A could lead to a voltage drop of 0.5 V (Chen et al., 2000). Furthermore, the current flow can vary during

electrolysis, which would cause the value of iR to change; hence the actual voltage would also alter. Another difficulty associated with the two-electrode system is that if the counter electrode reaction changed, the potential of the working electrode would also change in order to keep a constant potential difference. As a consequence, it is frequently difficult to obtain a fixed working electrode potential in two-electrode electrolysis.

Using a reference electrode in three-electrode electrolysis overcomes these problems by measuring the working electrode potential with respect to a constant reference potential. Very little current is allowed to flow through the reference electrode by the potentiostat, which means that the activities of the species inside the reference electrode do not change with time, leading to a constant potential (Monk, 2001). The very low current also means that any iR drop between the working and reference electrodes is minimised.

3.5 Three-Electrode Experiments

Three main types of three-electrode experiment were carried out in this study: cyclic voltammetry, chronoamperometry and galvanostatic chronopotentiometry. In all of the three-electrode experiments, control and data logging was carried out using a PGSTAT30 AUTOLAB potentiostat (Ecochemie) controlled by a computer using General Purpose Electrochemical Software (GPES). If it was considered that the current was likely to exceed 1 A, an attached current booster was used to raise the maximum current limit from 1 A to 10 A. For convenience, the acronyms WE, CE and RE are frequently used in figure captions throughout this thesis to refer to the working, counter and reference electrodes respectively. The three types of three-electrode experiment shall now be discussed in turn.

3.5.1 Cyclic voltammetry

For cyclic voltammetry, a stainless steel wire or platinum wire was used as the working electrode, which was submerged to as small a depth as practicable, whilst a stainless steel rod was used as the counter electrode. In every experiment, the counter electrode was immersed to

such a depth as to provide a substantially larger surface area in contact with the electrolyte, in comparison to the working electrode. The working electrode area was typically of the order of 0.1 cm^2, whilst the counter electrode surface area generally exceeded 5 cm^2. Thus the effect of any reactions occurring at the counter electrode was minimised in each experiment. The reference electrode used was the high temperature Ag/AgCl reference electrode described above.

Cyclic voltammetry was used for both qualitative and quantitative analyses of electrochemical reactions in various molten salt electrolytes. In this type of experiment, the potential of the working electrode is linearly varied at a constant, user-defined scan rate, whilst the direction of potential variation can be reversed and repeated in a cyclic manner. For studying cathodic reactions, the potential is made more negative from the starting potential until the first vertex potential is reached, at which point the direction of the potential scan is reversed. The potential is then made more positive at the same rate until the second vertex potential is reached, and the potential scan direction is reversed again.

One potential scan or cycle of cyclic voltammetry is complete once the starting potential is re-attained and a number of cycles can be performed to probe the response of the system. An example of a cyclic voltammogram for an electrochemically reversible system is given in Figure 3.4. Any mass transfer-limited reactions that occur during the cycles are indicated by the current becoming gradually independent of the potential variation, which is often observed following a current peak (Kissinger and Heineman, 1983). If a reaction is not limited by mass transfer, and all of the reactants and products are soluble in the electrolyte, then a peak would not form and merely an increase in current would be observed.

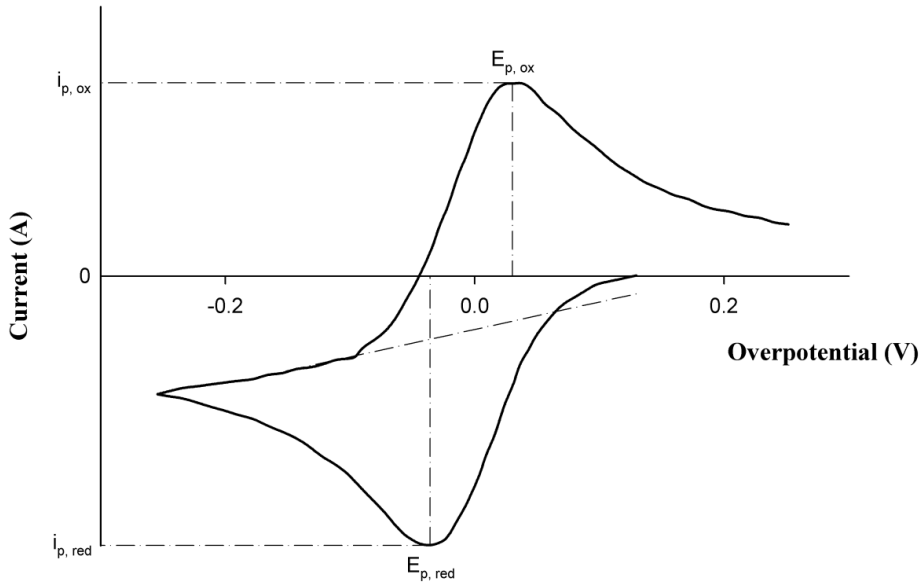

Figure 3.4: Example of a cyclic voltammogram for an electrochemically reversible system. Adapted from Fisher (1996).

In order to help elucidate the reactions responsible for current variations in cyclic voltammetry, four main approaches were employed. Firstly, the potential was held at certain user-defined values for a set period of time during a potential scan, after which the scan was allowed to continue. Holding the potential would allow reactions taking place at that potential to occur during the holding period, and the remainder of the potential scan, and possibly subsequent scans, would be affected as a result of this. An example of this is shown in Figure 3.5, where the second scan of cyclic voltammetry was held at a potential of -1.90 V vs. Ag/AgCl for 10 seconds. When the potential was held during the second scan, the heights of the anodic peaks labelled A1, A3 and A4 were considerably greater than in the first and third scans during which the potential was not held. A detailed discussion of the behaviour of this system is given in Chapter 4.

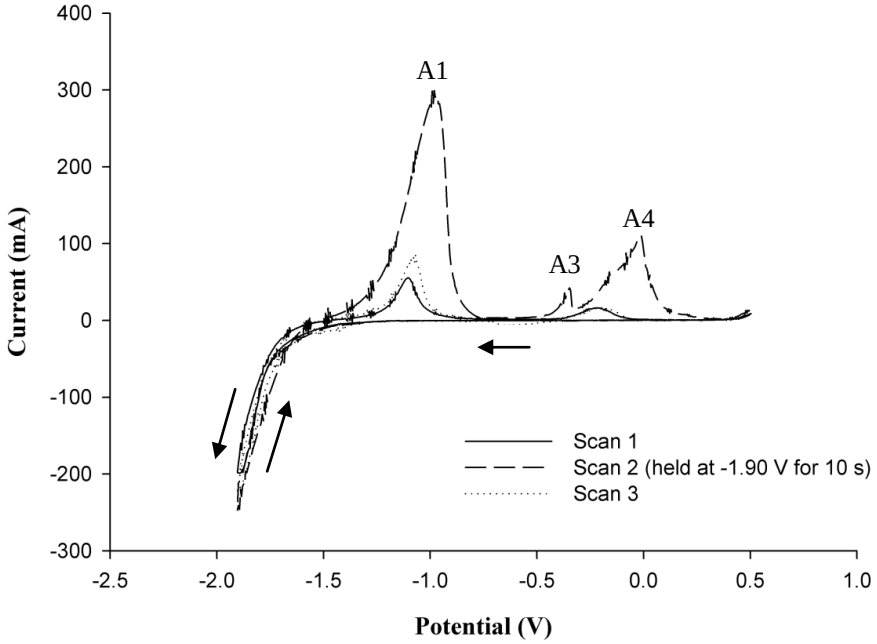

Figure 3.5: Cyclic voltammograms obtained using a platinum wire working electrode in a Li_2CO_3-Na_2CO_3 molten salt (molar ratio of 52:48), showing the effect of holding the potential at -1.90 V for 10 seconds during the second scan. Temperature: 703 °C; atmosphere: CO_2; scan rate: 100 mV/s; WE diameter: 0.25 mm; WE immersion depth: ca. 3.4 cm; CE: 6 mm diameter stainless steel rod; Ag/AgCl membrane RE.

Secondly, the direction of the potential scan could be reversed at a given potential at any point during the cathodic sweep. This would allow the potential scan to be reversed prior to a certain peak, for example, and the response of the reverse scan in light of this reversal could be noted. Figure 3.6 shows an example of this approach, where the second potential scan was reversed at a potential of -0.570 V vs. Ag/AgCl. The number and magnitude of the anodic peaks were observed to decrease as a result of this. Please refer to Section 6.2.2 for a more detailed discussion of this system.

Thirdly, the scan rate was varied and the changes to the voltammogram noted. For instance, for a reversible, mass transfer-limited reaction, the peak height is proportional to the square root of the scan rate (Kissinger and Heineman, 1983).

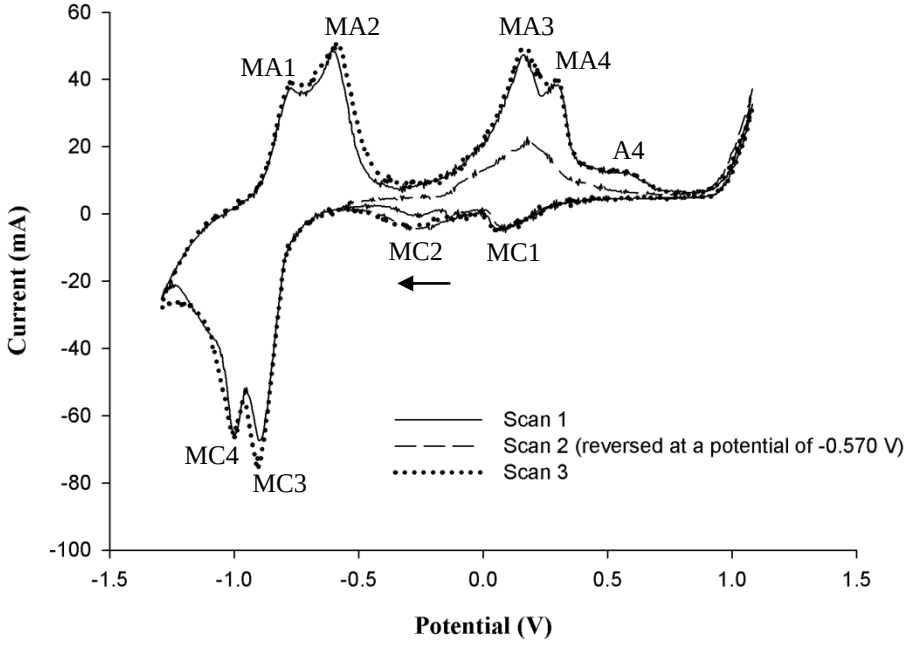

Figure 3.6: Cyclic voltammograms obtained from a Li_2CO_3-K_2CO_3 molten salt (molar ratio of 62:38) at a temperature of 708 °C under a CO_2 atmosphere. Note that the second potential scan was reversed at a potential of -0.570 V. Scan rate: 100 mV/s; WE: 0.25 mm diameter stainless steel wire; WE immersion depth: ca. 2.2 cm; CE: 6 mm diameter stainless steel rod; Ag/AgCl membrane RE.

Fourthly, for studies where platinum working electrodes were used, Q^+/Q^- (the ratio of the anodic charge passed to the cathodic charge passed) was calculated from cyclic voltammograms. This gave an indication of the proportion of cathodic products that remained at the working electrode surface to be re-oxidised during the anodic sweep. More details concerning this are given in Section 4.2.1.

3.5.2 Chronoamperometry

For chronoamperometry, a stainless steel rod was used as the counter electrode, whilst the reference electrode used was the same high temperature Ag/AgCl reference electrode described above. The working electrode material depended on the specific experiment being carried out.

In chronoamperometry, the potential of the working electrode is set at a constant value for a specific period of time and the variation of current with time is recorded. In this research, the charge passed during this process was recorded by the GPES software. Chronoamperometry was mainly used for three purposes. Firstly, it was used to test whether carbon was produced at certain cathodic peak potentials seen in cyclic voltammograms, using a stainless steel or platinum wire as the working electrode. Secondly, the technique was used to generate deposits of carbon for further analysis, where a mild steel rod was used as the working electrode. Thirdly, the technique was used to generate carbon for re-oxidation in galvanostatic chronopotentiometry, again using a mild steel rod as the working electrode.

Mild steel could potentially become corroded in a molten carbonate salt electrolyte. However, it was deemed an acceptable working electrode material, since the cathodic potential applied to it probably protected it from corrosion to some extent. The mild steel immersed in the salt also became covered by a protective layer of carbon as carbon electro-deposition proceeded.

3.5.3 Galvanostatic chronopotentiometry

Galvanostatic chronopotentiometry was used to re-oxidise carbon deposits produced in chronoamperometry; therefore a mild steel rod coated with a carbon deposit was used as the working electrode. A graphite counter electrode was used. A constant current was set for a specific period of time and the variation of potential with time was recorded, typically yielding a chronopotentiogram with several plateaux; an example is shown in Figure 3.7. In any given galvanostatic chronopotentiometry experiment, once the potential versus time trend had reached its final plateau, it was considered that all of the carbon had been oxidised. By dividing the charge passed during the deposition of carbon by the charge passed during re-oxidation (the charge passed prior to the final plateau being reached), Q^+/Q^- was calculated. Chronopotentiograms were also analysed to provide an insight into the electrochemical oxidation mechanism of electro-deposited carbon.

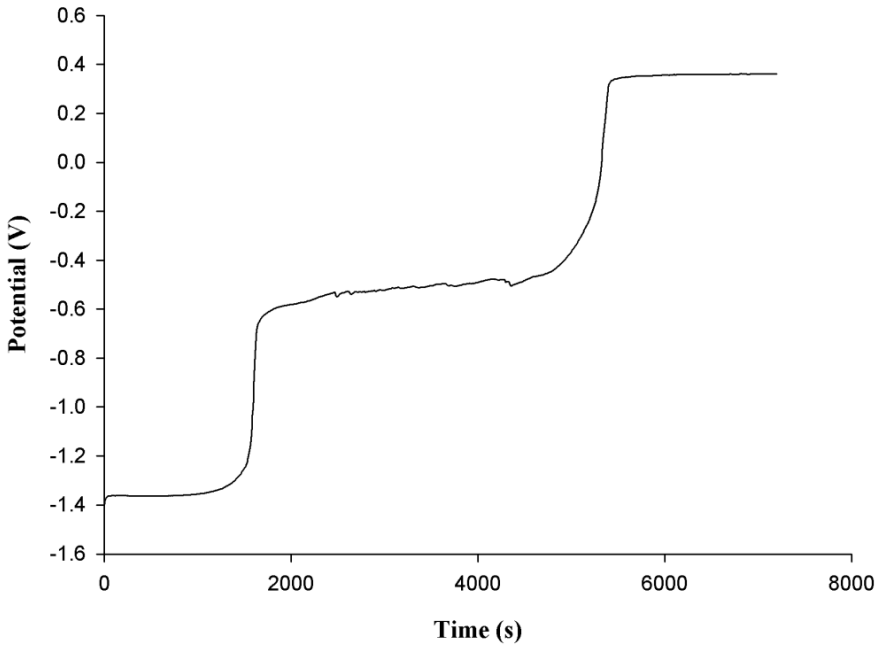

Figure 3.7: Variation of potential versus time for the re-oxidation of electro-deposited carbon in a Li_2CO_3-Na_2CO_3 (molar ratio: 52:48) molten salt mixture at a constant current of 150 mA, at a temperature of 747 °C under a CO_2 atmosphere. WE: 5 mm diameter mild steel rod (with carbon deposit still attached); CE: 10 mm diameter graphite rod; Ag/AgCl membrane RE.

3.6 Two-Electrode Electrolysis

Two-electrode electrolysis was carried out using an Agilent E3633A 20 A/10 V autoranging DC power supply and a laptop with an EXCEL add-on to collect data from the instrument. The cathode and anode materials were a mild steel rod and a stainless steel rod respectively. The potential difference was set at a constant value of 4 V in this study. A value of 4 V was chosen due to the fact that Siambun (2011b) was consistently able to obtain carbon deposits at this potential difference from the Li_2CO_3-K_2CO_3 electrolyte. Electrolysis was typically carried out for between 30 to 60 minutes to produce carbon deposits.

As mentioned in Section 3.4.2, one major disadvantage of two-electrode electrolysis is that the cathode potential is not controlled with respect to a reference electrode of fixed potential. Thus the cathode potential may shift during electrolysis, depending on the anode potential and the iR

drop. As a consequence, the electrochemical reactions occurring at the cathode are more difficult to control.

However, there are two main advantages in using two-electrode electrolysis, particularly from an industrial perspective. Firstly, reference electrodes in molten salts can only be used for limited periods of time before replacements are needed, which would be impractical for industrial application (Jewell, 2009). Secondly, currents in industrial molten salt processes can be high, of the order 10^3-10^5 A, which would be costly in terms of equipment if a three-electrode system were to be used (Wu et al., 2008).

3.7 Sample Analysis

3.7.1 Deposit handling

This sub-section describes the handling of deposits produced from electrolysis prior to further analysis via the techniques described in later sub-sections. Deposit handling was only carried out if further analysis of the deposit in question was desired; if a deposit was produced for the purposes of re-oxidation via galvanostatic chronopotentiometry (see Section 3.5.3), then the deposit was not processed in this manner.

After a deposit was produced during two or three-electrode electrolysis, the electrode was first removed from the electrochemical cell and allowed to cool. Once cooled, the deposit on the end of the electrode was immersed in magnetically stirred water held in a beaker at room temperature. A magnetic stirrer/hotplate (Gallenkamp) was used for stirring, albeit the hotplate function was not used. This stirring process was continued until all of the deposit became suspended in the water. The duration of stirring depended on the nature and quantity of the deposit but typically exceeded 24 hours.

Having removed the deposit from the electrode, the deposit suspension was filtered using a funnel containing a borosilicate filter of porosity grade 3 (Fisher Scientific; pore size of 15-40 μm). The deposit trapped by the filter was then washed with 20 mL of 0.56 mol/L hydrochloric

acid, which was created by diluting 35.5-37.5 % hydrochloric acid (Fisher Scientific) with distilled water. Next, the deposit was washed with 100 mL of distilled water. Finally, the deposit in the filter was dried overnight in a dryer (LTE Scientific Ltd.; model OP 100) at 60 °C.

As soon as the filter containing the deposit was taken out of the dryer, the deposit, which was usually in powder form by this point, was weighed and placed in a sealable glass vial. After carrying out this deposit handling procedure, samples of the deposit were then subjected to the analytical techniques described in the remainder of this section.

3.7.2 Combined thermogravimetric analysis (TGA) and differential scanning calorimetry (DSC)

Simultaneous thermogravimetric analysis (TGA) and heat-flux differential scanning calorimetry (DSC) of deposits was carried out using a TA Instruments SDT Q600. Note that heat-flux DSC is also known as calorimetric differential thermal analysis (Brown, 2001). This combined method of analysis was primarily used to ascertain the carbon content of a given sample, as well as the heat released when the sample was combusted.

In TGA, the change in weight of a sample is monitored over time as the temperature is varied according to a user-defined program (Davies, 2012). The sample weight is measured by the instrument using a microbalance. Furthermore, a controlled purge gas composition (nitrogen or air in this study) is supplied to the furnace in which the experiment is carried out.

When heat-flux DSC is carried out in the SDT Q600, the temperature difference between the sample pan and a reference pan is monitored using thermocouples, which are located under the pans on the weighing beams. When no transitions are taking place in the sample, the sample temperature tracks the reference temperature. However, if an exothermic reaction occurs, for example, the sample temperature would exceed the reference temperature. After the reaction is complete, the sample temperature would return to a similar temperature to the reference. This is illustrated in Figure 3.8(a). The instrument calculates the temperature difference between the

sample and reference to produce a plot of temperature difference against time; see Figure 3.8(b). For exothermic reactions, the observed peak in the temperature difference versus time plot points upwards and vice versa for endothermic reactions (Davies, 2012).

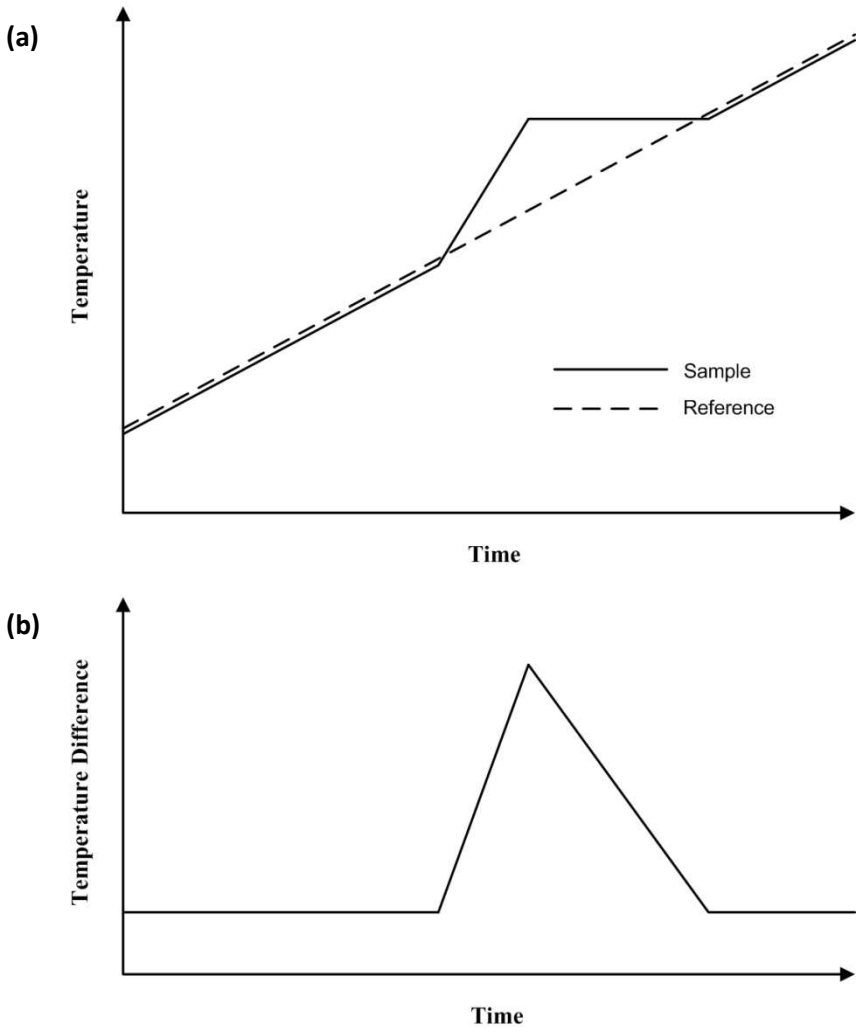

Figure 3.8: Hypothetical trends obtained during an exothermic transition in DSC, for (a) the sample and reference temperatures versus time, and (b) the temperature difference between the sample and reference versus time (adapted from Davies, 2012).

From the temperature difference signal obtained, the instrument can calculate the heat flow using the following equation (Brown, 2001):

$$\Delta H_s = (K \times A_s)/m_s \qquad (3.2)$$

Where: ΔH_s = enthalpy change of the thermal event; K = calibration factor; A_s = area under the endotherm/exotherm in the graph of ΔT vs. T obtained from the sample; m_s = sample mass.

The calibration factor K is determined by calibrating the instrument over its full operating temperature range. Sapphire was used when calibrating the heat-flux DSC function of the SDT Q600 used in the present research.

Note that the heat-flux DSC method described here has a different operating principle to the power-compensated DSC method, which was not used in this research. In power-compensated DSC, the DSC instrument endeavours to maintain the sample and reference materials at the same temperature throughout the user-defined temperature programme (Brown, 2001). Any differences between the power supplied to the sample and the reference are recorded. Therefore, any thermal events that occur in the sample appear as either exothermic or endothermic deviations of the sample heat flow from the DSC baseline heat flow (Brown, 2001). Power-compensated DSC has the advantage in that its response is faster than that of heat-flux DSC, albeit it is influenced more by the thermal properties of the sample.

The SDT Q600 uses a null position balance: the position of the pans in the furnace undergoes negligible change as the weight of the sample changes. This is important for three main reasons (Davies, 2012):

- The sample and reference beams barely move, which helps to maintain DSC baseline stability.
- The sample cannot move into different hot zones in the furnace as its weight alters.
- Purge gas-sample interaction remains constant throughout the experiment.

In this study, two clean 90 μL alumina pans (TA Instruments) were used as the sample and reference pans. The program used by the SDT Q600 was set as follows:

1. Select gas: nitrogen.

2. Ramp temperature to 200 °C at 20 °C/min.
3. Hold temperature at 200 °C for 15 minutes.
4. Select gas: air.
5. Ramp temperature to 1000 °C at 20 °C/min.

Stages 1 to 3 of the program ensured that any subsequent mass losses during step 5 were not due to the loss of adsorbed water from the sample. Compressed air (Air Products Ltd.) and nitrogen (99.999 % pure; Air Products Ltd.) were used as purge gases.

3.7.3 X-ray diffraction (XRD)

X-ray diffraction (XRD) is a non-destructive analytical technique used to analyse the crystal structures and chemical composition of a given sample. The principles of operation can be summarised as follows. When a sample is irradiated with X-rays, the incident radiation causes the sample electrons to move in a sinusoidal manner at the same frequency as the radiation. Due to the periodic acceleration and deceleration of the sample electrons, new X-rays are emitted from the sample, which is known as Thomson scattering (Waseda et al. 2011). The constructive and destructive interference of the scattered X-rays results in a diffraction pattern that is characteristic of the crystal structures and substances present in the sample. (Suryanarayana and Grant Norton, 1998).

X-rays are diffracted in specific directions according to the wavelength of the incident X-rays and the nature of the sample, in particular the spacing of the inter-atomic planes. Bragg's Law quantifies this (Suryanarayana and Grant Norton, 1998):

$$n\lambda = 2d \sin \theta \qquad (3.2)$$

Where: n = order of reflection, λ = wavelength of the incident radiation, d = distance between two crystal planes and θ = angle between the atomic planes and the incident wave.

XRD produces a spectrum of characteristic peaks at specific diffraction angles, which are plotted on axes of intensity versus diffraction angle. The measured intensity is proportional to the number of X-ray photons that have been counted for each angle 2θ. By comparing the spectrum obtained with those of known substances, the crystal planes and substances responsible for each intensity peak in the spectrum can be ascertained. Even amorphous substances can be studied using XRD to yield useful information. Typically, X-ray peaks broaden when the crystallite or grain size is lower than 0.1 μm, and the extent of broadening increases as the crystallite size decreases (Suryanarayana and Grant Norton, 1998).

In this study, XRD of deposits was carried out using a Hiltonbrooks X-ray Diffractometer, which was installed with a DG3 Cu-Kα generator and PW1050 goniometer. The goniometer was set to rotate at 2° 2θ/min, with a range of 0° to 80° and a step size of 0.05°. Jade 5.0 XRD analysis software with a 2004 powder diffraction file was used to interpret the diffraction pattern obtained.

Deposit samples were prepared for XRD analysis by first grinding to a fine powder in a pestle and mortar; this powder was then placed in the cavity of an aluminium sample holder to be used in the instrument.

3.7.4 Scanning electron microscopy (SEM), back-scattered scanning electron microscopy (BSEM) and energy-dispersive X-ray (EDX) spectroscopy

In the present work, scanning electron microscopy (SEM) was used to obtain high-resolution magnified images of the surface topography of deposit samples. Back-scattered scanning electron microscopy (BSEM) was also used to obtain highly magnified images of the surface topography of samples, but it was also used to show regions of the sample surface with different elemental compositions. Energy-dispersive X-ray (EDX) spectroscopy, also referred to as energy dispersive spectroscopy (EDS), was used to analyse the elements present in the deposit samples. The apparatus used to carry out EDX spectroscopy was located in the same instrument used to do SEM and BSEM.

In simple terms, electron microscopy is the production of magnified images of specimens using an electron beam. Electrons have a significantly greater resolving power than visible light: an SEM has a resolving power of approximately 3 or 4 nm, whereas the resolving power of a modern light microscope is around 200 nm at best (Fleger et al., 1993). The high resolving power of an SEM enables the production of highly magnified, high-resolution images.

Figure 3.9 shows a simple schematic representation of an SEM. The first stage in generating an image of the specimen is the production of a beam of electrons in an electron gun. This beam is controlled by a series of electromagnetic lenses placed along the path of the beam: the condenser lenses condense the beam, and the beam is focussed on a very fine point on the specimen via the objective lens. Note that an SEM operates under a high vacuum, so that air molecules do not interfere with the electron beam. The scan coils, located in the vicinity of the objective lens, produce a varying magnetic field and this is used to deflect the beam of electrons back and forth in a controlled raster pattern (Fleger et al., 1993).

As the beam scans across the specimen, the electrons undergo a complex series of reactions with the sample. Most of the kinetic energy of the primary electrons is converted to heat in the sample, but a small proportion of this energy may escape in the form of secondary electrons, light and X-rays. This is termed inelastic scattering: the primary electrons from the beam lose energy through interactions with the sample. (Goodhew et al., 2001). In addition, a proportion of the electrons from the primary beam are deflected out of the specimen by collisions with the specimen atoms; these electrons are referred to as back-scattered electrons (Watt, 1997). Back-scattered electrons result from the elastic scattering of primary electrons, where the electrons do not lose detectable amounts of energy in their interactions with sample (Goodhew et al., 2001).

The principal difference between back-scattered electrons and secondary electrons is their energy. Electrons that are emitted from the specimen with energies of less than or equal to 50 eV are termed secondary electrons, whilst electrons with higher energies are considered back-scattered electrons (Thornton, 1968). Another difference is that secondary electrons tend to be

emitted from a few atomic layers below the sample surface, whilst back-scattered electrons can arise from depths of several nanometres below the sample surface (Croft, 2006).

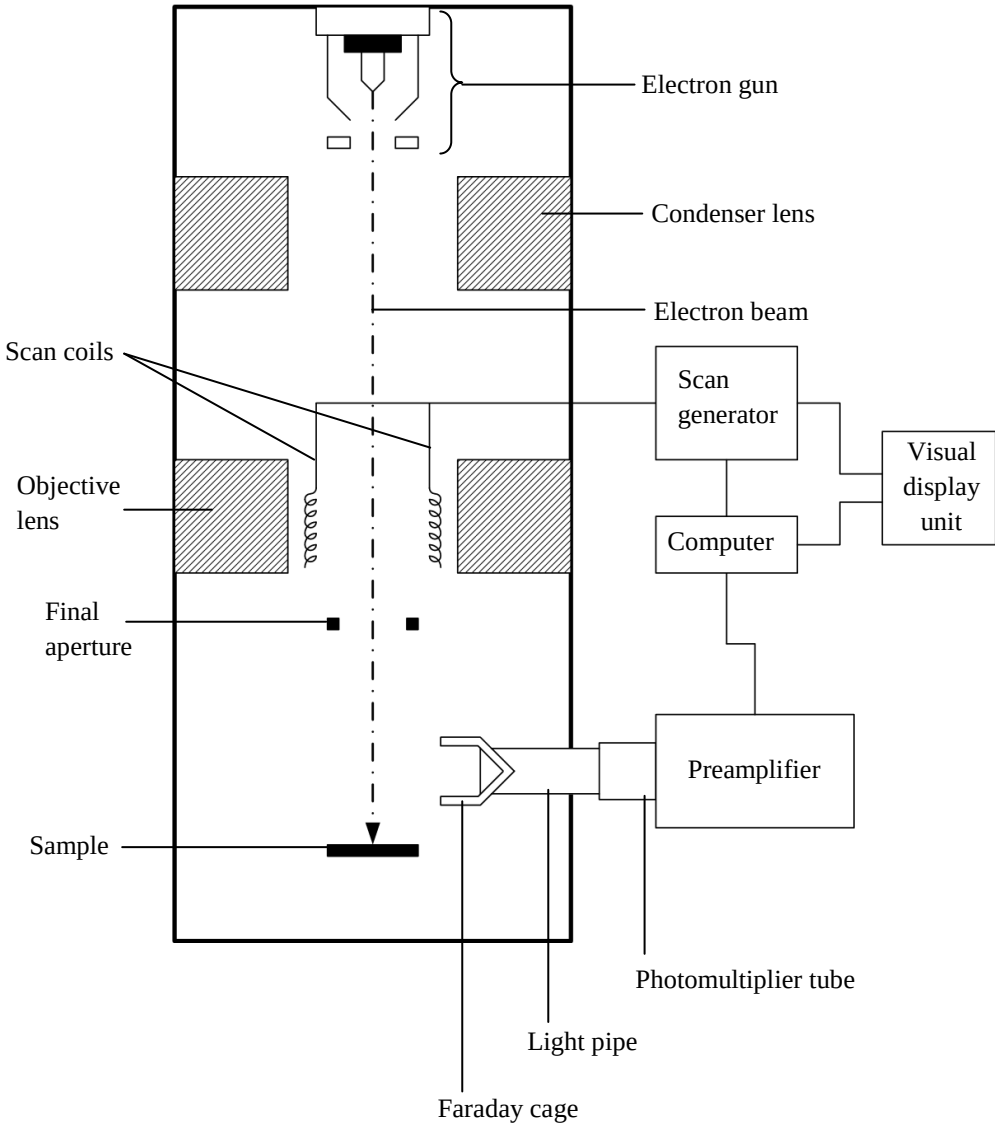

Figure 3.9: Schematic representation of the fundamental components of a scanning electron microscope (SEM). Adapted from Fleger et al. (1993).

Depending on the detector selected, either the secondary or back-scattered electrons are collected, converted to a voltage signal and then amplified. This signal is used to construct the micrograph on the display screen of the controlling computer; the brightness of each point in the resulting micrograph corresponds to the number of electrons that are detected at that point. Thus, a micrograph is constructed from thousands of points of varying brightness (Fleger et al., 1993).

The micrograph generated will exhibit different features depending on whether secondary or back-scattered electrons are used to generate it. When secondary electrons are collected, the SEM micrograph corresponds to the surface topography of the sample. For instance, if at a given instant the beam is incident on a projection on the surface of the specimen, a substantial number of secondary electrons will be detected, resulting in a large voltage and consequently a bright point on the micrograph. The reverse is true if the beam is incident on a depression in the sample: fewer secondary electrons will be detected, thus resulting in a lower voltage and a darker spot on the micrograph. Therefore, an SEM micrograph represents a topographic 'map' of the sample surface (Fleger et al., 1993).

When back-scattered electrons are collected, the BSEM micrograph clearly indicates regions of the sample surface with different atomic numbers, as well as the topography. As the atomic number of the back-scattering atoms increases, the intensity of back-scattered electrons increases sharply (Watt, 1997). As a consequence, regions of lower atomic number appear darker than those of higher atomic number. For instance, carbon-rich areas would appear darker than iron-rich areas. Furthermore, areas of higher elevation appear brighter than lower areas with the same elemental composition, since more electrons reach the detector from the higher regions. Since BSEM micrographs indicate the regions of the sample with different elemental compositions, they are useful for determining where best to conduct EDX spectroscopy of the sample, which shall now be discussed.

EDX spectroscopy is carried out in the same apparatus as SEM, with special accessory attachments. The technique is used to determine the elements present in the area of specimen-electron beam interaction based on the characteristic X-rays emitted from the sample. X-rays are emitted from the sample as a result of inelastic scattering: the electron beam causes electrons to be ejected from the sample, leading to vacancies in the electronic structures of atoms. A vacancy in the inner orbital shell of an atom is filled by an electron from a higher energy shell, and the energy difference between the shells can be emitted as an X-ray (Fleger et al., 1993). The energies and wavelengths of these X-rays are characteristic of the element producing them. Therefore, by detecting and analysing these X-rays, EDX spectroscopy

permits the user to determine the elements present in the sample, in addition to the quantity and distribution of these elements (Fleger et al., 1993).

EDX spectroscopy is very advantageous in that it allows composition to be measured on a spatial basis: the composition of different parts of the sample may be compared by changing the location upon which the electron beam is incident. However, the analytical spatial resolution of EDX spectroscopy (5 nm) is slightly poorer than that of SEM (4 nm) (Fleger et al., 1993). Another disadvantage of EDX spectroscopy is that it cannot detect the element lithium (Croft, 2006). Lithium compounds were a major constituent of several electrolytes studied in the present investigation; not being able to detect the element was thus a major disadvantage from the point of view of this study.

In the present work, an FEI ESEM instrument was used to conduct SEM, BSEM and EDX spectroscopy. The instrument was fitted with a hairpin thermionic emission source and an EDAX Genesis 2000 EDX detector. The electron acceleration voltage used was normally 25 kV. The working distances used were normally 10 mm for SEM and 11.5 mm for BSEM and EDX spectroscopy. Inside the instrument, powdered samples were held on aluminium stubs by means of double-sided carbon sticky tabs. For a given sample, BSEM and EDX spectroscopy were carried out first, before coating the sample with a thin layer of gold and carrying out SEM. Gold coatings were applied to the carbon samples prior to SEM in order to improve their electrical conductivity and hence enhance the image quality.

CHAPTER 4

REACTIONS ASSOCIATED WITH THE ELECTRO-DEPOSITION OF CARBON AND ITS RE-OXIDATION IN MOLTEN Li_2CO_3-Na_2CO_3

In this fourth chapter, the results of a study of carbon electro-deposition and re-oxidation reactions are presented. The more general aspects of these processes are focussed on here; the effect of different cations in the electrolyte is considered in Chapter 5. This chapter begins by giving the motivations for studying this topic. Subsequent sections cover the findings obtained from the cyclic voltammetry of the molten Li_2CO_3-Na_2CO_3 electrolyte, where platinum was used as the working electrode material.

4.1 Reasons for Studying Carbon Electro-deposition and its Associated Reactions

At present, our understanding of the electro-deposition of carbon in molten carbonates, and the reactions associated with its re-oxidation, is relatively weak. Cyclic voltammetry is a useful tool for investigating this, as carbon deposits can be generated during the cathodic sweep and then re-oxidised during the anodic sweep. The resulting voltammograms can provide an abundant source of information concerning the nature of the electrochemical reactions occurring.

In order to properly study this topic, cyclic voltammetry must be conducted at working electrodes that are effectively inert over the experimental timescales considered. If the working electrode material is not inert in the molten carbonate electrolyte under consideration, then additional peaks will arise due to electrochemical interactions between the working electrode material and the electrolyte. These additional peaks make it difficult to identify the peaks associated with carbon and its re-oxidation, as well as peaks related to other reactions associated with the electrochemical decomposition of the electrolyte.

In the literature published to date, Ingram et al. (1966), Bartlett and Johnson (1967), Lantelme et al. (1999), Kaplan et al. (2002) and Le Van et al. (2009) have presented voltammetric studies of carbon electro-deposition carried out using inert electrode materials. The key findings of Ingram et al. (1966) and Le Van et al. (2009) are given in Section 2.5.1 of the present thesis. Ingram et al. (1966) obtained linear sweep voltammograms in Li_2CO_3 and Li_2CO_3-Na_2CO_3-K_2CO_3 at gold working electrodes, whilst Bartlett and Johnson (1967) obtained a linear sweep voltammogram at a platinum working electrode in Li_2CO_3-Na_2CO_3. Lantelme et al. (1999), Kaplan et al. (2002) and Le Van et al. (2009) all studied the cyclic voltammetry of Li_2CO_3-Na_2CO_3-K_2CO_3 using vitreous carbon working electrodes.

Due to the fact that their works were published more than forty years ago, Ingram et al. (1966) and Bartlett and Johnson (1967) only used the technique of linear sweep voltammetry. Bartlett and Johnson (1967) only carried out one sweep in the cathodic direction, which limited the usefulness of the work in that it provided no information about carbon re-oxidation. Ingram et al. (1966) on the other hand carried out a cathodic sweep, depositing carbon that they then re-oxidised by performing a sweep in the anodic direction. By carrying out anodic stripping coulometry of electro-deposited carbon they were able to provide supporting evidence for their explanation of the anodic peaks that they observed. Thus, the work of Ingram et al. (1966) is the more useful of these two papers. However, neither Bartlett and Johnson (1967) nor Ingram et al. (1966) reported the effect of changing parameters such as the negative potential limit of the voltammogram or the scan rate.

The more recent works of Lantelme et al. (1999), Kaplan et al. (2002) and Le Van et al. (2009) did report the effect of a number of simple manipulations in cyclic voltammetry, such as holding the potential or making the negative potential limit more negative. However, they did not use the technique of cyclic voltammetry to anywhere near its full potential. These authors generally did not present much evidence for their attribution of anodic peaks to specific reactions. On the other hand, workers considering corrosion in molten carbonate fuel cells (MCFCs), such as Keijzer et al. (1999), did tend to subject their systems to more rigorous

investigations via cyclic voltammetry, but since their purpose was not to investigate carbon electro-deposition their works are of only limited value to the present topic.

The work described in this chapter seeks to address the above limitations by presenting the first truly rigorous study of carbon electro-deposition and its re-oxidation via cyclic voltammetry, in the mixed carbonate electrolyte Li_2CO_3-Na_2CO_3. Notably, this is also the first time that such a study has been conducted using Li_2CO_3-Na_2CO_3. Most authors preferred to investigate the Li_2CO_3-Na_2CO_3-K_2CO_3 electrolyte only, which was principally due to the fact that it has a lower eutectic temperature than Li_2CO_3-Na_2CO_3.

4.2 Cyclic Voltammetry of Li_2CO_3-Na_2CO_3 at Platinum Working Electrodes

The cyclic voltammetry of Li_2CO_3-Na_2CO_3 (molar ratio of 52:48) was carried out using platinum working electrodes at temperatures of 599 °C and 703 °C. 600 °C and 700 °C were the desired electrolyte temperatures. However, it was difficult in practice to obtain the exact temperatures required due to the fact that the electrolyte temperature could only be adjusted by changing the furnace set temperature. The furnace temperature controller had an accuracy of ±1 °C, although the electrolyte temperature was also influenced by factors such as the effectiveness of the furnace insulation and the ambient temperature, which were difficult to keep constant for all experiments. Figures 4.1(a) and 4.1(b) show voltammograms obtained at scan rates of 10 mV/s and 1000 mV/s respectively, at a temperature of 599 °C. Figure 4.2 shows voltammograms obtained at a scan rate of 10 mV/s and a temperature of 703 °C.

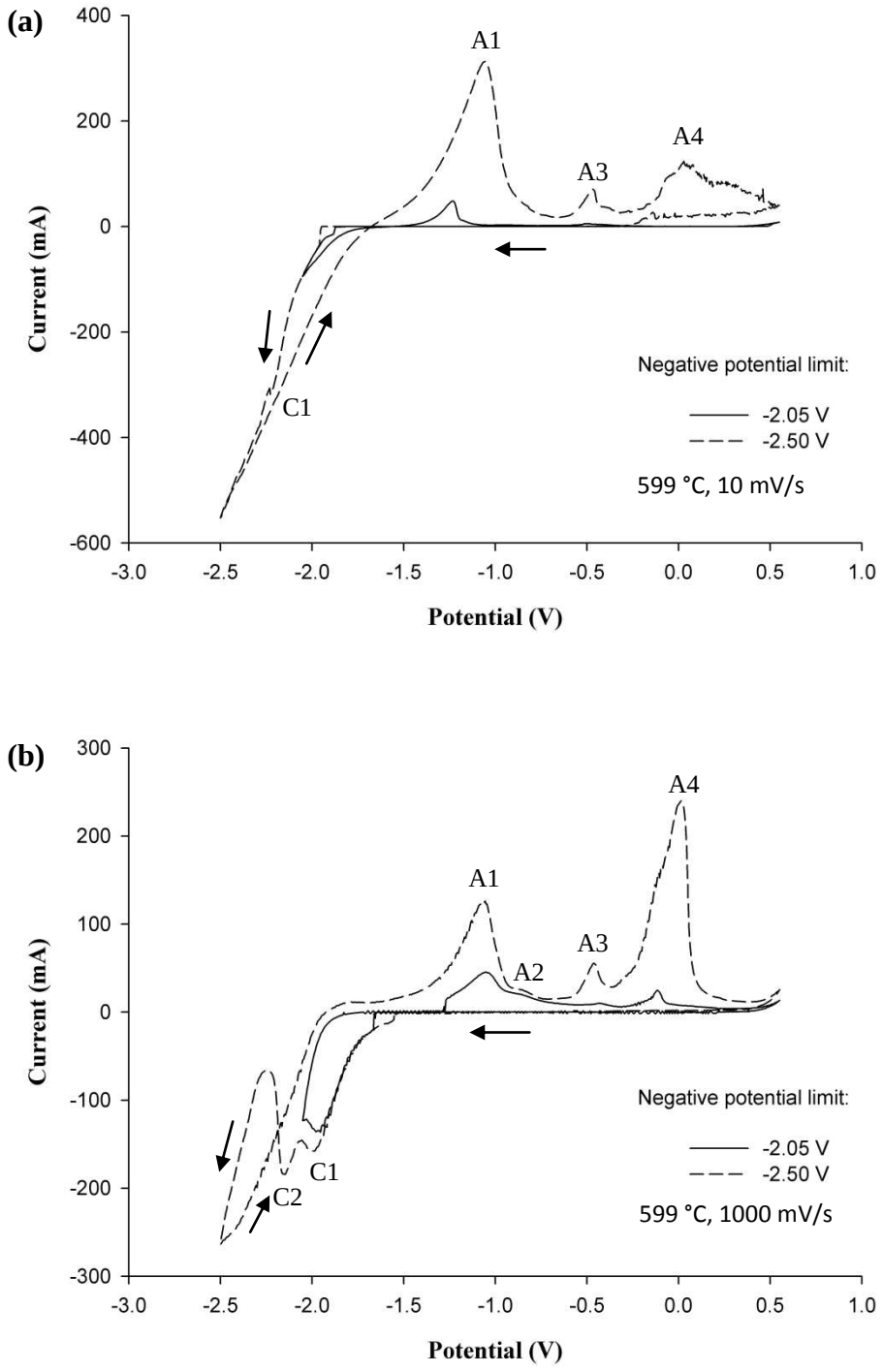

Figure 4.1: Cyclic voltammograms obtained using a platinum wire working electrode in a molten Li_2CO_3-Na_2CO_3 electrolyte (molar ratio of 52:48) at 599 °C, at scan rates of (a) 10 mV/s and (b) 1000 mV/s, for negative potential scan limits of -2.05 V and -2.50 V. Atmosphere: CO_2; WE diameter: 0.25 mm; WE immersion depth: ca. 0.9 cm; CE: 6 mm diameter stainless steel rod; RE: alumina membrane Ag/AgCl.

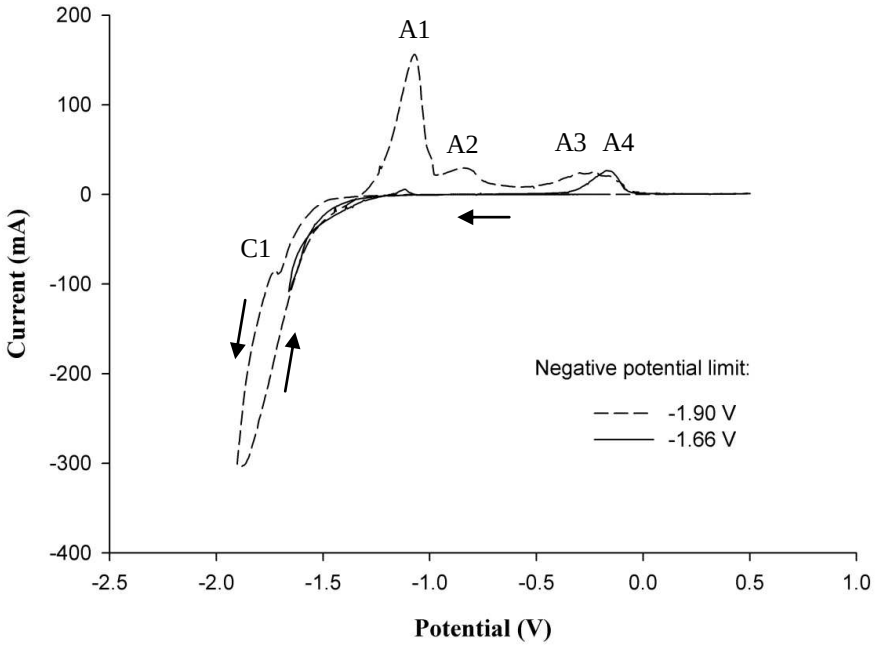

Figure 4.2: Cyclic voltammograms obtained using two different negative potential limits, for a Li_2CO_3-Na_2CO_3 molten salt mixture (molar ratio of 52:48) at a temperature of 703 °C under a CO_2 atmosphere. Scan rate: 10 mV/s; WE: 0.25 mm diameter platinum wire; WE immersion depth: ca. 3.4 cm; CE: 6 mm diameter stainless steel rod; alumina membrane Ag/AgCl RE.

4.2.1 Cathodic phenomena

Several prominent features are observed in Figures 4.1 and 4.2. Firstly, no cathodic peaks are visible prior to the start of the current wave at around the cathodic limit. This would imply that platinum is inert in Li_2CO_3-Na_2CO_3, at least within the relatively short experimental timescale considered here. Thus the anodic peaks are all likely to have arisen from the oxidation of products formed at the cathodic limit. This conclusion is reasonable based on the appearance of voltammograms obtained at other so-called inert electrode materials such as gold (Ingram et al., 1966) and vitreous carbon (Le Van et al., 2009), which also do not exhibit any cathodic peaks. Please refer to Figures 2.6, 2.7 and 2.9 in this thesis for examples of voltammograms obtained at vitreous carbon and gold working electrodes. The absence of any cathodic peaks prior to the current wave at the cathodic limit is entirely consistent with the linear sweep

voltammogram obtained by Bartlett and Johnson (1967), who used a platinum working electrode in molten Li_2CO_3-Na_2CO_3 at a temperature of 550 °C.

Lantelme et al. (1999) observed a cathodic peak prior to the cathodic limit when they conducted cyclic voltammetry at a platinum working electrode, at a temperature of 450 °C, in a Li_2CO_3-Na_2CO_3-K_2CO_3 molten salt; their voltammogram is shown in Figure 2.10 of this thesis. This cathodic peak was attributed to the following reaction:

$$PtO_3^{2-} + 4e^- \rightarrow Pt + 3O^{2-} \qquad (4.1)$$

Lantelme et al. (1999) made this attribution on the basis that Janz et al. (1963) observed the formation of Li_2PtO_3 when platinum was immersed in carbonate-based molten salts. However, the peak was very slight in comparison with all the other peaks, and it is likely that the formation of Li_2PtO_3 was slow due to the nobility of platinum metal. Therefore, considering the short experimental timescales used in the present work, it is reasonable that such a cathodic peak was not observed. Reaction 4.1 is evidently absent from both Figures 4.1 and 4.2.

Carbon electro-deposition probably occurred at the cathodic limit according to the following reaction (Ingram et al., 1966):

$$CO_3^{2-} + 4e^- \rightarrow C + 3O^{2-} \qquad (4.2)$$

The fact that cathodic loops were observed, as shown in Figures 4.1 and 4.2, indicates that a new phase was formed on the working electrode surface, which was very probably electro-deposited carbon. Cathodic loops form because the electro-deposition of carbon onto carbon usually requires a lower overpotential than electro-deposition onto a foreign substrate such as a metal. As a consequence of this, the rate of carbon electro-deposition increased as deposition progressed, leading to a higher reduction current at the same potentials after the scan direction reversed at the negative potential limit of the scan. Another explanation for the formation of

cathodic loops is that the surface area of the electrode has effectively increased after the electro-deposition of carbon.

Furthermore, carbon deposition has been physically observed to occur at potentials beyond the cathodic limit. At 703 °C, carbon was successfully electro-deposited onto platinum at a potential of -1.66 V vs. Ag/AgCl; note that this potential lies just prior to the small peak C1 in the cathodic current wave in Figure 4.2. At 599 °C and 703 °C, carbon deposits were obtained on mild steel rod working electrodes at potentials 0.6 V, 1.0 V and 1.4 V more negative than the potential at the start of the current wave at the cathodic limit (observed in cyclic voltammetry) – please see Chapter 7 for more details regarding these depositions.

The theoretical standard reaction potentials of possible cathodic reactions also corroborate well with the evidence for carbon deposition beyond the cathodic limit. In addition to Reaction 4.2 above, Le Van et al. (2009) suggested that the following three reactions could occur at the cathodic limit:

$$2Li^+ + 2CO_3^{2-} + 10e^- \rightarrow 6O^{2-} + Li_2C_2 \quad (4.3)$$

$$M^+ + e^- \rightarrow M \quad \text{(M represents an alkali metal)} \quad (4.4)$$

$$CO_3^{2-} + 2e^- \rightarrow CO + 2O^{2-} \quad (4.5)$$

If the oxidation of carbonate ions is used as the reference reaction:

$$CO_3^{2-} \rightarrow CO_2 + ½O_2 + 2e^- \quad (4.6)$$

Then Reactions 4.2 through 4.5 can be written as (where M represents an alkali metal):

$$3M_2CO_3 \rightarrow 3M_2O + 2CO_2 + O_2 + C \quad (4.7)$$

$$7Li_2CO_3 \rightarrow 6Li_2O + 5CO_2 + 2.5O_2 + Li_2C_2 \quad (4.8)$$

$$M_2CO_3 \rightarrow CO_2 + 0.5O_2 + 2M \quad (4.9)$$

$$2M_2CO_3 \rightarrow 2M_2O + CO_2 + 0.5O_2 + CO \quad (4.10)$$

Figure 4.3 shows the variation of standard potentials vs. CO_3^{2-}/CO_2-O_2 with temperature, for Reactions 4.2 through to 4.5. Evidently, at 599 °C and 703 °C, the three most favourable cathodic reactions are the formation of carbon, lithium carbide and carbon monoxide, all from the electro-reduction of Li_2CO_3. Carbon formation is the most favourable of the three reactions at both temperatures.

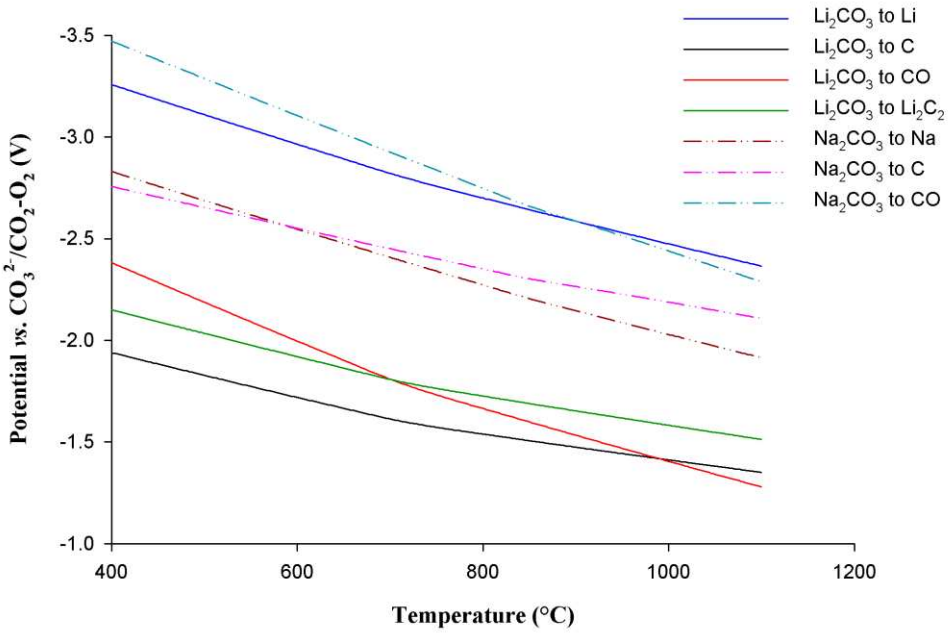

Figure 4.3: Standard potentials against temperature for the conversion of Li_2CO_3 or Na_2CO_3 to various cathodic products: carbon (C), alkali metal (Li or Na), carbon monoxide (CO) and lithium carbide (Li_2C_2). The potentials were calculated with the assistance of HSC Chemistry software (Version 6.12; Outokumpu Research) and are reported versus the CO_3^{2-}/CO_2-O_2 reference reaction (Reaction 4.6). Appendix I gives details of how these standard potentials were determined.

Li_2C_2 is not the only possible carbide compound that could have been formed during electrolysis. Several different carbide compounds could have been formed from either lithium or sodium ions via the following two reactions, where M represents lithium or sodium (Chen et al., 1998):

$$M^+ + e^- \rightarrow M \qquad (4.11)$$

$$iM + xC \rightarrow M_iC_x \qquad (x \geq i \geq 2) \qquad (4.12)$$

If carbide formation had proceeded in accordance with Reactions 4.11 and 4.12 instead of via Reaction 4.3, then the standard potential for alkali metal cation reduction to alkali metal (Reaction 4.11) would have influenced the quantity of alkali metal carbides that could have been produced.

In Figures 4.1(a) and 4.2, a small peak labelled C1 is observed in the current wave at the cathodic limit. This kind of peak was observed by Le Van et al. (2009) during cyclic voltammetry when the negative potential limit was made increasingly negative. They considered that the peak could have been associated with the formation of lithium carbide (according to Reaction 4.3) or the formation of adsorbed peroxides. Le Van et al. (2009) hypothesised that peroxides could be formed via the following reaction:

$$2CO_3^{2-} + 2e^- \rightarrow 2C + 3O_2^{2-} \qquad (4.13)$$

At very negative potentials, Le Van et al. (2009) considered that the surface of the electro-deposited carbon could become saturated with lithium oxide and peroxide, leading to a reduction in the active surface area and inducing a peak in the current wave at the cathodic limit. However, Le Van et al. (2009) calculated that the theoretical standard potential for Reaction 4.13 was -5.98 V vs. CO_3^{2-}/CO_2-O_2 at 450 °C. This very negative potential makes it seem unlikely that peroxides were formed during their cyclic voltammetry, as the most negative potential that they attained was around -2.6 V vs. CO_3^{2-}/CO_2-O_2. Thus, their suggestion that the cathodic peak was formed by the saturation of the working electrode surface by oxides and peroxides is thrown into question.

From the evidence collected in the present study, it seems likely that peaks such as C1 in Figures 4.1(a) and 4.2 were caused by multiple reactions occurring in competition beyond the cathodic limit. Furthermore, it was deduced that carbon electro-deposition only became the

dominant reaction once the working electrode had become coated with a layer of carbon. The evidence for these statements shall now be discussed.

Firstly, the cathodic limit observed in Figure 4.1(a) actually consists of at least three electrochemical reactions. When the scan rate was drastically increased from 10 mV/s to 1000 mV/s (cf. Figures 4.1(a) and 4.1(b)), two cathodic peaks C1 and C2 appeared in a region where an almost continuous increase in current was observed at 10 mV/s. The fact that these two peaks were only fully revealed at 1000 mV/s is evidence that the reactions responsible were kinetically-controlled[*]. Based on the thermodynamic potentials given in Figure 4.3, it is likely that carbon monoxide formation (Reaction 4.5) and lithium carbide formation (Reaction 4.3) also took place beyond the cathodic limit, both from the electro-reduction of Li_2CO_3. The formation of alkali metal from the electro-reduction of alkali metal cations (Reaction 4.4) cannot be ruled out either, since the overpotential for the deposition of alkali metal onto the platinum working electrode surface would probably be lower than that for carbon deposition. Regardless of the specific reactions responsible for peaks C1 and C2 in Figure 4.1(b), the fact that they only fully appeared at a very high scan rate is evidence that several competing reactions took place at the cathodic limit, including the electro-deposition of carbon.

Secondly, by considering empirical current efficiencies for carbon electro-deposition, as well as Q^+/Q^- values for the re-oxidation of cathodic products, it was deduced that carbon deposition at the cathode only became the dominant reaction once the metal working electrode had become completely coated with carbon.

Table 4.1 gives Q^+/Q^- values for the re-oxidation of cathodic products produced at the cathodic limit during cyclic voltammetry. Q^+/Q^- was calculated from cyclic voltammograms as follows. Firstly, the reduction charge passed at the cathodic limit was calculated by integrating both the forward and reverse current-time curves of the current wave at the cathodic limit[†]. Secondly,

[*] However, it is possible that these peaks were artefacts caused by the very high scan rate.
[†] The potential axis of a cyclic voltammogram can be converted to a time axis by dividing the potential change by the scan rate.

the oxidation charge passed at the anodic peaks was determined by integrating the current-time curves of these peaks. From these two charge values, Q^+/Q^- was calculated by dividing the oxidation charge by the reduction charge. Note that the same platinum working electrode was used for all of the tests carried out at a given temperature.

Table 4.1: Average Q^+/Q^- values for the re-oxidation of cathodic products produced during cyclic voltammetry, at different scan rates and negative potential limits. Electrolyte: Li_2CO_3-Na_2CO_3 (molar ratio of 52:48); WE: platinum (0.25 mm diameter); CE: stainless steel (6 mm diameter); RE: Ag/AgCl.

Electrolyte Temperature (°C)	**Scan Rate (mV/s)**	**Negative Potential Limit (V)**	**Average Q^+/Q^- (%)**
703	100	-1.53	17.1
	100	-1.66	20.5
	100	-1.72	20.2
	100	-1.90	28.1
	80	-1.90	28.1
	60	-1.90	29.7
	40	-1.90	30.0
	20	-1.90	30.2
	10	-1.90	36.6
	10	-1.66	19.4
599	100	-2.05	36.6
	80	-2.05	25.8
	60	-2.05	27.7
	40	-2.05	31.6
	10	-2.05	44.6
	10	-2.50	53.9

The results in Table 4.1 clearly show that Q^+/Q^- was generally low: the highest value at 703 °C was 36.6 %, whilst at 599 °C the highest value was 53.9 %. Generally, Q^+/Q^- increased when the negative potential limit of the scan was made more negative and when the scan rate was reduced. The result for a scan rate of 100 mV/s at 599 °C does not fit the observed trend; this may be due to the fact that there were traces of un-oxidised carbon on the surface of the working electrode from the previous voltammogram. In addition, Q^+/Q^- increased when the

potential was held at the negative potential limit for 10 seconds during a scan, as the results in Table 4.2 show.

The low Q^+/Q^- values shown in Table 4.1 indicate that significant amounts of cathodic product were not detected during the anodic potential scans. However, in voltammograms where the potential was held beyond the cathodic limit for longer periods of time, a greater proportion of the cathodic products remained at the working electrode to be re-oxidised during the anodic sweep. This is indicated by the higher Q^+/Q^- values obtained at lower scan rates, at more negative potential limits and when the potential was held at the negative potential limit during a scan.

Table 4.2: Q^+/Q^- values for the re-oxidation of cathodic products produced during cyclic voltammetry, comparing scans where the potential was held for 10 seconds to scans where the potential was not held. Electrolyte: Li_2CO_3-Na_2CO_3 (molar ratio of 52:48); temperature: 703 °C; WE: platinum (0.25 mm diameter); CE: stainless steel (6 mm diameter); RE: Ag/AgCl.

Scan Rate (mV/s)	**Scan Number**	**Negative Potential Limit (V)**	**Holding Potential (V)**	**Duration of Holding (s)**	**Q^+/Q^- (%)**
100	1	-1.66	N/A	N/A	20.0
100	2	-1.66	-1.66	10	68.5
100	3	-1.66	N/A	N/A	20.0
100	1	-1.90	N/A	N/A	27.1
100	2	-1.90	-1.90	10	100
100	3	-1.90	N/A	N/A	31.0

Furthermore, the current efficiencies for carbon electro-deposition via chronoamperometry were all relatively high: the lowest for Li_2CO_3-Na_2CO_3 was 54.8 %, and the highest was 93.7 % (see Chapter 7). Note that chronoamperometry was carried out for 30 minutes to electro-deposit carbon in these experiments. Such high current efficiencies would be unattainable if most of the cathodic product was lost during chronoamperometry. Therefore, the reactions that initially occurred at a bare metal working electrode were not exclusively associated with

carbon formation. However, once the electrode had become covered by a layer of carbon, it would appear that carbon deposition dominated, as indicated by the high current efficiencies from chronoamperometry, and the higher Q^+/Q^- values obtained when carbon deposition occurred over longer periods of time. This may have been due to the fact that a smaller overpotential is required to deposit carbon onto carbon, as opposed to carbon onto metal. It is also possible that the bare metal electrode surface catalysed some of the other reactions taking place on it; this catalysis may not have occurred once the electrode had become coated with a layer of carbon.

Considering the general situation when the working electrode is bare metal at the start of carbon electro-deposition, carbon deposition does not dominate and other reactions take place at comparable rates to carbon formation, probably carbon monoxide formation and alkali metal cation reduction. The products of these other reactions do not stay at the working electrode as easily as carbon: carbon monoxide bubbles away and alkali metals may dissolve in the electrolyte. Thus, Q^+/Q^- would be low. However, carbon deposition would gradually cover the whole of the metal working electrode with a layer of carbon. Once carbon has covered the entirety of the metal working electrode, carbon deposition dominates because the overpotential for its deposition becomes much lower, which leads to a significantly higher deposition rate. One important factor is that the three most thermodynamically favourable cathodic reactions all use Li_2CO_3 as their reactant (see Figure 4.3). If carbon deposition is occurring at a much higher rate, then it follows that there will be little Li_2CO_3 available for the other reactions. As a consequence, carbon can be deposited at high current efficiencies when the working electrode is coated with carbon. This would in turn lead to a high Q^+/Q^-, if the carbon were to be re-oxidised.

4.2.2 Anodic phenomena

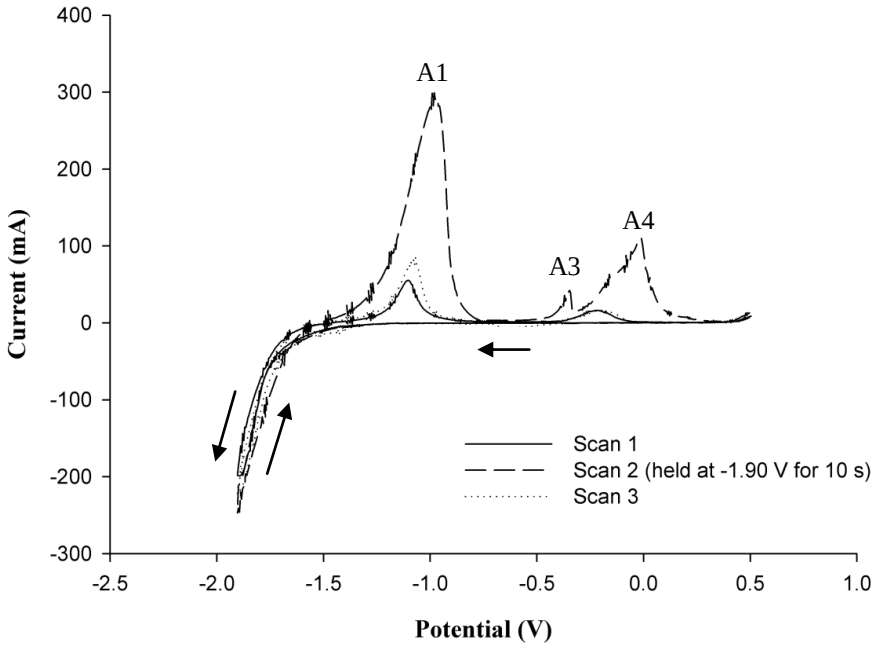

Figure 4.4: Cyclic voltammograms obtained using a platinum wire working electrode in a Li_2CO_3-Na_2CO_3 molten salt (molar ratio of 52:48), showing the effect of holding the potential at -1.90 V for 10 seconds during the second scan. Temperature: 703 °C; atmosphere: CO_2; scan rate: 100 mV/s; WE diameter: 0.25 mm; WE immersion depth: ca. 3.4 cm; CE: 6 mm diameter stainless steel rod; Ag/AgCl membrane RE.

The anodic phenomena observed in the cyclic voltammetry of the Li_2CO_3-Na_2CO_3 electrolyte are rather complex. As Figures 4.1 and 4.2 show, up to four anodic peaks could be observed during cyclic voltammetry at a platinum working electrode in Li_2CO_3-Na_2CO_3. As was mentioned in Section 4.2.1, the platinum working electrode was found to be inert and no cathodic peaks were observed at potentials more positive than the cathodic limit. As a consequence all of the anodic peaks observed in Figures 4.1 and 4.2 are likely to have been caused by the oxidation of products formed at the cathodic limit. This conclusion is supported by the fact that when the negative potential limit of a given scan was made more negative, all of the anodic peaks increased in height. Furthermore, when the potential was held beyond the cathodic limit potential for 10 seconds, the height of all of the anodic peaks increased, as is shown in Figure 4.4. Based on the results of this study and comparisons with relevant works in

the literature, it would appear that at least peaks A1 and A3 were due to the oxidation of electro-deposited carbon.

Ingram et al. (1966) observed three anodic peaks in their linear sweep voltammetry of electro-deposited carbon; this voltammogram is presented in Figure 2.7 of the present thesis. The carbon was electro-deposited by Ingram et al. (1966) onto a gold working electrode in a Li_2CO_3-Na_2CO_3-K_2CO_3 electrolyte at a temperature of 600 °C. The relative proportions of the anodic peaks in the voltammogram with the most negative limit in Figure 4.1(a) are very similar to those in Figure 2.7. In addition, the difference between the scan rates used in Figures 4.1(a) and 2.7 was only 5 mV/s, and the temperatures used were almost identical. Ingram et al. (1966) considered that electro-deposited carbon was re-oxidised in two principal stages – the same conclusion was reached in the present work. These stages could correspond to the following two carbon oxidation reactions, suggested by Le Van et al. (2009):

$$C + 2O^{2-} \rightarrow CO_2 + 4e^- \quad (4.14)$$

$$C + 2CO_3^{2-} \rightarrow 3CO_2 + 4e^- \quad (4.15)$$

Alternatively, it is quite possible that the two stages corresponded to the oxidation of portions of the carbon with different morphologies. However, it is difficult to specify exactly which reactions led to specific anodic peaks at this time.

The most obvious evidence for the re-oxidation of carbon via a two-stage process comes from the constant-current galvanostatic re-oxidation of electro-deposited carbon. Figure 4.5 shows a typical chronopotentiogram obtained from such an experiment. The carbon was obtained after 10 minutes of electrolysis at a potential of -2.77 V vs. Ag/AgCl[*], in the same electrolyte and using the same reference electrode that was used to obtain the cyclic voltammograms in Figure 4.1. The temperature of the molten salt was also the same at 599 °C. Chronopotentiograms such as this are considered in more detail in Chapter 8, albeit there are several conclusions that

[*] Note that this applied potential is significantly more negative than the cathodic limit in Figures 4.1 and 4.2. Such a negative potential was applied in order to increase the carbon deposition rate and hence obtain a suitable quantity of carbon deposit in a relatively short period of time.

can be drawn from them that are relevant to the interpretation of the anodic peaks in cyclic voltammetry.

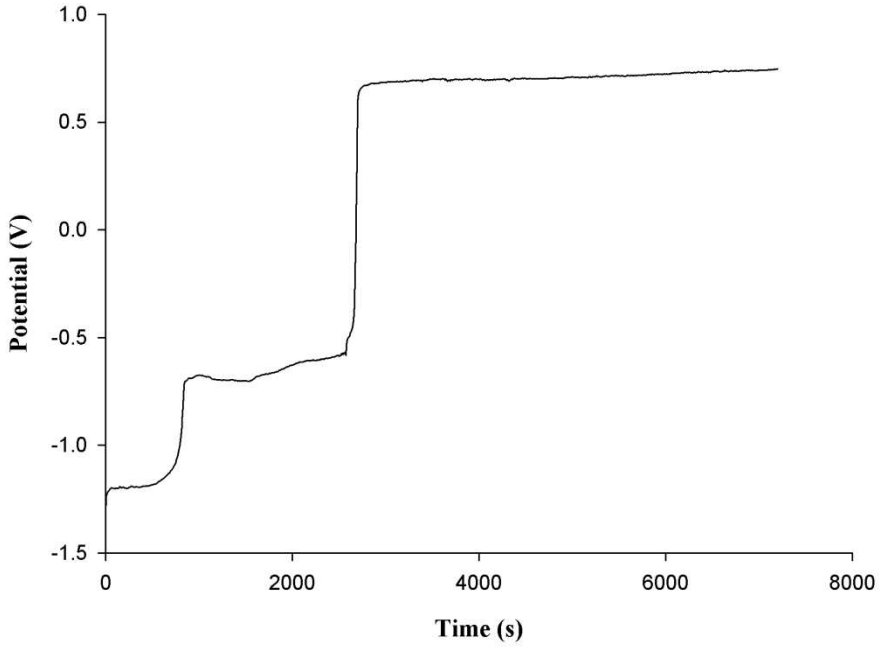

Figure 4.5: Variation of potential versus time during the re-oxidation of electro-deposited carbon in a Li_2CO_3-Na_2CO_3 molten salt (molar ratio: 52:48) at a constant current of 150 mA, at a temperature of 599 °C, under a CO_2 atmosphere. The carbon was electro-deposited at an applied potential of -2.77 V vs. Ag/AgCl. WE: 5 mm diameter mild steel rod (with carbon deposit still attached); CE: 10 mm diameter graphite rod; Ag/AgCl membrane RE.

The most important conclusion that can be drawn from these chronopotentiograms is that the electro-deposited carbon was oxidised in two principal stages, as indicated by the first and second plateaux in Figure 4.5. The third and final plateau probably corresponds to the oxidation of carbonate ions at the anodic limit. Comparing Figure 4.5 with the voltammograms in Figure 4.1, it is apparent that the plateaux in Figure 4.5 correspond to specific anodic current waves in the voltammograms. Starting with the first plateau at around -1.3 V, this corresponds to the start of the current wave of peak A1, whose peak value is around -1.1 V. The second plateau at -0.7 V appears to correspond to peak A3, whose peak lies at around -0.5 V. From these two correspondences, it is highly likely that peaks A1 and A3 were associated with the oxidation of electro-deposited carbon. Note that the peak potentials of peaks A1 and A3 were

dependent on the scan rate, the peak current and the quantity of carbon deposited. Thus, the small differences between the plateaux potentials in Figure 4.5 and the peak potentials in Figures 4.1, 4.2 and 4.5 are not unexpected. As for the third plateau at 0.6 V, this matches the experimentally-observed anodic limit of the voltammograms (this is not particularly apparent in Figure 4.1 but was observed in other voltammograms). These observations agree well with the experimental observations of Ingram et al. (1966).

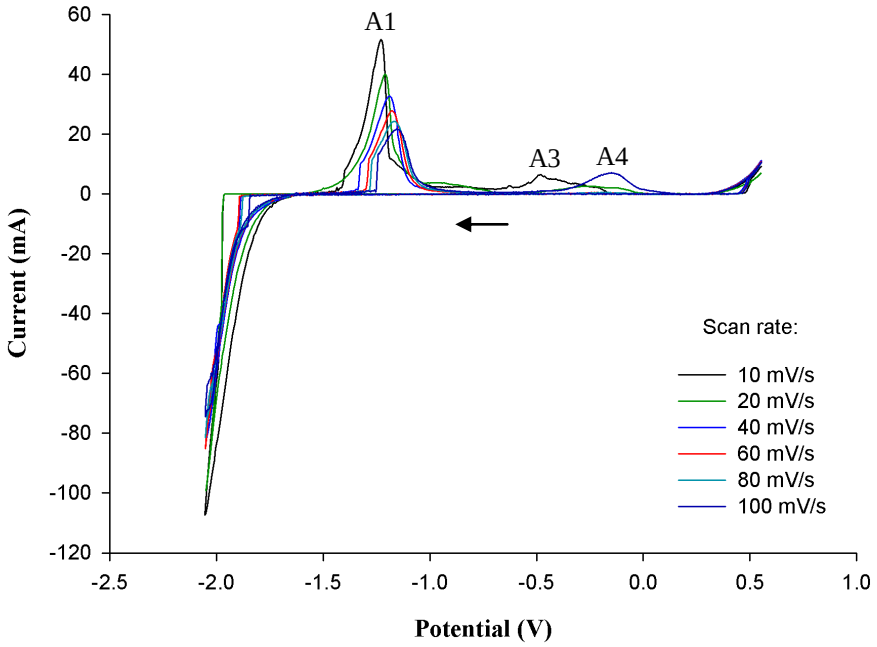

Figure 4.6: Cyclic voltammograms obtained at various scan rates, for a Li_2CO_3-Na_2CO_3 molten salt mixture (molar ratio of 52:48) at a temperature of 599 °C under a CO_2 atmosphere. WE: 0.25 mm diameter platinum wire; WE immersion depth: 0.9 cm; CE: 6 mm diameter stainless steel rod; Ag/AgCl membrane RE.

In addition, when the scan rate was varied in cyclic voltammetry, peak A1 responded in a manner that was compatible with it being attributed to carbon re-oxidation. Figure 4.6 shows the effect of varying the scan rate between 10 mV/s and 100 mV/s on the cyclic voltammetry. From this figure, it is very apparent that peak A1 was associated with the oxidation of a product that remained at the electrode surface: as the scan rate decreased, the area and height of peak A1 increased. At lower scan rates there was more time available for the carbon electro-deposition reaction to occur and so more carbon was produced. This in turn led to larger anodic peaks for the oxidation of this carbon.

The anodic limit in Figures 4.1 and 4.2 probably corresponds to the oxidation of carbonate ions in accordance with Reaction 4.6. Carbonate ions should be present throughout the electrolyte at a very high activity; thus it should not be possible to deplete the diffusion layer around the working electrode of carbonate ions. As a result, the oxidation of carbonate ions should not be limited by mass transfer and hence no peak would be observed for it in Figures 4.1 and 4.2. Carbonate ion oxidation was considered to be the anodic limit in voltammetry by many authors, including Ingram et al. (1966), Bartlett and Johnson (1967), Lantelme et al. (1999) and Le Van et al. (2009).

Thus far in this discussion, anodic peaks A1 and A3 in Figures 4.1 and 4.2 have been explained, but peaks A2 and A4 have not. The re-oxidation of carbon with different morphologies or the oxidation of carbide compounds may have been responsible for these peaks.

In the above discussion, it is particularly apparent that no peaks were attributed to the oxidation of alkali metal (Li or Na). The anodic peak for the re-oxidation of metal produced at the cathodic limit usually exhibits a characteristically sharp shape at potentials just positive of the cathodic limit (Hu, 2011); this was not observed in the voltammograms obtained. This may be because the alkali metal entered the bulk electrolyte too rapidly to be re-oxidised. Alternatively, it is possible that no alkali metals were actually produced at the cathodic limit. In such circumstances no anodic peak would be observed for their oxidation. One other possible explanation for the apparent absence of anodic peaks for alkali metal re-oxidation is that when alkali metals were formed at the working electrode, they reacted with carbon that had already been electro-deposited to form carbide compounds.

4.2.3 The effect of temperature

From the results obtained in this research, it is apparent that the cyclic voltammetry of Li_2CO_3-Na_2CO_3 was similar at temperatures of 599 °C and 703 °C. As Figure 4.3 shows, the order of cathodic reaction potentials is the same at both temperatures, although carbon monoxide

formation is comparatively more favourable at 703 °C. Thus the extent of similarity exhibited is reasonable. Furthermore, it would appear that the carbon re-oxidation processes were very similar, if not identical, at both temperatures studied.

4.3 Conclusions

Firstly, carbon deposition was found to occur at the cathodic limit in a molten Li_2CO_3-Na_2CO_3 electrolyte, probably via the following reaction:

$$CO_3^{2-} + 4e^- \rightarrow C + 3O^{2-} \qquad (4.16)$$

This agrees well with a large proportion of the published literature on carbon electro-deposition in pure carbonate electrolytes.

One novel finding of this investigation is that carbon electro-deposition competed with several other cathodic reactions at the cathodic limit, which included alkali metal carbide formation, alkali metal cation reduction and carbon monoxide formation. Q^+/Q^- values, deduced using cyclic voltammetry, were compared with current efficiencies that were obtained from carbon electro-depositions that were of long duration, which were carried out using chronoamperometry. From this comparison it was found that carbon deposition only dominated over the other competing reactions once the working electrode had become coated with a layer of carbon. This is because the overpotential needed for the deposition of carbon onto carbon is lower than that required for the deposition of carbon onto metal. Furthermore, it is likely that the bare metal working electrode surface catalysed the other competing reactions, before the metal working electrode surface became coated with electro-deposited carbon.

Electrochemical re-oxidation of electro-deposited carbon was found to take place via a process with at least two distinct stages. These stages may have corresponded to the oxidation of portions of the carbon with different morphologies.

CHAPTER 5

A PRELIMINARY STUDY OF CATION INFLUENCES ON ELECTRODE REACTIONS IN MOLTEN ALKALI CARBONATE SALTS: THE K^+ ION VERSUS THE Na^+ ION

In this fifth chapter, the effect of cations on carbon electro-deposition and re-oxidation in molten alkali carbonate electrolytes is considered. The first section in this chapter discusses the reasons for investigating this topic. In subsequent sections, the results obtained from the cyclic voltammetry of the molten Li_2CO_3-K_2CO_3 electrolyte are considered, which was carried out using a platinum working electrode. These results are compared with those obtained from the molten Li_2CO_3-Na_2CO_3 electrolyte at similar temperatures (whose results are presented in Chapter 4). Thus, some insights can be gleaned concerning the effect of changing the 'second cation' in the electrolyte from the Na^+ ion to the K^+ ion.

5.1 Reasons for Studying Cation Influences on Carbon Electro-Deposition and Re-Oxidation

In general, there is a dearth of information in the published literature concerning the effect of cations on carbon electro-deposition and re-oxidation in molten carbonate electrolytes. Ingram et al. (1966) showed that it was possible to electro-deposit carbon from Li_2CO_3 and Li_2CO_3-Na_2CO_3-K_2CO_3 electrolytes at a temperature of 750 °C. However, they were unable to electro-deposit carbon from a Na_2CO_3-K_2CO_3 electrolyte at the same temperature. The work of Ingram et al. (1966) represents the only study of the effect of removing the lithium ion on carbon electro-deposition, for molten carbonate electrolytes. No studies whatsoever appear to have been published in the literature regarding the effect of the Na^+ and K^+ ions on carbon electro-deposition and re-oxidation. Most authors tended to focus on one electrolyte only, and as a result were unable to gauge the effect of the cations present.

Thus, this chapter seeks to address this by comparing the results obtained from cyclic voltammetry at a platinum working electrode in molten Li_2CO_3-K_2CO_3, with the results obtained in molten Li_2CO_3-Na_2CO_3 at similar temperatures[*]. Furthermore, there is one additional novel aspect of this study: this is the first time that a rigorous study of carbon electro-deposition and re-oxidation has been carried out in the Li_2CO_3-K_2CO_3 electrolyte, using cyclic voltammetry.

5.2 Cyclic Voltammetry of Li_2CO_3-K_2CO_3 at Platinum Working Electrodes

The cyclic voltammetry of Li_2CO_3-K_2CO_3 (molar ratio of 62:38) was carried out using platinum working electrodes at temperatures of 579 °C and 708 °C. The desired electrolyte temperatures were 600 °C and 700 °C, although in practice it was difficult to attain these temperatures because the electrolyte temperature could only be controlled via the furnace set temperature. The furnace temperature controller had an accuracy of ±1 °C, but the electrolyte temperature was also affected by the effectiveness of the furnace insulation and the ambient temperature, which were difficult to keep constant between experimental runs. Figures 5.1(a) and 5.1(b) show voltammograms obtained at scan rates of 100 mV/s and 500 mV/s respectively, at a temperature of 579 °C. Figures 5.2(a) and 5.2(b) show voltammograms obtained at scan rates of 10 mV/s and 1000 mV/s respectively, at a temperature of 708 °C. Overall, the cyclic voltammograms obtained for Li_2CO_3-K_2CO_3 are rather similar to those obtained from Li_2CO_3-Na_2CO_3, so one would expect many of the reactions to be the same.

[*] The results for the Li_2CO_3-Na_2CO_3 electrolyte have already been presented in Chapter 4 of the present thesis.

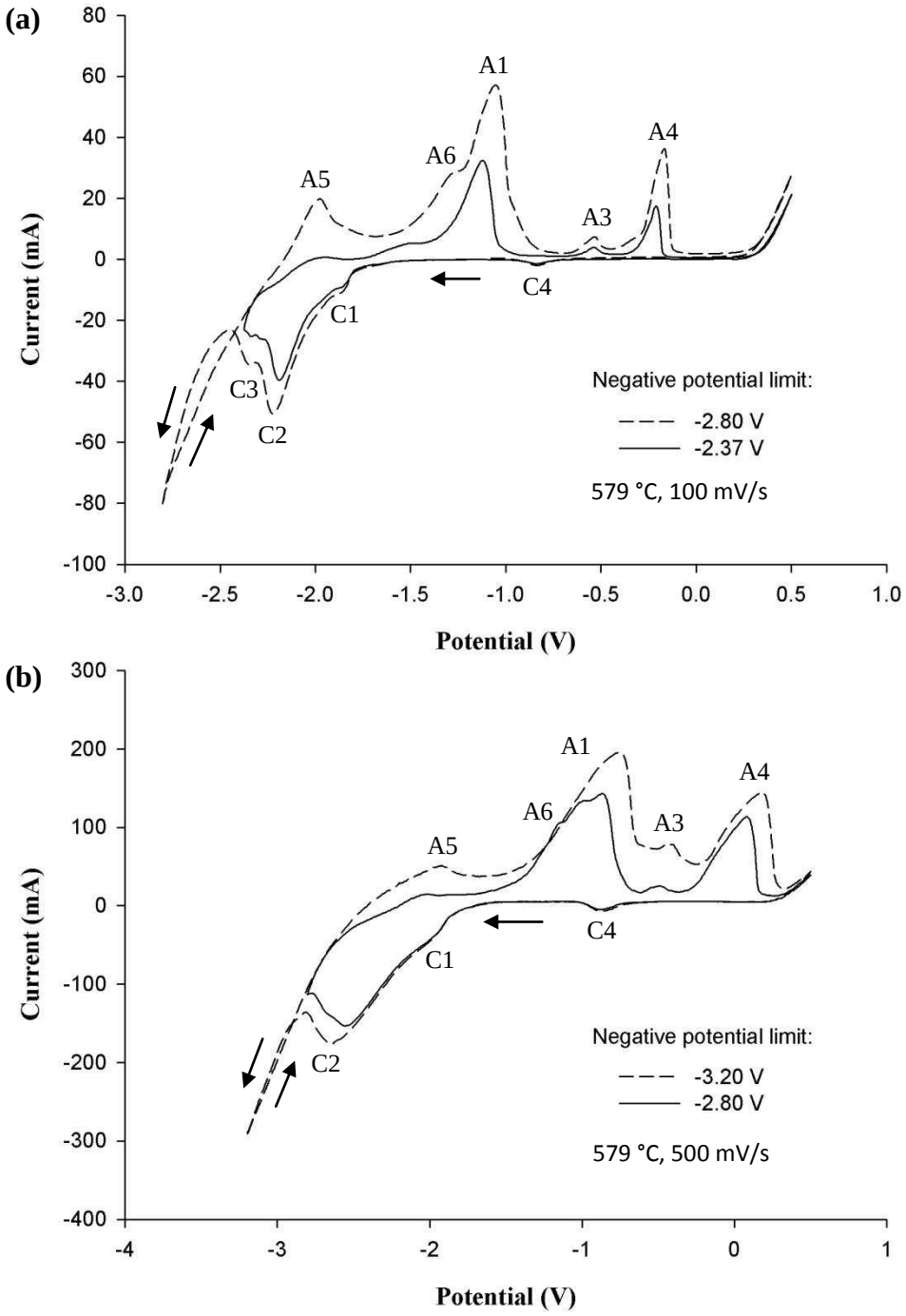

Figure 5.1: Cyclic voltammograms obtained from a platinum wire working electrode in a molten Li_2CO_3-K_2CO_3 electrolyte (molar ratio of 62:38) at 579 °C, at scan rates of (a) 100 mV/s and (b) 500 mV/s, at different negative potential scan limits. Atmosphere: CO_2; WE diameter: 0.25 mm; WE immersion depth: 0.3 cm; CE: 6 mm diameter stainless steel rod; RE: Ag/AgCl.

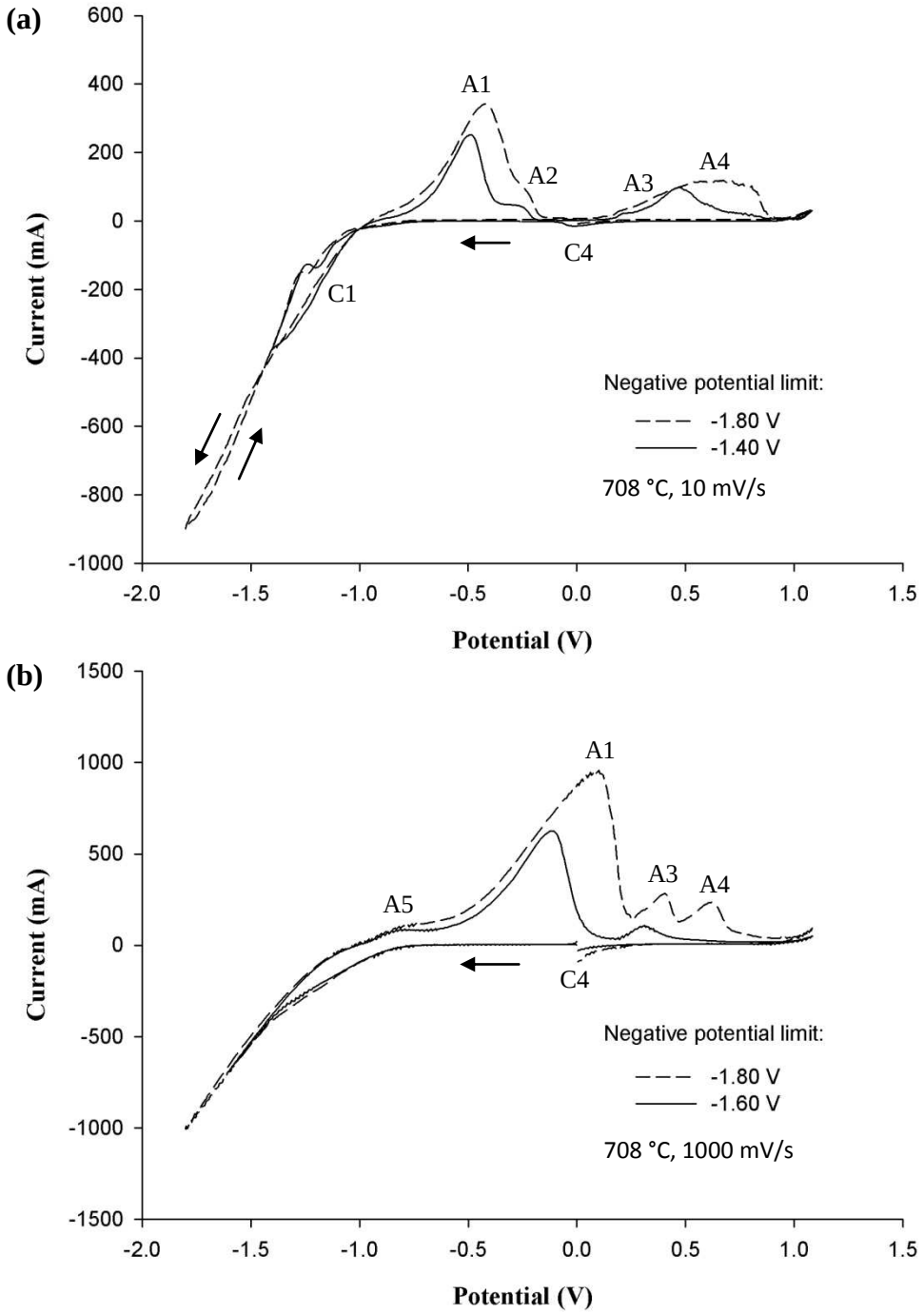

Figure 5.2: Cyclic voltammograms obtained from a platinum wire working electrode in a molten Li_2CO_3-K_2CO_3 electrolyte (molar ratio of 62:38) at 708 °C, at scan rates of (a) 10 mV/s and (b) 1000 mV/s, at different negative potential scan limits. Atmosphere: CO_2; WE diameter: 0.25 mm; WE immersion depth: 2.5 cm; CE: 6 mm diameter stainless steel rod; RE: Ag/AgCl.

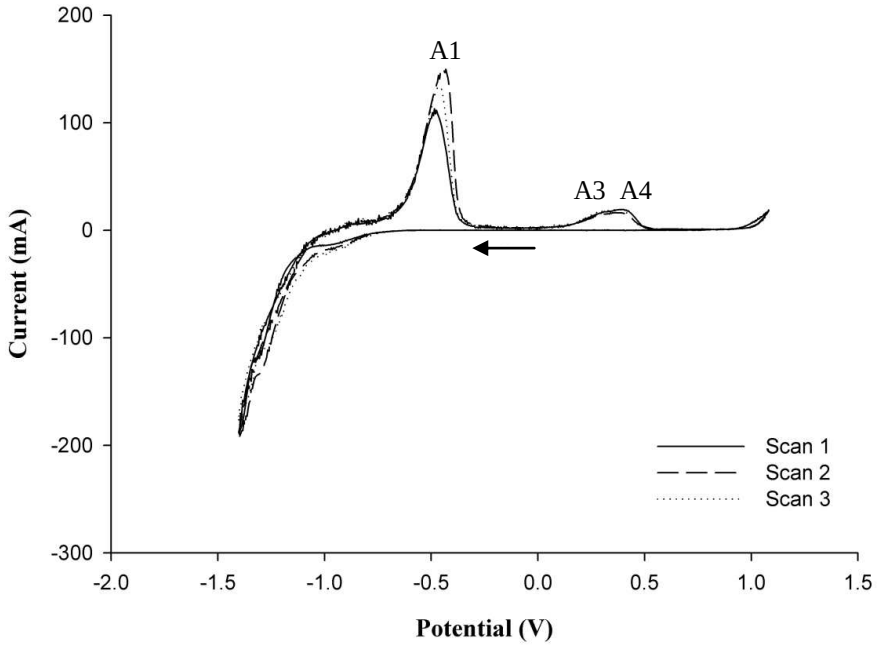

Figure 5.3: Cyclic voltammograms obtained from a platinum wire working electrode immersed in a Li_2CO_3-K_2CO_3 electrolyte (molar ratio of 62:38) at a temperature of 708 °C under a CO_2 atmosphere. Scan rate: 100 mV/s; WE: diameter: 0.25 mm; WE immersion depth: 2.5 cm; CE: 6 mm diameter stainless steel rod; Ag/AgCl membrane RE.

5.2.1 Cathodic phenomena

Starting with the cathodic phenomena, there are many significant features present in Figures 5.1 and 5.2. Firstly, unlike the voltammograms observed for Li_2CO_3-Na_2CO_3, a small cathodic peak C4 is present at both temperatures studied. This peak is very similar to one that was observed by Lantelme et al. (1999) in their cyclic voltammogram that was obtained at a platinum working electrode in a Li_2CO_3-Na_2CO_3-K_2CO_3 molten salt (cf. Figures 2.10, 5.1 and 5.2). As was mentioned in Chapter 4, this peak was attributed to the reduction of PtO_3^{2-} ions:

$$PtO_3^{2-} + 4e^- \rightarrow Pt + 3O^{2-} \qquad (5.1)$$

The experimental timescales used in this research were similar for both the Li_2CO_3-Na_2CO_3 and Li_2CO_3-K_2CO_3 electrolytes, so it is possible that platinum oxidation occurs faster in the

Li_2CO_3-K_2CO_3 electrolyte, resulting in the formation of a cathodic peak for the reduction of PtO_3^{2-} ions in Figures 5.1 and 5.2. One observation that supports this is that peak C4 was not observed in voltammograms conducted near the very beginning of an experimental session; one such voltammogram is shown in Figure 5.3. At such an early stage it is possible that too little Li_2PtO_3 was formed for a significant reduction peak to be observed. Thus, it is reasonable to attribute peak C4 to the reduction of PtO_3^{2-} ions via Reaction 5.1.

As with the Li_2CO_3-Na_2CO_3 electrolyte, the cathodic limit in Figures 5.1 and 5.2 probably corresponds to the electro-deposition of carbon via carbonate ion reduction:

$$CO_3^{2-} + 4e^- \rightarrow C + 3O^{2-} \qquad (5.2)$$

The fact that cathodic loops were observed in cyclic voltammetry is evidence for this. In addition, carbon electro-deposition was physically observed in the Li_2CO_3-K_2CO_3 electrolyte. At a temperature of 708 °C, carbon was successfully electro-deposited onto a platinum working electrode at a potential of -1.17 V vs. Ag/AgCl; this potential lies beyond the cathodic limit in Figure 5.2. At both 579 °C and 708 °C, carbon deposits were obtained on mild steel rod working electrodes at potentials 0.6 V, 1.0 V and 1.4 V more negative than the potential at the start of the current wave at the cathodic limit (observed in cyclic voltammetry) – see Chapter 7 for more details regarding these depositions.

Thermodynamic calculations provide further evidence for the formation of carbon beyond the cathodic limit in Li_2CO_3-K_2CO_3. Apart from carbon electro-deposition, possible reactions at the cathodic limit include the following:

$$2Li^+ + 2CO_3^{2-} + 10e^- \rightarrow 6O^{2-} + Li_2C_2 \qquad (5.3)$$

$$M^+ + e^- \rightarrow M \quad (\text{M represents an alkali metal: Li or K}) \qquad (5.4)$$

$$CO_3^{2-} + 2e^- \rightarrow CO + 2O^{2-} \qquad (5.5)$$

In Figure 5.4, the theoretical standard potentials vs. CO_3^{2-}/CO_2-O_2 for Reactions 5.4, 5.5, 5.6 and 5.7 are given at temperatures between 400 °C and 1100 °C. At 579 °C and 708 °C, the most favourable reactions are the formation of carbon, lithium carbide and carbon monoxide, all from Li_2CO_3. Carbon electro-deposition is the most thermodynamically favourable reaction, as it has the least negative potential.

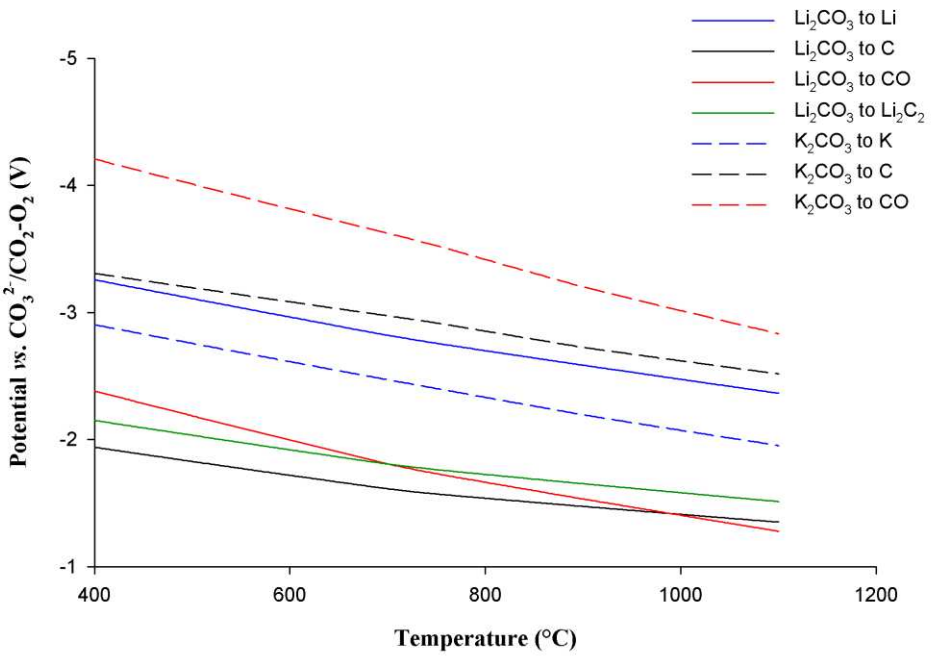

Figure 5.4: Standard potentials against temperature for the conversion of Li_2CO_3 or K_2CO_3 to various cathodic products: carbon (C), alkali metal (Li or K), carbon monoxide (CO) and lithium carbide (Li_2C_2). The potentials were calculated using HSC Chemistry software (Version 6.12; Outokumpu Research) and are reported versus the CO_3^{2-}/CO_2-O_2 reference reaction (Reaction 5.11).

In Section 4.2.1, for Li_2CO_3-Na_2CO_3, cathodic peaks such as C1 and C2 were ascribed to reactions occurring in competition with carbon electro-deposition beyond the cathodic limit. This would also appear to be the case for Li_2CO_3-K_2CO_3 in Figures 5.1 and 5.2, although the behaviour of these peaks differs somewhat from those of Li_2CO_3-Na_2CO_3. At 708 °C (Figure 5.2), the small peak C1 was visible at a scan rate of 10 mV/s but was not visible at 1000 mV/s. On the other hand, at 579 °C (Figure 5.1), at least two cathodic peaks were visible even at a scan rate of 100 mV/s.

5.2.2 Analysing Q^+/Q^-

The Q^+/Q^- trends observed in Li_2CO_3-K_2CO_3 for the re-oxidation of cathodic products were rather different in some respects to those obtained from Li_2CO_3-Na_2CO_3. The Q^+/Q^- trends at 708 °C also differed from those observed at 579 °C. Generally, it would appear the surface of the platinum working electrode became modified as successive scans of cyclic voltammetry were carried out. This modification appeared to make it easier for carbon deposition to compete with the other cathodic reactions.

Table 5.1: The effect of changing the scan rate on Q^+/Q^-, for the Li_2CO_3-K_2CO_3 (molar ratio of 62:38) electrolyte at a temperature of 708 °C. WE: platinum (0.25 mm diameter); CE: stainless steel (6 mm diameter); RE: Ag/AgCl.

Scan Rate (mV/s)	**Negative Potential Limit (V)**	**Q^+ (C)**	**Q^- (C)**	**Q^+/Q^- (%)**
100	-1.40	1.776	3.575	49.7
80	-1.40	3.151	6.220	50.7
60	-1.40	3.362	6.524	51.5
40	-1.40	5.737	10.75	53.4
20	-1.40	14.41	25.56	56.4
10	-1.40	47.701	73.93	64.5

At 708 °C, some trends were similar to those observed for Li_2CO_3-Na_2CO_3. Firstly, when the scan rate was reduced, Q^+/Q^- increased, as was observed for Li_2CO_3-Na_2CO_3; this trend is shown in Table 5.1. Note that the same platinum working electrode was used in all of the tests carried out. As was stated in Section 4.2.1, an increase in Q^+/Q^- implies that more of the cathodic products were retained at the working electrode to be re-oxidised during the anodic sweep. Thus, as for the Li_2CO_3-Na_2CO_3 electrolyte, it can be concluded that the reactions initially occurring at a bare metal working electrode were not exclusively associated with carbon formation, although after the working electrode had become coated with carbon, carbon deposition dominated over the other cathodic reactions. This is further supported by the high current efficiencies obtained for carbon deposition via chronoamperometry: the lowest for Li_2CO_3-K_2CO_3 was 69.5 %; the highest was 84.5 % (see Chapter 7 for details of these depositions). Note that, in these cases, chronoamperometry was carried out for 30 minutes to

electro-deposit carbon. Such high current efficiencies could not be obtained if most of the cathodic product were lost during chronoamperometry.

However, comparing the data for temperatures of around 700 °C in Tables 4.1 (for Li_2CO_3-Na_2CO_3) and 5.4, it is evident that the Q^+/Q^- values obtained from Li_2CO_3-K_2CO_3 were higher than those for Li_2CO_3-Na_2CO_3 under similar conditions. This implies that a greater proportion of the cathodic products remained at the working electrode to be re-oxidised during the anodic sweep in Li_2CO_3-K_2CO_3. As was noted above, the same platinum working electrode was used in the potential scans from which the data in Table 5.1 was obtained. The cycles were carried out consecutively and also some cycles of cyclic voltammetry had been performed prior to the scan rate investigation. Perhaps the reason for the higher Q^+/Q^- values in Table 5.1 was that the working electrode surface was modified in earlier cycles, in such a way as to reduce the overpotential for carbon deposition and hence increase the rate of its deposition over the short timescales considered – this shall be elaborated on later in this section.

Table 5.2 gives the Q^+/Q^- values for the re-oxidation of cathodic products for the initial cyclic voltammograms carried out in the Li_2CO_3-K_2CO_3 electrolyte at 708 °C. The first voltammogram yielded a Q^+/Q^- of 21.0 %, which is similar to the Q^+/Q^- values observed in the Li_2CO_3-Na_2CO_3 electrolyte. However, the Q^+/Q^- values for the second and third voltammograms in Table 5.2 were much higher: 74.1 % and 47.7 % respectively. From the third voltammogram onwards, Q^+/Q^- remained relatively stable but its value was consistently more than twice the Q^+/Q^- obtained from the first voltammogram. During the anodic stripping of carbon that was electro-deposited from Li_2CO_3-Na_2CO_3-K_2CO_3, Ingram et al. (1966) observed that some carbon remained on the working electrode even after the potential had risen to the melt oxidation potential. This was also observed by the present author in the re-oxidation of electro-deposited carbon in both Li_2CO_3-K_2CO_3 and Li_2CO_3-Na_2CO_3 at temperatures around 600 °C (see Chapter 8 for more details). Thus, it would appear that not all of the carbon was re-oxidised during the anodic sweep of the first voltammogram in Table 5.2. Consequently, carbon could deposit at a faster rate during the cathodic sweep of the second and later

voltammograms because there was already a layer of carbon on the working electrode surface, which reduced the overpotential for carbon deposition.

Table 5.2: Q^+/Q^- values for the re-oxidation of cathodic products obtained from successive scans of cyclic voltammetry, for the Li_2CO_3-K_2CO_3 (molar ratio of 62:38) electrolyte at a temperature of 708 °C. Scan rate: 100 mV/s; WE: platinum (0.25 mm diameter); CE: stainless steel (6 mm diameter); RE: Ag/AgCl.

Order in which Voltammograms were Obtained	**Negative Potential Limit (V)**	**Q^+ (C)**	**Q^- (C)**	**Q^+/Q^- (%)**
1	-1.72	3.135	14.91	21.0
2	-1.40	2.669	3.602	74.1
3	-1.40	1.326	2.781	47.7
4	-1.40	1.323	2.806	44.0
5	-1.40	1.659	3.326	48.8
6	-1.40	1.521	3.141	48.4
7	-1.40	1.520	3.129	48.6
8	-1.40	1.771	3.641	48.7
9	-1.40	1.776	3.575	49.7

The fact that the second voltammogram in Table 5.2 yielded a greater Q^+/Q^- than later voltammograms can be explained by the change in the negative potential limit from -1.72 V vs. Ag/AgCl to -1.40 V vs. Ag/AgCl. When a more negative potential limit was used during the first voltammogram, more carbon would have been deposited than during the second voltammogram. Some of the un-oxidised carbon from the first voltammogram could therefore have been re-oxidised during the second voltammogram. On the whole, it would seem that a portion of the electro-deposited carbon was not re-oxidised during any given scan in the Li_2CO_3-K_2CO_3 electrolyte at 708 °C. This supposition is supported by the fact that Q^+/Q^- generally increased from the third voltammogram (47.7 %) to the ninth voltammogram (49.7 %). Although this increase is rather slight, it suggests that the amount of un-oxidised carbon on the platinum surface was gradually increasing with each successive voltammogram, which would have increased the number of sites at which carbon could have electro-deposited at a

lower overpotential during subsequent scans. Thus the extent to which carbon deposition dominated over other cathodic reactions would have increased.

Table 5.3: Q^+/Q^- values for the re-oxidation of cathodic products produced from successive scans of cyclic voltammetry, for the Li_2CO_3-K_2CO_3 (molar ratio of 62:38) electrolyte at a temperature of 579 °C. Scan rate: 100 mV/s; WE: platinum (0.25 mm diameter); CE: stainless steel (6 mm diameter); RE: Ag/AgCl.

Order in which Voltammograms were Obtained	**Negative Potential Limit (V)**	**Q^+ (C)**	**Q^- (C)**	**Q^+/Q^- (%)**
1	-2.30	0.370	1.288	20.4
2	-2.35	0.492	1.803	24.8
3	-2.35	0.678	2.297	37.1
4	-2.35	0.732	2.332	40.2
5	-2.37	0.650	2.133	31.5
6	-2.37	0.868	2.541	40.9
7	-2.37	0.926	2.629	42.1

For the Li_2CO_3-K_2CO_3 electrolyte at a temperature of 579 °C, it would seem that this incomplete carbon re-oxidation effect was particularly strong. Table 5.3 shows Q^+/Q^- values for the re-oxidation of cathodic products obtained from successive Li_2CO_3-K_2CO_3 voltammograms at a temperature of 579 °C. The same platinum working electrode was used to obtain these voltammograms. From Table 5.3 it is apparent that Q^+/Q^- generally increased with each successive scan, even when the negative potential limit of the scan was kept the same. This implies that, with each successive voltammogram, more and more cathodic product remained at the working electrode to be re-oxidised during the anodic sweep. One possible explanation for this is that increasing amounts of un-oxidised carbon were left on the working electrode surface after each successive voltammogram, as has already been discussed.

Due to the rising Q^+/Q^- with each successive scan, the effect of changing the scan rate on Q^+/Q^- at 579 °C was investigated using a fresh platinum working electrode for each

voltammogram carried out. Table 5.4 gives the results of this study and from this table it is apparent that there was no trend in the variation of Q^+/Q^- with scan rate.

Table 5.4: The effect of scan rate on Q^+/Q^- for the re-oxidation of cathodic products produced during cyclic voltammetry, when a fresh working electrode was used for each scan rate, for the Li_2CO_3-K_2CO_3 (molar ratio of 62:38) electrolyte at a temperature of 574 °C. WE: platinum (0.25 mm diameter); CE: stainless steel (6 mm diameter); RE: Ag/AgCl.

Scan Rate (mV/s)	**Negative Potential Limit (V)**	**Q^+ (C)**	**Q^- (C)**	**Q^+/Q^- (%)**
100	-2.06	0.078	0.278	32.0
80	-2.06	0.256	0.469	47.8
60	-2.06	0.06	0.394	32.9
40	-2.06	0.096	0.631	22.0
20	-2.06	0.058	1.104	24.7
10	-2.06	0.34	1.899	31.4

From the Q^+/Q^- values obtained in Li_2CO_3-K_2CO_3, it is particularly clear that modification of the surface of the platinum working electrode took place with each successive scan, to a much greater extent than in Li_2CO_3-Na_2CO_3. This modification appeared to reduce the overpotential required for carbon electro-deposition in later scans, probably because un-oxidised carbon remained on the working electrode surface after each successive scan of cyclic voltammetry.

Carbon could have remained un-oxidised after a given anodic sweep if the rate of re-oxidation was too slow to re-oxidise all of the carbon during the anodic sweep in question. Ingram et al. (1966) observed that the last portion of their electro-deposited carbon could only be re-oxidised at low currents during anodic stripping. This implies a slow rate of oxidation for the last stage of carbon re-oxidation and is consistent with the results presented in this chapter.

One might ask why the same behaviour was not observed in the Li_2CO_3-Na_2CO_3 electrolyte. Based on the observations made in this chapter, it would appear that the carbon deposits obtained in Li_2CO_3-K_2CO_3 were more difficult to completely re-oxidise during a given anodic sweep, particularly at the lower temperature of 579 °C. However, until more detailed structural

studies of the carbon deposits from the Li_2CO_3-Na_2CO_3 and Li_2CO_3-K_2CO_3 electrolytes have been carried out (eg. by transmission electron microscopy and by Brunauer-Emmett-Teller gas adsorption studies), it will be difficult to ascertain the exact reason why the carbon deposits obtained from Li_2CO_3-K_2CO_3 were more difficult to completely re-oxidise during a given anodic sweep of cyclic voltammetry.

5.2.3 Anodic phenomena

On the basis of the evidence obtained in the present work, carbon re-oxidation appears to have taken place according to a similar process in both Li_2CO_3-Na_2CO_3 and Li_2CO_3-K_2CO_3. Since this re-oxidation process has already been discussed in detail in Section 4.2.2, the evidence for it shall only be reviewed here.

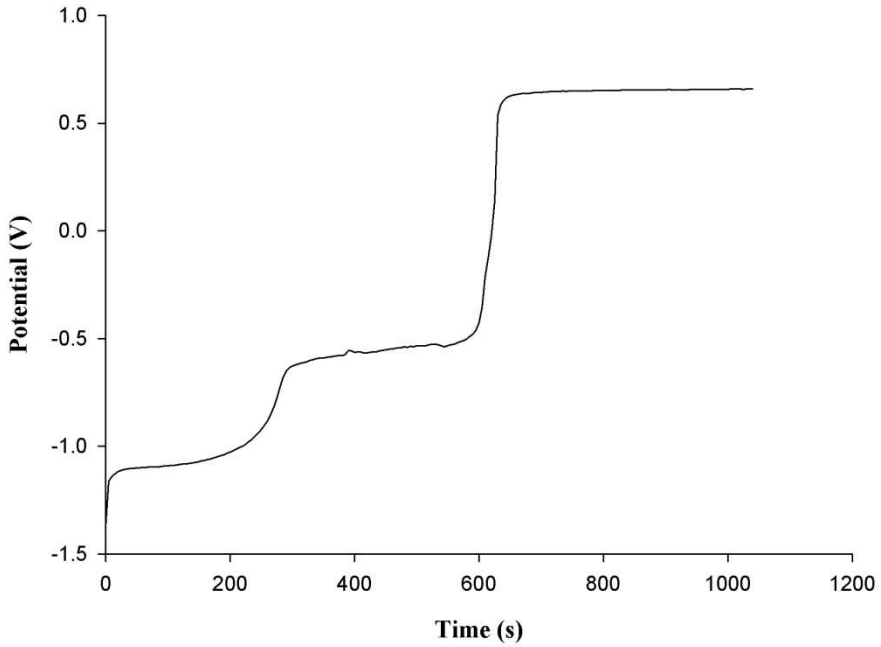

Figure 5.5: Variation of potential versus time during the re-oxidation of electro-deposited carbon in a Li_2CO_3-K_2CO_3 (molar ratio: 62:38) molten salt mixture at a constant current of 450 mA, at a temperature of 574 °C, under a CO_2 atmosphere. The carbon was electro-deposited at an applied potential of -2.56 V vs. Ag/AgCl. WE: 5 mm diameter mild steel rod (with carbon deposit still attached); CE: 10 mm diameter graphite rod; Ag/AgCl membrane RE.

Peaks A1 and A3 probably correspond to the re-oxidation of electro-deposited carbon according to the aforementioned carbon oxidation process described in Section 4.2.2, which holds for Li_2CO_3-K_2CO_3 for two main reasons. Firstly, chronopotentiograms obtained from the galvanostatic re-oxidation of electro-deposited carbon in Li_2CO_3-K_2CO_3 indicated that the carbon was re-oxidised in two principal stages, corresponding to peaks A1 and A3. Figure 5.5 shows a typical chronopotentiogram obtained at a temperature of 574 °C in the Li_2CO_3-K_2CO_3 molten salt. The reference electrode used was the same as the one that was used to produce the voltammograms in Figure 5.1. Comparing Figures 5.1(a) and 5.5, it is apparent that the first plateau at -1.1 V in Figure 5.5 corresponds to Peak A1 in Figure 5.1(a). The second plateau at −0.55 V corresponds to Peak A3. The third plateau at 0.65 V is similar to the anodic limit in Figure 5.1(a), at which oxidation of the electrolyte took place.

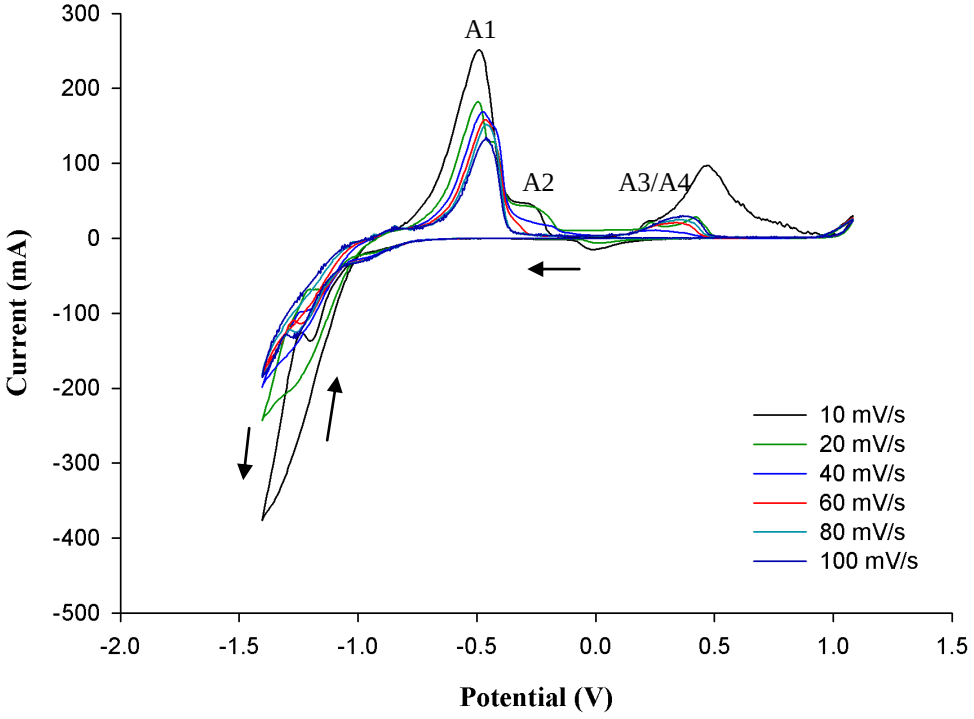

Figure 5.6: Cyclic voltammograms obtained at various scan rates, for a Li_2CO_3-K_2CO_3 molten salt mixture (molar ratio of 62:38) at a temperature of 708 °C under a CO_2 atmosphere. WE: 0.25 mm diameter platinum wire; WE immersion depth: 2.5 cm; CE: 6 mm diameter stainless steel rod; Ag/AgCl membrane RE.

Secondly, the response of peak A1 to changing scan rate is compatible with it being ascribed to carbon re-oxidation. Figure 5.6 shows the effect of varying the scan rate between 10 mV/s and 100 mV/s. Peak A1 increased in height as the scan rate was reduced, which implies that it was associated with the oxidation of a product that remained at the electrode surface, probably carbon. Peak A3 was also observed to increase in height with decreasing scan rate, implying that it was also associated with the oxidation of electro-deposited carbon.

As with the Li_2CO_3-Na_2CO_3 electrolyte, the anodic limit can be attributed to the oxidation of carbonate ions (see Section 4.2.3 for a justification of this):

$$CO_3^{2-} \rightarrow CO_2 + \tfrac{1}{2}O_2 + 2e^- \qquad (5.6)$$

Peaks A2 and A4 may have been due to the re-oxidation of carbon with different morphologies, as with the Li_2CO_3-Na_2CO_3 electrolyte.

Two additional minor anodic peaks A5 and A6 were observed in Figures 5.1 and 5.2, which were not observed in any of the voltammograms obtained in Li_2CO_3-Na_2CO_3. Peak A6 was only observed at a temperature of 579 °C and it always appeared as a 'step' on the side of peak A1. Based on this, it is possible that peak A6 was simply caused by the re-oxidation of electro-deposited carbon. Peak A5 is analogous to an anodic peak observed in a voltammogram obtained by Le Van et al. (2009), although they did not actually acknowledge its existence[*]. According to the position of peak A5, it is likely that it corresponds to the re-oxidation of one of the other products of the cathodic reactions that competed with carbon electro-deposition. Thus, peak A5 could be ascribed to the oxidation of lithium metal and/or potassium metal, or to the oxidation of alkali metal carbides.

[*] See Figure 2.6 in the present thesis for the voltammogram in question that was obtained by Le Van et al. (2009).

5.2.4 The effect of temperature

Comparing Figures 5.1 and 5.2, at temperatures of 579 °C and 708 °C respectively, it is apparent that much of the electrochemical behaviour was the same. Anodic peaks A1, A3 and A4 were all observed and behaved in similar ways at both temperatures; cathodic peak C4 was also observed at both temperatures. However, at 579 °C, the cathodic peaks just prior to the cathodic limit were considerably more prominent than at 708 °C. This may have been due to slower rates of carbon formation at 579 °C, which would have meant that these peaks were not concealed by the current wave at the cathodic limit to such a great extent as at 708 °C. Furthermore, as has already been remarked, it would appear that carbon re-oxidation was slower at 579 °C, leading to the accumulation of un-oxidised carbon on the working electrode surface, which increased the degree to which carbon electro-deposition dominated at the cathodic limit, with each successive scan of cyclic voltammetry (see Section 5.2.2).

5.3 Conclusions

Generally, the carbon electro-deposition and re-oxidation reactions in Li_2CO_3-K_2CO_3 were found to be similar to those in Li_2CO_3-Na_2CO_3. Firstly, carbon electro-deposition was found to take place at the cathodic limit, probably according to the following reaction:

$$CO_3^{2-} + 4e^- \rightarrow C + 3O^{2-} \qquad (5.14)$$

Secondly, carbon deposits were found to be re-oxidised according to a similar two-stage process in both electrolytes. As with the Li_2CO_3-Na_2CO_3 electrolyte, it is highly likely that carbon electro-deposition in the Li_2CO_3-K_2CO_3 electrolyte competed with a number of other cathodic reactions at the cathodic limit. Carbon deposition was found to dominate only after the working electrode had become coated with a layer of carbon.

Based on the Q^+/Q^- values obtained for the re-oxidation of cathodic products, it would seem that some electro-deposited carbon remained un-oxidised after re-oxidation during a given

anodic sweep of cyclic voltammetry in the Li_2CO_3-K_2CO_3 electrolyte. Some of this un-oxidised carbon remained on the working electrode surface and probably increased the number of sites at which carbon electro-deposition could occur at a lower overpotential. This phenomenon was particularly evident at lower temperatures close to 600 °C in Li_2CO_3-K_2CO_3, although at temperatures nearer to 700 °C the effect of un-oxidised carbon appeared to be considerably smaller. Perhaps the rate of re-oxidation was insufficient for all of the carbon to be re-oxidised quickly enough during the anodic sweep. Notably, this effect did not appear to occur to any great extent in the Li_2CO_3-Na_2CO_3 electrolyte. However, until more detailed structural analyses of electro-deposited carbon are performed, it will be difficult to account for the difference in carbon re-oxidation behaviour between the Li_2CO_3-Na_2CO_3 and Li_2CO_3-K_2CO_3 electrolytes.

CHAPTER 6

CYCLIC VOLTAMMETRY OF STAINLESS STEEL WORKING ELECTRODES IN DIFFERENT MOLTEN CARBONATES

Having considered the electro-deposition of carbon and its re-oxidation at the inert platinum working electrode in Chapters 4 and 5, this sixth chapter broadens the scope of the investigation by presenting a comparative study of the cyclic voltammetry of stainless steel electrodes in four different molten carbonate electrolytes: Li_2CO_3-Na_2CO_3, Li_2CO_3-K_2CO_3, Na_2CO_3 and K_2CO_3. This chapter aims to achieve an understanding of the reactions occurring at a cheaper and more practical working electrode. The first section concerns the motivations for studying this topic. In later sections, the electrolytes are divided into two main groups: those that contain lithium cations and those that do not; the cyclic voltammetry of each electrolyte is discussed in turn. Note that some preliminary studies of the Li_2CO_3-Na_2CO_3-K_2CO_3, Li_2CO_3 and Na_2CO_3-K_2CO_3 electrolytes have also been carried out and are presented in Appendix II.

6.1 Reasons for Studying this Topic

Very few works in the published literature compare carbon electro-deposition and re-oxidation in different molten salt electrolytes. Most authors limited themselves to only one or two electrolyte compositions, which may have led them to draw conclusions that are not universally applicable to the other carbonate-only salts. A study of several carbonate electrolytes under similar conditions may allow an objective evaluation of their relative merits and disadvantages. Despite the fact that it was published over forty years ago, the work of Ingram et al. (1966) is the only paper published in English that directly compares carbon electro-deposition in different carbonate electrolytes under similar conditions. However, their work suffers in that it was published before cyclic voltammetry was widely used, which limited the extent to which they were able to explore the voltammetry of their systems. However,

despite this shortcoming, it is still one of the more thorough papers on the voltammetry of pure carbonate electrolytes. As has been already pointed out in Sections 4.1 and 5.1, most authors have not probed the cyclic voltammetry of their systems very rigorously, and have often made peak attributions on the basis of little evidence.

The findings presented in this chapter will help to address the issues raised here. This study also represents the first comprehensive, comparative investigation of carbon electro-deposition and re-oxidation in four molten carbonate electrolytes by cyclic voltammetry.

6.2 Cyclic Voltammetry of Carbonate Electrolytes that contain Lithium Cations: Li_2CO_3-Na_2CO_3 and Li_2CO_3-K_2CO_3

Ingram et al. (1966) considered that the presence of lithium in the electrolyte was essential in order for carbon electro-deposition to occur; the same conclusion has been reached in the present study. The molten carbonate electrolytes that contain lithium cations shall be considered first, before moving onto the electrolytes that lack lithium cations.

6.2.1 Cyclic voltammetry of stainless steel in molten Li_2CO_3-Na_2CO_3

The cyclic voltammetry of Li_2CO_3-Na_2CO_3 (molar ratio of 52:48) was carried out using stainless steel working electrodes at temperatures of 599 °C, 627 °C and 703 °C. Figure 6.1 shows two voltammograms that were carried out at a temperature of 627 °C, at two different negative potential limits of -1.81 V and -1.88 V vs. Ag/AgCl. Figure 6.1 exhibits features that were observed in all of the voltammograms obtained at stainless steel working electrodes in the Li_2CO_3-Na_2CO_3 electrolyte, regardless of the specific temperature used.

By comparing Figure 6.1 with the voltammograms obtained at platinum working electrodes in Chapter 4, it is possible to ascertain which peaks were caused by interactions between the molten carbonate electrolyte and the stainless steel working electrode. Peaks that were considered to be due to reactions involving substances from the stainless steel working

electrode have a letter 'M' at the start of their labels. Peaks that were identified in Chapter 4 use the labels that were assigned to them in that chapter. First, the peaks associated with reactions that did not involve substances originating from the working electrode material shall be identified, which should be the same as those observed in Chapter 4 at platinum working electrodes. Please refer to Chapter 4 for a detailed discussion of the phenomena responsible for these peaks.

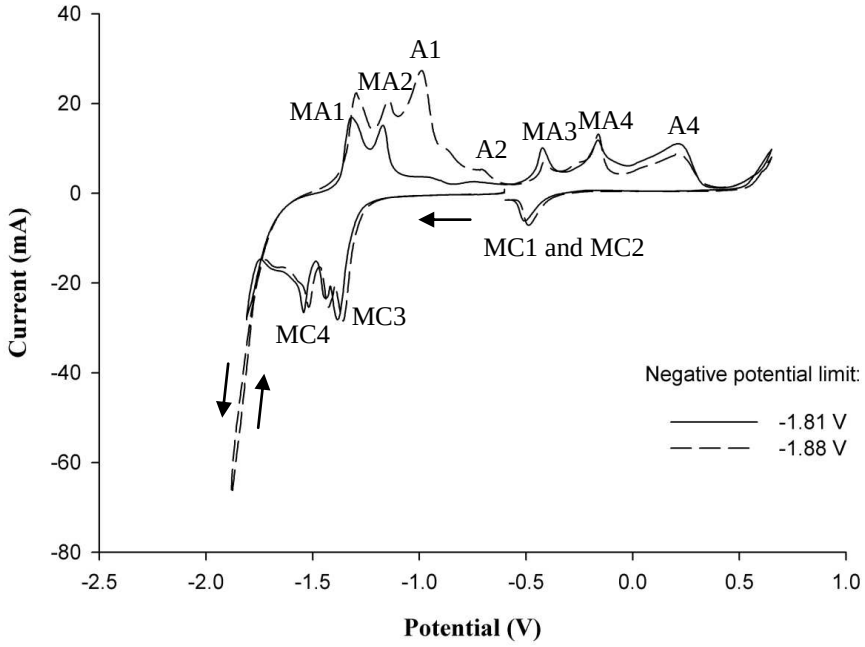

Figure 6.1: Cyclic voltammograms obtained using a stainless steel wire working electrode in a molten Li_2CO_3-Na_2CO_3 electrolyte (molar ratio of 52:48) at 627 °C, at a scan rate of 100 mV/s, for negative potential limits of -1.81 V and -1.88 V. Atmosphere: CO_2; WE diameter: 0.25 mm; WE immersion depth: ca. 1.5 cm; CE: 6 mm diameter stainless steel rod; RE: alumina membrane Ag/AgCl.

The cathodic limit in Figure 6.1 probably corresponds to carbon electro-deposition:

$$CO_3^{2-} + 4e^- \rightarrow C + 3O^{2-} \qquad (6.1)$$

As was stated in Chapter 4, carbon electro-deposition has been observed to occur at potentials beyond the cathodic limit in the Li_2CO_3-Na_2CO_3 electrolyte. In addition to carbon electro-

deposition, it is likely that other competing reactions took place at the cathodic limit, such as alkali metal cation reduction and carbon monoxide formation.

Peak A1 was also observed using the platinum working electrode and can be attributed to the re-oxidation of electro-deposited carbon. In Chapter 4, it was shown that peak A1 increased in height when the negative potential limit of the scan was made more negative (see Figure 4.1), or when the scan rate was decreased (see Figure 4.6). Both of these behaviours have been observed at stainless steel working electrodes. Figure 6.1 shows that the height of peak A1 increased when the negative potential limit was changed from -1.81 V to -1.88 V vs. Ag/AgCl. Figure 6.2 shows the effect of changing the scan rate at temperatures of 599 °C and 703 °C. At both temperatures, the height of peak A1 increased as the scan rate was made smaller. Note that there is a large difference in the currents observed between Figures 6.2(a) and 6.2(b), which is probably due to the difference in working electrode immersion depth, as well as the more negative potential limit used in Figure 6.2(b). However, the trend for peak A1 is the same in both cases. Since peaks MA1 and MA2 do not exhibit comparable behaviour to that described for peak A1 in Chapter 4, it is reasonable to assign peak A1 as indicated in Figure 6.1.

Furthermore, when the potential was held at the negative potential limit of the scan for ten seconds, peak A1 drastically increased in height compared to when the potential was not held, as is shown in Figure 6.3. This supports the attribution of peak A1 argued above. Generally, holding the potential at the negative potential limit yielded similar results to when the negative potential limit was made more negative.

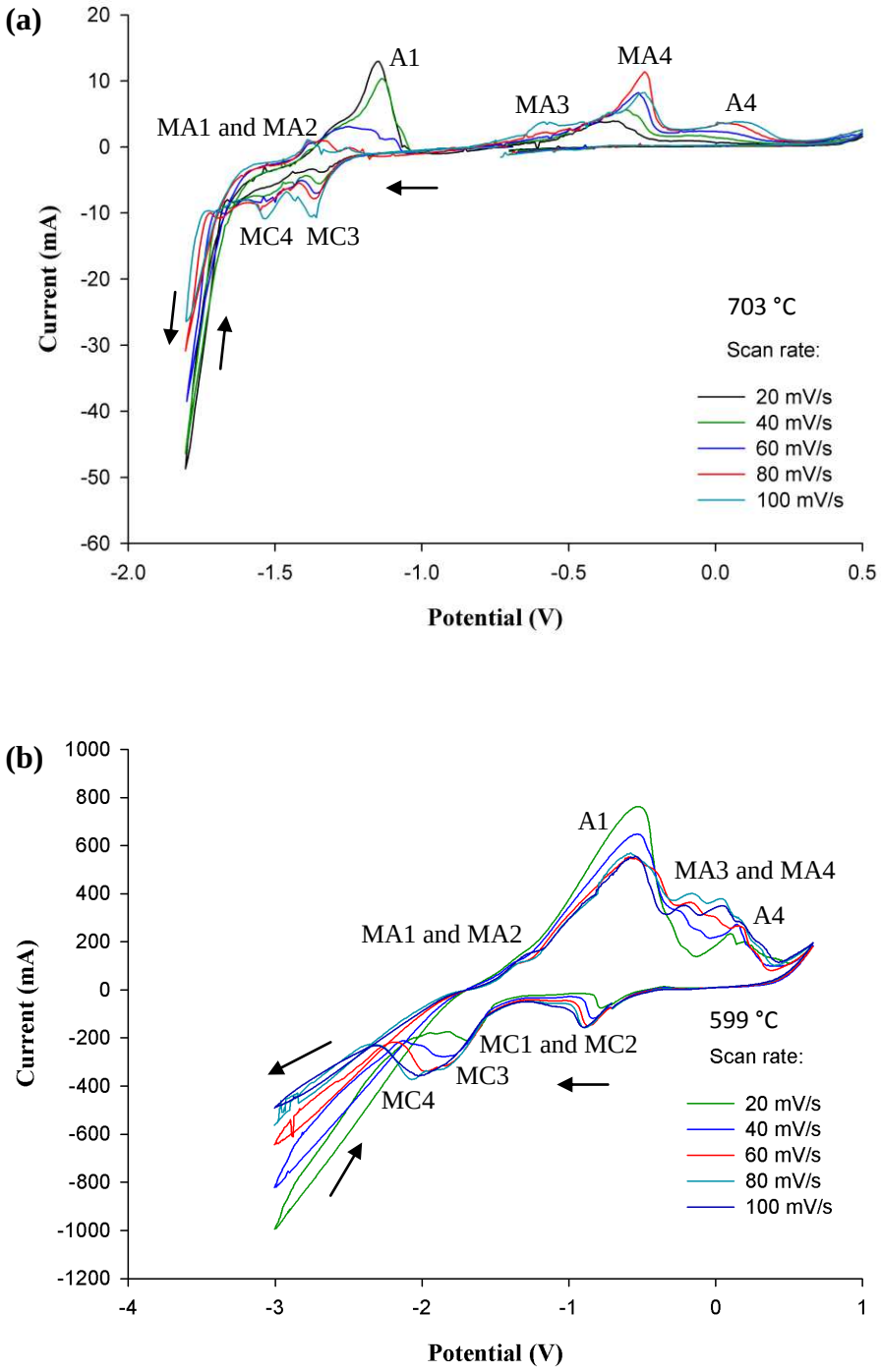

Figure 6.2: Cyclic voltammograms obtained at various scan rates, for a Li_2CO_3-Na_2CO_3 molten salt mixture (molar ratio of 52:48) at temperatures of (a) 703 °C and (b) 599 °C. Atmosphere: CO_2; WE: 0.25 mm diameter stainless steel wire; WE immersion depths: (a) ca. 2.3 cm, (b) ca. 2.7 cm; CE: 6 mm diameter stainless steel rod; Ag/AgCl membrane RE.

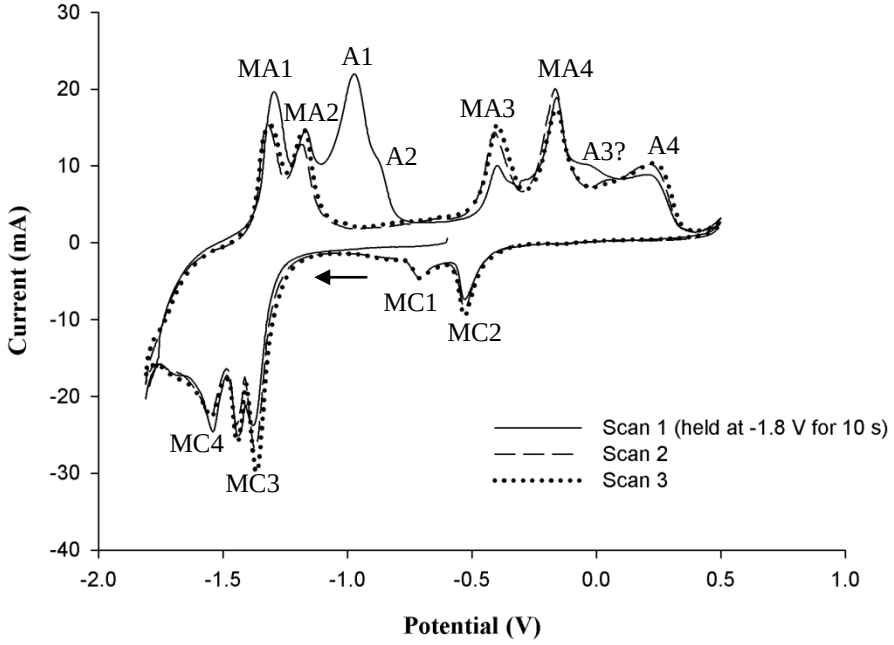

Figure 6.3: Cyclic voltammograms obtained from a Li_2CO_3-Na_2CO_3 molten salt (molar ratio of 52:48) at a temperature of 627 °C, under a CO_2 atmosphere. Note that the potential was held at -1.8 V for 10 s during the first scan. Scan rate: 100 mV/s; WE: 0.25 mm diameter stainless steel wire; WE immersion depth: ca. 1.5 cm; CE: 6 mm diameter stainless steel rod; Ag/AgCl membrane RE.

In Chapter 4, a peak labelled A3 was also ascribed to the oxidation of carbon. However, since peak A3 was usually rather small in the cyclic voltammograms presented in Chapter 4, it is quite likely that peak A3 has been concealed by peaks MA3 and MA4.

Now the peaks that were likely to have been caused by interactions between the working electrode material (stainless steel) and the Li_2CO_3-Na_2CO_3 electrolyte shall be considered. One point worth mentioning here is that carbon electro-deposition eventually covers the bare metal of the working electrode surface during electrolysis, effectively converting the working electrode into a carbon electrode. In addition, the focus of the present work is carbon electro-deposition and re-oxidation. Thus, the following discussion is restricted to findings from cyclic voltammetry in comparison with the very limited literature available.

In Figure 6.1, two sets of anodic and cathodic peaks are present that were associated with reactions involving substances that originated from the working electrode material. The first set consists of the two cathodic peaks MC3 and MC4, and the two anodic peaks MA1 and MA2. The second set consists of the two cathodic peaks MC1 and MC2, and the two anodic peaks MA3 and MA4. Keijzer et al. (1999) observed anodic peaks that are comparable to MA1, MA2, MA3 and MA4 in their cyclic voltammetry at a stainless steel working electrode, using a Li_2CO_3-Na_2CO_3 electrolyte at 650 °C (see Figure 2.11(b) of the present thesis). They also observed a pair of cathodic peaks that are comparable to cathodic peaks MC1 and MC2, but did not observe any peaks that were analogous to MC3 or MC4. However, Biedenkopf et al. (1998) did observe a similar peak to MC3 in cyclic voltammetry at a chromium working electrode, using a molten Li_2CO_3-K_2CO_3 electrolyte at 650 °C.

Identifying which reactions were specifically responsible for peaks MC1, MC2, MC3, MC4, MA1, MA2, MA3 and MA4 is not straightforward from the point of view of this investigation, particularly since stainless steel contains three metals that may react with the electrolyte: iron, nickel and chromium[*]. Based on the findings of this work and those of Biedenkopf et al. (1998) and Keijzer et al. (1999), it seems likely that several reaction peaks associated with transition metals from stainless steel coincide. As a result, no attempt to identify the specific transition-metal-related reactions occurring has been made in this study. Section 2.5.3 of the present thesis may be consulted for details of the likely transition-metal-related oxidation and reduction reactions that Keijzer et al. (1999) considered to take place in the molten Li_2CO_3-Na_2CO_3 and the Li_2CO_3-K_2CO_3 electrolytes.

The set of peaks MA3-MA4-MC1-MC2 seems to be associated with iron oxidation and reduction at the very least, as the conclusions of Keijzer et al (1999) and Biedenkopf et al. (1998) are concordant on this matter. Keijzer et al (1999) also considered that nickel oxidation and reduction took place at this set of peaks, in addition to some reactions associated with chromium. Note that the heights of the anodic peaks MA3 and MA4 are greater than their corresponding cathodic peaks MC1-MC2. Perhaps this is because some of the products of the

[*] The stainless steel wire working electrode used in this investigation consisted of 18 % chromium and 10 % nickel, with the balance being iron.

oxidation reactions responsible for peaks MA3 and MA4 diffused away from the working electrode, so less of these products remained in the vicinity of the working electrode to be reduced at peaks MC1 and MC2. Since Biedenkopf et al. (1998) observed a peak that is analogous to peak MC3 at a chromium working electrode, it seems likely that a number of chromium-related reactions took place at the set of peaks MA1-MA2-MC3-MC4.

6.2.2 Cyclic voltammetry of stainless steel in molten Li_2CO_3-K_2CO_3

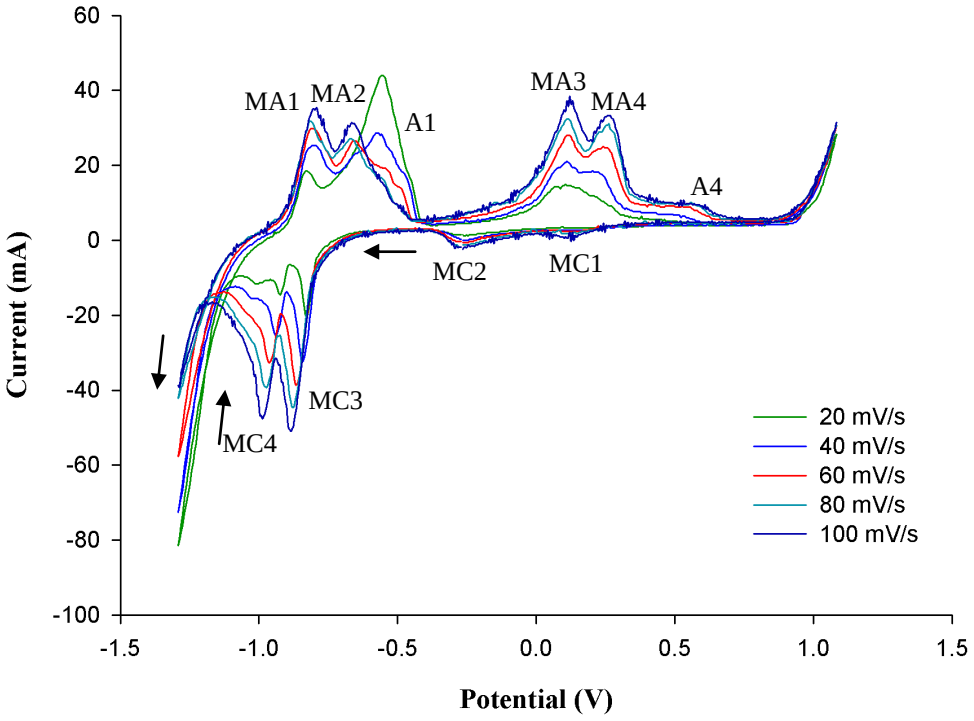

Figure 6.4: Cyclic voltammograms obtained at various scan rates, for a Li_2CO_3-K_2CO_3 molten salt mixture (molar ratio of 62:38) at a temperature of 708 °C under a CO_2 atmosphere. WE: 0.25 mm diameter stainless steel wire; WE immersion depth: ca. 2.2 cm; CE: 6 mm diameter stainless steel rod; Ag/AgCl membrane RE.

Generally, the cyclic voltammetry of stainless working electrodes in the Li_2CO_3-K_2CO_3 electrolyte yielded very similar results to those of the Li_2CO_3-Na_2CO_3 electrolyte. Furthermore, this electrolyte has already been considered in detail in Chapter 5. Therefore, the results from the Li_2CO_3-K_2CO_3 electrolyte will be discussed briefly, since most of the phenomena that have been observed have already been treated in depth in Chapters 4 and 5, and in Section 6.2.1.

Moreover, the peak labels used in this section correspond to the same peak attributions that were made in Section 6.2.1.

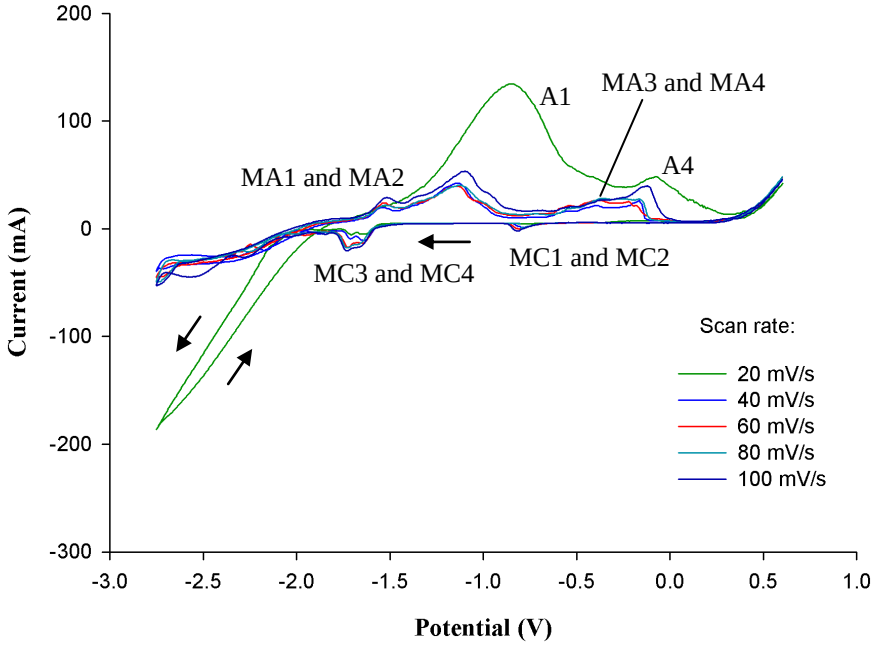

Figure 6.5: Cyclic voltammograms obtained at various scan rates, for a Li_2CO_3-K_2CO_3 molten salt mixture (molar ratio of 62:38) at a temperature of 579 °C under a CO_2 atmosphere. WE: 0.25 mm diameter stainless steel wire; WE immersion depth: ca. 0.7 cm; CE: 6 mm diameter stainless steel rod; Ag/AgCl membrane RE.

The cyclic voltammetry of Li_2CO_3-K_2CO_3 (molar ratio of 62:38) was carried out using stainless steel working electrodes at temperatures of 579 °C and 708 °C. Figure 6.4 shows five cyclic voltammograms that were carried out at different scan rates at 708 °C. Figure 6.4 exhibits very similar responses to those observed in Figure 6.2 for Li_2CO_3-Na_2CO_3: the height of peak A1 increased with decreasing scan rate, whilst the peaks associated with substances from the stainless steel decreased in height with decreasing scan rate. At a temperature of 579 °C, comparable responses were observed, as is shown in Figure 6.5, although the scans did not vary to any great extent as the scan rate was decreased until it reached 20 mV/s. At 20 mV/s, it seems that a much more substantial quantity of carbon was deposited compared to at lower scan rates, as indicated by the larger current wave at the cathodic limit and the higher peak A1.

Notably, cathodic loops were observed in both Figures 6.4 and 6.5, which is indicative of carbon formation taking place at the working electrode surface.

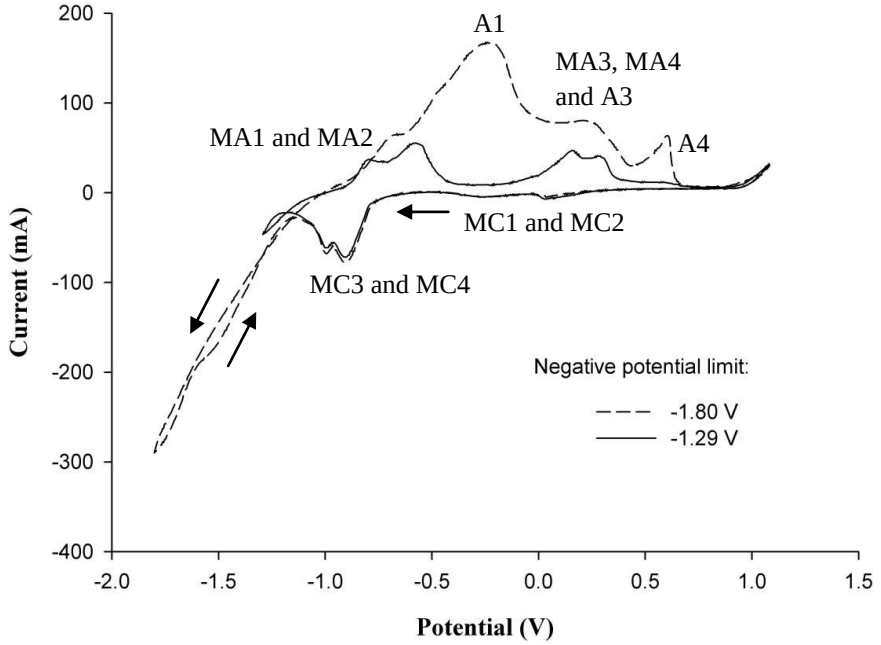

Figure 6.6: Cyclic voltammograms obtained using a stainless steel wire working electrode in a molten Li_2CO_3-K_2CO_3 electrolyte (molar ratio of 62:38) at 708 °C, at a scan rate of 100 mV/s, for negative potential limits of -1.29 V and -1.80 V. Atmosphere: CO_2; WE diameter: 0.25 mm; WE immersion depth: ca. 2.2 cm; CE: 6 mm diameter stainless steel rod; RE: alumina membrane Ag/AgCl.

When the negative potential limit was changed, the cyclic voltammograms obtained from the Li_2CO_3-K_2CO_3 electrolyte also responded in a similar way to the Li_2CO_3-Na_2CO_3 electrolyte. Figure 6.6 shows two cyclic voltammograms obtained from the Li_2CO_3-K_2CO_3 electrolyte at 708 °C at negative potential limits of -1.29 V and -1.80 V vs. Ag/AgCl. In both Figures 6.1 and 6.6, a substantial increase in the height of peak A1 was observed when the negative potential limit was made more negative. However, in Figure 6.6, peaks MA3 and MA4 both increased in height as well. This is probably due to the fact that the difference between the negative potential limits considered in Figure 6.6 was much larger (0.51 V) than the difference considered in Figure 6.1 (0.07 V). As was remarked in Section 6.2.1, peak A3 probably coincided with peaks MA3 and MA4. Therefore, the increase in height of the peak(s) labelled

'MA3, MA4 and A3' may have been primarily caused by an increase in the height of peak A3. This is reasonable because peak A3 corresponds to the oxidation of carbon; at more negative potential limits, greater quantities of carbon were produced, which would have lead to larger peaks (A1 and A3) for the re-oxidation of the carbon.

Figure 6.7 shows the effect of reversing the cathodic sweep at a potential prior to the cathodic peak MC3, for the Li_2CO_3-K_2CO_3 electrolyte. As with Figure 6.4 for Li_2CO_3-Na_2CO_3, this kind of reversal resulted in the disappearance of peak A4, and the only significant peaks that are present in the reversed scan of Figure 6.7 are the set of anodic peaks MC1-MC2-MA3-MA4.

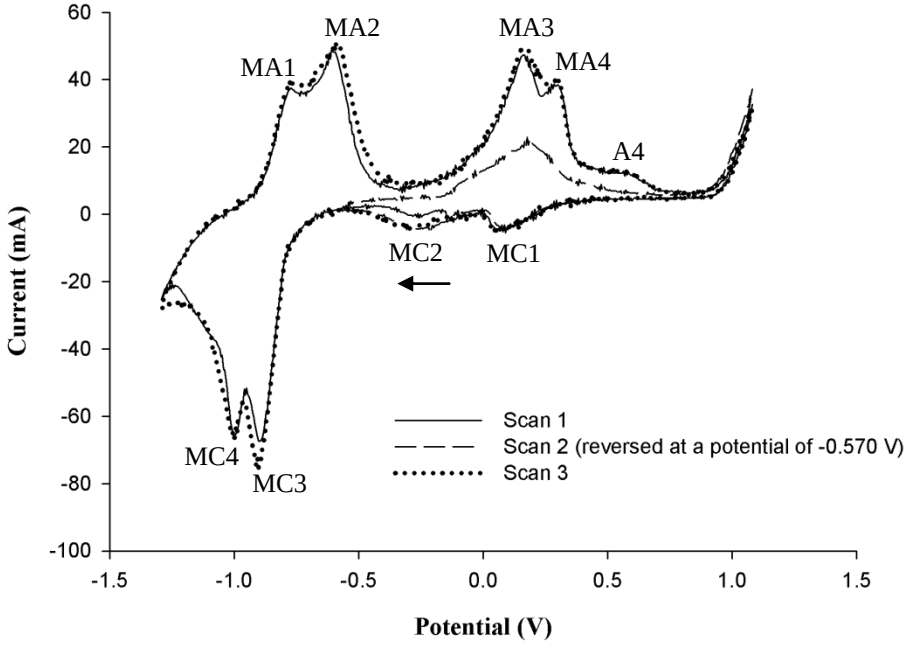

Figure 6.7: Cyclic voltammograms obtained from a Li_2CO_3-K_2CO_3 molten salt (molar ratio of 62:38) at a temperature of 708 °C under a CO_2 atmosphere. Note that the second potential scan was reversed at a potential of -0.570 V. Scan rate: 100 mV/s; WE: 0.25 mm diameter stainless steel wire; WE immersion depth: ca. 2.2 cm; CE: 6 mm diameter stainless steel rod; Ag/AgCl membrane RE.

Regarding the simultaneous occurrence of stainless-steel-related anodic peaks and carbon re-oxidation anodic peaks, it seems that perhaps the working electrode was not completely coated with carbon during a given cycle of cyclic voltammetry, leaving some proportion of the

working electrode surface exposed to the electrolyte. In addition, it is quite possible that some of the oxides containing transition metals dissolved in the electrolyte. For example, Li_2CrO_4, NiO and FeO can all dissolve in molten carbonate electrolytes (Keijzer et al.,1999). Such dissolved species could still undergo electrochemical reactions at the working electrode regardless of whether a layer of electro-deposited carbon was present or not.

6.3 Cyclic Voltammetry of Carbonate Electrolytes that do not contain Lithium Cations: Na_2CO_3 and K_2CO_3

In the second half of this chapter, the cyclic voltammetry of two carbonate-only electrolytes that do not contain lithium cations is considered: Na_2CO_3 and K_2CO_3. No carbon deposits could be obtained from these two electrolytes, and this observation supports the claim of Ingram et al. (1966) that the presence of lithium cations is required to electro-deposit carbon from carbonate-only electrolytes.

6.3.1 Cyclic voltammetry of stainless steel in molten Na_2CO_3

Figure 6.8 shows a typical cyclic voltammogram obtained from a pure Na_2CO_3 electrolyte using a stainless steel working electrode, at a temperature of 900 °C. Comparing Figure 6.8 with the cyclic voltammograms presented in Section 6.2, it is apparent that the behaviour of the pure Na_2CO_3 electrolyte was rather different from the molten carbonate electrolytes that contained Li_2CO_3.

No carbon deposits could be obtained from the pure Na_2CO_3 electrolyte during two-electrode electrolysis at a temperature of 900 °C, at an applied potential difference of 4 V (which would have led to a cathode potential of around -2.8 V vs. Ag/AgCl). The cathode material was mild steel. Such a negative cathode potential (beyond the cathodic limit) would have lead to the production of carbon deposits in the molten carbonate electrolytes that contained Li_2CO_3. Siambun (2011b) carried out potentiostatic electrolyses at -1.8 V and -2.0 V vs. Ag/AgCl at a temperature of 910 °C using stainless steel working electrodes, but was not able to obtain any

carbon deposits using the pure Na_2CO_3 electrolyte. Furthermore, no cathodic loops were observed in the cyclic voltammetry of the pure Na_2CO_3 electrolyte, which usually accompany the electro-deposition of carbon. Therefore, it seems that the reaction(s) occurring at the cathodic limit in Figure 6.8 did not include the electro-deposition of carbon.

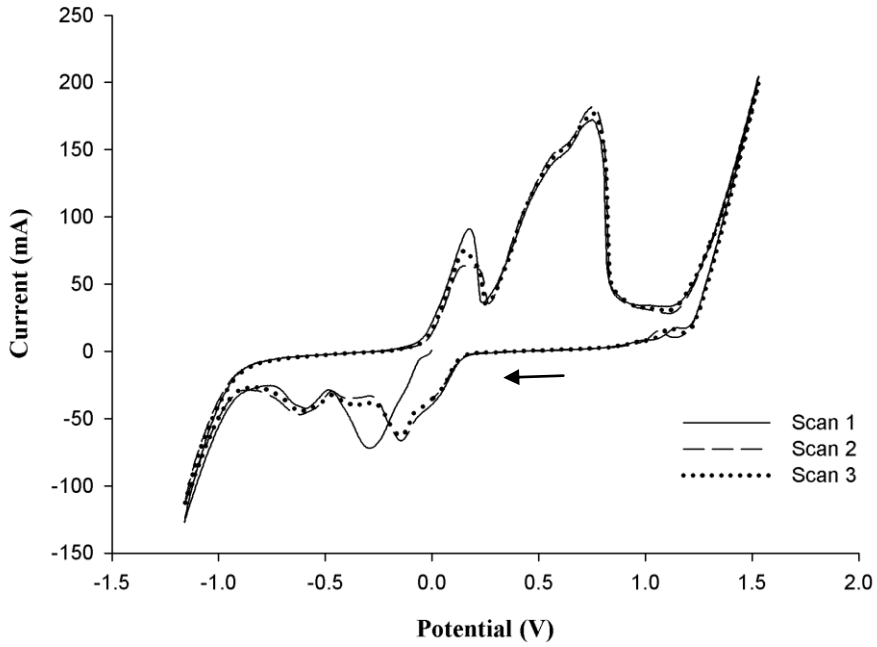

Figure 6.8: Cyclic voltammograms obtained for a pure Na_2CO_3 molten salt at a temperature of 900 °C under a CO_2 atmosphere. Scan rate: 100 mV/s; WE: 0.25 mm diameter stainless steel wire; CE: 6 mm diameter stainless steel rod; Ag/AgCl membrane RE.

The condition of the pure Na_2CO_3 electrolyte after two-electrode electrolysis also supports the conclusion that no carbon electro-deposition had taken place. Normally, when carbon was electro-deposited in any molten carbonate electrolyte, some of the carbon produced fell off the working electrode and sank to the bottom of the crucible[*]. Thus, when the crucible was cleaned after shutting down an experiment, this carbon powder would be observed. No such carbon powder was present in the bottom of the crucible after two-electrode electrolysis had been carried out in the pure Na_2CO_3 electrolyte, which implies that no carbon electro-deposition had taken place to any significant extent.

[*] This issue is considered in more detail in Chapter 7.

The following three cathodic reactions could potentially occur at the cathodic limit in Na_2CO_3:

$$Na^+ + e^- \rightarrow Na \quad (6.2)$$

$$CO_3^{2-} + 4e^- \rightarrow C + 3O^{2-} \quad (6.3)$$

$$CO_3^{2-} + 2e^- \rightarrow CO + 2O^{2-} \quad (6.4)$$

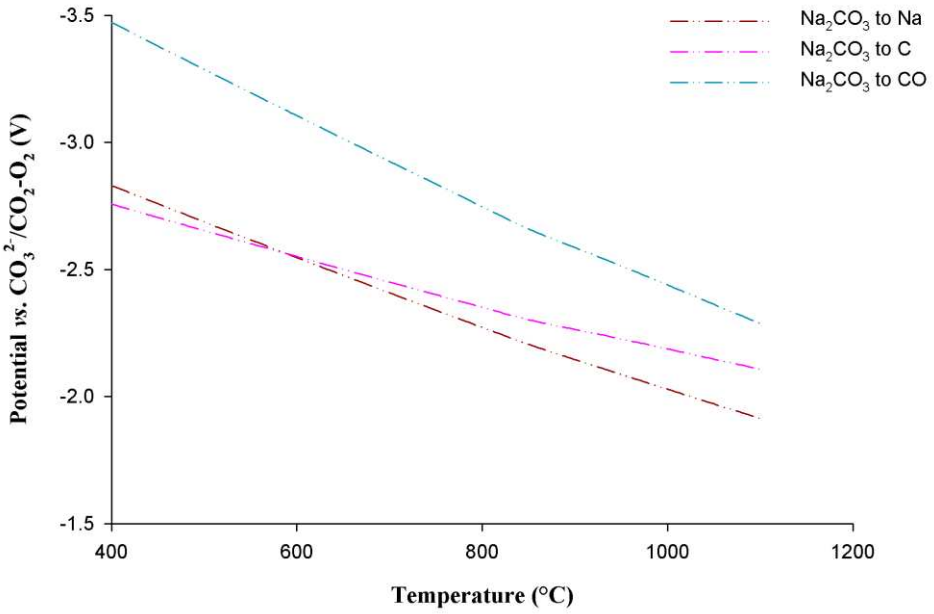

Figure 6.9: Standard potentials against temperature for the conversion of Na_2CO_3 to various cathodic products: carbon (C), sodium metal (Na) and carbon monoxide (CO).The potentials were calculated with the assistance of HSC Chemistry software (Version 6.12; Outokumpu Research) and are reported versus the CO_3^{2-}/CO_2-O_2 reference reaction. Appendix I gives details of how these standard potentials were determined.

Figure 6.9 shows the variation of theoretical standard potentials against temperature, for Reactions 6.2, 6.3 and 6.4 in the pure Na_2CO_3 electrolyte. The most thermodynamically favourable reaction at 900 °C is sodium metal formation via Reaction 6.2. The standard potential for carbon monoxide formation via Reaction 6.4 is the most negative of the three reactions at all of the temperatures shown in Figure 6.9, albeit it cannot be ruled out as a possible cathodic reaction. Even though the standard potential of Reaction 6.3 is not much more negative than that of Reaction 6.2, it is surprising that no carbon deposits could be

obtained from the pure Na_2CO_3 electrolyte. Perhaps carbon electro-deposition was not observed because the overpotential required for Reaction 6.3 to occur was too high. Hence, it would appear that the principal reaction at the cathodic limit was Reaction 6.2.

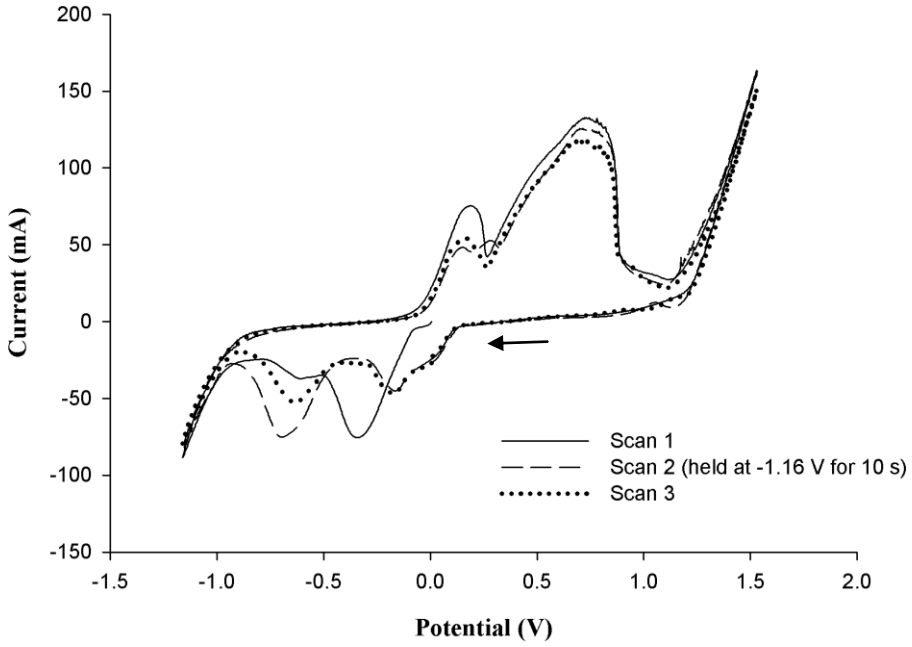

Figure 6.10: Cyclic voltammograms obtained for a pure Na_2CO_3 molten salt at a temperature of 900 °C under a CO_2 atmosphere. Note that the potential was held at -1.16 V for 10 seconds during the second scan. Scan rate: 100 mV/s; WE: 0.25 mm diameter stainless steel wire; CE: 6 mm diameter stainless steel rod; Ag/AgCl membrane RE.

From the evidence obtained, it is apparent that none of the products formed at the cathodic limit remained at the working electrode to be re-oxidised during the anodic sweep. Figure 6.10 shows the effect of holding the potential at the cathodic limit for 10 seconds during the second scan. Holding the potential appears to have had no effect on any of the anodic peaks compared to when the potential was not held. Figure 6.11 shows the effect of changing the scan rate on the cyclic voltammograms obtained from the Na_2CO_3 electrolyte. The heights of all the anodic and cathodic peaks decreased when the scan rate was decreased. This behaviour is similar to that expected from peaks associated with substances from the working electrode metal, as was observed in Section 6.2 for the electrolytes that contained Li_2CO_3. In addition, no anodic peaks exhibited an increase in height with decreasing scan rate in Figure 6.11. This implies that no

carbon was produced at the cathodic limit, since at least one of the characteristic carbon re-oxidation peaks (peak A1) tends to show an increase in height with decreasing scan rate.

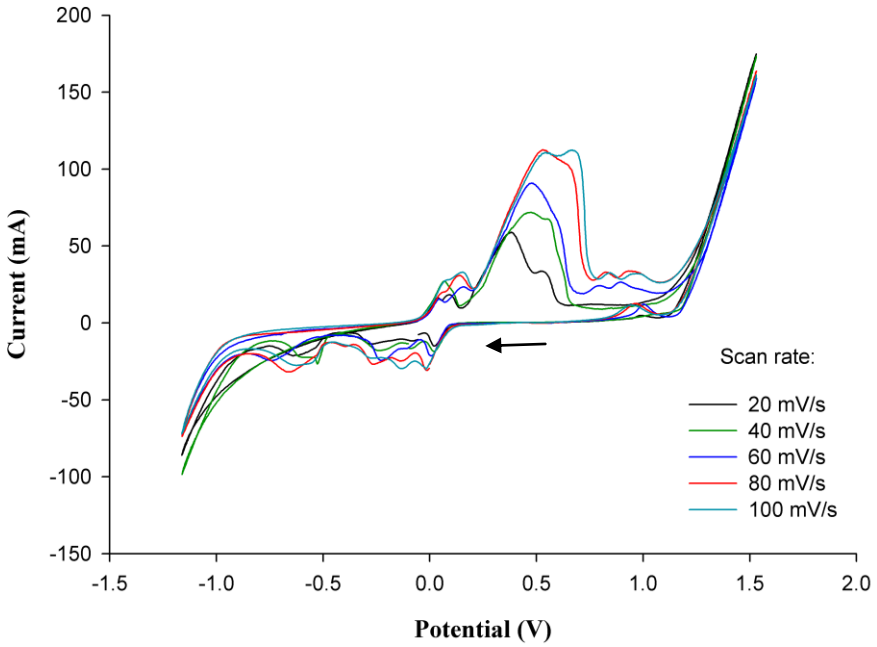

Figure 6.11: Five cyclic voltammograms obtained at various scan rates from a Na_2CO_3 molten salt at a temperature of 900 °C under a CO_2 atmosphere. WE: 0.25 mm diameter stainless steel wire; CE: 6 mm diameter stainless steel rod; Ag/AgCl membrane RE.

Although no anodic peaks were identified that were apparently connected with the oxidation of products that were produced at the cathodic limit, this observation was not entirely unexpected. Any sodium metal that was produced at the cathodic limit would have been a vapour at 900 °C, as its boiling point is 883 °C (Knovel Corporation, 2008). Thus, any sodium metal that was produced would have probably evaporated before it could be detected during the anodic sweep. Similarly, if any carbon monoxide were produced at the cathodic limit, this might also have moved away from the working electrode surface too quickly for it to be re-oxidised.

All of the anodic and cathodic peaks observed in Figure 6.8 were probably caused by reactions involving substances from the working electrode material. On the other hand, the anodic limit probably corresponds to the oxidation of carbonate ions. It would appear that the two major anodic peaks in Figure 6.8 are paired with the two major cathodic peaks. This is apparent when

the potential scan was reversed before the cathodic peaks were reached, as is shown in Figure 6.12. When the scan direction was reversed just before the end of the first scan, no anodic peaks were detected during the anodic sweep. Since no studies of the stainless steel working electrode composition before and after electrolysis have been carried out in the present work, it is not possible to assign specific reactions to the anodic and cathodic peaks. Petrushina et al. (2000) investigated the cyclic voltammetry of stainless steel in the Na_2CO_3-K_2CO_3 electrolyte at a temperature of 730 °C. Petrushina et al. (2000) did not suggest any specific reactions for the peaks observed in the Na_2CO_3-K_2CO_3 electrolyte, but did state that Na^+ ions were involved in the formation of oxide layers on the surface of the stainless steel.

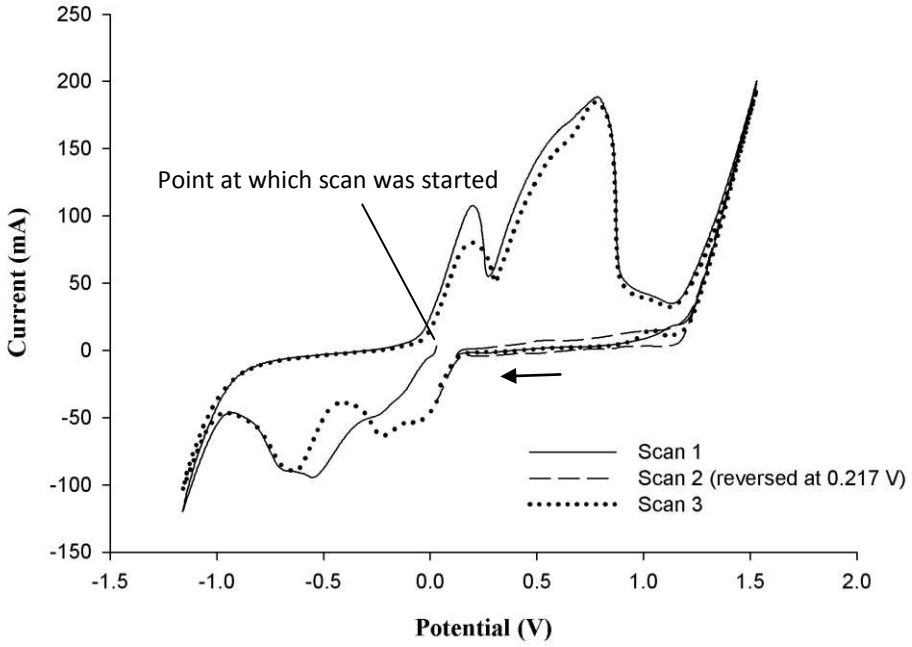

Figure 6.12: Cyclic voltammograms obtained for a pure Na_2CO_3 molten salt at a temperature of 900 °C under a CO_2 atmosphere. Note that the second scan was started by reversing the first scan at a potential of 0.217 V. Scan rate: 100 mV/s; WE: 0.25 mm diameter stainless steel wire; CE: 6 mm diameter stainless steel rod; Ag/AgCl membrane RE.

Petrushina et al. (2000) considered that one of the peaks observed in the voltammetry of the Na_2CO_3-K_2CO_3 electrolyte involved the anodic dissolution of the stainless steel. This is almost certainly the case for the pure Na_2CO_3 electrolyte considered in this section as well, as the immersed part of the working electrode broke off after around 42 consecutive scans of cyclic

voltammetry. This anodic dissolution of stainless steel in pure Na_2CO_3 may have been exacerbated by the fact that no $LiFeO_2$ could be formed at the working electrode surface. When $LiFeO_2$ is formed at the surface of the stainless steel, it protects the stainless steel to a certain extent due to the fact that it has a low solubility in molten carbonate electrolytes (Biedenkopf et al., 1998). This may be why little significant anodic dissolution was observed in the molten carbonate electrolytes that contained Li_2CO_3.

6.3.2 Cyclic voltammetry of stainless steel in molten K_2CO_3

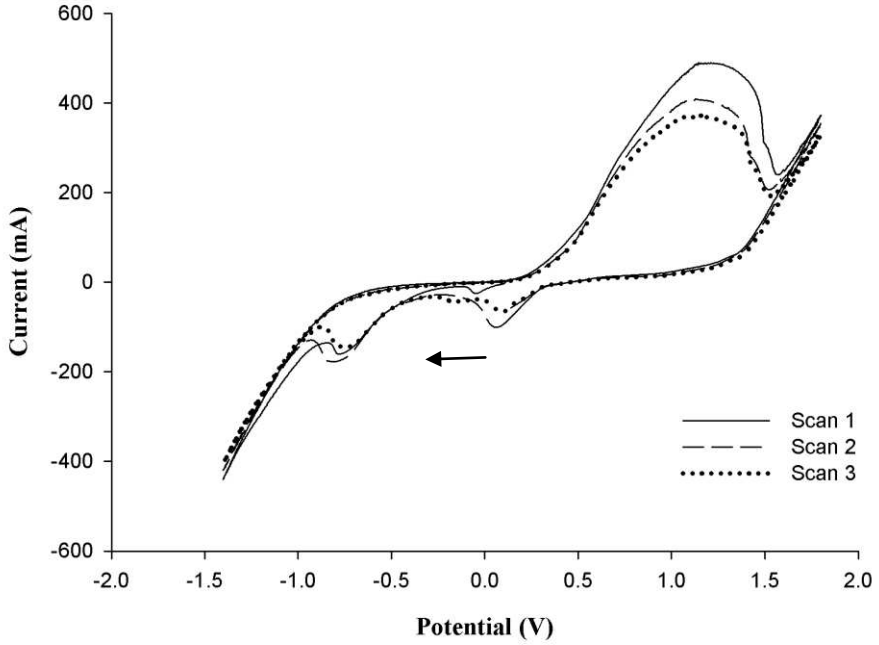

Figure 6.13: Cyclic voltammograms obtained from a pure K_2CO_3 molten salt at a temperature of 930 °C under a CO_2 atmosphere. Scan rate: 100 mV/s; WE: 0.25 mm diameter stainless steel wire; CE: 6 mm diameter stainless steel rod; Ag/AgCl membrane RE.

Figure 6.13 shows a typical cyclic voltammogram obtained at a stainless steel working electrode in the pure K_2CO_3 electrolyte at 930 °C. Evidently, the general appearance of Figure 6.13 is very different to the cyclic voltammograms presented in Section 6.2 for the molten carbonate electrolytes that contain Li_2CO_3.

No carbon deposits could be obtained from the pure K_2CO_3 under the conditions studied in this research. Electrolysis was carried out using a mild steel working electrode, at a temperature of 930 °C and an applied potential difference of 4 V (which would have corresponded to a cathode potential of around -2.7 V vs. Ag/AgCl). Siambun (2011b) carried out potentiostatic electrolyses at -1.8 V and -2.0 V vs. Ag/AgCl at a temperature of 980 °C using stainless steel working electrodes, but was not able to obtain any carbon deposits from the K_2CO_3 electrolyte. Furthermore, two other observations indicate that no carbon electro-deposition took place under the conditions studied in the present research. Firstly, no cathodic loops were observed in cyclic voltammetry; the observance of such loops appears to be indicative of carbon electro-deposition. Secondly, no traces of any carbon were found in the electrolyte after shutting down the experiment.

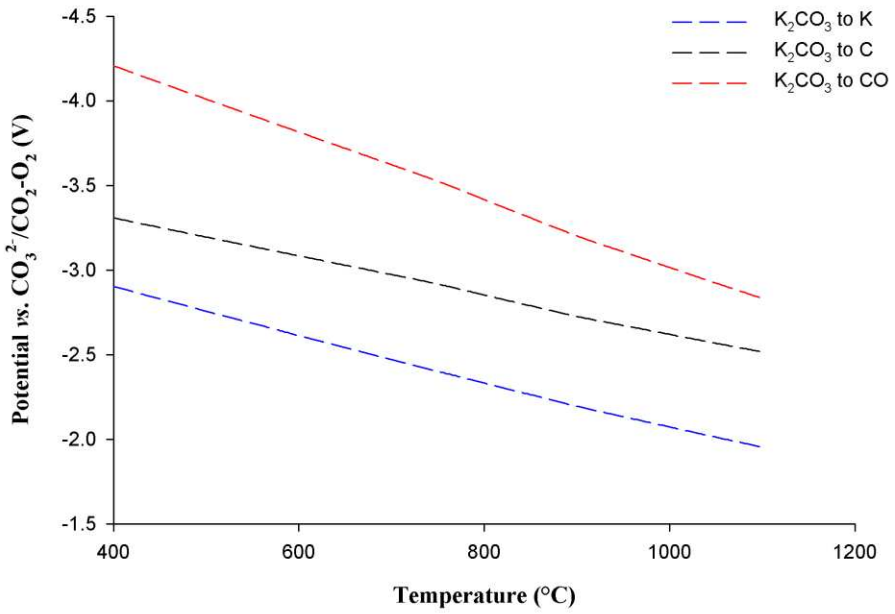

Figure 6.14: Standard potentials against temperature for the conversion of K_2CO_3 to various cathodic products: carbon (C), potassium metal (K) and carbon monoxide (CO).The potentials were calculated with the assistance of HSC Chemistry software (Version 6.12; Outokumpu Research) and are reported versus the CO_3^{2-}/CO_2-O_2 reference reaction. Appendix I gives details of how these standard potentials were determined.

Regarding the reactions that occurred at the cathodic limit in the pure K_2CO_3 electrolyte, the following reactions could potentially have taken place:

$$K^+ + e^- \rightarrow K \quad (6.5)$$

$$CO_3^{2-} + 4e^- \rightarrow C + 3O^{2-} \quad (6.6)$$

$$CO_3^{2-} + 2e^- \rightarrow CO + 2O^{2-} \quad (6.7)$$

The variation of the theoretical standard potentials of Reactions 6.5, 6.6 and 6.7 with temperature are shown in Figure 6.14. Evidently, the most thermodynamically favourable reaction at 930 °C in Figure 6.14 is Reaction 6.5, followed by Reaction 6.6 and lastly Reaction 6.7. In light of the standard potentials presented in Figure 6.14 and the experimental evidence presented thus far, it seems likely that Reaction 6.5 was the principal reaction at the cathodic limit in the pure K_2CO_3 electrolyte.

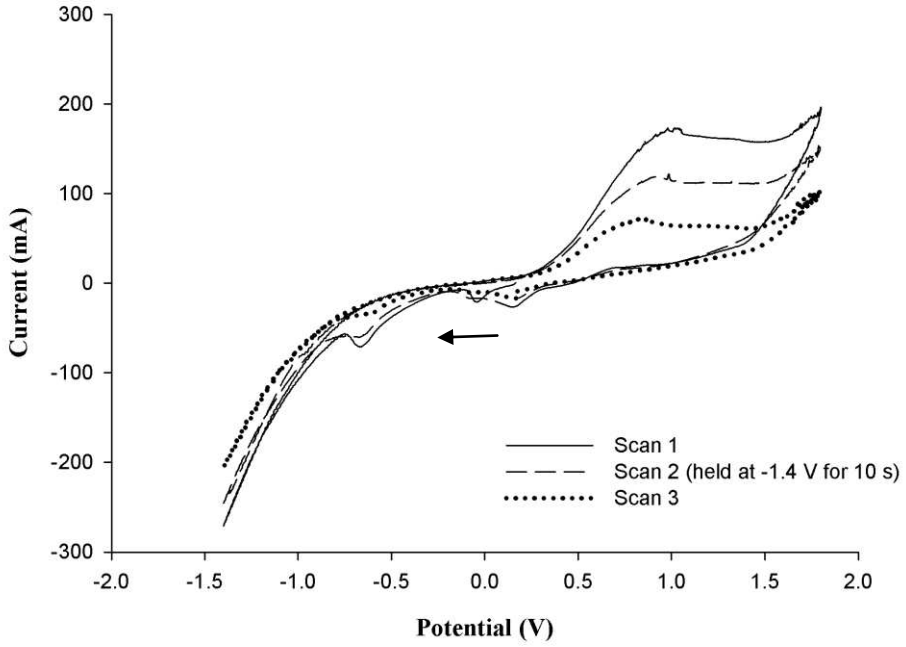

Figure 6.15: Cyclic voltammograms obtained from a pure K_2CO_3 molten salt at a temperature of 930 °C under a CO_2 atmosphere. Note that the potential was held at -1.4 V for 10 s during the second scan. Scan rate: 100 mV/s; WE: 0.25 mm diameter stainless steel wire; CE: 6 mm diameter stainless steel rod; Ag/AgCl membrane RE.

All of the peaks observed in Figure 6.13 appear to have been associated with reactions involving substances from the stainless steel working electrode, whilst the oxidation of carbonate ions probably occurred at the anodic limit. When the potential was held at the negative potential limit for 10 seconds, the anodic peak did not increase in height, as is shown in Figure 6.15. This suggests that none of the products produced at the cathodic limit were oxidised during the anodic sweep. This is not unexpected, as the boiling point of potassium metal is 760 °C (Knovel Corporation, 2008). As a consequence, it is likely that any potassium metal produced at the cathodic limit evaporated too quickly for it to be re-oxidised during the anodic sweep. Note that there is a general decrease in current with each successive scan in Figure 6.15. This current decrease is indicative of anodic dissolution, and implies that the anodic peak is associated with the anodic dissolution of the stainless steel working electrode. When the working electrode was removed from the electrolyte after cyclic voltammetry, the electrode was found to have become much thinner where it had been immersed, which is strong evidence for anodic dissolution.

Figure 6.16 shows the effect of changing the scan rate on the cyclic voltammetry obtained at a stainless steel working electrode in the pure K_2CO_3 electrolyte. All of the peaks decreased in height with decreasing scan rate. On the basis of the behaviour observed in the cyclic voltammgrams that were presented in Section 6.2, this is consistent with the behaviour of peaks that were associated with reactions involving substances from the working electrode metal.

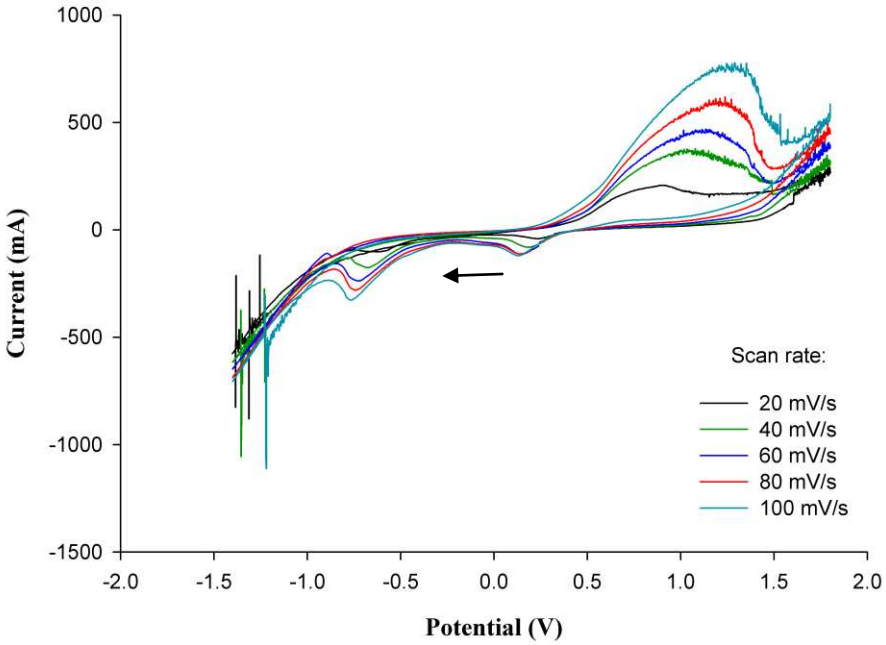

Figure 6.16: Five cyclic voltammograms obtained at five different scan rates from a K_2CO_3 molten salt at a temperature of 930 °C under a CO_2 atmosphere. Working electrode: 0.25 mm diameter stainless steel wire; counter electrode: 6 mm diameter stainless steel rod; Ag/AgCl membrane reference electrode.

6.4 Conclusions

Electro-deposited carbon could be obtained from all of the carbonate-only electrolytes that contained Li_2CO_3 in the present work: Li_2CO_3-Na_2CO_3, Li_2CO_3-K_2CO_3, Li_2CO_3 and Li_2CO_3-Na_2CO_3-K_2CO_3[*]. However, no carbon electro-deposition was found to take place in the lithium-free, carbonate-only electrolytes: Na_2CO_3, K_2CO_3 and Na_2CO_3-K_2CO_3[†]. Thus, the findings of this chapter support the conclusion of Ingram et al. (1966) that the presence of lithium cations is necessary in order for carbon electro-deposition to occur in carbonate-only electrolytes. Whilst this agrees with the thermodynamic analyses of possible cathodic reactions, it is still unclear if the overpotential necessary for carbon electro-deposition in the

[*] See Appendix II for the results obtained from the Li_2CO_3 and Li_2CO_3-Na_2CO_3-K_2CO_3 electrolytes.
[†] See Appendix II for the results obtained from the Na_2CO_3-K_2CO_3 electrolyte.

Na_2CO_3, K_2CO_3 and Na_2CO_3-K_2CO_3 electrolytes was too high and hence was not attained in the present study.

Carbon electro-deposition was found to occur at the cathodic limit of all the carbonate electrolytes that contained Li_2CO_3. The mixtures of Li_2CO_3-Na_2CO_3 and Li_2CO_3-K_2CO_3 exhibited similar cyclic voltammetry at stainless steel working electrodes; thus the electrochemical reactions occurring in these electrolytes were very similar. The peaks associated with carbon re-oxidation were identified by comparison with the voltammograms presented in Chapters 4 and 5, and by their responses to the manipulation of cyclic voltammetry (i.e. changing the scan rate, holding the potential and reversing the potential scan). Two sets of anodic and cathodic peaks in the voltammograms were found to be associated with reactions involving the working electrode material itself. Each set of peaks consisted of four paired peaks: two anodic peaks and two cathodic peaks. These peaks were probably associated with the formation of a variety of oxides from the chromium, nickel and iron present in the working electrode. These reactions involving substances from the working electrode material would not have a drastic effect on long-term carbon electro-deposition due to the fact that the metal working electrode would become coated with a layer of electro-deposited carbon.

Moving on to the Na_2CO_3 and K_2CO_3 electrolytes, alkali metal formation was probably the main reaction taking place at the cathodic limit of these electrolytes. However, none of the products formed at the cathodic limit were found to be re-oxidised during the anodic sweep of cyclic voltammetry at stainless steel working electrodes. This is probably because any alkali metal produced at the working electrode evaporated or entered the electrolyte too quickly for it to be detected during the anodic sweep. Thus, all of the anodic and cathodic peaks were found to be associated with reactions involving substances from the stainless steel working electrode material itself. The specific reactions responsible for these peaks is not clear at present, but at least some of the reactions led to the anodic dissolution of the working electrode. It would appear that stainless steel is more susceptible to anodic dissolution in the carbonate-only electrolytes that lack Li_2CO_3, and this was probably due to the fact that $LiFeO_2$ could not be

formed in such electrolytes. When $LiFeO_2$ forms, it protects the stainless steel to a certain extent because it is not very soluble in molten carbonates (Biedenkopf et al., 1998).

CHAPTER 7

THE ELECTRO-DEPOSITION OF CARBON AND ITS PROPERTIES

This seventh chapter presents the results of a study of carbon electro-deposition via potentiostatic electrolysis, in which the carbon deposits produced have been analysed using a variety of different techniques. The chapter begins by giving the motivations for studying this topic, followed by sections covering the following areas: chronoamperometry; deposition rate and current efficiency; thermogravimetric analysis (TGA) and heat-flux differential scanning calorimetry (DSC); scanning electron microscopy (SEM); back-scattered scanning electron microscopy (BSEM) and energy-dispersive X-ray (EDX) spectroscopy; and X-ray diffraction (XRD). This chapter focuses on the Li_2CO_3-Na_2CO_3 and Li_2CO_3-K_2CO_3 electrolytes, albeit some results from the Li_2CO_3-Na_2CO_3-K_2CO_3 electrolyte are also presented.

7.1 Reasons for Studying the Potentiostatic Electro-Deposition of Carbon and the Properties of the Carbon Produced

As Section 2.7 in the Literature Review of this thesis demonstrates, the properties of electro-deposited carbon have already been investigated in some detail, for a variety of different deposition conditions and using many different kinds of analysis technique. However, insofar as carbonate-only electrolytes are concerned, only Kaplan et al. (2002) and Le Van et al. (2009) have carried out detailed studies of the properties of electro-deposited carbon, and they have both limited their studies to the Li_2CO_3-Na_2CO_3-K_2CO_3 electrolyte. Thus, there is a need to study other carbonate-only electrolytes, such as Li_2CO_3-Na_2CO_3 and Li_2CO_3-K_2CO_3, in order to ascertain the properties of the electro-deposited carbon that can be produced from them. In addition, no comparative studies of the properties of carbon from different carbonate-only electrolytes have been carried out.

Even though Kaplan et al. (2002) Le Van et al. (2009) studied the electro-deposition of carbon in some detail, neither of these authors attempted to determine current efficiencies or production rates for carbon electro-deposition. In fact, there is a paucity of results regarding the production rates and current efficiencies of carbon deposition. Another area of analysis that has been neglected in the literature is thermal and thermochemical analysis of the carbon using methods such as thermogravimetric analysis (TGA).

This chapter seeks to address the above issues by presenting a comparative study of the electro-deposition of carbon in the Li_2CO_3-Na_2CO_3, Li_2CO_3-K_2CO_3 and Li_2CO_3-Na_2CO_3-K_2CO_3 electrolytes. The results of carbon analysis are presented for each of these three electrolytes for several different sets of electro-deposition conditions.

7.2 Electro-Deposition of Carbon via Potentiostatic Electrolysis (Chronoamperometry)

The carbon deposits that are considered in this chapter were all electro-deposited via chronoamperometry using a three-electrode system; the methodology for this type of experiment is described in Section 3.5.2. In each electro-deposition, the working electrode was a 5 mm diameter mild steel rod[*], the counter electrode was a 6 mm diameter stainless steel rod, and the reference electrode was an alumina membrane Ag/AgCl reference electrode (please see Section 3.4.2 for details). Each electro-deposition experiment had a fixed duration of 30 minutes. As has already been related in the preceding chapters, carbon was electro-deposited via the following reaction:

$$CO_3^{2-} + 4e^- \rightarrow C + 3O^{2-} \qquad (7.1)$$

[*] Graphite could be used as an alternative working electrode material for carbon electro-deposition, but it was not used in the present work because it has been shown that the intercalation of alkali metal ions can cause graphite to disintegrate in molten salts (Chen et al., 1998). Although the overpotential for the deposition of carbon onto carbon is probably lower than that required to deposit carbon onto metal, in practice a carbon coating is formed relatively quickly on the working electrode surface during electrolysis. Therefore, long-duration electrolyses would probably not be significantly affected by whether the working electrode material was mild steel or graphite.

The resulting carbon deposit was cooled and then washed with 0.56 mol/L hydrochloric acid and distilled water - this deposit handling procedure is described in detail in Section 3.7.1. Table 7.1 gives the sets of conditions under which carbon deposits were produced. Deposition potentials were chosen to be approximately 0.6 V, 1.0 V and 1.4 V more negative than the potential at the start of the current wave at the cathodic limit observed in cyclic voltammetry, for each electrolyte in question. Such negative potentials were chosen in order to ensure that sufficient quantities of carbon would be produced during the deposition period for analysis purposes. The two target electrolyte temperatures were 600 °C and 700 °C, although it was difficult to attain these in practice due to the nature of the furnace temperature control mechanism (see Section 4.2 for further details of this issue).

Table 7.1: Conditions under which carbon deposits were produced via chronoamperometry in carbonate-only molten salts. Note that the deposition potentials chosen for each electrolyte were approximately 0.6 V, 1.0 V and 1.4 V more negative than the potential at the start of the current wave at the cathodic limit observed in cyclic voltammetry, for each electrolyte in question.

Molten Salt Composition (Molar Ratio in Brackets)	**Temperature (°C)**	**Deposition Potential (V vs. Ag/AgCl)**
Li_2CO_3-Na_2CO_3 (52:48)	703	-2.60
	703	-3.00
	703	-3.40
	599	-3.07
	599	-3.47
	599	-3.87
Li_2CO_3-K_2CO_3 (62:38)	708	-2.18
	708	-2.58
	708	-2.98
	579	-3.06
	579	-3.46
	579	-3.86
Li_2CO_3-Na_2CO_3-K_2CO_3 (43.5:31.5:25.0)	709	-2.60
	709	-3.00
	709	-3.40

Figure 7.1 shows two typical carbon deposits obtained from the Li_2CO_3-Na_2CO_3-K_2CO_3 electrolyte at potentials of -2.60 V and -3.00 V vs. Ag/AgCl, at a temperature of 709 °C. Generally, all carbon deposits obtained in the present work were of a similar appearance when

removed from the furnace, regardless of the electrolyte and process conditions used. Note that, in Figure 7.1(b), it would appear that a portion of the carbon deposit had fallen off the working electrode into the electrolyte.

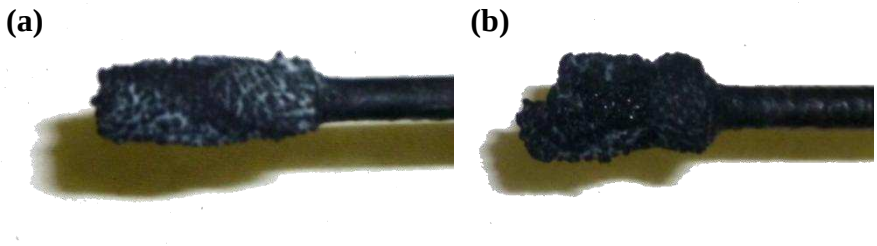

Figure 7.1: 5 mm diameter mild steel rod working electrodes coated with carbon, which was electro-deposited from a Li_2CO_3-Na_2CO_3-K_2CO_3 electrolyte (molar ratio of 43.5:31.5:25.0) at a temperature of 709 °C, and at applied potentials of (a) -2.60 V and (b) -3.00 V vs. Ag/AgCl. The deposition time was 30 minutes in both cases.

Figure 7.2 shows two chronoamperograms obtained from the Li_2CO_3-K_2CO_3 electrolyte at temperatures of 579 °C and 708 °C. These chronoamperograms exhibit typical trends that were observed at temperatures of ca. 600 °C and ca. 700 °C, irrespective of the electrolyte and the applied potential used – i.e. the temperature had an obvious effect on the current-time trend obtained, whilst the electrolyte composition and the applied potential did not. Figure 7.2(a) shows that the current became more negative with time, and is quite similar to the chronoamperogram presented by Le Van et al. (2009) for carbon electro-deposition onto a nickel cathode in a Li_2CO_3-Na_2CO_3-K_2CO_3 electrolyte at a temperature of 450 °C. Le Van et al. (2009) attributed this trend to an increase in the electro-active surface area with time, due to the growth of the carbon deposit, which seems a reasonable explanation.

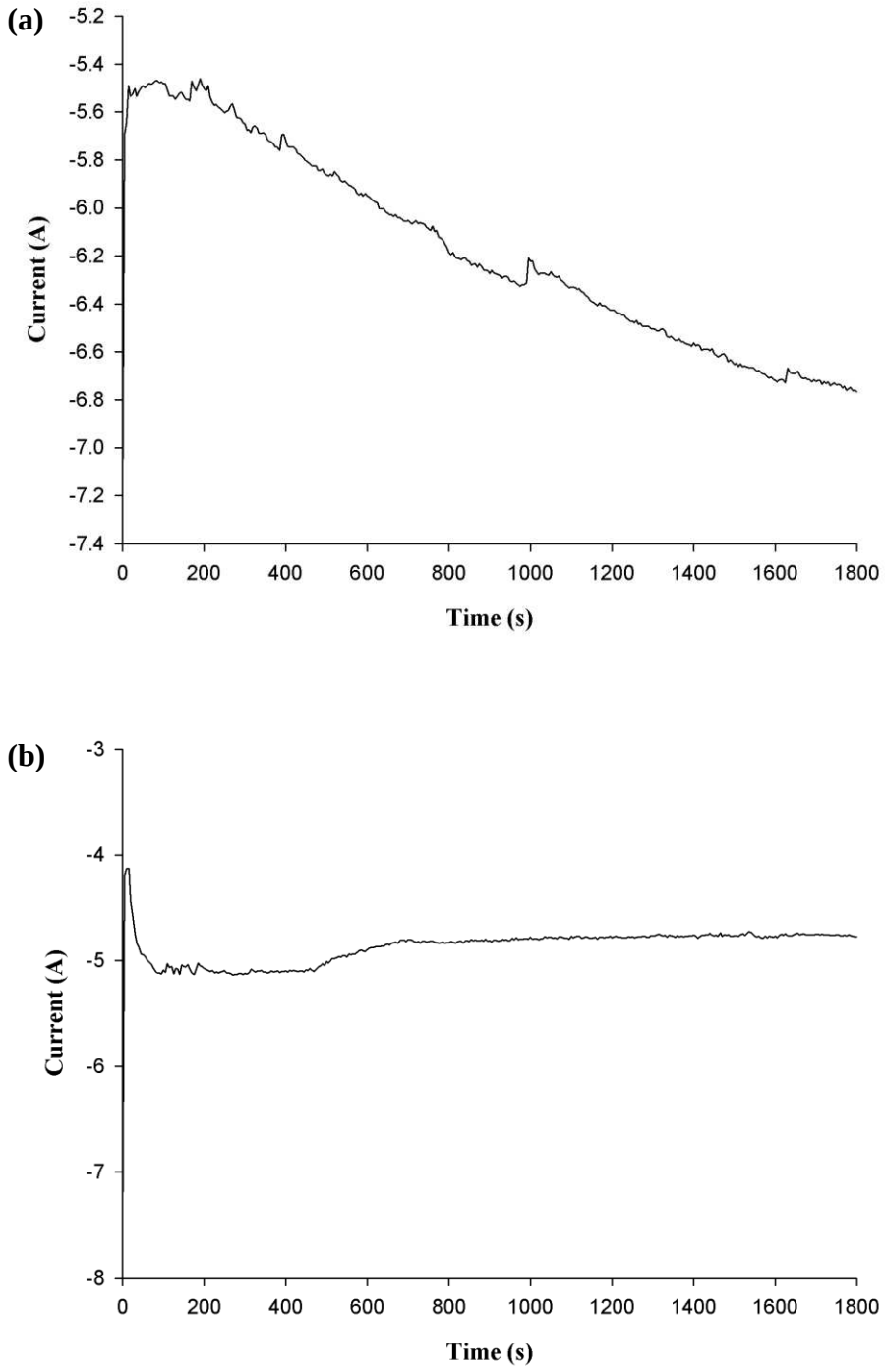

Figure 7.2: Typical variation of current versus time during carbon electro-deposition in a Li_2CO_3-K_2CO_3 electrolyte (molar ratio of 62:38) at temperatures of (a) 708 °C and (b) 579 °C, under a CO_2 atmosphere. The applied working electrode potentials were (a) –2.98 V and (b) −3.86 V. WE: 5 mm diameter mild steel rod; CE: 6 mm diameter stainless steel rod; alumina membrane Ag/AgCl RE.

However, Figure 7.2(b) at ca. 600 °C does not show a comparable trend to Figure 7.2(a). After an initial peak at around 300 seconds in Figure 7.2(b), the current gradually became less negative at a very low rate, even though the carbon deposit would have been growing throughout the electrolysis. This trend may have been due to a trade-off between an increase in the electro-active surface area and an increase in the kinetic and/or electrical resistance.

The transmission electron micrographs obtained by Le Van et al. (2009) for their electro-deposited carbon indicate that their carbon contained substantial amounts of amorphous carbon (see Figure 2.13 in Section 2.7.1). Amorphous carbon tends to have a relatively high electrical resistivity compared to crystalline graphite due to the random orientation of its crystallites (Pierson, 1993), which hinders the formation of extensive networks of delocalised electrons through the π-bonds of its graphene sheets. The electrical resistivity of amorphous carbon is 0.091 Ω.cm, whereas the resistivity of crystalline graphite is only 0.029 Ω.cm. Hence, as the carbon deposit grew larger with time at ca. 600 °C, its resistance would have probably increased as its thickness increased. Such an increase in resistance would have increased the iR drop, and would have made the practically achieved potential of the working electrode less negative (i.e. the potential difference between the working and reference electrodes would have decreased). Thus, this increase in resistance may have lowered the rate of carbon electro-deposition at the deposit surface to such an extent that it compensated for any increase in the electro-active surface area. Such an effect was not observed at temperatures ca. 700 °C (Figure 7.2(a)), which could have been due to the fact that the rate of carbon electro-deposition was intrinsically higher at that temperature. Therefore, any increase in deposit resistance at ca. 700 °C may not have been sufficient to retard the deposition rate significantly.

Earlier in this section it was mentioned that a proportion of the carbon deposit appeared to have been lost from the working electrode in Figure 7.1(b). Two other observations support this idea of carbon loss from the working electrode during electrolysis. Firstly, in the chronoamperogram that was obtained from the electro-deposition of the deposit shown in Figure 7.1(b), a significant ‘kink’ was observed in the positive current direction at around 1700 seconds; this chronoamperogram is shown in Figure 7.3. Such a kink would suggest that a

reduction in the electro-active surface area had occurred. Similar, smaller kinks can also be seen in Figure 7.2(a).

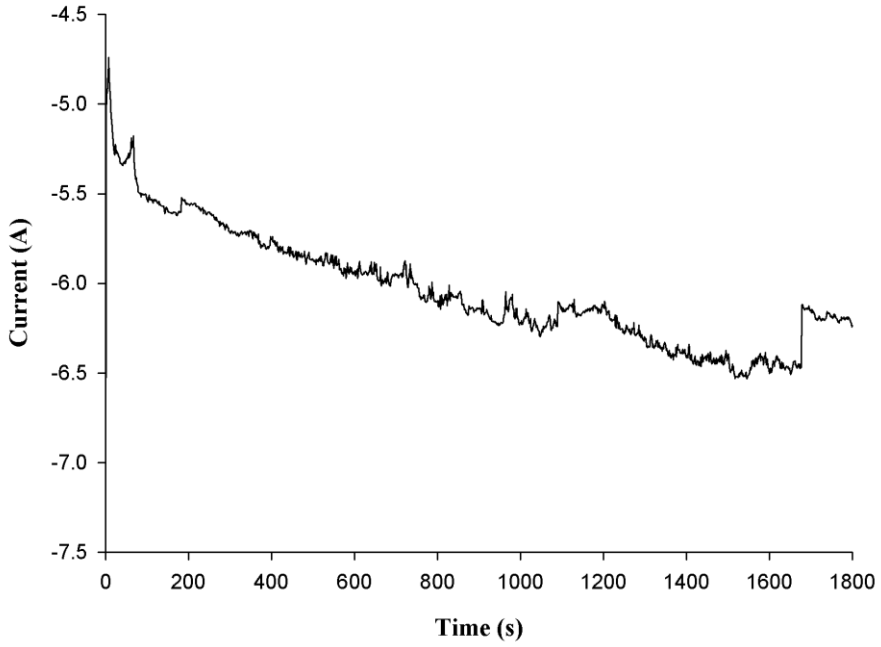

Figure 7.3: Variation of current versus time during carbon electro-deposition in a Li_2CO_3-Na_2CO_3 electrolyte (molar ratio of 52:48) at a temperature of 703 °C, at an applied working electrode potential of -3.00 V, under a CO_2 atmosphere. Note that this figure shows the chronoamperogram of the carbon electro-deposition experiment that produced the carbon deposit shown in Figure 7.1(b). WE: 5 mm diameter mild steel rod; CE: 6 mm diameter stainless steel rod; alumina membrane Ag/AgCl RE.

Secondly, when carbon deposits were produced in a given experiment, some black material was invariably observed at the bottom of the solidified electrolyte after cooling and shutting down the reactor. This black material was probably carbon that fell off the working electrode during electrolysis. Figure 7.4 shows the appearance of a typical solidified electrolyte after carbon electro-deposition had been carried out in earlier experiments. When electrolysis experiments were carried out using the Na_2CO_3, K_2CO_3 and Na_2CO_3-K_2CO_3 electrolytes, no carbon was electro-deposited (see Sections 6.3 and AII.3 for more details) and no black material was found to be present at the bottom of the solidified electrolyte. This observation

supports the idea that the black material observed at the bottom of the electrolyte after carbon electro-deposition had taken place was indeed carbon.

Figure 7.4: Solidified electrolyte removed from the reactor after carbon electro-deposition experiments in a Li_2CO_3-Na_2CO_3-K_2CO_3 electrolyte at a temperature of 702 °C. Note that the electrolyte has been placed upside-down so that the black material at the bottom of the electrolyte can be seen.

In general, the observation of black material at the bottom of the electrolyte and kinks in the chronoamperograms were typical observations for all of the experimental runs in which carbon electro-deposition was carried out. Two principal reasons for these carbon losses were probably the amorphous nature of the carbon deposit and the poor adhesion of the deposit onto the metal working electrode. The amorphous structure of the carbon would possibly have made it easier for portions of the deposit to become detached due to a lack of long-range crystalline order. As for the poor adhesion of the carbon, this would have been caused by the fact that the carbon consists of multiple graphene sheets held together by van der Waals forces (Pierson, 1993), whilst the metal working electrode consists of metal cations bound together in a lattice by electrostatic attraction to delocalised electrons. Any interactions between the carbon and the working electrode metal would as a result be relatively weak van der Waals forces. The intercalation of alkali metal ions into the carbon structure may also have caused some carbon losses. Chen et al. (1998) observed the disintegration of graphite cathodes in chloride molten salts, which was apparently caused by this effect.

7.3 Apparent Carbon Electro-Deposition Rates and Current Efficiencies

Table 7.2: Apparent rates of carbon electro-deposition in the Li_2CO_3-Na_2CO_3, Li_2CO_3-K_2CO_3 and Li_2CO_3-Na_2CO_3-K_2CO_3 electrolytes at several different applied potentials, at temperatures of ca. 600 °C and ca. 700 °C. Note that the carbon production rate refers to the mass of carbon in the deposit, not the overall deposit mass. WE: 5 mm diameter mild steel rod; CE: 6 mm diameter stainless steel rod; alumina membrane Ag/AgCl RE.

Molten Salt Composition (Molar Ratio in Brackets)	**Temperature (°C)**	**Applied Potential (V vs. Ag/AgCl)**	**Apparent Carbon Production Rate ($g/cm^2.h$)**
Li_2CO_3-Na_2CO_3 (52:48)	703	-2.60	0.0309
	703	-3.00	0.103
	703	-3.40	0.164
	599	-3.07	0.0762
	599	-3.47	0.075
	599	-3.87	0.173
Li_2CO_3-K_2CO_3 (62:38)	708	-2.18	0.0618
	708	-2.58	0.128
	708	-2.98	0.183
	579	-3.06	0.0468
	579	-3.46	0.0692
	579	-3.86	0.0706
Li_2CO_3-Na_2CO_3-K_2CO_3 (43.5:31.5:25.0)	709	-2.60	0.0539
	709	-3.00	0.0737
	709	-3.40	0.0887

Table 7.2 gives the apparent carbon electro-deposition rates for the three electrolytes considered in this chapter. The apparent carbon electro-deposition rate was calculated for each electrolyte using the following equation:

$$\text{Deposition Rate} = \frac{\text{Mass of Deposit} \times \text{Mass Percentage of Carbon}}{\text{Immersed Area of Working Electrode} \times \text{Duration of Deposition}} \qquad (7.2)$$

The values that were inserted into this equation were determined as follows. The ‘mass of deposit’ was the mass of the deposit in question after the washing and drying process had been completed. A sample of the deposit was then tested by simultaneous thermogravimetric analysis (TGA) and heat-flux differential scanning calorimetry (DSC) to determine the ‘mass

percentage of carbon present in the deposit' (see Section 7.4 for further details of TGA-DSC analysis of carbon deposits). The 'immersed area of working electrode' was calculated using the measured immersion depth of the working electrode and the electrode diameter.

As for the current efficiency of carbon electro-deposition, this was calculated using the following equation:

$$\text{Current Efficiency} = \frac{\text{Charge Required to Deposit Carbon}}{\text{Charge Supplied During Electrolysis}} \times 100 \qquad (7.3)$$

The values that were inserted into this equation were determined as follows. The 'charge supplied during electrolysis' was simply recorded by the potentiostat during the electrolysis. To calculate the 'charge required to deposit carbon', the stoichiometry of Reaction 7.1 was used first to determine the number of electrons required to deposit a given carbon deposit*; the number of electrons required was then multiplied by the Faraday constant (96485 C/mol) to obtain the 'charge required to deposit carbon'.

Two major trends in the carbon production rate can be observed in Table 7.2. Firstly, the carbon production rate increased as the applied potential was made more negative. As was observed in the cyclic voltammograms presented in Chapters 4 and 5, carbon electro-deposition occurred at the cathodic limit and did not appear to be limited by mass transfer under the conditions considered in the present work. Thus, one would expect the current to increase with increasing overpotential as described by the Butler-Volmer equation (Bard and Faulkner, 2001):

$$i = i_0 \left[e^{\frac{-\alpha F \eta}{RT}} - e^{\frac{(1-\alpha) F \eta}{RT}} \right] \qquad (7.4)$$

Where: i = current, i_0 = exchange current, α = transfer coefficient, F = Faraday's constant, R = molar gas constant, T = absolute temperature and η = overpotential.

* Note that the mass of carbon was used in calculation of this value, not the mass of the overall deposit.

Hence, when a more negative potential was applied during carbon electro-deposition, the overpotential would have been larger, resulting in a larger current and as a consequence a larger carbon production rate.

Secondly, it would appear that the carbon production rates attained were generally higher at higher temperatures. This is not unexpected considering the presence of -1/T in the powers of the exponentials in Equation 7.4. However, if the temperature were to exceed 1000 °C, then one might expect the rate of carbon electro-deposition to drop due to the formation of carbon monoxide. As Figure 4.3 in Section 4.2.1 shows, the theoretical standard potential for carbon monoxide formation only becomes less negative than that for carbon electro-deposition at around 1000 °C.

Comparing the carbon electro-deposition rates obtained for each of the three electrolytes at a given temperature, it would appear that the Li_2CO_3-Na_2CO_3 and Li_2CO_3-K_2CO_3 electrolytes had fairly similar carbon deposition rates, whilst the Li_2CO_3-Na_2CO_3-K_2CO_3 electrolyte had the lowest deposition rates.

Table 7.3: Current efficiencies for carbon electro-deposition in the Li_2CO_3-Na_2CO_3, Li_2CO_3-K_2CO_3 and Li_2CO_3-Na_2CO_3-K_2CO_3 electrolytes, at temperatures of ca. 600 °C and 700 °C.

Electrolyte	**Current Efficiency Range (%)**	**Average Current Efficiency (%)**
Li_2CO_3-Na_2CO_3	54.8 to 93.7	74.4
Li_2CO_3-K_2CO_3	69.5 to 84.5	79.0
Li_2CO_3-Na_2CO_3-K_2CO_3	44.7 to 61.8	51.2

As for the current efficiencies of carbon electro-deposition, these did not appear to exhibit any trend with potential or temperature. Table 7.3 shows the range of current efficiencies for carbon electro-deposition, as well as the average current efficiency. The rather high current efficiencies obtained from the Li_2CO_3-Na_2CO_3 and Li_2CO_3-K_2CO_3 electrolytes indicate that carbon electro-deposition was the principal reaction taking place. In other words, the extent to which competing cathodic reactions took place was limited. Competing reactions would have

included alkali metal formation, alkali metal carbide formation and carbon monoxide formation, as discussed in Chapters 4 and 5. Therefore, these high current efficiencies support the conclusion drawn in Chapters 4 and 5 that carbon electro-deposition dominated over the other cathodic reactions once the working electrode had become coated with a layer of carbon, which would have happened at quite an early stage in the 30-minute electrolysis process considered in this chapter.

When interpreting carbon production rates and current efficiencies, one factor that needs to be taken into account is the effect of the loss of carbon from the working electrode. This would have lead to a drop in the calculated values of carbon production rate and current efficiency, and may not necessarily have occurred to the same extent in every experiment. The loss of carbon from the working electrode may be the reason why the rates and current efficiencies obtained from the Li_2CO_3-Na_2CO_3-K_2CO_3 electrolyte were lower than those of the other two electrolytes. This effect may also be the reason why no trend was observed in the current efficiency when the potential or temperature was changed – if indeed there was any trend to be observed. In future work, the effect of carbon losses might be minimised by limiting the length of electro-deposition experiments to 10 minutes or less. Larger deposits may well lose more carbon than smaller deposits, as it would be harder for larger masses of carbon to adhere to the metal working electrode surface.

7.4 Thermogravimetric Analysis (TGA) and Differential Scanning Calorimetry (DSC)

Each of the carbon deposits considered in this chapter was analysed using simultaneous thermogravimetric analysis (TGA) and heat-flux differential scanning calorimetry (DSC). This technique was used to ascertain the mass percentage of carbon in each deposit, the energy released from each deposit upon oxidation and the onset temperature of oxidation of each deposit. Section 3.7.2 can be consulted for a detailed explanation of the experimental procedure used. Figure 7.5 shows typical results obtained from the TGA-DSC analysis of carbon that was electro-deposited from the Li_2CO_3-K_2CO_3 electrolyte at a temperature of 579 °C and at an

applied potential of -3.06 V. Note that all of the carbon deposits[*] studied in this research yielded results of comparable form to Figure 7.5, irrespective of the electrolyte, temperature or applied potential used to obtain the deposit in question.

The general trends in Figure 7.5 will be discussed first before moving on to considering quantitative data obtained from all of the carbon deposits studied. Initially, the temperature was raised at a rate of 20 °C/min to 200 °C, where it was held constant for 15 minutes; the purge gas used during this part of the experiment was nitrogen. The weight loss during this period probably corresponds to the loss of adsorbed water from the sample (8.9 % of the initial sample weight). Although the sample was dried before being stored in an air-tight vial (as described in Section 3.7.1), it was not possible to completely remove all the moisture from the sample because some moisture would have been adsorbed during sample handling.

After the isothermal period at 200 °C had finished, the temperature was raised at a constant rate of 20 °C/min to 1000 °C; during this period the purge gas was supplied from a compressed air cylinder. Carbon oxidation started to occur at an onset temperature of around 356 °C, causing the sample weight remaining to drop sharply by 80.5 %. It is very likely that this weight loss was due to the oxidation of carbon due to the fact that there is a substantial heat flow peak in Figure 7.5(b) that coincides with the sharp weight loss in Figure 7.5(a). A very marginal weight loss followed after oxidation had finished – this may have been caused by the thermal decomposition of carbonate impurities present in the deposit. After the experiment had finished, 10.6 % of the original deposit mass remained, which probably consisted of alkali metal carbonate compounds, alkali metal oxides, metal and metal oxide impurities and carbon that did not combust. The impurities present in the carbon deposit will be considered in more detail in Sections 7.6 and 7.7.

[*] The term ‘carbon deposits’ is not used to imply that the entire deposit consisted of carbon, merely that carbon was a significant constituent of the deposits obtained from electro-deposition experiments.

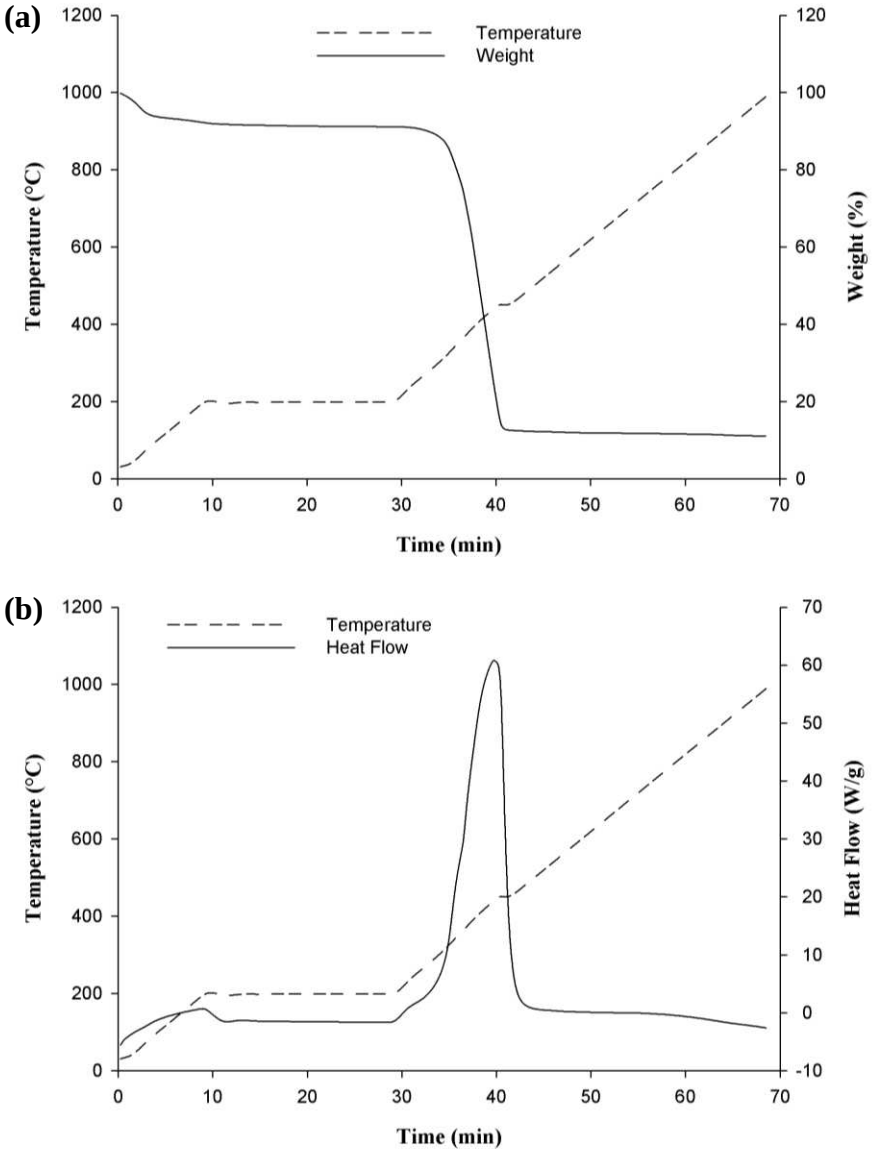

Figure 7.5: Results from the simultaneous TGA-DSC analysis of a deposit produced from the Li_2CO_3-K_2CO_3 electrolyte (molar ratio of 62:38) at a temperature of 579 °C, at an applied potential of -3.06 V vs. Ag/AgCl. (a) Change in deposit weight (expressed as a percentage of the initial sample mass) with time. (b) Change in heat flow with time. The manner in which the temperature was controlled with respect to time is represented by the dashed line. Note that the purge gas used in TGA-DSC was nitrogen up until the end of the isothermal region at 200 °C, after which the gas was changed to air. Please consult Section 3.7.2 for more details on the technique and the experimental program used.

Generally, all of the carbon deposits yielded similar results in TGA-DSC experiments, with no apparent trends with changing electro-deposition potential or electrolyte temperature. The average mass percentages of carbon present in the deposits obtained from each electrolyte were (on a dry basis): 82.1 % for Li_2CO_3-Na_2CO_3, 84.7 % for Li_2CO_3-K_2CO_3 and 84.5 % for Li_2CO_3-Na_2CO_3-K_2CO_3. The fact that all of the mass percentages of carbon obtained in this study were similar, regardless of the specific electro-deposition conditions used, can be accounted for as follows. Firstly, as was argued in Chapters 4 and 5, carbon electro-deposition became the dominant reaction once the working electrode had become coated with a layer of carbon, which would have happened at a relatively early stage in a 30-minute electro-deposition. Secondly, the other major cathodic products that could be produced, namely alkali metal and carbon monoxide would probably not have remained at the working electrode surface. Therefore, it is reasonable that the deposit collected at the working electrode mainly consisted of carbon.

The average temperatures for the onset of oxidation of carbon from each of the three electrolytes were: 337 °C for Li_2CO_3-Na_2CO_3, 357 °C for Li_2CO_3-K_2CO_3 and 348 °C for Li_2CO_3-Na_2CO_3-K_2CO_3. Siambun (2011b) tested a commercial KS-10 graphite powder (which had a particle size of approximately 6 μm) using TGA-DSC and found that its onset temperature was around 700 °C, which is considerably higher than the onset temperatures of the carbon deposits studied in this research. Welham and Williams (1998) compared the oxidation of graphite and amorphous activated carbon and observed that the onset temperature for amorphous carbon was around 340 °C lower than that of graphite. As was discussed in Section 2.7.1, electro-deposited carbon contains significant amounts of amorphous carbon[*], so the relatively low onset temperatures are consistent with the findings of Welham and Williams (1998). Jiang et al. (2000) found that natural graphite with an increased surface area and a greater fraction of edge sites combusted at lower temperatures compared to graphite with smaller surface areas and a smaller fraction of edge sites. Thus, these two factors probably contributed to the low onset temperatures observed in the present study.

[*] This was confirmed by XRD results presented in Section 7.6.

Furthermore, Neeft et al. (1996) found that the alkali metal carbonates Li_2CO_3, Na_2CO_3 and K_2CO_3 acted as catalysts in soot (carbon) oxidation, reducing the temperature of oxidation from 894 °C to 690 °C, 680 °C and 650 °C respectively, when the catalysts were in close contact with the carbon to be combusted. This catalytic effect could very possibly have contributed to the low onset temperatures of oxidation obtained in the present research.

The heat released from the oxidation of the carbon deposits also did not appear to vary with deposition potential or electrolyte temperature. The average amounts of heat released from the deposits obtained from each electrolyte were[*]: 19900 J/g for Li_2CO_3-Na_2CO_3, 21000 J/g for Li_2CO_3-K_2CO_3 and 22500 J/g for Li_2CO_3-Na_2CO_3-K_2CO_3 (note that these energies are given per gram of deposit on a dry basis). For the carbon deposits obtained from the Li_2CO_3-Na_2CO_3 electrolyte, the amount of energy released as heat upon oxidation represented 20.6 % to 26.2 % of the initial electrical energy required to deposit the carbon via electrolysis. For the Li_2CO_3-K_2CO_3 electrolyte, this range was 25.2 % to 36.3 % of the electrical energy input, whereas for the Li_2CO_3-Na_2CO_3-K_2CO_3 electrolyte, this range was 10.5 % to 16.5 %.

7.5 Scanning Electron Microscopy (SEM)

Scanning electron microscopy (SEM) was used to analyse the carbon deposits produced from the Li_2CO_3-Na_2CO_3 and Li_2CO_3-K_2CO_3 electrolytes, producing high-resolution magnified images of the surface topography of the deposit samples. Section 3.7.4 gives details of the SEM technique and how it was used to generate images of carbon deposits in this study.

[*] Note that the uncertainty in the weight measured was ± 0.1 μg, whilst the uncertainty in the temperature measured (from which the calorimetric data were derived) was ± 0.001 °C.

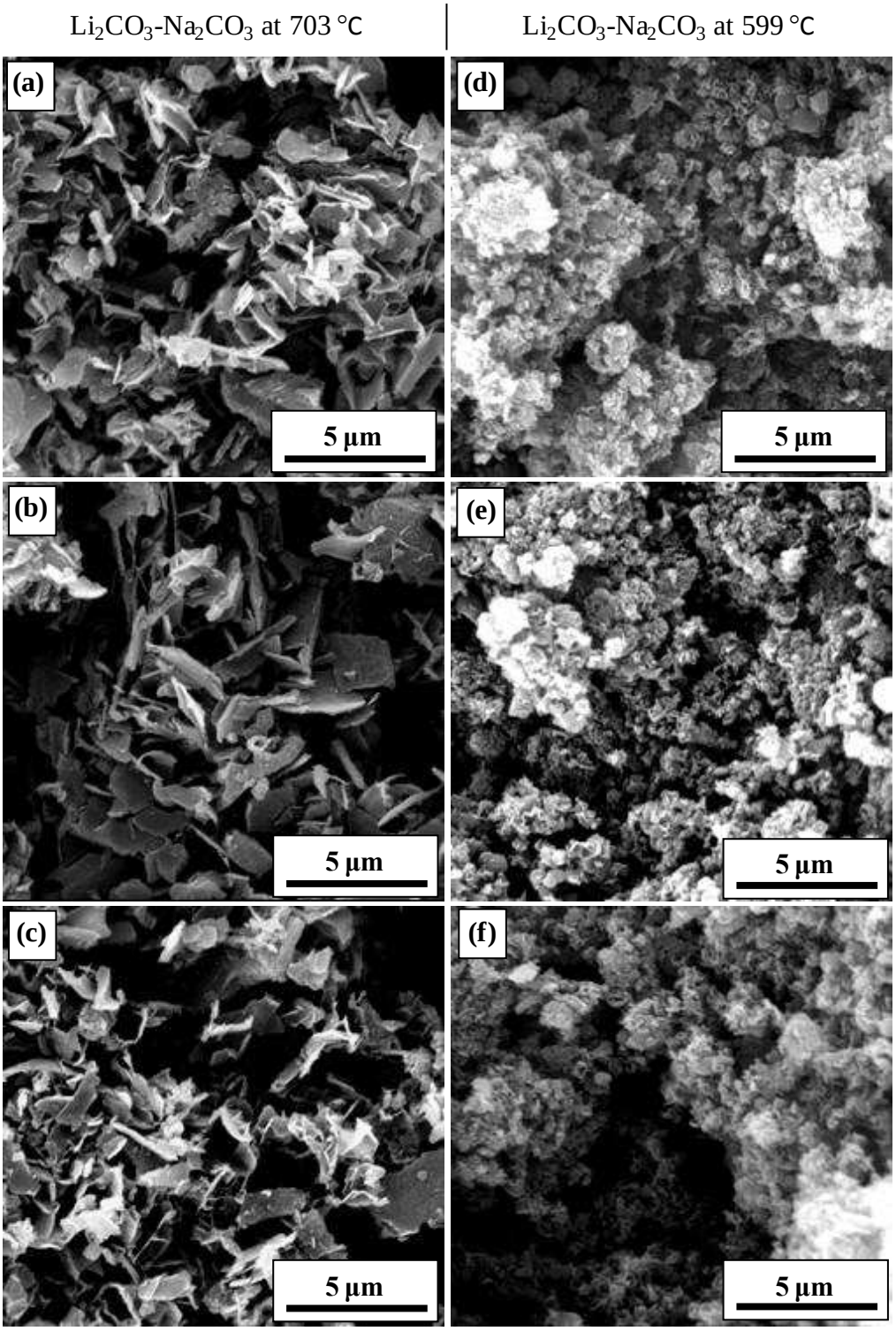

Figure 7.6: SEM images of carbon deposits produced from the Li_2CO_3-Na_2CO_3 electrolyte (molar ratio of 52:48) at temperatures of 703 °C (a-c) and 599 °C (d-f). The deposits were *obtained at the following applied potentials vs. Ag/AgCl: (a) −2.60 V, (b) −3.00 V, (c) −3.40 V, (d) −3.07 V, (e) −3.47 V and (f) −3.87 V. Note that the magnification used for all these* images was 16000×.

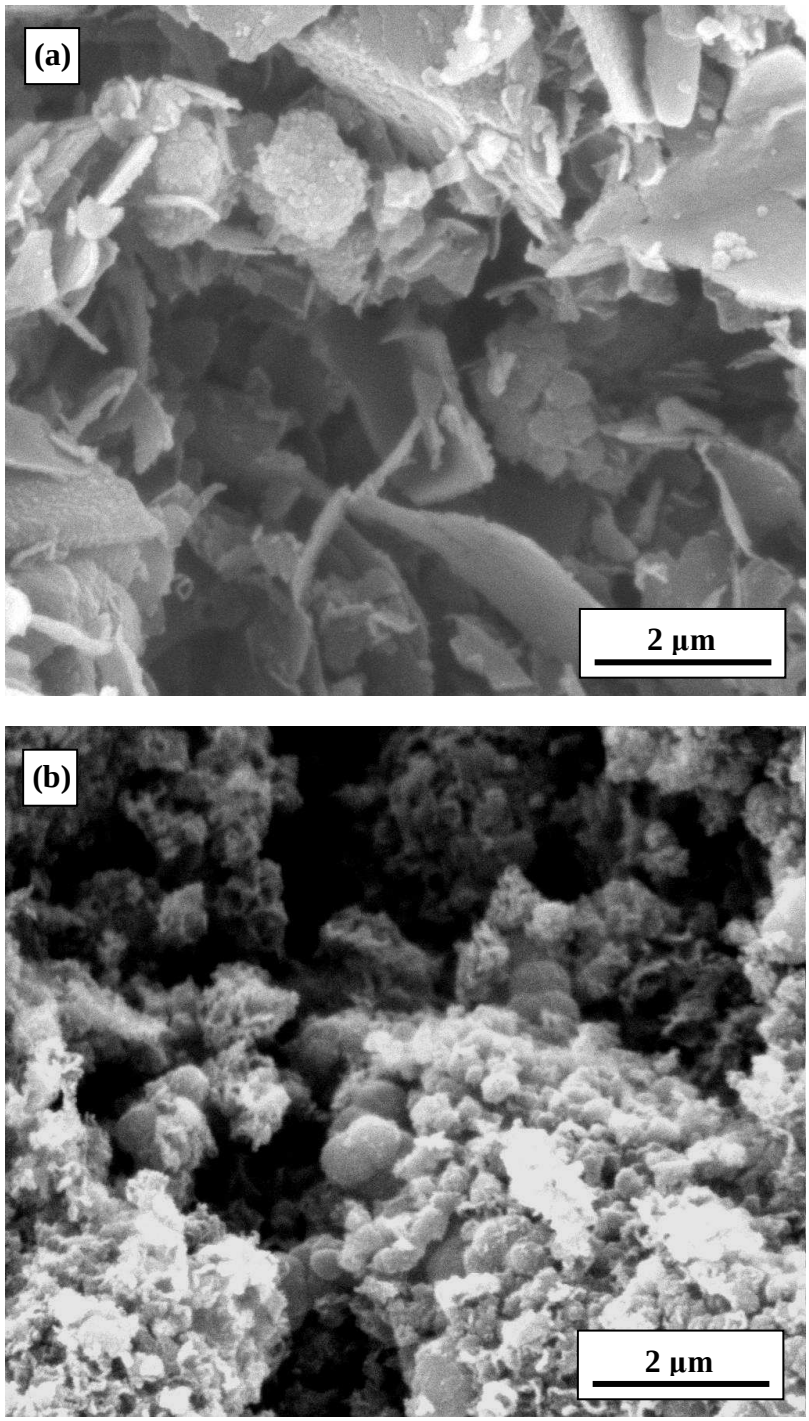

Figure 7.7: Higher magnification SEM images of carbon deposits produced from the Li_2CO_3-Na_2CO_3 electrolyte (molar ratio of 52:48) at temperatures of 703 °C (a) and 599 °C (b). The *deposits were obtained at the following applied potentials vs. Ag/AgCl: (a) −3.00 V and (b)* −3.07 V. Note that the magnification used for these two images was 30000×.

Figure 7.6 shows SEM images of the carbon deposits obtained from the Li_2CO_3-Na_2CO_3 electrolyte. All of these images are comparable to the SEM images that were obtained by Le Van et al. (2009) from carbon that was electro-deposited from a Li_2CO_3-Na_2CO_3-K_2CO_3 electrolyte[*]. Generally, the carbon deposits shown in Figure 7.6 consist of flake-shaped and quasi-spherical particles, where the quasi-spherical particles have nanometre-scale dimensions whereas the flake-shaped particles have micrometre-scale lengths.

Figure 7.7 shows two higher magnification images of the deposits. The flake-shaped particles appear to be formed from agglomerated quasi-spherical particles. On close examination of Figures 7.7(a) and (b), quasi-spherical particles with a diameter of around 60 nm can be discerned. This value is close to the average particle diameter of 30-50 nm given by Le Van et al. (2009) for their electro-deposited carbon. Thus, it is reasonable to infer that some carbon nanopowder was obtained via electro-deposition in the present work[†].

The flake-shaped agglomerates appear to be the principal carbon structure observed at the higher temperature of 703 °C. This observation is consistent with the work of Le Van et al. (2009), who found that elongated particles were typically observed at higher temperatures. However, some quasi-spherical particles are also present at this temperature, as is evident in the higher magnification image presented in Figure 7.7(a). At a temperature of 599 °C, the dominant carbon structure would appear to be the fine, quasi-spherical carbon particles that were observed by Le Van et al. (2009) at lower temperatures closer to 450 °C. As with the work of Le Van et al. (2009), there appeared to be no obvious change in particle size or morphology with increasing deposition potential, as shown in Figure 7.6.

Figure 7.8 shows SEM images of the carbon deposits produced from the Li_2CO_3-K_2CO_3 electrolyte, at temperatures of 708 °C and 579 °C. All of these images are fairly comparable to those obtained from the Li_2CO_3-Na_2CO_3 electrolyte, except from the fact that flake-shaped agglomerates do not appear to be present to any significant extent at either temperature in

[*] Four SEM images obtained by Le Van et al. (2009) are given in Figure 2.15.
[†] The presence of such nanopowder may be one of the reasons why carbon losses occurred so easily from the working electrode during electro-deposition.

Figure 7.8 – the dominant carbon morphology appears to be fine, quasi-spherical particles at both 708 °C and 579 °C.

As with the carbon obtained from the Li_2CO_3-Na_2CO_3 electrolyte, there appears to be no change in the particle size or morphology with increasing deposition potential in Figure 7.8. Figure 7.9 shows two higher magnification images of carbon deposits obtained from the Li_2CO_3-K_2CO_3 electrolyte. Particles as small as 60 nm can be discerned in both Figures 7.9(a) and (b) which shows that carbon nanopowder was also produced in Li_2CO_3-K_2CO_3.

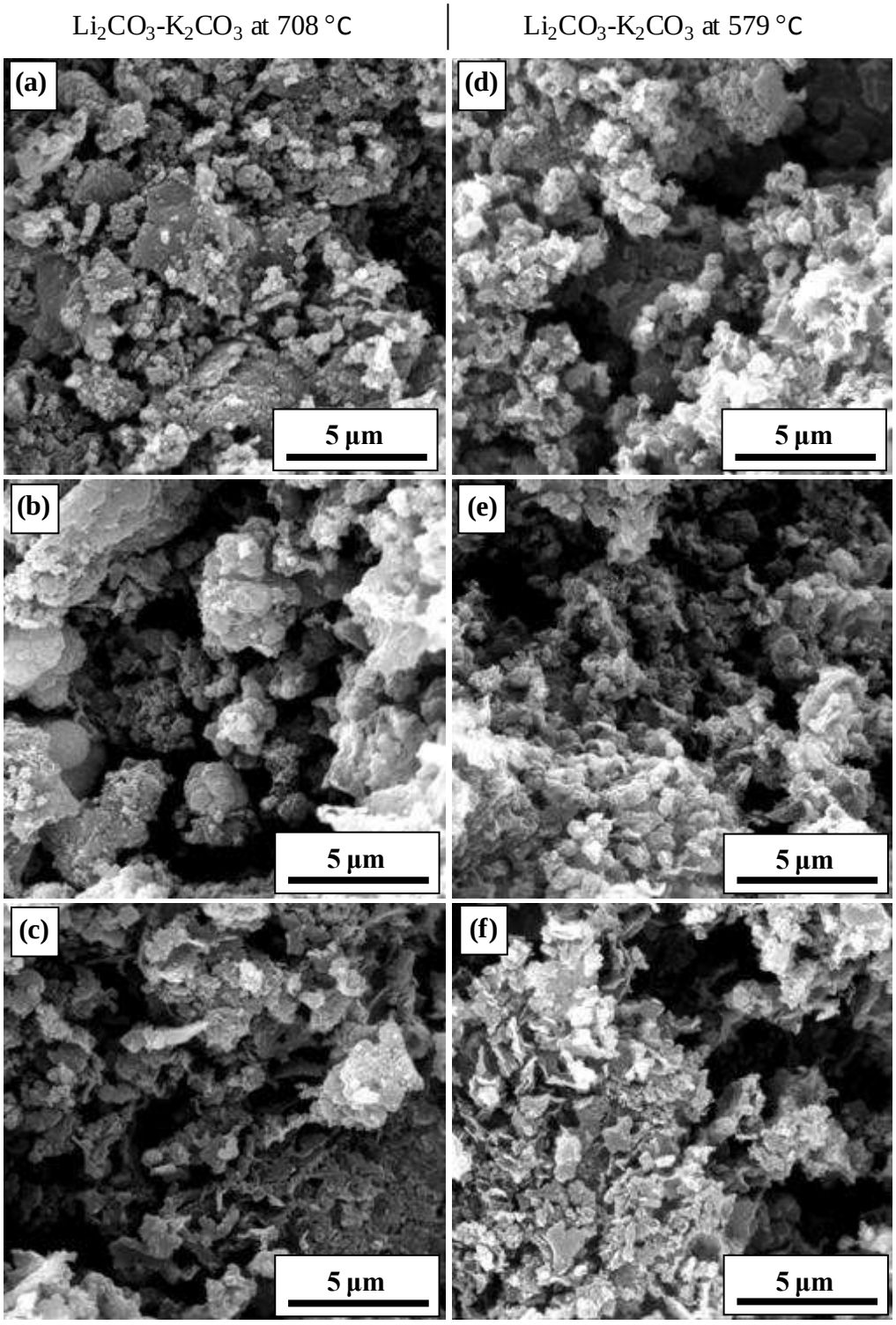

Figure 7.8: SEM images of carbon deposits produced from the Li_2CO_3-K_2CO_3 electrolyte (molar ratio of 62:38) at temperatures of 708 °C (a-c) and 579 °C (d-f). The deposits were obtained *at the following applied potentials vs. Ag/AgCl: (a) −2.18 V, (b) −2.58 V, (c) −2.98 V, (d) −3.06 V, (e) −3.46 V and (f) −3.86 V. Note that the magnification used for all these* images was 16000×.

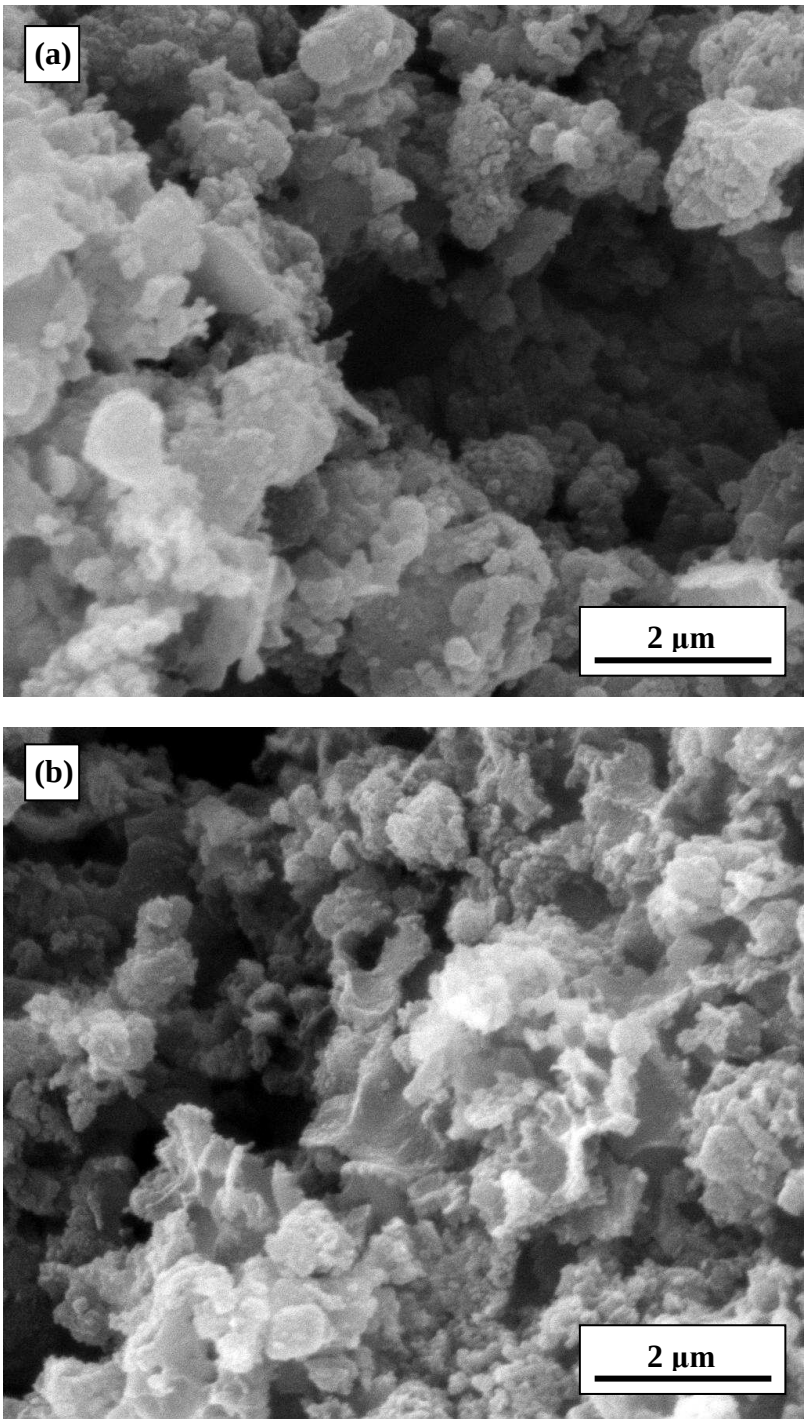

Figure 7.9: Higher magnification SEM images of carbon deposits produced from the Li_2CO_3-K_2CO_3 electrolyte (molar ratio of 62:38) at temperatures of 708 °C (a) and 579 °C (b). The *deposits were obtained at the following applied potentials vs. Ag/AgCl: (a) −2.58 V and (b)* −3.06 V. Note that the magnification used for these two images was 30000×.

7.6 X-Ray Diffraction (XRD)

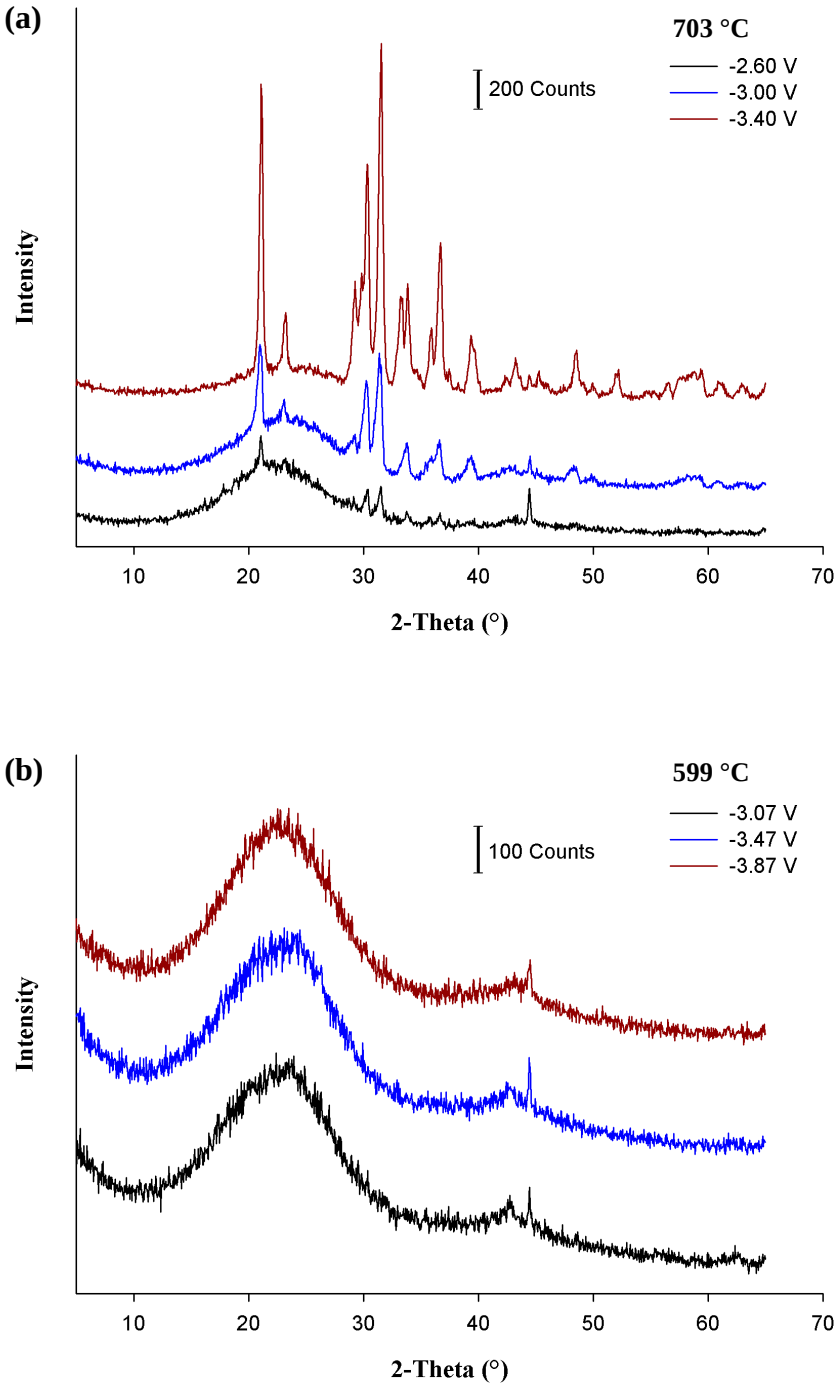

Figure 7.10: XRD spectra of carbon deposits obtained from the Li_2CO_3-Na_2CO_3 electrolyte (molar ratio of 52:48) at temperatures of (a) 703 °C and (b) 599 °C, at various applied potentials. Note that the peaks at an angle of 44.3° were caused by a machine fault.

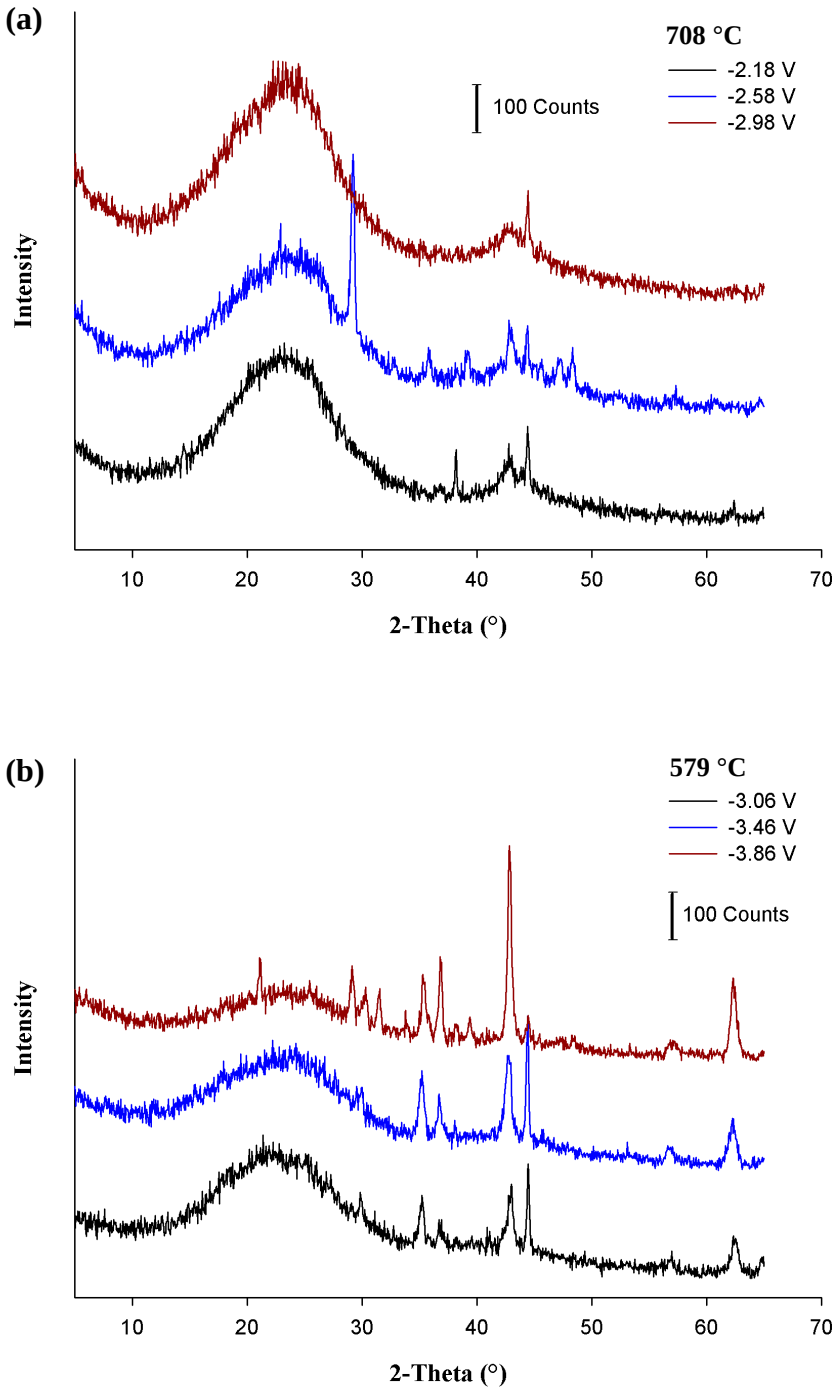

Figure 7.11: XRD spectra of carbon deposits obtained from the Li_2CO_3-K_2CO_3 electrolyte (molar ratio of 62:38) at temperatures of (a) 708 °C and (b) 579 °C, at various applied potentials. Note that the peaks at an angle of 44.3° were caused by a machine fault.

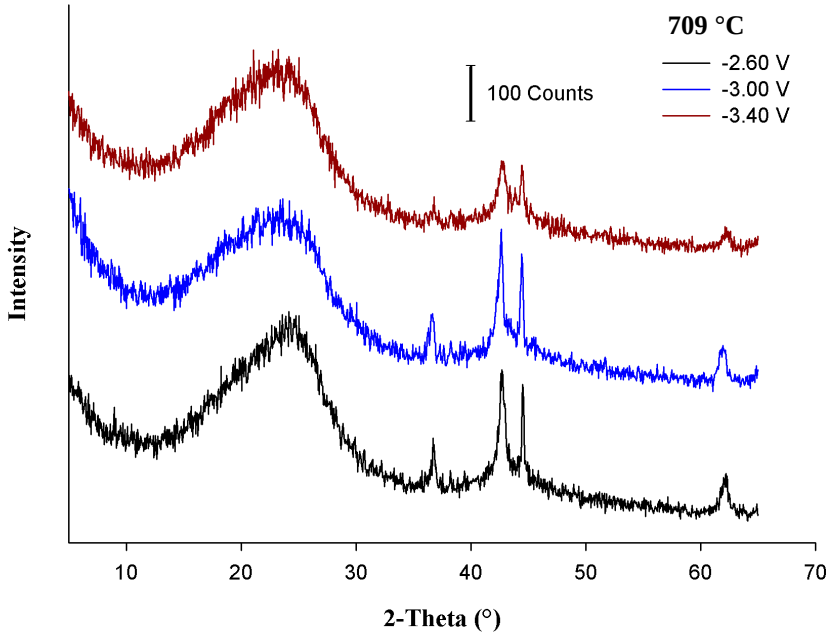

Figure 7.12: XRD spectra of carbon deposits obtained from the Li_2CO_3-Na_2CO_3-K_2CO_3 electrolyte (molar ratio of 43.5:31.5:25.0) at a temperature of 709 °C, at various applied potentials. Note that the peaks at an angle of 44.3° were caused by a machine fault.

X-ray diffraction (XRD) was used to help determine the crystal structures and chemical compositions of the carbon deposits. Section 3.7.3 can be consulted for further information on the XRD technique. Figures 7.10, 7.11 and 7.12 show XRD spectra of all the carbon deposits considered in the present chapter. All of the spectra show a broad peak centred at around 23.0°, which is characteristic of amorphous carbon (Welham and Williams, 1998). Le Van et al. (2009) observed a sharp peak at approximately 26.4°, which corresponded to the (002) reflection of graphitised carbon. However, this sharp peak is absent from the spectra presented in Figures 7.10, 7.11 and 7.12, which implies that significant amounts of graphitised carbon were not present in the carbon deposits studied in this chapter.

Characteristic peaks for several other substances are present in Figures 7.10, 7.11 and 7.12. Firstly, in the spectra presented in Figure 7.10(a), all of the sharp peaks can be attributed to Li_2CO_3. The characteristic peaks observed at around 21.1°, 23.2°, 29.3°, 30.4°, 31.6°, 33.9°, 35.9°, 36.9°, 48.6° in the -3.86 V spectra in Figure 7.11(b) can also be attributed to Li_2CO_3.

The presence of Li_2CO_3 was not unexpected due to the fact that it was a major constituent of the electrolytes used. Furthermore, Li_2CO_3 was more difficult to remove by washing because it has a low solubility in water of 12.63 g/dm^3 compared to Na_2CO_3 and K_2CO_3, whose solubilities in water are 293.1 g/dm^3 and 1118 g/dm^3 respectively (Linke, 1958). This difference in solubility explains why no characteristic peaks for Na_2CO_3 or K_2CO_3 were observed in Figures 7.10, 7.11 and 7.12. However, one would have expected that the 0.56 mol/dm^3 hydrochloric acid used in the washing process would have removed most of the Li_2CO_3 present. Perhaps some Li_2CO_3 was inaccessible to the acid during the washing process, in the deposits where it was detected via XRD.

In Section 7.5 it was noted that flake-shaped agglomerates were the principal carbon structure observed in the three carbon deposits that were obtained from the Li_2CO_3-Na_2CO_3 electrolyte at 703 °C. Figure 7.10(a) shows the XRD traces obtained from these three deposits, which indicate the presence of significant amounts of Li_2CO_3. The fact that flake-shaped agglomerates were only observed in these three deposits suggests that the flake-shaped agglomerates were caused by Li_2CO_3 still being present after washing rather than the temperature and the electrolyte used.

The spectra shown in Figures 7.10, 7.11 and 7.12 also indicate the presence of a number of different iron-containing compounds in many of the deposits, which almost certainly originated from the mild steel working electrodes used. These iron compounds could also have arisen from the stainless steel counter electrodes used. The presence of peaks at 41.9°, 42.8° and 43.8° in Figures 7.10(b), 7.11 and 7.12 suggests that the deposits that produced these spectra contained iron carbide (Fe_2C). The deposits whose spectra are shown in Figures 7.11(b) and 7.12 appear to have contained $Li_5Fe_5O_8$, as indicated by peaks at 37.0°, 43.0° and 62.5°. Furthermore, iron oxide (Fe_3O_4) was detected in the spectra shown in Figure 7.11, as indicated by peaks at approximately 29.9°, 35.3°, 42.9°, 53.3°, 56.8° and 62.4°. Both $Li_5Fe_5O_8$ and Fe_3O_4 can be formed during iron corrosion in molten carbonates (Biedenkopf et al., 1998), so it is reasonable to observe these two compounds in some of the carbon deposits that were obtained

in the present work. On the other hand, iron carbide probably formed where carbon particles were in direct contact with the mild steel working electrode.

In Chapters 4 and 5, it was suggested that lithium and potassium carbides could be formed during carbon electro-deposition. However, no peaks for alkali metal carbides are present in Figures 7.10, 7.11 or 7.12. When Kaplan et al. (2002) and Le Van et al. (2009) analysed their electro-deposited carbon via XRD, they were also unable to detect any alkali metal carbides. This is very probably because alkali metal carbides are highly reactive: all of the alkali metal carbides present probably reacted with the water and the hydrochloric acid used in the washing process.

In general, the XRD spectra presented in Figures 7.10, 7.11 and 7.12 seem to suggest that the impurities present in the electro-deposited carbon depend more on the efficacy of the washing process rather than the electrolysis conditions – there appears to be no major trend with potential, temperature or electrolyte composition. Most of the impurities appear to have arisen from either the electrode materials or the electrolyte.

7.7 Back-Scattered Scanning Electron Microscopy (BSEM) and Energy-Dispersive X-ray (EDX) Spectroscopy

Back-scattered scanning electron microscopy (BSEM) was carried out in conjunction with energy dispersive X-ray (EDX) spectroscopy to analyse the elemental compositions of the carbon deposits. Section 3.7.4 describes the use of these two techniques in detail. The compositions of the deposits obtained did not vary significantly with electrolyte temperature or deposition potential, although there were minor differences in composition between deposits produced from different electrolytes. Table 7.4 gives the average mass percentages of various elements detected via EDX spectroscopy for carbon deposits obtained from the Li_2CO_3-Na_2CO_3, Li_2CO_3-K_2CO_3 and Li_2CO_3-Na_2CO_3-K_2CO_3 electrolytes. Note that when the EDX measurements used to acquire the data for Table 7.4 were carried out, the electron beam was

not focussed on a single point on each sample surface, but was incident on a relatively large area of each sample surface.

Table 7.4: Average mass percentages of various elements detected by EDX spectroscopy, for carbon deposits obtained from the Li_2CO_3-Na_2CO_3, Li_2CO_3-K_2CO_3 and Li_2CO_3-Na_2CO_3-K_2CO_3 electrolytes.

Electrolyte Composition	**Average Mass Percentages of Elements Detected (%)**									
	C	**O**	**Na**	**Al**	**Si**	**S**	**Cl**	**K**	**Fe**	**Mg**
Li_2CO_3-Na_2CO_3	65.1	29.4	2.7	0.3	1.8	0.1	0.3	0.0	0.4	0.0
Li_2CO_3-K_2CO_3	70.4	22.4	0.1	1.0	0.9	0.1	0.2	1.9	2.9	0.1
Li_2CO_3-Na_2CO_3-K_2CO_3	74.0	22.8	0.3	0.0	0.2	0.1	0.3	1.4	1.0	0.0

Table 7.4 shows that carbon was the most abundant element in the deposits, which agrees well with TGA and XRD results presented in Sections 7.4 and 7.6 respectively. However, a proportion of the carbon detected by EDX spectroscopy does arise from alkali metal carbonate impurities in the deposits. Li_2CO_3 was detected by XRD in four of the carbon deposits but no characteristic peaks for Na_2CO_3 or K_2CO_3 were detected in XRD. Thus, Li_2CO_3 was probably the only alkali metal carbonate that could have been present at a relatively high concentration in any of the washed deposits. However, EDX spectroscopy cannot detect lithium (Croft, 2006), so the technique cannot be used to verify whether Li_2CO_3 was present in the deposits or not.

Oxygen was the second most abundant element detected, which could have been present in alkali metal oxides, Li_2CO_3, iron oxides or lithium-iron oxides. The presence of the element iron in all of the deposits corroborates well with the XRD results presented in Section 7.6, which indicated the presence of Fe_2C, $Li_5Fe_5O_8$ and Fe_3O_4 in many of the deposits. Such iron compounds almost certainly originated from the mild steel working electrodes used.

Table 7.4 shows that small quantities of sodium and potassium were present in the deposits, albeit no potassium was detected in the deposits obtained from the Li_2CO_3-Na_2CO_3 electrolyte, and the quantity of sodium detected in the deposits from Li_2CO_3-K_2CO_3 was very small (0.1

%). The presence of sodium and potassium could indicate that Na_2O or K_2O were present in the deposits. No Na_2CO_3 or K_2CO_3 was detected in XRD (see Section 7.6), which suggests that these two compounds were not present in any of the deposits in large quantities. The detection of small quantities of chlorine (0.2 % to 0.3 %) also suggests that some LiCl, NaCl and/or KCl could have been present. Alkali metal chlorides would most likely have been produced when the deposits were washed with dilute hydrochloric acid.

The presence of silicon and aluminium in the deposits was almost certainly due to the fact that all of the deposits were filtered using borosilicate glass filters.

One limitation of the EDX spectroscopy technique is that elements lighter than sodium are difficult to detect accurately, and lithium cannot be detected at all (Croft, 2006). As a consequence, the mass percentages given in Table 7.4 can only be taken as approximations.

Figures 7.13, 7.14 and 7.15 show some typical BSEM images of carbon deposits that were obtained in the present study. Generally, all of the BSEM images obtained were similar in terms of appearance, so only images from five of the deposits have been presented here. Three kinds of feature can be observed in the BSEM images obtained. Firstly, small white spots are distributed fairly evenly across the deposit surfaces; these spots are particularly obvious in Figures 7.14(a) and (b). Secondly, the small white spots are concentrated in some places on the surfaces of the deposits (prominent examples of this kind of feature are labelled ‘C’ in Figures 7.13 and 7.14). Both of these features probably arose due to the presence of iron compounds in the deposit, as regions of higher atomic number are brighter than regions of lower atomic number in BSEM images. This was confirmed by carrying out EDX spectroscopy at the point labelled ‘C’ in Figure 7.14(b); the mass percentage of iron detected was 31.2 %, which is much higher than the overall average iron content of 2.9 % for deposits produced from Li_2CO_3-K_2CO_3. EDX spectroscopy of similar groups of white spots in other carbon deposits yielded comparable iron contents in the range of 25 % to 47 % by mass.

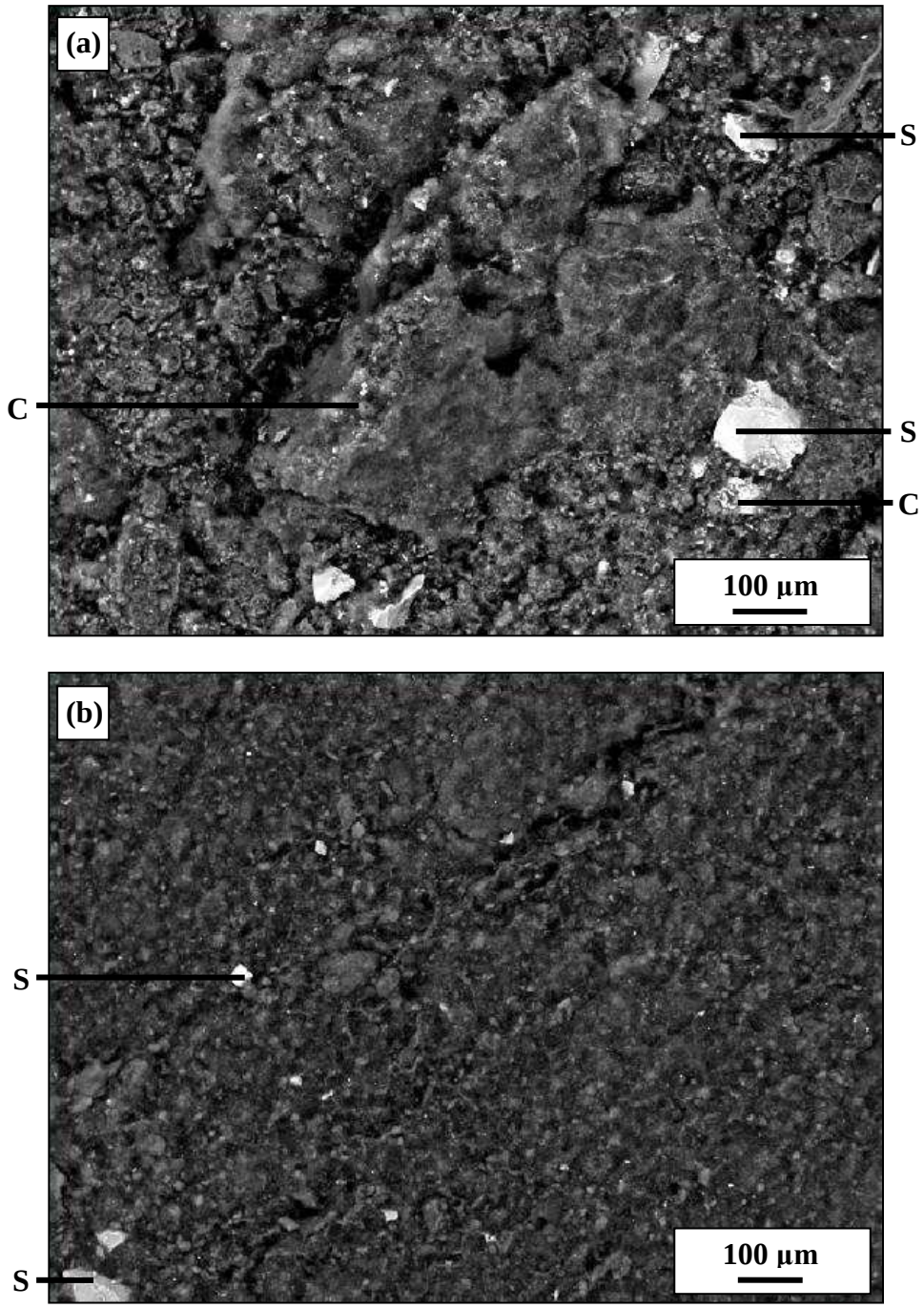

Figure 7.13: BSEM images of two carbon deposits produced from the Li_2CO_3-Na_2CO_3 electrolyte (molar ratio of 52:48) at temperatures of (a) 703 °C and (b) 599 °C. The deposits *were obtained at the following applied potentials vs. Ag/AgCl: (a) −3.40 V and (b) −3.47 V.* Note that the magnification used for both these images was 200×.

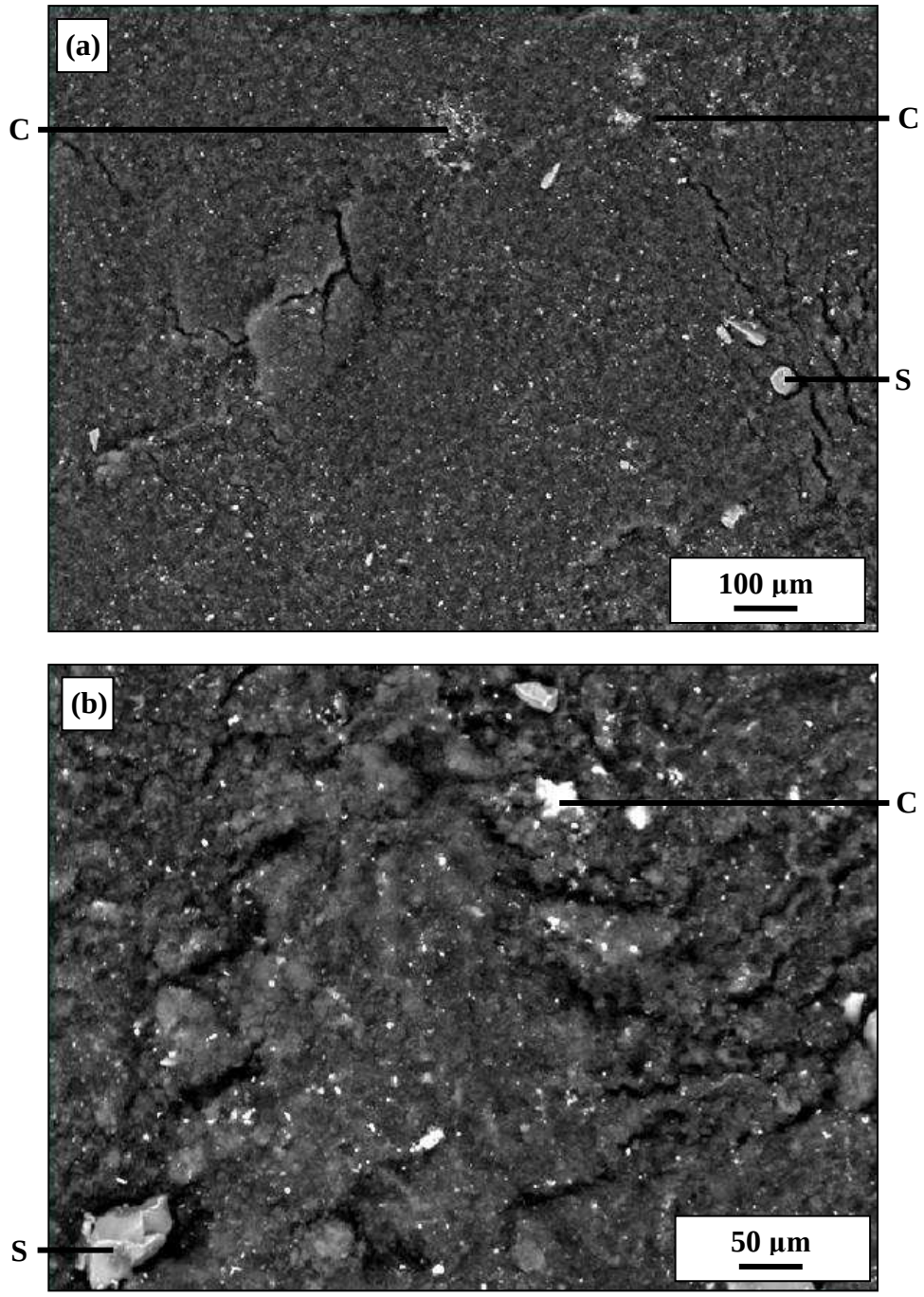

Figure 7.14: BSEM images of two carbon deposits produced from the Li_2CO_3-K_2CO_3 electrolyte (molar ratio of 62:38) at temperatures of (a) 708 °C and (b) 579 °C. The deposits *were obtained at the following applied potentials vs. Ag/AgCl: (a) −2.58 V and (b) −3.46 V.* Note that the magnifications used for these images were (a) 200× and (b) 400×.

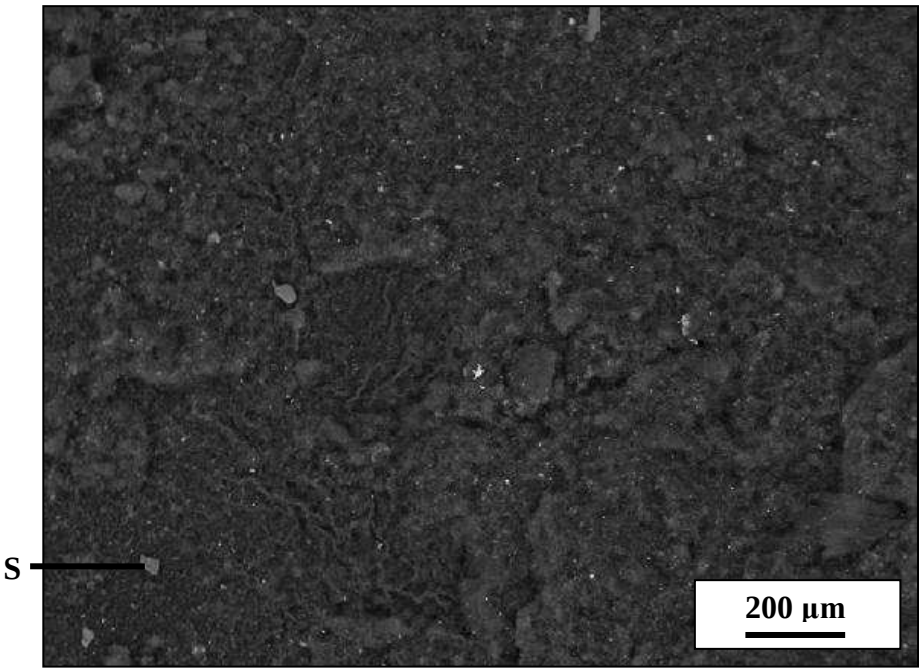

Figure 7.15: BSEM image of a carbon deposit produced from the Li_2CO_3-Na_2CO_3-K_2CO_3 electrolyte (molar ratio of 43.5:31.5:25.0) at a temperature of 709 °C. The deposit was *obtained at an applied potential of −3.00 V vs. Ag/AgCl. Note that the magnification used for* this image was 150×.

The third kind of feature present in Figures 7.13, 7.14 and 7.15 are large, irregular lumps with smooth, flat sides; a number of representative examples are labelled 'S'. These lumps were almost certainly derived from the borosilicate glass filters used in the washing process. Carrying out EDX spectroscopy of the largest lump in Figure 7.13(a) gave mass percentages of 30.1 % for silicon and 55.4 % for oxygen – these are much higher than the overall mass percentages for these elements in Table 7.4. SiO_2 is the principal constituent of borosilicate glass (Dulsky, 1996), so these mass percentages imply that the large lumps are indeed pieces of borosilicate glass. EDX spectroscopy of similar lumps in other carbon deposits gave silicon contents in the range of 21.5 % to 33.4 % by mass, and oxygen contents in the range of 27.6 % to 59.1 % by mass.

7.8 Conclusions

Carbon was electro-deposited from the Li_2CO_3-Na_2CO_3 and Li_2CO_3-K_2CO_3 electrolytes at temperatures of ca. 600 °C and ca. 700 °C, and from the Li_2CO_3-Na_2CO_3-K_2CO_3 electrolyte at a temperature of ca. 700 °C. Electro-deposition was carried out via chronoamperometry in a three-electrode system, at potentials approximately 0.6 V, 1.0 V and 1.4 V more negative than the potential at the start of the current wave at the cathodic limit observed in cyclic voltammetry.

In chronoamperograms carried out at ca. 700 °C, the current became increasingly negative with time (i.e. the magnitude of the current became larger) as carbon electro-deposition proceeded. This was attributed to a growth in the electro-active surface area with time. However, at ca. 600 °C, the current very gradually became less negative with time, which was ascribed to a trade-off between an increase in the electro-active surface area and an increase in the deposit resistance with time. Apparently, the deposit resistance at ca. 700 °C was not sufficient to retard the electro-deposition rate.

The apparent carbon electro-deposition rate was found to increase with temperature from ca. 600 °C to ca. 700 °C, and was also found to increase as the applied potential was made more negative (i.e. as the overpotential was made larger). The highest apparent electro-deposition rate obtained was 0.183 $g/cm^2.h$ at an applied potential of -2.98 V vs. Ag/AgCl, using a Li_2CO_3-K_2CO_3 electrolyte at 708 °C. The average current efficiencies obtained for carbon electro-deposition were generally high: 74.4 % for Li_2CO_3-Na_2CO_3, 79.0 % for Li_2CO_3-K_2CO_3 and 51.2 % for Li_2CO_3-Na_2CO_3-K_2CO_3.

Simultaneous thermogravimetric analysis (TGA) and heat-flux differential scanning calorimetry (DSC) revealed that average mass percentages of carbon present in the deposits obtained from each electrolyte were (on a dry basis): 82.1 % for Li_2CO_3-Na_2CO_3, 84.7 % for Li_2CO_3-K_2CO_3 and 84.5 % for Li_2CO_3-Na_2CO_3-K_2CO_3. The average temperatures for the onset of oxidation of carbon from each of the three electrolytes were: 337 °C for Li_2CO_3-Na_2CO_3,

357 °C for Li_2CO_3-K_2CO_3 and 348 °C for Li_2CO_3-Na_2CO_3-K_2CO_3. These onset temperatures are much lower than that of commercial KS-10 graphite powder, which has an onset temperature of around 700 °C (Siambun, 2011b). Two main factors probably contributed to the low onset temperatures of the electro-deposited carbon: the high surface area of the carbon (due to its fine particle size) and the presence of alkali metal carbonate impurities (which can have a catalytic effect on oxidation). The average amounts of energy released from the deposits during oxidation were (on a dry basis): 19900 J/g for Li_2CO_3-Na_2CO_3, 21000 J/g for Li_2CO_3-K_2CO_3 and 22500 J/g for Li_2CO_3-Na_2CO_3-K_2CO_3.

Scanning electron microscopy (SEM) of electro-deposited carbon from Li_2CO_3-Na_2CO_3 and Li_2CO_3-K_2CO_3 revealed that the carbon primarily consisted of fine, quasi-spherical particles, some as small as 60 nm in diameter. Therefore, at least some of the carbon can be said to be nanopowder. Some of the quasi-spherical particles were agglomerated into micrometre-scale flakes in the carbon from Li_2CO_3-Na_2CO_3 at 703 °C. X-ray diffraction (XRD) of the carbon deposits revealed that the carbon was amorphous – there was little indication of any graphitised carbon.

Energy-dispersive X-ray (EDX) spectroscopy and XRD showed that several other substances were present in the carbon deposits as impurities. Iron compounds such as Fe_2C, $Li_5Fe_5O_8$ and Fe_3O_4 were detected in a number of the deposits, as was Li_2CO_3. The majority of the impurities present seem to have arisen from either the working electrode material (iron compounds) or from the electrolyte (Li_2CO_3).

CHAPTER 8

RE-OXIDATION OF ELECTRO-DEPOSITED CARBON AND THE EFFECT OF PROCESS CONDITIONS ON Q^+/Q^-

This chapter presents a study of the re-oxidation of electro-deposited carbon and the efficiency of this process. In the first section of the chapter, the reasons for studying this topic are outlined. In the second section, the production of carbon deposits for re-oxidation studies is considered, whilst the third section discusses the general process by which the re-oxidation of electro-deposited carbon proceeds. The effect of process conditions on this re-oxidation process are considered in the fourth section. Finally, the fifth section looks at potential ways of improving re-oxidation efficiency by changing the molten salt reactor design or method of operation.

8.1 Reasons for Studying the Re-oxidation of Electro-deposited Carbon

When electricity is used to electro-deposit carbon in the present molten salt process, electrical energy is stored as chemical potential energy in the carbon produced. As a consequence, the electro-deposited carbon acts as an energy store. This stored energy could be released as heat via the combustion of the carbon. However, if it were desired that the stored energy be converted back to electricity, the efficiency of converting the heat from carbon combustion to electricity would be relatively low. To convert the heat from carbon combustion into electricity, the heat would be used to raise steam to drive a turbine connected to an electrical generator, as in a conventional coal-fired power station. However, there is a fundamental limit to the efficiency of conversion of heat to work imposed by the Second Law of Thermodynamics: even an ideal heat engine cannot ever attain an efficiency of 100 % (Rogers and Mayhew, 1992). Considering the Carnot Cycle of a reversible heat engine, the maximum efficiency for the conversion of heat to work is given by (Rogers and Mayhew, 1992):

$$\eta = \frac{T_1 - T_2}{T_1} \qquad (8.1)$$

Where: η = efficiency for the conversion of heat to work; T_1 = temperature of hot reservoir from which heat is drawn (in degrees Kelvin); and T_2 = temperature of cold sink to which the remaining heat is rejected (in degrees Kelvin).

From Equation 8.1, it can be seen that for 100 % efficiency to be attained, either the temperature of the cold sink must be absolute zero or the hot reservoir must have a temperature of infinity, both of which are practically unattainable. Therefore, it would be impossible for the turbine to convert all the energy supplied to it from the steam into work (rotational motion), in order to drive the electrical generator. As a consequence, it would be less desirable to convert the chemical potential energy of electro-deposited carbon into electrical energy via the combustion route.

However, if the carbon were to be electrochemically re-oxidised directly in a device such as the direct carbon fuel cell (DCFC), it would be possible to attain much better efficiencies for the conversion of stored chemical energy to electrical energy. Firstly, this is due to the fact that there is no need to convert heat to work and so the maximum efficiency limit imposed by Equation 8.1 no longer applies. Secondly, the overall reaction for the oxidation of carbon to carbon dioxide has favourable thermodynamics. If oxygen is supplied to a DCFC, the carbon is re-oxidised according to the following overall reaction (Cherepy et al., 2005):

$$C + O_2 \rightarrow CO_2 \qquad (8.2)$$

The half-cell reactions in a DCFC were considered by Cherepy et al. (2005) to be the following:

$$\text{Anode: } C + 2CO_3^{2-} \rightarrow 3CO_2 + 4e^- \qquad (8.3)$$

$$\text{Cathode: } O_2 + 2CO_2 + 4e^- \rightarrow 2CO_3^{2-} \qquad (8.4)$$

The entropy change of Reaction 8.2 is very low, only 2.9 J/mol.K (Cherepy et al., 2005). As a consequence the theoretical efficiency for the conversion of the chemical energy to electrical

energy via this reaction approaches 100 % due to low entropic heat evolution[*] (Cherepy et al., 2005). Hence the direct electrochemical re-oxidation route would be a much more efficient way of converting the energy stored in electro-deposited carbon to electricity, in comparison with the aforementioned combustion route.

From the above paragraphs, it is apparent that the direct electrochemical re-oxidation of electro-deposited carbon is a more efficient way of converting the energy stored within the carbon to electricity. However, in the published literature, the re-oxidation of electro-deposited carbon in molten salts has only been studied by Ingram et al. (1966) for a rather narrow set of conditions. Ingram et al. (1966) only studied re-oxidation in a ternary Li_2CO_3-Na_2CO_3-K_2CO_3 electrolyte at a temperature of 600 °C; the only parameters that were varied were the initial quantity of carbon to be re-oxidised and the re-oxidation current. Therefore, there is a need to conduct a more wide-ranging study of the re-oxidation of electro-deposited carbon. This chapter seeks to address this issue by presenting a study of the re-oxidation of electro-deposited carbon in four different molten carbonate electrolytes, considering factors such as the electrolyte temperature, the potential at which the carbon was electro-deposited and the re-oxidation current applied.

8.2 Preparation of Carbon Deposits for Re-Oxidation

Before it is possible to discuss the re-oxidation of electro-deposited carbon, it is necessary to describe how carbon deposits were prepared for re-oxidation experiments. The four electrolytes investigated were: Li_2CO_3, Li_2CO_3-Na_2CO_3, Li_2CO_3-K_2CO_3 and Li_2CO_3-Na_2CO_3-K_2CO_3[†]. Carbon deposits were prepared by chronoamperometry in a three-electrode system, which is described in more detail in Section 3.5.2. In each electro-deposition, the working electrode was a 5 mm diameter mild steel rod, the counter electrode was a 6 mm diameter stainless steel rod, and the reference electrode was an alumina membrane Ag/AgCl reference electrode, which is described in Section 3.4.2. The electro-deposition of carbon was typically carried out for 10

[*] Note: $\Delta G = \Delta H - T\Delta S$; theoretical efficiency = $\Delta G/\Delta H = 1 - T\Delta S/\Delta H$).

[†] The principal electrolytes considered were Li_2CO_3-Na_2CO_3 and Li_2CO_3-K_2CO_3; some supplementary results obtained from the Li_2CO_3 and Li_2CO_3-Na_2CO_3-K_2CO_3 electrolytes are given in Appendix III.

minutes. The specific process conditions under which the carbon was electro-deposited are considered in Section 8.4 and Appendix III, such as the electrolyte temperature. Note that electro-deposition potentials were chosen to be more negative than the observed cathodic limit potentials in cyclic voltammetry, in order to obtain a suitable quantity of carbon for re-oxidation in a relatively short time.

Figure 8.1 shows two chronoamperograms obtained from carbon electro-deposition experiments carried out in a Li_2CO_3-K_2CO_3 electrolyte, at temperatures of 708 °C and 574 °C. Generally speaking, the chronoamperograms presented in Figure 8.1 are typical of those obtained from carbon electro-deposition in all four of the electrolytes considered in this chapter. Chronoamperograms such as those shown in Figure 8.1 are discussed in more detail in Chapter 7, but there are a number of points worth raising here. Firstly, after the initial peak in Figure 8.1, the current at both temperatures gradually became more negative with time. This is indicative of the thickness of the carbon deposit increasing with time as electro-deposition proceeded, leading to a greater surface area onto which carbon electro-deposition could occur and hence a greater current. The gradient of the curve after the peak is steeper at 708 °C as opposed to that at 574 °C, suggesting that the deposition rate was higher at 708 °C.

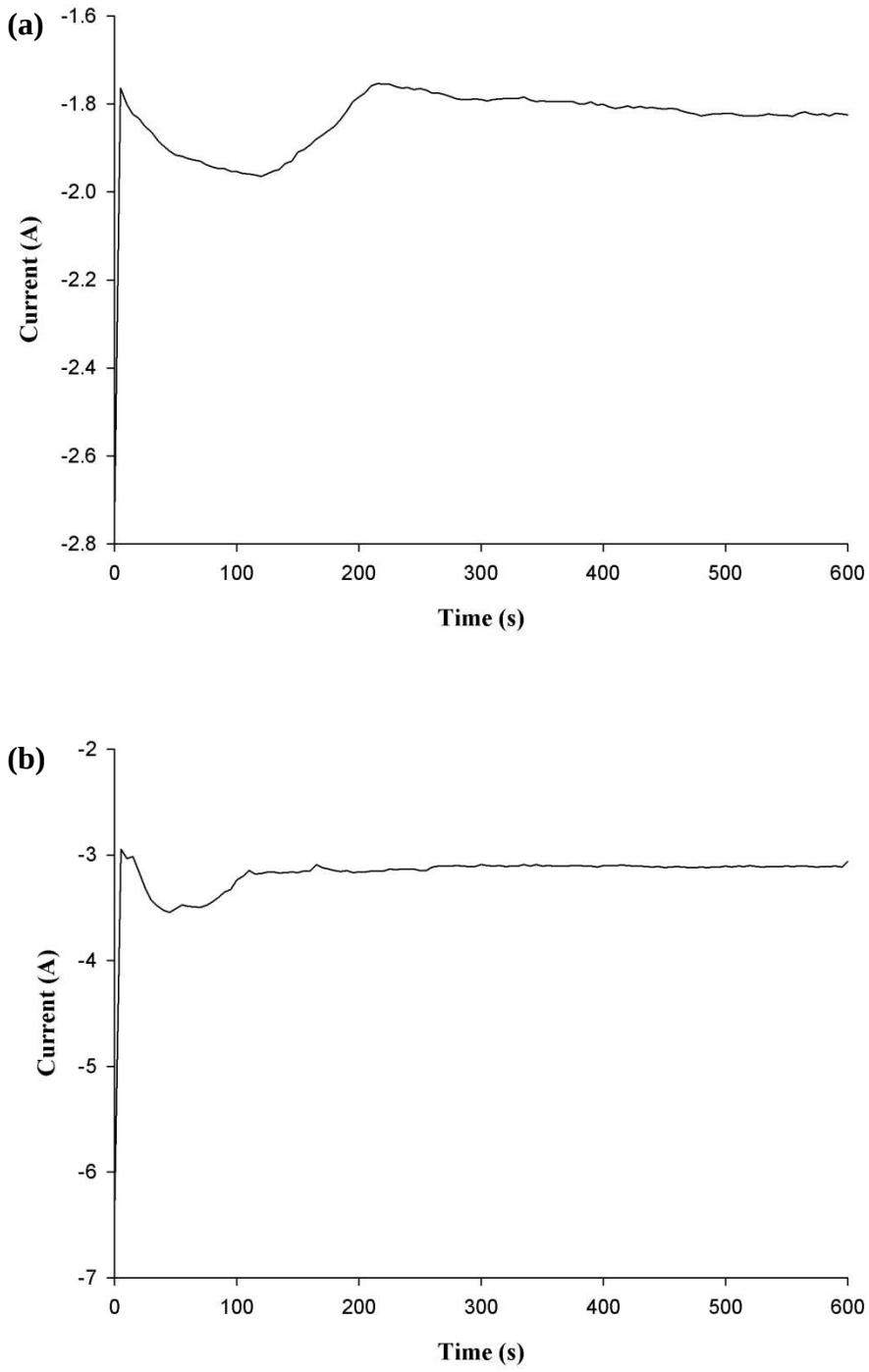

Figure 8.1: Typical variation of current versus time during carbon electro-deposition in a Li_2CO_3-K_2CO_3 electrolyte (molar ratio of 62:38) at temperatures of (a) 708 °C and (b) 574 °C, under a CO_2 atmosphere. The applied working electrode potentials were (a) –1.68 V and (b) −3.16 V. WE: 5 mm diameter mild steel rod; CE: 6 mm diameter stainless steel rod; alumina membrane Ag/AgCl RE.

Secondly, the chronoamperograms obtained from 10-minute depositions generally did not show many 'kinks' in the positive current direction, and where these kinks did occur there were not particularly large deviations from the observed trend. Conversely, kinks such as these were generally observed to have a greater magnitude in the chronoamperograms obtained from 30-minute depositions, which are considered in Chapter 7. Such kinks may represent parts of the carbon deposit falling off the working electrode, as this would have led to a smaller surface area for carbon deposition and hence a lower current. Carbon falling off the working electrode perhaps did not occur to such a great extent during shorter electro-deposition experiments, as the carbon deposit would not have been so thick. However, it is important to bear in mind that some carbon may have fallen off the working electrode during both electro-deposition and re-oxidation.

8.3 General Features of the Carbon Re-Oxidation Process

In this section, some general observations are made regarding the re-oxidation of electro-deposited carbon, i.e. these observations apply to all of the electrolytes considered: Li_2CO_3, Li_2CO_3-Na_2CO_3, Li_2CO_3-K_2CO_3 and Li_2CO_3-Na_2CO_3-K_2CO_3. The effects of specific process conditions, such as the electrolyte temperature, are considered in Section 8.4.

In Section 4.2.2 of the present thesis, it was proposed that carbon re-oxidation took place via a process consisting of at least two stages. Based on the findings of authors such as Vutetakis et al. (1987), it seems likely that carbon dioxide was the principal product of carbon re-oxidation. Evidence from both cyclic voltammetry and the re-oxidation of electro-deposited carbon via chronopotentiometry was used to support this mechanism. In this section, the evidence for the two-stage oxidation process is considered.

Section 3.5.3 of the present thesis describes the methodology for the re-oxidation of electro-deposited carbon via chronopotentiometry in a three-electrode system. In each re-oxidation experiment, the working electrode was a mild steel rod where the immersed part of the rod had been coated with carbon during chronoamperometry (as described in Section 8.2). The counter

electrode was a 10 mm diameter graphite rod, whilst the reference electrode was an alumina membrane Ag/AgCl reference electrode. Re-oxidation experiments were typically carried out for up to two hours, by which time the plateau corresponding to the oxidation of the carbonate ion was invariably observed.

Irrespective of the specific conditions used to electro-deposit or re-oxidise carbon in this investigation, all re-oxidation experiments carried out via chronopotentiometry yielded chronopotentiograms of the same fundamental form. A typical potentiogram is given in Figure 8.2, which shows three plateaux. The first and second plateaux probably correspond to two stages of oxidation of the electro-deposited carbon, whilst the third plateau almost certainly corresponds to the oxidation of the carbonate ion.

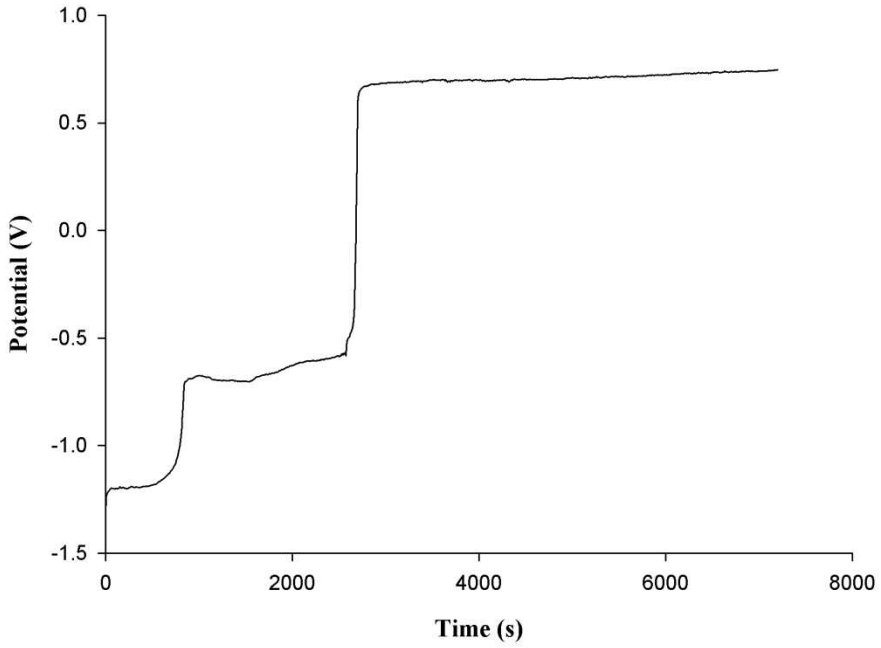

Figure 8.2: Variation of potential versus time during the re-oxidation of electro-deposited carbon in a Li_2CO_3-Na_2CO_3 molten salt (molar ratio: 52:48) at a constant current of 150 mA, at a temperature of 599 °C, under a CO_2 atmosphere. The carbon was electro-deposited in the same electrolyte at an applied potential of -2.77 V vs. Ag/AgCl. WE: 5 mm diameter mild steel rod (with carbon deposit still attached); CE: 10 mm diameter graphite rod; Ag/AgCl membrane RE.

As was pointed out in Chapter 4, the anodic limit potential of the cyclic voltammograms obtained from Li_2CO_3-Na_2CO_3 and Li_2CO_3-K_2CO_3 is very similar to the potential of the third plateau observed in chronopotentiograms such as Figure 8.2, when the same reference electrode was used for both cyclic voltammetry and chronopotentiometry. This in itself is strong evidence for attributing the third plateau to the oxidation of carbonate ions:

$$CO_3^{2-} \rightarrow CO_2 + \tfrac{1}{2}O_2 + 2e^- \qquad (8.5)$$

Further evidence for this comes from the fact that no carbon remained on the working electrode once the third plateau had been reached, except in a few limited cases that shall be considered later in Section 8.4.

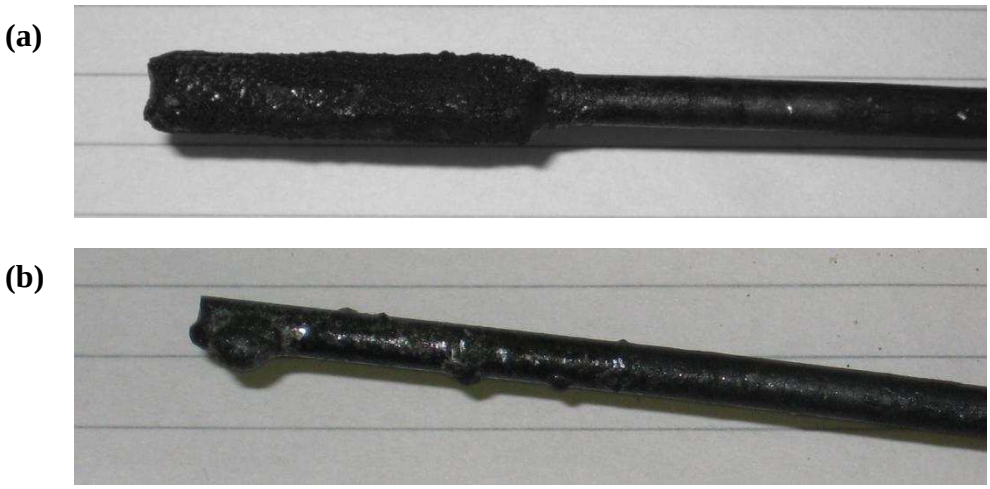

Figure 8.3: (a) 5 mm diameter mild steel rod working electrode coated with carbon that was electro-deposited from a pure Li_2CO_3 electrolyte at a temperature of 800 °C, at an applied potential of -1.8 V vs. Ag/AgCl. (b) The same working electrode after re-oxidation via chronopotentiometry, where the applied current was 100 mA; the re-oxidation process was stopped before the end of the second potential plateau.

The evidence presented in this chapter and Chapters 4 and 5 support a two-stage oxidation mechanism in chronopotentiometry. Firstly, if carbon re-oxidation by chronopotentiometry was stopped during the second plateau, then traces of carbon were still observed to be present on the working electrode surface. Figure 8.3(a) shows a working electrode coated with a layer of

carbon that was electro-deposited in a pure Li_2CO_3 electrolyte at a temperature of 800 °C, at an applied potential of -1.8 V vs. Ag/AgCl; Figure 8.3(b) shows the same working electrode after re-oxidation at an applied current of 100 mA, where the re-oxidation process was stopped during the second plateau, before the third plateau was reached. Evidently some carbon was still present on the working electrode shown in Figure 8.3(b). This is good evidence that carbon was still being oxidised during the second plateau, as generally no carbon was observed to be present after the third plateau had been reached in chronopotentiometry.

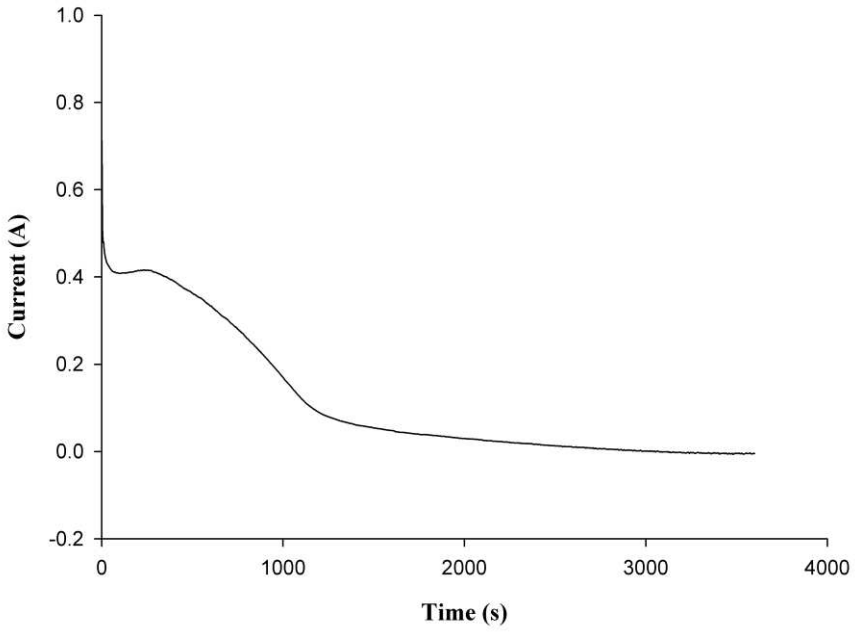

Figure 8.4: Variation of current versus time during the re-oxidation of electro-deposited carbon in a Li_2CO_3-Na_2CO_3 molten salt mixture (molar ratio: 52:48) at a constant potential of -1.20 V, at a temperature of 599 °C, under a CO_2 atmosphere. The carbon was electro-deposited in the same electrolyte at an applied potential of -2.77 V vs. Ag/AgCl. WE: 5 mm diameter mild steel rod (with carbon deposit still attached); CE: 10 mm diameter graphite rod; Ag/AgCl membrane RE.

Further evidence for the two-stage oxidation process was obtained from carbon re-oxidation via chronoamperometry. In each re-oxidation experiment, the working electrode potential was fixed at a potential similar to that of the first plateau from earlier chronopotentimetry experiments, which were carried out under identical conditions using the same reference

electrode. The carbon deposits that were re-oxidised in such experiments were electro-deposited via chronoamperometry, as described earlier in Section 8.2. Figure 8.4 shows a typical chronoamperogram obtained from the potentiostatic re-oxidation of electro-deposited carbon. Once the current had fallen to approximately zero, the working electrode was removed; in the majority of cases, a significant quantity of electro-deposited carbon remained on the working electrode. For example, for the experiment from which Figure 8.4 was produced, the working electrode was still covered by a layer of carbon that was at least 1 mm thick. Observations such as this imply that both the first and second plateaux each correspond to specific stages of the re-oxidation of electro-deposited carbon. The transition from the second plateau to the third plateau probably occurred when there was either insufficient carbon to be oxidised at a rate needed to meet the applied current, or when the carbon re-oxidation rate had become too slow to meet the applied current.

Before the effect of process conditions on the re-oxidation process is considered, it is worth noting the following observation from the literature. When a coal-derived anode was electrochemically oxidised in a molten carbonate electrolyte, it was observed that active material was shed during oxidation (Vutetakis et al., 1987). Thus, it is very likely that a proportion of the electro-deposited carbon was lost during re-oxidation in the present work.

8.4 The Effect of Process Conditions on the Re-Oxidation of Electro-Deposited Carbon

8.4.1 Re-oxidation of electro-deposited carbon in the Li_2CO_3-Na_2CO_3 electrolyte

Table 8.1 shows the Q^+/Q^- values obtained for the re-oxidation of electro-deposited carbon via chronopotentiometry, at a number of different process conditions[*]. Q^+/Q^- was calculated by dividing the oxidation charge passed up to the end of the second plateau by the reduction charge passed during electro-deposition. Thus, Q^+/Q^- also takes into account the re-oxidation of other cathodic products, if indeed any others were produced. Regardless of the specific conditions used, the majority of the Q^+/Q^- values lie within the range of 55 % to 65 %. Varying

[*] Note that the targeted reactor temperatures were 600 °C and 700 °C, although these temperatures were difficult to precisely achieve in practice due to the nature of the furnace temperature control mechanism.

quantities of carbon probably became detached from the working electrode during re-oxidation (and probably electro-deposition as well), which may be the reason why higher Q^+/Q^- values were not generally obtained. In addition, as has been discussed in Section 4.2.1, it is likely that other cathodic products would have been produced during carbon electro-deposition, such as carbon monoxide and alkali metals. If these products left the vicinity of the working electrode, it would not be possible to re-oxidise them, resulting in a drop in the Q^+/Q^- observed.

Table 8.1: Q^+/Q^- values for the re-oxidation of electro-deposited carbon via chronopotentiometry, for the Li_2CO_3-Na_2CO_3 electrolyte (molar ratio of 52:48) at various process conditions; Q^+/Q^- values at the ends of the first and second plateaux are shown. NB. Carbon re-oxidation was considered to have stopped at the end of the second plateau.

Salt Temperature (°C)	**Deposition Potential vs. Ag/AgCl (V)**	**Reduction Charge Passed (C)**	**Re-Oxidation Current (mA)**	**Q^+/Q^- (%)**		**All Carbon Removed?**
				At End of 1st Plateau	**At End of 2nd Plateau**	
703	-2.30	-1147	150	32.0	69.4	Yes
703	-2.30	-1385	150	41.0	61.5	Yes
703	-2.30	-1482	300	51.2	63.4	Yes
725	-2.30	-1326	450	47.0	105.0	Yes
725	-2.60	-1917	300	43.3	95.2	Yes
725	-3.00	-1519	300	15.6	34.4	Yes
599	-2.77	-664	150	18.3	60.6	No
599	-2.77	-732	150	22.4	60.5	No
597	-2.77	-1275	300	40.5	63.9	Yes
597	-2.77	-1108	450	45.1	60.1	Yes
597	-3.07	-2197	300	37.1	63.7	Yes
597	-3.67	-1575	300	15.4	55.8	Yes

The loss of carbon during electro-deposition and/or re-oxidation may be responsible for the fact that there are no discernible trends in Q^+/Q^- with changing electro-deposition potential or discharge rate, although it is possible that the Q^+/Q^- did not change when these parameters were altered. However, it would appear that carbon re-oxidation in the Li_2CO_3-Na_2CO_3 electrolyte was comparatively more difficult at temperatures of 597 °C and 599 °C. This is apparent from the observation that not all of the carbon was re-oxidised during both

experimental runs at 599 °C. Li et al. (2008) found that higher temperatures led to greater carbon re-oxidation rates in DCFCs, which is consistent with this observation.

Ingram et al. (1966) studied the anodic stripping of electro-deposited carbon in a Li_2CO_3-Na_2CO_3-K_2CO_3 electrolyte at a temperature of 600 °C, obtaining Q^+/Q^- values between 32 % and 57 %. The fact that Ingram et al. (1966) generally stopped re-oxidation at the end of the first plateau may account for the relatively low Q^+/Q^- values obtained. Indeed, many of the Q^+/Q^- values calculated at the end of the first plateau in Table 8.1 lie within the range given by Ingram et al. (1966).

Due to the fact that each experimental run in Table 8.1 took around three hours in total, there was insufficient time to collect larger amounts of data for the Li_2CO_3-Na_2CO_3 electrolyte, which would have allowed any trends or anomalies to be more easily discerned. In addition, Ingram et al. (1966) were not able to observe any trends in their Q^+/Q^- data either.

8.4.2 Re-oxidation of electro-deposited carbon in the Li_2CO_3-K_2CO_3 electrolyte

Moving onto the Li_2CO_3-K_2CO_3 electrolyte, Table 8.2 shows the Q^+/Q^- values obtained for the re-oxidation of electro-deposited carbon via chronopotentiometry, at a number of different process conditions. The Q^+/Q^- values obtained from this electrolyte seem to be generally lower than those obtained from the Li_2CO_3-Na_2CO_3 electrolyte; the overall average of all the Q^+/Q^- values in Table 8.1 for Li_2CO_3-Na_2CO_3 is 66.1 %, whereas the overall average of all the Q^+/Q^- values in Table 8.2 for Li_2CO_3-K_2CO_3 is 48.5 %. Perhaps this is because the proportion of carbon that fell off the working electrode during re-oxidation was greater in the Li_2CO_3-K_2CO_3 electrolyte[*], which may have been due to poorer cohesion of carbon particles or poorer adhesion of the carbon to the working electrode surface. However, until more detailed studies of electro-deposited carbon structures and surface properties have been carried out (eg. by transmission electron microscopy and by Brunauer-Emmett-Teller gas adsorption studies), it

[*] The average current efficiencies given in Chapter 7 for carbon electro-deposition in both the Li_2CO_3-Na_2CO_3 and Li_2CO_3-K_2CO_3 electrolytes were similar (74.4 % and 79.0 % respectively). Thus, it seems unlikely that carbon losses were higher during electro-deposition in the Li_2CO_3-K_2CO_3 electrolyte.

will be difficult to determine the precise reason why the carbon produced from the Li_2CO_3-Na_2CO_3 electrolyte yielded higher re-oxidation Q^+/Q^- values.

Table 8.2: Q^+/Q^- values for the re-oxidation of electro-deposited carbon via chronopotentiometry, for the Li_2CO_3-K_2CO_3 electrolyte (molar ratio of 62:38) at various process conditions; Q^+/Q^- values at the ends of the first and second plateaux are shown. NB. Carbon re-oxidation was considered to have stopped at the end of the second plateau.

Salt Temperature (°C)	**Deposition Potential vs. Ag/AgCl (V)**	**Reduction Charge Passed (C)**	**Re-Oxidation Current (mA)**	**Q^+/Q^- (%)**		**All Carbon Removed?**
				At End of 1st Plateau	**At End of 2nd Plateau**	
708	-1.68	-1102	150	24.5	77.8	Yes
708	-1.68	-1017	150	25.8	83.3	Yes
704	-1.68	-973.6	300	17.4	47.6	Yes
704	-1.68	-1301	450	18.2	34.1	Yes
704	-1.98	-1764	300	16.3	32.2	Yes
704	-2.28	-2318	300	14.9	27.6	Yes
579	-2.56	-658.6	150	19.8	54.9	Yes
574	-2.56	-756.0	300	33.8	61.4	Yes
574	-2.56	-841.3	450	14.4	33.4	Yes
574	-2.86	-1205	300	3.61	39.3	No
574	-3.16	-1897	300	5.46	41.5	No

In Table 8.2, the range of Q^+/Q^- values observed at temperatures near to 700 °C is 27.6 % to 83.3 %, whereas at temperatures nearer to 600 °C the range is 33.4 % to 61.4 %. Carbon re-oxidation appears to have been somewhat more difficult at around 600 °C for two reasons. Firstly, some of the carbon remained un-oxidised after two of the runs at 574 °C. Secondly, the maximum Q^+/Q^- attained at temperatures near 600 °C was 61.4 %, which is lower than that obtained at temperatures near 700 °C (83.3 %). This conclusion is consistent with the findings from cyclic voltammetry that are considered in Section 5.2.2; Q^+/Q^- values for the re-oxidation of cathodic products in cyclic voltammetry indicated that a proportion of the electro-deposited carbon remained un-oxidised after a given anodic sweep in the Li_2CO_3-K_2CO_3 electrolyte, particularly at temperatures near 600 °C.

A number of trends in Q^+/Q^- seem to be apparent in Table 8.2. Firstly, the more negative the potential at which the carbon was electro-deposited, the lower the Q^+/Q^- attained. This would appear to be related to the fact that larger amounts of carbon would have been deposited at more negative potentials, as is indicated by the larger reduction charges passed at more negative potentials. If larger amounts of carbon were present on the working electrode, then it would have been more likely that some of the electro-deposited carbon would have fallen off the electrode during electro-deposition* and/or re-oxidation. Secondly, the Q^+/Q^- appears to decrease with increasing discharge current, which may be because the higher rate of carbon re-oxidation caused a larger proportion of the carbon to fall off the working electrode.

As with the Li_2CO_3-Na_2CO_3 electrolyte, due to the fact that three hours were required to carry out each experimental run in Table 8.2, it was not possible to collect larger quantities of data for the Li_2CO_3-K_2CO_3 electrolyte.

8.5 Improving Q^+/Q^-

From Tables 8.1 and 8.2, it is apparent that Q^+/Q^- values over 65 % were not frequently attained for the re-oxidation of electro-deposited carbon. However, if the electro-deposition and re-oxidation processes were to be used to store energy, it would be desirable to increase the Q^+/Q^- values attained. As was mentioned earlier in Sections 8.2 and 8.3, it is likely that some carbon was lost from the working electrode during both electro-deposition and re-oxidation. This effect was probably the main reason why higher Q^+/Q^- values were generally not observed.

In molten carbonate DCFCs, the carbon fuel can be dispersed between the anode and cathode in particulate form. For example, Li et al. (2008) were able to oxidise carbon particles suspended in a ternary Li_2CO_3-Na_2CO_3-K_2CO_3 electrolyte, where the concentration of carbon was 1, 5 or 10 wt %; note that the suspension was maintained by means of a stirring rod with a half-circle impeller. The electro-deposited carbon produced in the present work could be

* This issue is considered in more detail in Chapter 7.

collected, pulverised and then re-oxidised in such a DCFC arrangement. Since the carbon powder does not need to be in direct contact with the anode at all times in order to be re-oxidised in such a DCFC system, it would be possible to re-oxidise all of the carbon powder. However, one disadvantage of this method of re-oxidising the carbon is that removing the carbon and pulverising it would take some time and effort to achieve. In addition, this method does not prevent carbon losses during the electro-deposition stage, unless the same electrolyte is used for both electro-deposition and re-oxidation, in which case any lost carbon would be suspended along with the pulverised carbon.

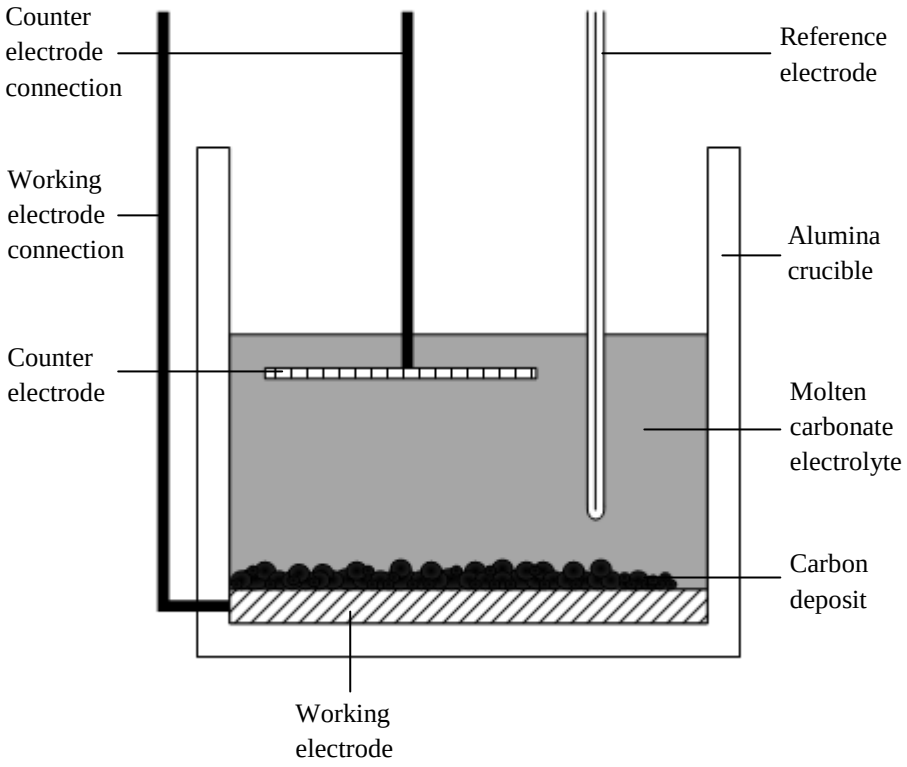

Figure 8.5: Possible electrode arrangements in an electrochemical cell for the electro-deposition and subsequent re-oxidation of carbon.

For the purposes of energy storage, it would be more convenient to be able to electro-deposit and re-oxidise carbon in the same electrochemical cell. One relatively simple way of reducing the amount of carbon lost from the working electrode would be to make the working electrode a flat metal plate at the very bottom of the electrolyte container, as shown in Figure 8.5. This arrangement would help to prevent any loss of carbon from the working electrode caused by

gravity during both electro-deposition (where the working electrode serves as the cathode) and re-oxidation (where the working electrode serves as the anode), which would lead to much more reliable Q^+/Q^- values being obtained.

However, it may not be possible to completely eliminate losses of carbon from the working electrode surface due to the fact that the electro-deposited carbon primarily consists of amorphous carbon particles, which are often aggregated into larger particles[*]. As scanning electron microscopy (SEM) images presented in Section 7.5 show, the carbon deposits contained carbon nanoparticles as small as 60 nm. Such nanoparticles could easily become detached from the carbon deposit and become suspended in the electrolyte, due to small electrolyte disturbances (eg. turbulence). Due to the very small size of these nanoparticles, it would take a long time for them to settle under gravity, although it seems unlikely that large quantities of carbon could be lost in this way.

In a practical system for re-oxidising electro-deposited carbon to generate electricity, oxygen would need to be supplied at the counter electrode during re-oxidation, in order to allow Reaction 8.4 to occur. Since obtaining reliable Q^+/Q^- values is the main priority at this early stage in the present research, such a means of supplying oxygen at the counter electrode is not included in the set-up represented in Figure 8.5. The counter electrode in Figure 8.5 could be made of some kind of mesh (such as a platinum mesh) in order to provide a high surface area.

8.6 Conclusions

Firstly, the most important conclusion that can be drawn from the results presented in this chapter is that electro-deposited carbon was re-oxidised in two electrochemical stages, which supports the two-stage carbon re-oxidation process proposed in Chapters 4 and 5. This conclusion was found to be applicable to all of the electrolytes from which carbon could be electro-deposited: Li_2CO_3, Li_2CO_3-Na_2CO_3, Li_2CO_3-K_2CO_3 and Li_2CO_3-Na_2CO_3-K_2CO_3[†].

[*] See Chapter 7 for more details.
[†] Please see Appendix III for some Q^+/Q^- results that were obtained from the Li_2CO_3 and Li_2CO_3-Na_2CO_3-K_2CO_3 electrolytes.

Re-oxidation of electro-deposited carbon via galvanostatic chronopotentiometry produced chronopotentiograms with three distinct plateaux. The first two plateaux were found to correspond to carbon re-oxidation, due to the fact that significant amounts of carbon were still observed to be present if re-oxidation was stopped before the end of the second plateau. Furthermore, if the electro-deposited carbon was re-oxidised at the potential of the first plateau via potentiostatic electrolysis (chronoamperometry), it was found that significant quantities of carbon still remained on the working electrode even after the current flow had dropped to zero. However, carbon deposits were seldom observed to be present on the working electrode surface once the third plateau had been reached in chronopotentiometry. Hence, the third plateau was ascribed to the oxidation of carbonate ions.

Q^+/Q^- values for the re-oxidation of electro-deposited carbon were determined at a number of different sets of process conditions for the Li_2CO_3-Na_2CO_3 and Li_2CO_3-K_2CO_3 electrolytes. Generally, the re-oxidation of carbon deposits from Li_2CO_3-Na_2CO_3 yielded higher Q^+/Q^- values; the average Q^+/Q^- for this electrolyte was 66.1 %, as opposed to 48.5 % for the Li_2CO_3-K_2CO_3 electrolyte. Without more detailed structural investigations of the electro-deposited carbon, it is difficult to account for this difference. Carbon re-oxidation was found to be more difficult at temperatures near to 600 °C than at temperatures near to 700 °C, for both electrolytes. This was indicated by incomplete re-oxidation of carbon in some experiments, and also by lower Q^+/Q^- values at 600 °C in the case of Li_2CO_3-K_2CO_3. Li et al. (2008) found that electrochemical carbon oxidation rates in molten carbonate were higher at higher temperatures, so these observations are consistent with the findings of Li et al. (2008).

When the re-oxidation current was made larger or when the electro-deposition potential was more negative, Q^+/Q^- values were found to decrease for the Li_2CO_3-K_2CO_3 electrolyte, although no such trend was observed for Li_2CO_3-Na_2CO_3. The lower Q^+/Q^- values at these conditions may have been caused by increased losses of carbon from the working electrode during re-oxidation and/or electro-deposition. These same losses may also have been the reason why no comparable trends were observed for Li_2CO_3-Na_2CO_3. In future work, one could use a ‘flat plate’ working electrode at the base of the electrolyte container; this would

help to reduce losses of electro-deposited carbon from the working electrode by preventing carbon from falling off it.

CHAPTER 9

CONCLUSIONS AND FUTURE WORK

The research presented in this thesis has covered a range of fundamental areas concerning the production of carbon from carbon dioxide via molten carbonate electrolysis, in addition to carbon re-oxidation. The work has encompassed studies of cyclic voltammetry and galvanostatic chronopotentiometry to deduce the reactions taking place. Furthermore, the electro-deposited carbon produced has been examined using a variety of different analysis techniques, including scanning electron microscopy and X-ray diffraction, in order to determine its properties. The most important conclusions that can be drawn from the preceding chapters are reiterated in the following paragraphs.

Firstly, using cyclic voltammetry carried out at platinum working electrodes, carbon was found to be electro-deposited at the cathodic limit in the Li_2CO_3-Na_2CO_3 and Li_2CO_3-K_2CO_3 electrolytes at temperatures of ca. 600 °C and ca. 700 °C, probably via the following reaction:

$$CO_3^{2-} + 4e^- \rightarrow C + 3O^{2-} \qquad (9.1)$$

One novel finding of this research is that the carbon electro-deposition reaction was found to compete with a number of other cathodic reactions at the cathodic limit, which included alkali metal carbide formation, alkali metal cation reduction and carbon monoxide formation. By calculating Q^+/Q^- values for the re-oxidation of cathodic products from cyclic voltammetry, it was found that carbon deposition did not dominate over the other cathodic reactions until the working electrode was covered with a layer of carbon. This is probably because the overpotential required to electro-deposit carbon onto carbon is lower than that necessary to electro-deposit carbon onto metal. Furthermore, the bare metal working electrode probably catalysed the other cathodic reactions before it became covered with carbon.

Electrochemical re-oxidation of electro-deposited carbon was found to take place via a process consisting of at least two stages, which was deduced using cyclic voltammetry in conjunction with carbon re-oxidation via chronopotentiometry.

Electro-deposited carbon could be obtained from all of the carbonate electrolytes studied that contained Li_2CO_3: Li_2CO_3-Na_2CO_3, Li_2CO_3-K_2CO_3, Li_2CO_3 and Li_2CO_3-Na_2CO_3-K_2CO_3. However, no carbon could be obtained from carbonate electrolytes that lacked Li_2CO_3. The reason for this is unclear, although the electro-deposition of carbon from Li_2CO_3 has the least negative potential out of all the possible cathodic reactions at temperatures below 1000 °C. In electrolytes lacking Li_2CO_3, such as Na_2CO_3 and K_2CO_3, alkali metal formation appears to have been the principal reaction that occurred at the cathodic limit.

Carbon was electro-deposited onto mild steel working electrodes via chronoamperometry in the Li_2CO_3-Na_2CO_3, Li_2CO_3-K_2CO_3 and Li_2CO_3-Na_2CO_3-K_2CO_3 electrolytes. The highest apparent electro-deposition rate obtained was 0.183 g/cm^2.h at an applied potential of -2.98 V vs. Ag/AgCl, using the Li_2CO_3-K_2CO_3 electrolyte at 708 °C. The average current efficiencies obtained for carbon electro-deposition were: 74.4 % for Li_2CO_3-Na_2CO_3, 79.0 % for Li_2CO_3-K_2CO_3 and 51.2 % for Li_2CO_3-Na_2CO_3-K_2CO_3. Scanning electron microscopy (SEM), X-ray diffraction (XRD) and energy dispersive X-ray (EDX) spectroscopy revealed that the washed carbon deposits mostly consisted of fine quasi-spherical carbon particles, some as small as 60 nm in diameter. All of the electro-deposited carbon appeared to be amorphous.

Carbon samples were also subjected to simultaneous thermogravimetric analysis (TGA) and heat-flux differential scanning calorimetry (DSC). The average mass percentages of carbon present in the deposits obtained from each electrolyte were (on a dry basis): 82.1 % for Li_2CO_3-Na_2CO_3, 84.7 % for Li_2CO_3-K_2CO_3 and 84.5 % for Li_2CO_3-Na_2CO_3-K_2CO_3. The average amounts of energy released from the deposits during oxidation were (on a dry basis): 19900 J/g for Li_2CO_3-Na_2CO_3, 21000 J/g for Li_2CO_3-K_2CO_3 and 22500 J/g for Li_2CO_3-Na_2CO_3-K_2CO_3. The average temperatures for the onset of oxidation of carbon from each of the three electrolytes were: 337 °C for Li_2CO_3-Na_2CO_3, 357 °C for Li_2CO_3-K_2CO_3 and 348 °C

for Li_2CO_3-Na_2CO_3-K_2CO_3. These onset temperatures are much lower than those of a commercial graphite powder (KS-10 graphite powder has an onset temperature of around 700 °C), which may have been due to the presence of alkali metal carbonate impurities in the deposits (which can have a catalytic effect on oxidation) and/or the high surface area of the carbon (due to the fine particle sizes present).

The following items could be considered in future work to follow up this PhD project:

- In the present research, it appeared that carbon deposits produced in the Li_2CO_3-K_2CO_3 electrolyte could not be re-oxidised as quickly as those produced from the Li_2CO_3-Na_2CO_3 electrolyte, at similar temperatures. Possibly some structural differences between the carbon deposits were responsible for this. Hence, it would be appropriate to carry out more detailed structural analyses of carbon deposits produced from these two electrolytes, using techniques such as transmission electron microscopy and Brunauer-Emmett-Teller gas adsorption studies.
- Electro-deposition and re-oxidation experiments could be carried out in a cell where the working electrode is a flat plate at the base of the cell – this would help to minimise losses of carbon from the working electrode and yield more accurate current efficiencies and deposition rates.
- The cyclic voltammetry of the Li_2CO_3, Li_2CO_3-Na_2CO_3-K_2CO_3, Na_2CO_3, K_2CO_3 and Na_2CO_3-K_2CO_3 electrolytes needs to be studied using an inert working electrode such as platinum, as this will prevent additional peaks from arising due to reactions between the working electrode material and the electrolyte. Carbon electro-deposition and re-oxidation could also be studied in more detail in these electrolytes.
- The performance of the electro-deposited carbon in energy storage devices such as supercapacitors could be tested further than has already been done in the literature.

REFERENCES

AZUMA, M., K. HASHIMOTO, M. HIRAMOTO, M. WATANABE and T. SAKATA (1990), Electrochemical Reduction of Carbon Dioxide on Various Metal Electrodes in Low-Temperature Aqueous KHCO3 Media, Journal of the Electrochemical Society, Vol. 137, No. 6., pgs 1772-1778.

BARD, A. J. and L. R. FAULKNER (2001), Electrochemical Methods: Fundamentals and Applications, John Wiley & Sons Inc., New York.

BARNETT, R., K. T. KILBY and D. J. FRAY (2009), Reduction of Tantalum Pentoxide Using Graphite and Tin-Oxide-Based Anodes via the FFC-Cambridge Process, Metallurgical and Materials Transactions B, Vol. 40, No. 2, pgs 150-157.

BARROSSE-ANTLE, L. E. and R. G. COMPTON (2009), Reduction of carbon dioxide in 1-butyl-3-methylimidazolium acetate, Chemical Communications, pgs 3744-3746.

BARTLETT, H. E. and K. E. JOHNSON (1967), Electrochemical Studies in Molten Li_2CO_3-Na_2CO_3, Journal of the Electrochemical Society, Vol. 114, No. 5, pgs 457-461.

BELEY, M., J. P. COLLIN, R. RUPPERT and J. P. SAUVAGE (1986), Electrocatalytic reduction of carbon dioxide by nickel cyclam2+ in water: study of the factors affecting the efficiency and the selectivity of the process, Journal of the American Chemical Society, Vol. 108, No. 24, pgs 7461-7467.

BHUGUN, I, D. LEXA and J.-M. SAVÉANT (1996), Catalysis of the Electrochemical Reduction of Carbon Dioxide by Iron(0) Porphyrins: Synergystic Effect of Weak Brönsted Acids, Journal of the American Chemical Society, Vol. 118, No. 7, pgs 1769-1776.

BIEDENKOPF, P., M. SPIEGEL and H. J. GRABKE (1998), The corrosion behaviour of iron and chromium in molten $(Li_{0.62}K_{0.38})_2CO_3$, Electrochimica Acta, Vol. 44, pgs 683-692.

BORUCKA, A. (1977), Evidence for the Existence of Stable $CO_2^{=}$ Ion and Response Time of Gas Electrodes in Molten Alkali Carbonates, Journal of the Electrochemical Society, Vol. 124, No. 7, pgs 972-976.

BROWN, M. E. (2001), Introduction to Thermal Analysis: Techniques and Applications (2nd Edition), Kluwer Academic Publishers, Secaucus, USA.

CHASE, M. W. JR. (1998), NIST-JANAF Thermochemical Tables (4th Edition), National Institute of Standards, Gaithersberg.

CHEN, G. Z., I. KINLOCH, M. S. P. SHAFFER, D. J. FRAY and A. H. WINDLE (1998), Electrochemical investigation of the formation of carbon nanotubes in molten salts, High Temperature Material Processes, Vol. 2, No. 4, pgs 459-469.

CHEN, G. Z., D. J. FRAY and T. W. FARTHING (2000), Direct electrochemical reduction of titanium dioxide to titanium in molten calcium chloride, Nature, Vol. 407, pgs 361-364.

CHEN, G. Z., S. M. JUNG, N. SIAMBUN, D. JEWELL and G. RICE (2009), Final Report for the Brian Mercer Feasibility Award: A Feasibility Study of Solar-Electrochemical Cells for Capturing Atmospheric Carbon, University of Nottingham, Nottingham.

CHEN, G., Z. SHI, D. SHI, X. HU, B. GAO, Z. WANG and Y. YU (2010), Research on electro-deposition of carbon from LiF-NaF-Na_2CO_3 molten salt system, Proceedings of the 2010 World Non-Grid-Connected Wind Power and Energy Conference, WNWEC 2010, Nanjing, pgs 1-3.

CHEREPY, N. J., R. KRUEGER, K. J. FIET, A. F. JANKOWSKI and J. F. COOPER (2005), Direct Conversion of Carbon Fuels in a Molten Carbonate Fuel Cell, Journal of the Electrochemical Society, Vol. 152, No. 1, pgs A80-A87.

COSTENTIN, C, M. ROBERT and J.-M. SAVÉANT (2013), Catalysis of the electrochemical reduction of carbon dioxide, Chemical Society Reviews, Vol. 42, pgs 2423-2436.

CREUTZ, C and E. FUJITA (2001), Carbon Dioxide as a Feedstock, in: Carbon Management: Implications for R&D in the Chemical Sciences and Technology: A Workshop Report to the Chemical Sciences Roundtable, National Academy Press, Washington D. C., pgs 83-92.

CROFT, W. J. (2006), Under the Microscope: A Brief History of Microscopy, World Scientific, River Edge, New Jersey.

DAVIES, P. (2012), SDT Q600 Training Course, TA Instruments, Elstree (held on 15th February 2012).

DAVIS, J. R. (2002), Process Selection Guide in the Surface Hardening of Steels: Understanding the Basics, ASM International, Ohio.

DEANHARDT, M. L., K. H. STERN and A. KENDE (1986), Thermal Decomposition and Reduction of Carbonate Ion in Fluoride Melts, Journal of the Electrochemical Society, Vol. 133, No. 6, pgs 1148-1152.

DELIMARSKII, YU. K., O. V. GORODIS'KII and V. F. GRISHCHENKO (1964), Cathode liberation of carbon from molten carbonates, Doklady Akademii Nauk SSSR, Vol. 156, No. 3, pgs 650-651.

DELIMARSKII, YU. K., V. F. GRISHCHENKO and A. V. GORODYSKII (1965), Reactions taking place during electrolysis of fused carbonates, Ukrainskii Khimicheskii Zhurnal, Vol. 31, No. 1, pgs 32-37.

DELIMARSKII, YU. K., V. I. SHAPOVAL, V. F. GRISHCHENKO and V. A. VASILENKO (1968), Cathodic liberation of carbon in the electrolysis of molten carbonates, Doklady Akademii Nauk SSSR, Vol. 183, No. 6, pgs 1332-1334.

DELIMARSKII, YU. K., V. F. GRISHCHENKO and V. A. VASILENKO (1969), Electrolysis of molten alkali metal carbonates, Zhurnal Prikladnoi Khimii, Vol. 42, No. 1, pgs 224-226.

DELIMARSKII, YU. K., V. I. SHAPOVAL, V. A. VASILENKO and V. F. GRISHCHENKO (1970a), Electrolysis of fused carbonates of alkali metals under pressure, Zhurnal Prikladnoi Khimii, Vol. 43, No. 12, pgs 2634-2638.

DELIMARSKII, YU. K., V. F. GRISHCHENKO, N. KH. TUMANOVA and V. I. SHAPOVAL (1970b), Products of the electrolytic decomposition of fused carbonates, Ukrainskii Khimicheskii Zhurnal, Vol. 36, No. 2, pgs 136-141.

DELIMARSKII, YU. K., V. I SHAPOVAL and V. A. VASILENKO (1971), Importance of the kinetic process during the electroreduction of CO_3^{2-} in molten potassium chloride-sodium chloride, Elektrokhimiya, Vol. 7, No. 9, pgs 1301-1304.

DELIMARSKII, YU. K., V. I. SHAPOVAL, V. A. VASILENKO and V. F. GRISHCHENKO (1975), Electrolytic production of pure carbon, Otkrytiya, Izobret., Prom. Obraztsy, Tovarnye Znaki, Vol. 52, No. 35, pgs 176-177.

DEVYATKIN, S. V. (2012), Chemical and Electrochemical Behavior of Titanium, Silicon, and Boron Oxides in Molten Carbonates, Russian Journal of Electrochemistry, Vol. 48, No. 10, pgs 1000-1004.

DIMITROV, A. (2009), Study of molten Li_2CO_3 electrolysis as a method for production of carbon nanotubes, Macedonian Journal of Chemistry and Chemical Engineering, Vol. 28, No. 1, pgs 111-118.

DULSKY, T. R. (1996), A Manual for the Chemical Analysis of Metals, ASTM International, West Conshohocken, Pennsylvania.

EGGINS, B. R., C. ENNIS, R. MCCONNELL and M. SPENCE (1997), Improved yields of oxalate, glyoxylate and glycolate from the electrochemical reduction of carbon dioxide in methanol, Journal of Applied Electrochemistry, Vol. 27, No. 6, pgs 706-712.

FACILITY FOR THE ANALYSIS OF CHEMICAL THERMODYNAMICS (2012), FTsalt-FACT Salt Database, FactSage, http://www.crct.polymtl.ca/fact/documentation/FTsalt/FTsalt_Figs.htm (accessed in October 2012)

FISHER, A. C. (1996) Electrode Dynamics, Oxford University Press, Oxford.

FLAVELL-WHILE, C. (2011) Chemengers who changed the world: power player, The Chemical Engineer, Issue 836, pgs 42-44.

FLEGER, S. L., J. W. HECKMAN and K. L. KLOMPARENS (1993), Scanning and Transmission Electron Microscopy: An Introduction, W. H. Freeman and Company, New York.

GATTRELL, M., N. GUPTA and A. CO (2006), A review of the aqueous electrochemical reduction of CO_2 to hydrocarbons at copper, Journal of Electroanalytical Chemistry, Vol. 594, pgs 1-19.

GOODHEW, P. J., J. HUMPHREYS and R. BEANLAND (2001), Electron Microscopy and Analysis, Taylor and Francis, London.

GROULT, H. and D. DEVILLIERS (1998), Fluorine evolution reaction in KF-2HF: Influence of Ni-doping particles on the electrochemical properties of the carbon-fluorine surface film, Journal of Fluorine Chemistry, Vol. 87, pgs 151-156.

GROULT, H., B. KAPLAN, S. KOMABA, N. KUMAGAI, V. GUPTA, T. NAKAJIMA and B. SIMON (2003), Lithium Insertion into Carbonaceous Anode Materials Prepared by Electrolysis of Molten Li-K-Na Carbonates, Journal of the Electrochemical Society, Vol. 150, No. 2, pgs G67-G75.

GROULT, H, B. KAPLAN, F. LANTELME, S. KOMABA, N. KUMAGAI, H. YASHIRO, T. NAKAJIMA, B. SIMON and A. BARHOUN (2006), Preparation of carbon nanoparticles from electrolysis of molten carbonates and use as anode materials in lithium-ion batteries, Solid State Ionics, Vol. 177, pgs 869-875.

GUO, Y., J. QI, Y. JIANG, S. YANG, Z. WANG and H. XU (2003), Performance of electrical double layer capacitors with porous carbons derived from rice husk, Materials Chemistry and Physics, Vol. 80, pgs 704-709.

HARA, K., A. KUDO and T. SAKATA (1995), Electrochemical reduction of carbon dioxide under high pressure on various electrodes in an aqueous electrolyte, Journal of Electroanalytical Chemistry, Vol. 391, pgs 141-147.

HAUPIN, W. E. and W. B. FRANK, in BOCKRIS, J. O'M, B. E. CONWAY, E. YEAGER and R. E. WHITE (1981), Comprehensive Treatise of Electrochemistry Volume 2: Electrochemical Processing, Plenum Press, New York, pgs 301-325.

HAWECKER, J., J.-M. LEHN and R. ZIESSEL (1984), Electrocatalytic reduction of carbon dioxide mediated by Re(bipy)$(CO)_3Cl$ (bipy = 2,2'-bipyridine), Journal of the Chemical Society, Chemical Communications, pgs 328-330.

HEINZE, J. (1984), Cyclic Voltammetry – "Electrochemical Spectroscopy", Angewandte Chemie, Vol. 23, No. 11, pgs 831-918.

HORI, Y., K. KIKUCHI, A. MURATA and S. SUZUKI (1986), Production of methane and ethylene in electrochemical reduction of carbon dioxide at copper electrode in aqueous hydrogencarbonate solution, Chemistry Letters, pgs 897-898.

HORI, Y. and A. MURATA (1990), Electrochemical evidence of intermediate formation of adsorbed CO in cathodic reduction of CO_2 at a nickel electrode, Electrochimica Acta, Vol. 35, pgs 1777-1780.

HU, D. (2011), Near-Net-Shape Electrochemical Metallisation of Oxide Precursors into Ti-6Al-4V Products in Molten $CaCl_2$ (PhD Thesis), University of Nottingham, Nottingham.

IJIJE, H. V. (2012), Unpublished First Year Annual Report, University of Nottingham, Nottingham.

INGRAM, M. D., B. BARON and G. J. JANZ (1966), The electrolytic deposition of carbon from fused carbonates, Electrochimica Acta, Vol. 11, pgs. 1629-1639.

ITO, Y., T. SHIMADA and H. KAWAMURA (1992), Electrochemical formation of thin carbon film from molten chloride system, Proceedings of the Electrochemical Society, Vol. 16, pgs 574-585.

ITO, Y. (2011), Formation of a carbon film by the molten salt electrochemical process and its applications (溶融塩電気化学プロセスによる炭素めっき), TANSO 2011 (炭素 2011), No. 248, pgs 144-151.

JANZ, G. J., A. CONTE and E. NEUENSCHWANDER (1963), Corrosion of Platinum, Gold, Silver and Refractories in Molten Carbonates, Corrosion, Vol. 19, pgs 292-294.

JANZ, G. J. and A. CONTE (1964a), Potentiostatic polarization studies in fused carbonates-I. the noble metals, silver and nickel, Electrochimica Acta, Vol. 9, pgs 1269-1278.

JANZ, G. J. and A. CONTE (1964b), Potentiostatic polarization studies in fused carbonates-II. stainless steel, Electrochimica Acta, Vol. 9, pgs 1279-1287.

JEWELL, D. (2009), Novel Electrochemical Engineering for the Intelligent Extraction of Titanium (PhD Thesis), University of Nottingham, Nottingham,

JIANG, W., G. NADEAU, K. ZAGHIB and K. KINOSHITA (2000), Thermal analysis of the oxidation of natural graphite — effect of particle size, Thermochimica Acta, Vol. 351, No. 1-2, pgs 85-93.

JITARU, M., D. A. LOWY, M. TOMA, B. C. TOMA and L. ONICIU (1997), Electrochemical reduction of carbon dioxide on flat metallic cathodes, Journal of Applied Electrochemistry, Vol. 27, No. 8, pgs 875-889.

KANECO, S., K. IIBA, S.-K. SUZUKI, K. OHTA and T. MIZUNO (1999), Electrochemical Reduction of Carbon Dioxide to Hydrocarbons with High Faradaic Efficiency in LiOH/Methanol, Journal of Physical Chemistry B, Vol. 103, pgs 7456-7460.

KANECO, S., K. IIBA, H. KATSUMATA, T. SUZUKI and K. OHTA (2007), Effect of sodium cation on the electrochemical reduction of CO_2 at a copper electrode in methanol, Journal of Solid State Electrochemistry, Vol. 11, pgs 490-495.

KAPLAN, B., H. GROULT, S. KOMABA, N. KUMAGAI and F. LANTELME (2001), Synthesis of Nanostructured Carbon Material by Electroreduction in Fused Alkali Carbonates, Chemistry Letters, Vol. 7, pgs 714-715.

KAPLAN, B., H. GROULT, A. BARHOUN, F. LANTELME, T. NAKAJIMA, V. GUPTA, S. KOMABA and N. KUMAGAI (2002), Synthesis and Structural Characterization of Carbon Powder by Electrolytic Reduction of Molten Li_2CO_3-Na_2CO_3-K_2CO_3, Journal of the Electrochemical Society, Vol. 149, No. 5, pgs D72-D78.

KAPLAN, V., E. WACHTEL, K. GARTSMAN, Y. FELDMAN and I. LUBOMIRSKY (2010), Conversion of CO_2 to CO by Electrolysis of Molten Lithium Carbonate, Journal of the Electrochemical Society, Vol. 157, No. 4, pgs B552-B556.

KAWAMURA, H. and Y. ITO (2000), Electrodeposition of cohesive carbon films on aluminum in a LiCl-KCl-K_2CO_3 melt, Journal of Applied Electrochemistry, Vol. 30, pgs 571-574.

KEIJZER, M., G. LINDBERGH, K. HEMMES, P. J. J. M VAN DER PUT, J. SCHOONMAN and J. H. W DE WIT (1999), Corrosion of 304 Stainless Steel in Molten-Carbonate Fuel Cells, Journal of the Electrochemical Society, Vol. 146, No. 7, pgs 2508-2516.

KISSINGER, P. T. and W. R. HEINEMAN (1983), Cyclic Voltammetry, Journal of Chemical Education, Vol. 60, No. 9, pgs 702-706.

KNOVEL CORPORATION (2008), Knovel Critical Tables (2nd Edition), Knovel Corporation, Norwich, New York. Online version available at:

http://www.knovel.com/web/portal/browse/display?_EXT_KNOVEL_DISPLAY_bookid=761&VerticalID=0

KUSHKHOV, KH. B., V. I. SHAPOVAL and I. A. NOVOSELOVA (1987), Electrochemical behavior of carbon dioxide gas under excess pressure in an equimolar melt of potassium and sodium chlorides, Elektrokhimiya¸Vol. 23, No. 7, pgs 952-956.

LANTELME, F., B. KAPLAN, H. GROULT and D. DEVILLIERS (1999), Mechanism for elemental carbon formation in molecular ionic liquids, Journal of Molecular Liquids, Vol. 83, pgs 255-269.

LE VAN, K., H. GROULT, F. LANTELME, M. DUBOIS, D. AVIGNANT, A. TRESSAUD, S. KOMABA, N. KUMAGAI and S. SIGRIST (2009), Electrochemical formation of carbon nano-powders with various porosities in molten alkali carbonates, Electrochimica Acta, Vol. 54, pgs 4566-4573.

LE, M., M. REN, Z. ZHANG, P. T. SPRUNGER, R. L. KURTZ and J. C. FLAKE (2011), Electrochemical Reduction of CO_2 to CH_3OH at Copper Oxide Surfaces, Journal of the Electrochemical Society, Vol. 158, No. 5, pgs E45-E49.

LEE, K. S. (2012), Unpublished Masters Degree Dissertation, University of Nottingham, Nottingham.

LI, X., Z. H. ZHU, R. DE MARCO, A. DICKS, J. BRADLEY, S. LIU and G. Q. LU (2008), Factors that Determine the Performance of Carbon Fuels in the Direct Carbon Fuel Cell, Industrial and Engineering Chemistry Research, Vol. 47, pgs 9670-9677.

LICHT, S., B. WANG, S. GHOSH, H. AYUB, D. JIANG and J. GANLEY (2010), A New Solar Carbon Capture Process: Solar Thermal Electrochemical Photo (STEP) Carbon Capture, Journal of Physical Chemistry Letters, Vol. 1, pgs 2363-2368.

LINKE, W. F. (1958), Solubilities of Inorganic and Metal Organic Compounds, D. Van Nostrand Company Inc., Princeton.

LORENZ, P. K. and G. J. JANZ (1970), Electrolysis of molten carbonates: anodic and cathodic gas evolving reactions, Electrochimica Acta, Vol. 15, pgs 1025-1035.

MARTÍNEZ, E., U. WIKLUND, J. ESTEVE, F. MONTALÀ and L. L. CARRERAS (2002), Tribological performance of TiN supported molybdenum and tantalum carbide coatings in abrasion and sliding contact, Wear, Vol. 253, pgs 1182-1187.

MASSOT, L., P. CHAMELOT, F. BOUYER and P. TAXIL (2002), Electrodeposition of carbon films from molten alkaline fluoride media, Electrochimica Acta, Vol. 47, pgs 1949-1957.

MASSOT, L. P. CHAMELOT, F. BOUYER and P. TAXIL (2003), Studies of carbon nucleation phenomena in molten alkaline fluoride media, Electrochimica Acta, Vol. 48, pgs 465-471.

MIKKELSEN, M., M. Jørgensen and F. C. Krebs (2009), The teraton challenge. A review of fixation and transformation of carbon dioxide, Energy & Environmental Science, Vol. 3, pgs 43-81.

MONK, P. M. S. (2001), Fundamentals of Electroanalytical Chemistry, John Wiley & Sons, Chichester.

NEEFT, J. P. A., M. MAKKEE and J. A. MOULIJN (1996), Catalysts for the oxidation of soot from diesel exhaust gases. I. An exploratory study, Applied Catalysis B: Environmental, Vol. 8, pgs 57-78.

NOVOSELOVA, I. A., S. V. VOLKOV, N. F. OLIINYK and V. I. SHAPOVAL (2003), High-temperature electrochemical synthesis of carbon-containing inorganic compounds under excessive carbon dioxide pressure, Journal of Mining and Metallurgy, Vol. 39B, pgs 281-293.

NOVOSELOVA, I. A., N. F. OLIINYK and S. V. VOLKOV, Electrolytic production of carbon nano-tubes in chloride-oxide melts under carbon dioxide pressure, in: T. N. VEZIROGLU, S. YU. ZAGINAICHENKO, D. V. SCHUR, B. BARANOWSKI, A. P. SHPAK, V. V. SKOROKHOD and A. KALE (Eds.) (2007), Hydrogen Materials and Chemistry of Carbon Nanomaterials, Springer, Berlin, pgs 459-465.

NOVOSELOVA, I. A., N. F. OLIINYK, S. V. VOLKOV, A. A. KONCHITS, I. B. YANCHUK, V. S. YEFANOV, S. P. KOLESNIK and M. V. KARPETS (2008a), Electrolytic synthesis of carbon nanotubes from carbon dioxide in molten salts and their characterization, Physica E, Vol. 40, pgs 2231-2237.

NOVOSELOVA, I. A., N. F. OLIINYK, A. B. VORONINA and S. V. VOLKOV (2008b), Electrolytic generation of nano-scale carbon phases with framework structures in molten salts on metal cathodes, Z. Naturforsch, Vol. 63a, pgs 467-474.

OLAH, G. A. and G. K. S. PRAKASH (2010), Electrolysis of Carbon Dioxide in Aqueous Media to Carbon Monoxide and Hydrogen for Production of Methanol, US Patent 20100193370 A1.

PETRUSHINA, I. M., L. QINGFENG, F. BORUP and N. J. BJERRUM (2000), Corrosion protection of steel in molten Li2CO3–K2CO3 and Na2CO3–K2CO3 mixtures in a hydrogen-containing atmosphere, Journal of Applied Electrochemistry, Vol. 30, pgs 929-937.

PIERSON, H. O. (1993), Handbook of Carbon, Graphite, Diamond and Fullerenes: Properties, Processing and Applications, Noyes Publications, Park Ridge, New Jersey.

RAEBIGER, J. W., J. W. TURNER, B. C. NOLL, C. J. CURTIS, A. MIEDANER, B. COX and D. L DUBOIS (2006), Electrochemical Reduction of CO_2 to CO Catalyzed by a Bimetallic Palladium Complex, Organometallics, Vol. 25, No. 14, pgs 3345-3351.

ROGERS, G. F. C. and Y. R. MAYHEW (1992), Engineering Thermodynamics Work and Heat Transfer (4^{th} Edition), Prentice Hall, Harlow, UK.

SIAMBUN, N. J., H. MOHAMED, D. HU, D. JEWELL, Y. K. BENG and G. Z. CHEN (2011a), Utilisation of Carbon Dioxide for Electro-Carburisation of Mild Steel in Molten Carbonate Salts, Journal of the Electrochemical Society, Vol. 158, No. 11, pgs H1117-H1124.

SIAMBUN, N. J. (2011b), Electrolysis of Molten Carbonate Salts and its Applications (PhD Thesis), University of Nottingham, Nottingham.

SMIRNOV, M. V., I. YA. LYUBIMTSEVA and L. A. TSIOVKINA (1965), Cathodic processes on a gold electrode in the lithium oxide-lithium carbonate molten mixture, Elektrokhimiya, Vol. 7, No. 4, pgs 566-568.

SNUFFIN, L. L., L. W. WHALEY and L. YU (2011), Catalytic Electrochemical Reduction of CO_2 in Ionic Liquid $EMIMBF_3Cl$, Journal of the Electrochemical Society, Vol. 158, No. 9, pgs F155-F158.

SONG, Q., Q. XU and C. XING (2012), Preparation of a gradient Ti–TiOC-carbon film by electro-deposition, Electrochemistry Communications, Vol. 17, pgs 6-9.

STERN, K. H. and E. L. WEISE (1969), High Temperature Properties and Decomposition of Inorganic Salts: Part 2. Carbonates, Nat. Stand. Ref. Data Ser., National Bureau of Standards (U. S.).

STERN, K. H. and D. R. ROLISON (1989), Theme and Variations on Tantalum-Carbonate Reactions in Molten Fluorides, Journal of the Electrochemical Society, Vol. 136, No. 12, pgs 3760-3767.

STERN, K. H. (1992), Electrodeposition of refractory carbide coatings from fluoride melts, Journal of Applied Electrochemistry, Vol. 22, pgs 717-721.

SURYANARAYANA, C. and M. GRANT NORTON (1998), X-ray Diffraction: A Practical Approach, Plenum Press, New York.

TAGUCHI, S. and A. ARAMATA (1994), Surface-structure sensitive reduced CO_2 formation on Pt single crystal electrodes in sulfuric acid solution, Electrochimica Acta, Vol. 39, pgs 2533.

THORNTON, P. R. (1968), Scanning Electron Microscopy, Chapman and Hall Ltd, London.

TOKUMITSU, K., A. MABUCHI, H. FUJIMOTO and T. KASUH (1996), Electrochemical Insertion of Lithium into Carbon Synthesized from Condensed Aromatics, Vol. 143, No. 7, pgs 2235-2239.

TZVETKOFF, TZ. and J. KOLCHAKOV (2004), Mechanism of growth, composition and structure of oxide films formed on ferrous alloys in molten salt electrolytes - a review, Materials Chemistry and Physics, Vol. 87, pgs 201-211.

VOSSEN, J. P. T., L. PLOMP, J. H. W. DE WIT and G. RIETVELD (1995), Corrosion Behaviour of Stainless Steel and Nickel-Base Alloys in Molten Carbonate, Journal of the Electrochemical Society, Vol. 142, No. 10, pgs 3327-3335.

VOSSEN, J. P. T., R. C. MAKKUS and J. H. W. DE WIT (1996), Corrosion Behavior of Chromium in Molten Carbonate, Journal of the Electrochemical Society, Vol. 143, pgs 66-73.

VUTETAKIS, D. G., D. R. SKIDMORE and H. J. BYKER (1987), Electrochemical Oxidation of Molten Carbonate-Coal Slurries, Journal of the Electrochemical Society, Vol. 134, No. 12, pgs 3027-3034.

WAGMAN, D. D., W. H. EVANS, V. B. PARKER, R. H. SCHUMM, I. HALOW, S. M. BAILEY, K. L. CHURNEY and R. L. NUTALL (1982), The NBS tables of chemical thermodynamic properties; selected values for inorganic and C_1 and C_2 organic substances in SI units, US National Bureau of Standards, Washington DC.

WANG, H., N. J. SIAMBUN, L. YU and G. Z. CHEN (2012), A Robust Alumina Membrane Reference Electrode for High Temperature Molten Salts, Journal of the Electrochemical Society, Vol. 159, No. 9, pgs H740-H746.

WASEDA, Y., E. MATSUBARA and K. SHINODA (2011), X-ray diffraction crystallography: introduction, examples and solved problems (1st Edition), Springer-Verlag, Berlin.

WATT, I. M. (1997), The Principles and Practice of Electron Microscopy, Cambridge University Press, Cambridge.

WELHAM, N. J. and J. S. WILLIAMS (1998), Extended milling of graphite and activated carbon, Carbon, Vol. 36, No. 9, pgs 1309-1315.

WHIPPLE, D. T. and P. J. A. KENIS (2010), Prospects of CO_2 Utilization via Direct Heterogeneous Electrochemical Reduction, Journal of Physical Chemistry Letters, No. 1, pgs 3451-3458.

WHIPPLE, D. T., E. C. FINKE and P. J. A. KENIS (2010), Microfluidic Reactor for the Electrochemical Reduction of Carbon Dioxide: The Effect of pH, Electrochemical and Solid State Letters, Vol. 13, No. 9, B109-B111.

WU, T., W. XIAO, X. JIN, C. LIU, D. WANG and G. Z. CHEN (2008), Computer-aided control of electrolysis of solid Nb_2O_5 in molten $CaCl_2$, Physical Chemistry Chemical Physics, Vol. 10, pgs 1809-1818.

APPENDIX I

CALCULATING STANDARD POTENTIALS OF CATHODIC REACTIONS VS. CO_3^{2-}/CO_2-O_2

In Chapters 4, 5 and 6, the theoretical standard potentials of several reactions with respect to CO_3^{2-}/CO_2-O_2 were given; this appendix explains how these potentials were determined. Consider the following cathodic reaction:

$$Li^+ + e^- \rightarrow Li \qquad \text{(AI.1)}$$

The CO_3^{2-}/CO_2-O_2 reference reaction is the oxidation of the carbonate ion:

$$CO_3^{2-} \rightarrow CO_2 + ½O_2 + 2e^- \qquad \text{(AI.2)}$$

Combining the half-cell Reactions AI.1 and AI.2 a full reaction equation is obtained:

$$Li_2CO_3 \rightarrow CO_2 + ½O_2 + 2Li \qquad \text{(AI.3)}$$

The standard Gibbs free energy of this reaction is given by the following equation:

$$\Delta G^o_{Li_2CO_3/Li} = \Delta G^o_{CO_2} - \Delta G^o_{Li_2CO_3} \qquad \text{(AI.4)}$$

Where: $\Delta G°_X$ = Standard Gibbs free energy change of formation of substance X.

As a result the standard potential of Reaction AI.1 vs. CO_3^{2-}/CO_2-O_2 is:

$$E^o_{Li} = -\frac{\Delta G^o_{Li_2CO_3/Li}}{2F} \qquad \text{(AI.5)}$$

Where: $E°_{Li}$ = standard potential for lithium ion reduction to lithium metal and F = Faraday's constant (96.48 kC/mol).

Since Gibbs free energy is a function of temperature, the value of $E°_{Li}$ can be calculated at many different temperatures.

APPENDIX II

PRELIMINARY STUDIES OF THE Li_2CO_3-Na_2CO_3-K_2CO_3, Li_2CO_3 AND Na_2CO_3-K_2CO_3 ELECTROLYTES BY CYCLIC VOLTAMMETRY

In Chapter 6, the cyclic voltammetry of stainless steel electrodes was studied in four different molten carbonate electrolytes: Li_2CO_3-Na_2CO_3, Li_2CO_3-K_2CO_3, Na_2CO_3 and K_2CO_3. This appendix supplements Chapter 6 by presenting some preliminary studies of the cyclic voltammetry of stainless steel in the molten Li_2CO_3-Na_2CO_3-K_2CO_3, Li_2CO_3 and Na_2CO_3-K_2CO_3 electrolytes. Note that many of the equations, sections and figures referred to in this appendix will be found in Chapter 6.

AII.1 Cyclic Voltammetry of Stainless Steel in Molten Li_2CO_3-Na_2CO_3-K_2CO_3

From the preliminary studies that have been carried out, the cyclic voltammograms of the Li_2CO_3-Na_2CO_3-K_2CO_3 electrolyte obtained using stainless steel working electrodes appear to be rather similar to those of the Li_2CO_3-Na_2CO_3 and Li_2CO_3-K_2CO_3 electrolytes. Hence, the peak labels used in this section correspond to the same peak attributions that were made in Sections 6.2.1 and 6.2.2.

Figure AII.1 shows two voltammograms obtained at a stainless steel working electrode in the Li_2CO_3-Na_2CO_3-K_2CO_3 electrolyte at 707 °C, at negative potential limits of -2.45 V and -2.75 V vs. Ag/AgCl. Figure AII.1 shows typical features that were observed at all of the temperatures studied for the Li_2CO_3-Na_2CO_3-K_2CO_3 electrolyte: 496 °C, 577 °C and 707 °C. As with the Li_2CO_3-Na_2CO_3 and Li_2CO_3-K_2CO_3 electrolytes, peak A1 increased in height when the negative potential limit of the scan was made more negative. The number and positions of the peaks observed in Figure AII.1 are also similar to the aforementioned two electrolytes.

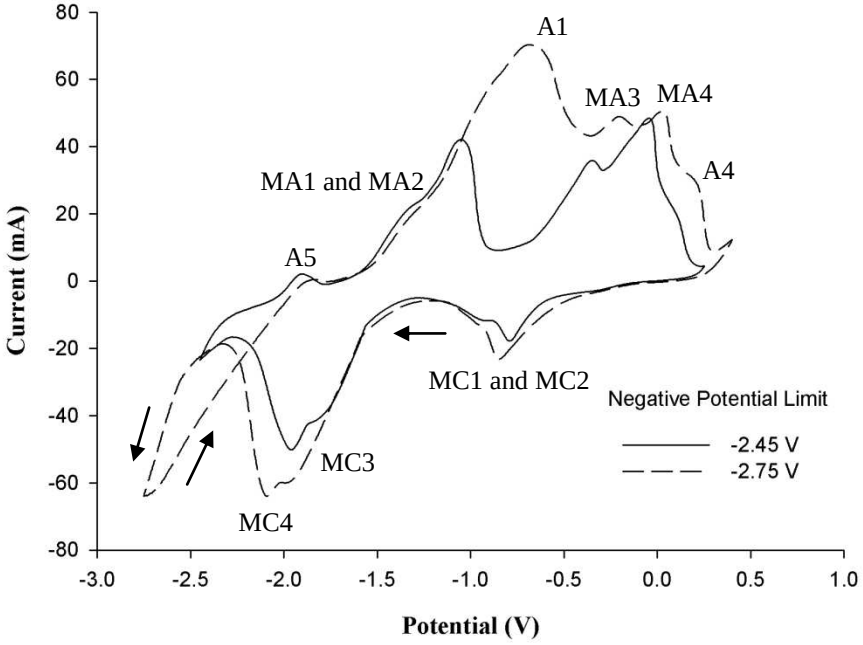

Figure AII.1: Cyclic voltammograms obtained using a stainless steel wire working electrode in a molten Li_2CO_3-Na_2CO_3-K_2CO_3 electrolyte (molar ratio of 43.5:31.5:25.0) at 707 °C, at a scan rate of 100 mV/s, for negative potential limits of -2.45 V and -2.75 V. Atmosphere: CO_2; WE diameter: 0.25 mm; CE: 6 mm diameter stainless steel rod; RE: alumina membrane Ag/AgCl.

Carbon electro-deposition has been experimentally confirmed in the Li_2CO_3-Na_2CO_3-K_2CO_3 electrolyte. At 709 °C, carbon deposits were obtained on mild steel rod working electrodes at potentials 0.6 V, 1.0 V and 1.4 V more negative than the potential at the start of the current wave at the cathodic limit (observed in cyclic voltammetry). These depositions are considered in more detail in Chapter 7 of the present thesis. Furthermore, Le Van et al. (2009) obtained carbon deposits from the Li_2CO_3-Na_2CO_3-K_2CO_3 electrolyte under various conditions, as shown in Table 2.1 in Chapter 2. In Figure AII.1, the scan with the more negative potential limit of -2.75 V vs. Ag/AgCl has a cathodic loop, which probably indicates that carbon was formed on the surface of the working electrode during that scan. Note that no cathodic loop is present in the scan with the less negative limit of -2.45 V vs. Ag/AgCl, despite the fact that the start of the current wave at the cathodic limit has been reached. As has been discussed in Chapters 4 and 5, it is likely that carbon electro-deposition did not dominate over other

competing cathodic reactions until the working electrode had become coated with a layer of carbon. Therefore, it is likely that the cathodic current flowing at the start of the current wave at the cathodic limit was largely, if not all due to the reactions that competed with carbon electro-deposition.

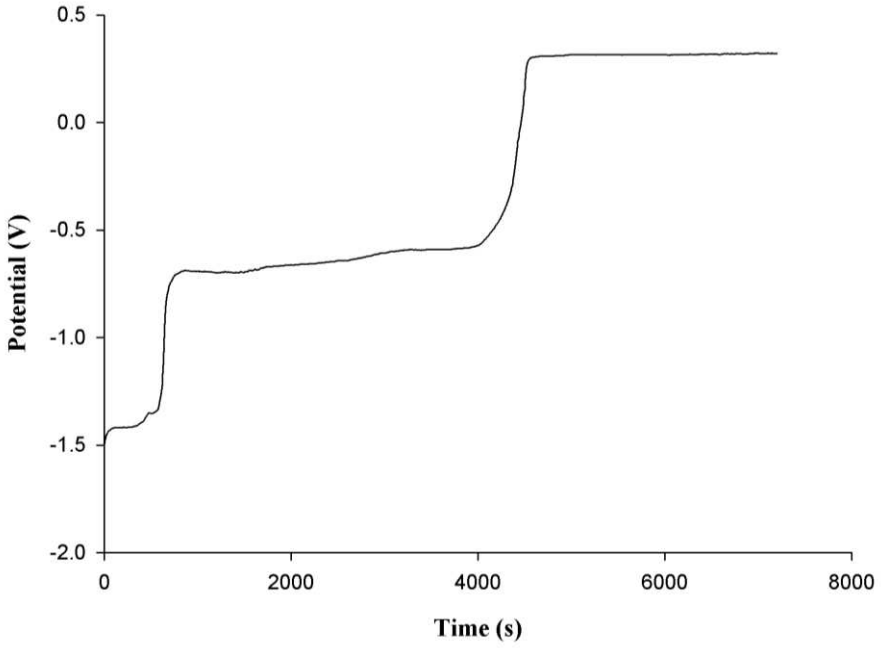

Figure AII.2: Variation of potential versus time during the re-oxidation of electro-deposited carbon in a Li_2CO_3-Na_2CO_3-K_2CO_3 molten salt (molar ratio of 43.5:31.5:25.0) at a constant current of 150 mA, at a temperature of 707 °C, under a CO_2 atmosphere. The carbon was electro-deposited at an applied potential of -2.1 V vs. Ag/AgCl. WE: 5 mm diameter mild steel rod (with carbon deposit still attached); CE: 10 mm diameter graphite rod; Ag/AgCl membrane RE.

The re-oxidation of electro-deposited carbon in the Li_2CO_3-Na_2CO_3-K_2CO_3 electrolyte was found to occur via a similar two-stage process that was observed using the Li_2CO_3-Na_2CO_3 and the Li_2CO_3-K_2CO_3 electrolytes. The strongest evidence for this was obtained from the galvanostatic re-oxidation of electro-deposited carbon. Figure AII.2 shows a typical chronopotentiogram obtained from the Li_2CO_3-Na_2CO_3-K_2CO_3 electrolyte. The carbon was obtained after 10 minutes of electrolysis at a potential of -2.1 V vs. Ag/AgCl, in the same electrolyte and using the same reference electrode as was used to obtain the cyclic voltammograms in Figure AII.1. The temperature of the molten salt was also the same at 707

°C. As with similar chronopotentiograms obtained from the Li_2CO_3-Na_2CO_3 and the Li_2CO_3-K_2CO_3 electrolytes, the first plateau corresponds to peak A1, the second plateau corresponds to peak A3, whilst the third plateau corresponds to the anodic limit (the oxidation of the carbonate ion). The potential of the first plateau in Figure AII.2 at around −1.41 V vs. Ag/AgCl corresponds to the start of the current wave of peak A1 in Figure AII.1. As for the second plateau in Figure AII.2 at approximately -0.65 V vs. Ag/AgCl, this corresponds to the current wave of peak A3, which was probably concealed by the anodic peaks MA3 and MA4 in Figure AII.1. The third plateau in Figure AII.2 at 0.32 V vs. Ag/AgCl corresponds quite well with the start of the current wave at the anodic limit in Figure AII.1.

Figure AII.3 shows cyclic voltammograms obtained at temperatures of 577 °C (a) and 496 °C (b). Generally, the voltammograms in Figure AII.3 appear to exhibit similar peaks to the voltammograms in Figure AII.1 at 707 °C. Note that peak A1 was not observed in Figure AII.3(b), and no cathodic loop was observed either. This was probably due to the negative potential limit of the scan not being negative enough for significant amounts of carbon electro-deposition to occur. The fact that peak A1 generally appeared when cathodic loops were observed is good evidence for ascribing peak A1 to carbon re-oxidation. One point worth mentioning here is that the lower temperature used when recording Figure AII.3(b) might have led to a lower ionic conductivity in the electrolyte, resulting in a larger iR drop that lead to the distortion of the voltammogram.

Due to the many similarities between the cyclic voltammograms obtained from the Li_2CO_3-Na_2CO_3, Li_2CO_3-K_2CO_3 and Li_2CO_3-Na_2CO_3-K_2CO_3 electrolytes, it is not difficult to account for the cyclic voltammetry observed at stainless steel working electrodes in the Li_2CO_3-Na_2CO_3-K_2CO_3 electrolyte. However, in the future, there is a need to conduct studies of the cyclic voltammetry of the Li_2CO_3-Na_2CO_3-K_2CO_3 electrolyte at platinum working electrodes. If such studies were carried out, it would be possible to interpret the cyclic voltammograms presented in this section with greater confidence.

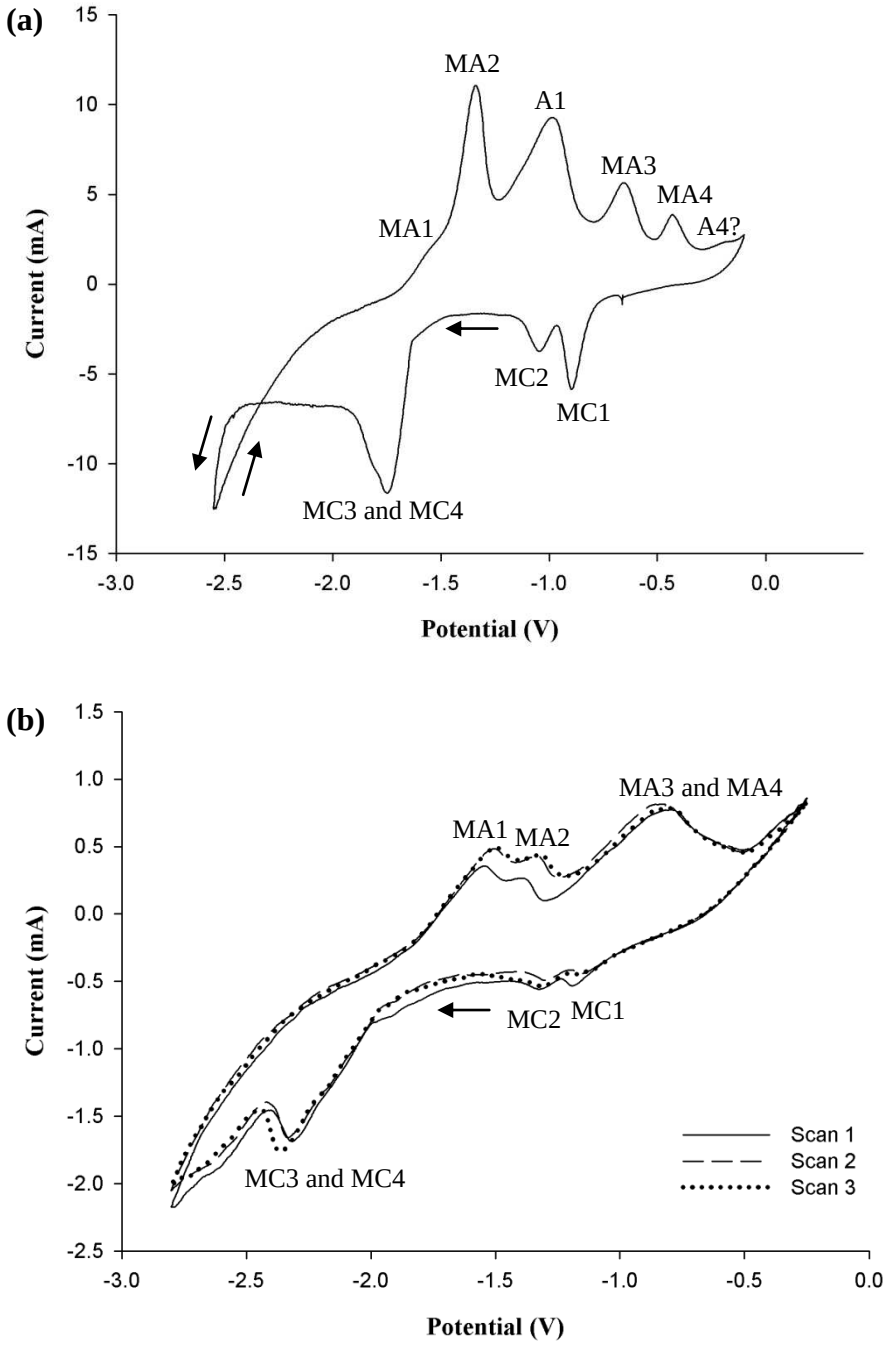

Figure AII.3: Cyclic voltammograms obtained using a stainless steel wire working electrode in a molten Li_2CO_3-Na_2CO_3-K_2CO_3 electrolyte (molar ratio of 43.5:31.5:25.0), at temperatures of (a) 577 °C and (b) 496 °C. Scan rates: (a) 100 mV/s, (b) 50 mV/s; atmosphere: CO_2; WE diameter: 0.25 mm; CE: 6 mm diameter stainless steel rod; RE: alumina membrane Ag/AgCl.

AII.2 Cyclic Voltammetry of Stainless Steel in Molten Li_2CO_3

Figure AII.4 shows typical cyclic voltammograms obtained from the Li_2CO_3 electrolyte using a stainless steel working electrode, at a temperature of 837 °C. Although there are some similarities between the cyclic voltammetry of the pure Li_2CO_3 electrolyte and that of the Li_2CO_3-Na_2CO_3, Li_2CO_3-K_2CO_3 and Li_2CO_3-Na_2CO_3-K_2CO_3 electrolytes, the voltammetry from pure Li_2CO_3 also exhibits some significant differences.

Carbon electro-deposition has been experimentally confirmed in the pure Li_2CO_3 electrolyte under a number of different process conditions. Firstly, in a two-electrode cell, at a temperature of 800 °C and an applied potential difference (or cell voltage) of 4 V (equivalent to a cathode potential of approximately -2.1 V vs. Ag/AgCl[*]), carbon was electro-deposited onto a mild steel cathode. Secondly, carbon was electro-deposited onto mild steel working electrodes in a three-electrode system at 800 °C, at a working electrode potential of -1.8 V vs. Ag/AgCl. Thirdly, carbon deposits have also been obtained using mild steel working electrodes in a three-electrode system at 753 °C, at an applied potential of -2.1 V vs. Ag/AgCl. All of these deposition potentials were chosen due to the fact that they lie beyond the cathodic limit potential at their respective temperatures. Note that a cathodic loop is present in Figure AII.4, which is indicative of carbon formation via Reaction 6.1.

[*] Note that the true cathode potential during two-electrode electrolysis is not known, due to the fact that the anode potential was almost certainly affected by the passage of current.

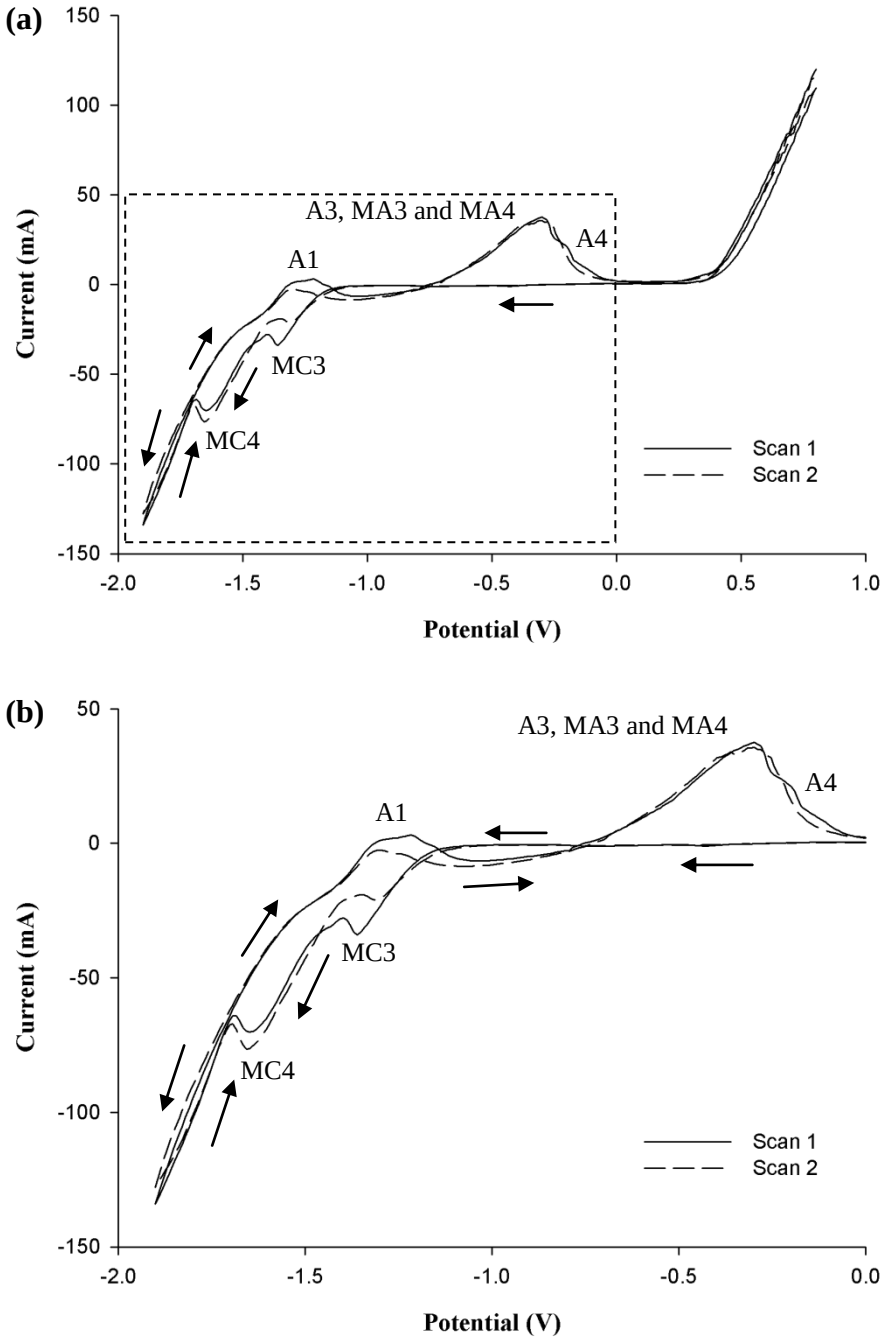

Figure AII.4: Cyclic voltammograms obtained from a pure Li_2CO_3 molten salt at a temperature of 837 °C, under a CO_2 atmosphere: (a) full scans; (b) enlarged view of the boxed region in (a). Scan rate: 50 mV/s; WE: 0.25 mm diameter stainless steel wire; CE: 6 mm diameter stainless steel rod; Ag/AgCl membrane RE.

As with the other molten carbonate electrolytes containing Li_2CO_3, electro-deposited carbon was found to be re-oxidised via a similar two-stage process. Figure AII.5 shows a chronopotentiogram obtained from the galvanostatic re-oxidation of a carbon deposit produced after 10 minutes of electro-deposition at a potential of -2.1 V vs. Ag/AgCl. The temperature of the electrolyte was 753 °C. By analogy with the other molten carbonate electrolytes containing Li_2CO_3, the first plateau corresponds to peak A1, the second plateau corresponds to peak A3 and the third plateau corresponds to the oxidation of carbonate ions at the anodic limit. Despite the significant difference in the temperatures used to obtain Figures 6.12 and 6.13, the first and second plateaux in Figure AII.5 seem to correspond well with the peaks labelled A1 and A3 in Figure AII.4 respectively.

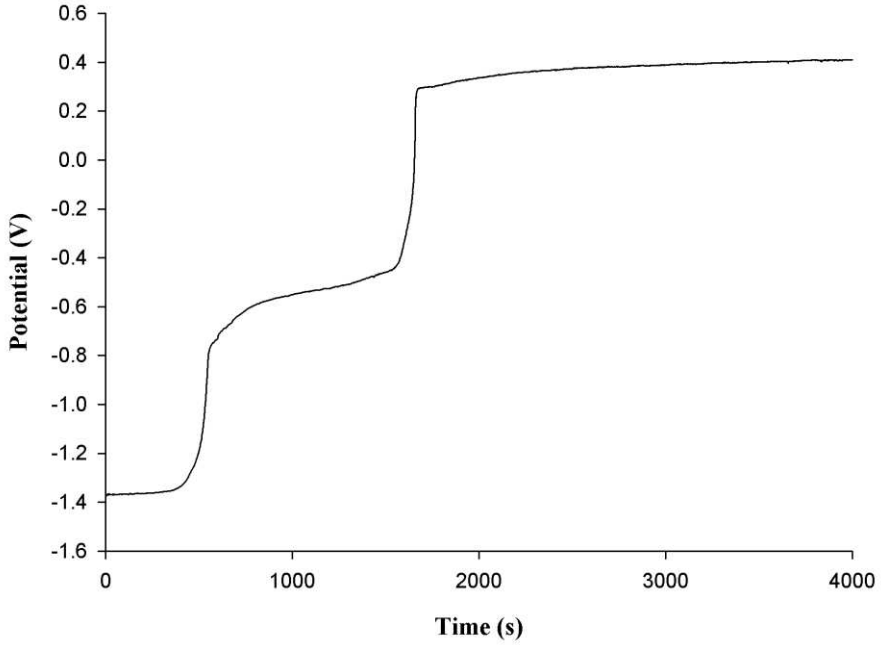

Figure AII.5: Variation of potential versus time during the re-oxidation of electro-deposited carbon in a pure Li_2CO_3 molten salt at a constant current of 150 mA, at a temperature of 753 °C, under a CO_2 atmosphere. The carbon was electro-deposited at an applied potential of -2.1 V vs. Ag/AgCl. WE: 5 mm diameter mild steel rod (with carbon deposit still attached); CE: 10 mm diameter graphite rod; Ag/AgCl membrane RE.

From the very limited results presented here, it is apparent that the behaviour of the pure Li_2CO_3 electrolyte was somewhat different to that observed in the Li_2CO_3-Na_2CO_3, Li_2CO_3-

K_2CO_3 and Li_2CO_3-Na_2CO_3-K_2CO_3 electrolytes. Regarding future work, there is a need to study the cyclic voltammetry of the pure Li_2CO_3 electrolyte using platinum working electrodes. This would allow the verification of the locations of peaks A1 and A3, and to improve our understanding of the system. There is also a need to investigate the physical properties of the carbon produced from the pure Li_2CO_3 electrolyte, as this may help to explain why peak A1 is somewhat smaller for this electrolyte.

AII.3 Cyclic Voltammetry of Stainless Steel in Molten Na_2CO_3-K_2CO_3

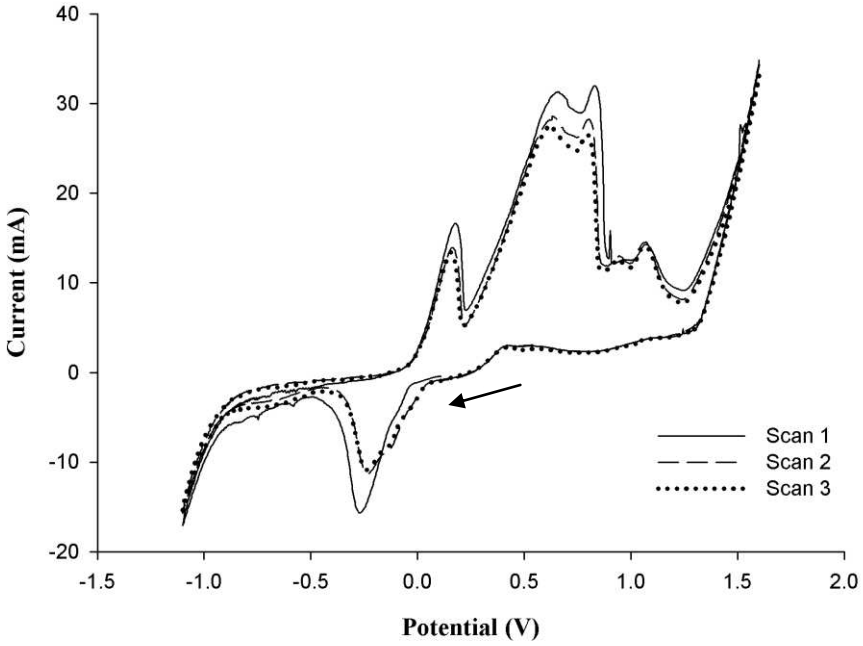

Figure AII.6: Cyclic voltammograms obtained from a Na_2CO_3-K_2CO_3 molten salt (molar ratio: 58:42) at a temperature of 847 °C under a CO_2 atmosphere. Scan rate: 50 mV/s; WE: 0.25 mm diameter stainless steel wire; CE: 6 mm diameter stainless steel rod; Ag/AgCl membrane RE.

Figure AII.6 shows typical cyclic voltammograms for the Na_2CO_3-K_2CO_3 electrolyte at a temperature of 847 °C. Figure AII.6 quite closely resembles Figure 6.8 for the pure Na_2CO_3 electrolyte, particularly in terms of the configuration of the anodic peaks. This suggests that the reactions that occurred in the Na_2CO_3-K_2CO_3 and the pure Na_2CO_3 electrolytes were similar.

No carbon could be electro-deposited from the Na_2CO_3-K_2CO_3 electrolyte at an applied potential difference of 4 V (which would correspond to a cathode potential of around -2.68 V vs. Ag/AgCl), at a temperature of 847 °C. The cathode material was mild steel. However, at a temperature of 800 °C, carbon could be electro-deposited from a pure Li_2CO_3 molten salt at an applied potential difference of 4 V, as was mentioned in Section AII.2.

Devyatkin (2012) obtained a cyclic voltammogram from a Na_2CO_3-K_2CO_3 electrolyte (molar ratio of 60:40) using a vitreous carbon working electrode at a temperature of 750 °C. The most striking feature of this voltammogram is that there are no anodic or cathodic peaks whatsoever between the anodic and cathodic limits. As was mentioned in Section 2.5.1, Le Van et al. (2009) found that the vitreous carbon working electrode was inert in a ternary Li_2CO_3-Na_2CO_3-K_2CO_3 electrolyte, so this is probably also the case for the Na_2CO_3-K_2CO_3 electrolyte. The fact that no anodic peaks were observed in the cyclic voltammogram of Devyatkin (2012) implies that none of the products produced at the cathodic limit were re-oxidised during the anodic sweep. Hence, it seems unlikely that any carbon was electro-deposited at the cathodic limit in the cyclic voltammogram obtained by Devyatkin (2012).

Petrushina et al. (2000) obtained a linear sweep voltammogram from a Na_2CO_3-K_2CO_3 electrolyte (molar ratio of 60:40), sweeping in the anodic direction, using a 316L stainless steel working electrode at a temperature of 730 °C. Two anodic peaks were identified by Petrushina et al. (2000), which were ascribed to the formation of mixed iron, nickel and chromium oxides, some of which could dissolve in the electrolyte.

In light of the voltammograms obtained by Devyatkin (2012) and Petrushina (2000), it can be inferred that all of the peaks in Figure AII.6 were associated with reactions that involved substances from the working electrode metal itself. In addition, none of the anodic peaks in Figure AII.6 appear to have been caused by the re-oxidation of products formed at the cathodic limit. Both of these inferences are also reasonable considering the findings from the pure Na_2CO_3 and K_2CO_3 electrolytes in the present research (see Sections 6.3.1 and 6.3.2).

Reactions 6.2 to 6.7 could possibly have occurred at the cathodic limit in the Na_2CO_3-K_2CO_3 electrolyte; Figure AII.7 shows the variation of the theoretical standard potentials for these six reactions. Evidently, at 847 °C, the most favourable three reactions are the formation of sodium metal, the formation of potassium metal, and the formation of carbon from Na_2CO_3, in that order. At 847 °C, potassium metal would be a vapour (its boiling point is 760 °C) but sodium metal would be a liquid (its melting point is 98 °C, whilst its boiling point is 883 °C). However, based on the voltammogram obtained by Devyatkin (2012), it seems unlikely that either of these products were re-oxidised during the anodic sweep in Figure AII.6. This may be because the sodium may have dissolved in the electrolyte, whilst the potassium would have evaporated. Therefore, the sodium and potassium metal products may have left the vicinity of the working electrode too quickly to be re-oxidised. Furthermore, perhaps no carbon was electro-deposited because the overpotential for its deposition was too high.

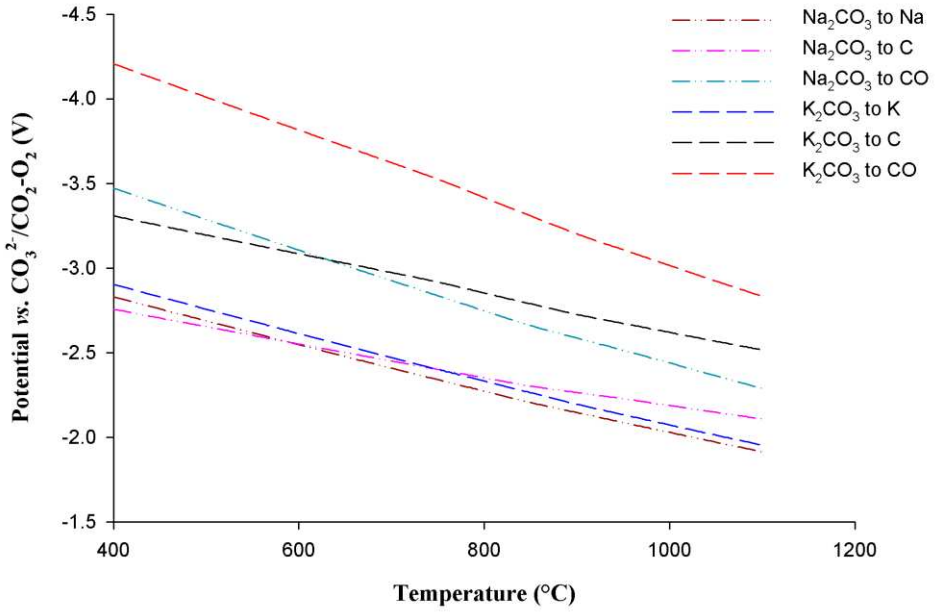

Figure AII.7: Standard potentials against temperature for the conversion of Na_2CO_3 and K_2CO_3 to various cathodic products: carbon (C), alkali metal (Na or K) and carbon monoxide (CO).The potentials were calculated with the assistance of HSC Chemistry software (Version 6.12; Outokumpu Research) and are reported versus the CO_3^{2-}/CO_2-O_2 reference reaction. Appendix I gives details of how these standard potentials were determined.

In order to properly verify the findings from the Na_2CO_3, K_2CO_3 and Na_2CO_3-K_2CO_3 electrolytes, it would be necessary to study them using a platinum working electrode. The comparison between voltammograms obtained at platinum electrodes and those obtained at stainless steel electrodes would enable the deduction of which peaks, if any, were associated with the re-oxidation of cathodic products. Furthermore, it may also be beneficial to carry out potentiostatic electrolysis at a number of different potentials beyond the cathodic limit potential, including at very negative potentials, as it may be possible that the overpotential required for carbon electro-deposition was not attained in the present study.

APPENDIX III

RE-OXIDATION OF ELECTRO-DEPOSITED CARBON IN THE Li_2CO_3 AND Li_2CO_3-Na_2CO_3-K_2CO_3 ELECTROLYTES

In Chapter 8, the Q^+/Q^- values for the re-oxidation of electro-deposited carbon in the Li_2CO_3-Na_2CO_3 and Li_2CO_3-K_2CO_3 electrolytes was considered in some detail. This appendix provides some supplementary Q^+/Q^- data for the re-oxidation of electro-deposited carbon in the Li_2CO_3 and Li_2CO_3-Na_2CO_3-K_2CO_3 electrolytes. Carbon deposits were electro-deposited via chronoamperometry, as has been described in Sections 3.5.2 and 8.2. These carbon deposits were then re-oxidised using chronopotentiometry, where the cell set-up used has already been described in Sections 3.5.3 and 8.3.

Table AIII.1: Q^+/Q^- values for the re-oxidation of electro-deposited carbon via chronopotentiometry, for the Li_2CO_3 and Li_2CO_3-Na_2CO_3-K_2CO_3 (molar ratio of 43.5:31.5:25.0) electrolytes at various process conditions; Q^+/Q^- values at the ends of the first and second plateaux are shown. NB. Carbon re-oxidation was considered to have stopped at the end of the second plateau.

Molten Salt	Salt Temperature (°C)	Deposition Potential vs. Ag/AgCl (V)	Reduction Charge Passed (C)	Re-Oxidation Current (mA)	Q^+/Q^- (%)		All Carbon Removed?
					At End of 1st Plateau	At End of 2nd Plateau	
Li_2CO_3	753	-2.1	-1191	150	6.87	20.9	Yes
Li_2CO_3-Na_2CO_3-K_2CO_3	702	-1.8	-787	150	11.5	42.0	Yes
	702	-1.8	-557	150	11.4	45.9	Yes

Table AIII.1 shows three Q^+/Q^- values for the re-oxidation of electro-deposited carbon via chronopotentiometry: two Q^+/Q^- values from the Li_2CO_3-Na_2CO_3-K_2CO_3 electrolyte and one Q^+/Q^- from the Li_2CO_3 electrolyte. Note that these two electrolytes were not studied to any great extent in the present research, which is why only three Q^+/Q^- values are presented for these two electrolytes. The two Q^+/Q^- values obtained from the Li_2CO_3-Na_2CO_3-K_2CO_3 electrolyte lie in the range of Q^+/Q^- values obtained by Ingram et al. (1966) for this electrolyte

at 600 °C (32 % to 57 %). They also lie in the range of change efficiencies obtained from both the Li_2CO_3-Na_2CO_3 and Li_2CO_3-K_2CO_3 electrolytes (27.6 % to 105 %), whilst the Q^+/Q^- obtained from the Li_2CO_3 electrolyte lies below the minimum value of this range. The cyclic voltammetry of the Li_2CO_3-Na_2CO_3-K_2CO_3 electrolyte presented in Appendix AII indicated that carbon re-oxidation in Li_2CO_3-Na_2CO_3-K_2CO_3 was largely similar to that in Li_2CO_3-Na_2CO_3 and Li_2CO_3-K_2CO_3. Thus, it is reasonable that the Q^+/Q^- values for these three electrolytes are generally comparable.

The comparatively low Q^+/Q^- of 20.9 % for Li_2CO_3 in Table AIII.1 may indicate that relatively large quantities of carbon fell off the electrode during electro-deposition and/or re-oxidation.